

The identification of neuronal binding partners for human soluble amyloid precursor protein alpha

A thesis submitted to the University of Manchester for the degree of Doctor of Philosophy in the Faculty of Biology, Medicine and Health

2023

Michael Haycox

School of Biological Sciences

List of contents

List of contents.....	2
List of Figures	6
List of Tables	9
List of abbreviations.....	10
Abstract.....	12
Declaration	13
Copyright statement.....	13
Acknowledgements.....	14
1. Introduction	15
1.1. An introduction to dementia.....	15
1.2. Alzheimer's disease	16
1.2.1. The neuropathology of Alzheimer's disease	17
1.2.1. Hyperphosphorylated tau	18
1.2.2. The normal physiological function of amyloid- β	19
1.2.3. A β in Alzheimer's disease	20
1.3. The amyloid precursor protein.....	22
1.3.1. The reciprocal proteolytic processing of APP.....	24
1.4. Causes and risk factors of AD.	26
1.5. Oxidative stress in AD.....	30
1.6. The failure of drug trials for AD.....	32
1.7. Soluble amyloid precursor protein (sAPP α).	35
1.7.1. sAPP α improved neuronal survival in the presence of toxic levels of A β	37
1.7.2. sAPP α protected neurons against glucose deprivation and glutamate excitotoxicity.....	37
1.7.3. sAPP α protected neuronal cells against A β -induced oxidative stress and reduced A β and ptau levels.	39
1.7.3. sAPP α is neurotrophic and stimulates neuronal growth.	40
1.7.4. sAPP α enhanced memory and LTP.....	41
1.7.5. sAPP α protected neurons against proteasomal stress.	42
1.7.6. sAPP α is significantly more protective than sAPP β and therefore has higher therapeutic potential.....	42
1.8. Known sAPP α receptors.	45
1.8.1. p75 neurotrophin receptor.	45

1.8.2. SORLA and Sortilin.	46
1.8.3. $\alpha 3$ -Na, K-ATPase.	46
1.8.4. GABA _B R1a.	47
1.9. Thesis aims.	47
2. Materials and Methods.....	49
2.1. Immortalised cell culture.	49
2.2. Construct generation and transfection into cells.....	49
2.3. Purification of secreted hexahistidine-tagged recombinant sAPP α and sAPP β	50
2.4. Preparation of whole cell lysates.	53
2.5. Biophysical analysis of recombinant purified sAPP α and sAPP β	53
2.6. Bicinchoninic acid (BCA) assay.	53
2.7. Sodium dodecyl sulphate polyacrylamide gel electrophoresis (SDS-PAGE).	53
2.8. Immunoblotting.....	54
2.9. Coomassie blue total protein gel stain.....	56
2.10. Bioinformatics.	56
2.11. The isolation of ligand-specific adhesion complexes using tosylactivated microbeads.	56
2.12. GeLC-MS/MS analysis.....	59
2.13. The differentiation of induced pluripotent stem cells into cortical neurons.	60
2.14. ROS assay.....	63
2.15. Assessing the binding of sAPP α to human cells through immunoblotting.	63
2.16. Assessing the binding of sAPP β to human cells through Mesoscale Discovery SH multiplex immunoassay.	63
2.17. siRNA knockdown of calyntenin-1, calyntenin-3 and GABABR1.....	63
2.18. RT-qPCR.	64
2.19. Immunofluorescence microscopy.	64
2.20. Detergent-free membrane enrichment.	65
2.21. Quartz Crystal Microbalance with Dissipation Monitoring.....	65
2.22. Statistics.....	67
3. The purification and biophysical characterisation of recombinant soluble amyloid precursor proteins alpha and beta	68
3.1. Introduction.....	68
3.1.1. Chapter aims.....	69

3.2. Generation of recombinant plasmids coding for sAPP α or sAPP β with N-terminal His-tags.	70
3.3. Expression and purification of recombinant his-tagged sAPP α and sAPP β	72
3.4. Immunoblot comparison of the purified sAPP α with commercial sAPP α	79
3.5. Biophysical analysis of lab purified sAPP α and sAPP β	79
3.6. Discussion.	82
3.6.1. Generation of HEK293 cell lines overexpressing N-terminal hexahistidine tagged sAPP α or sAPP β	82
3.6.2. IMAC-facilitated purification of hexahistidine tagged sAPP α and sAPP β	83
3.6.3. Comparison of lab-produced and commercially-acquired sAPP α	84
3.6.4. Biophysical analyses of sAPP α and sAPP β confirmed expected solubilities and lack of aggregation.	85
3.7. Chapter summary.	85
4. The binding and protective effects of soluble APP to neuronal cells.	87
4.1. Introduction.	87
4.1.1. Chapter aims.	89
4.2. The generation of iPSC-derived human neurons.	90
4.3. Investigation of the binding of purified sAPP α and sAPP β to iPSC-derived human cortical neurons.	93
4.4. Comparison of the effect of sAPP α and sAPP β on synaptic protein expression.	95
4.5. Demonstration of the binding of purified sAPP α and sAPP β to immortalised SH-SY5Y cells.	99
4.6. sAPP α reduced oxidative stress in SH-SY5Y cells.	103
4.7. Discussion.	107
4.7.1. The interaction between sAPP α , sAPP β and iPSC-derived human cortical neurons.	107
4.7.2. The interaction between sAPP α , sAPP β and SH-SY5Y neuroblastoma cells.	110
4.8. Chapter summary.	115
5. The unbiased identification of sAPP α and sAPP β binding partners.	116
5.1. Introduction.	116
5.1.1. Putative sAPP α and sAPP β receptors.	116
5.1.2. Microbead-based receptor identification methods.	117
5.1.3. QCM-D-based receptor identification methods.	118
5.1.4. Chapter aims.	119

5.2. The microbead-based identification of sAPP α and sAPP β binding partners.	120
5.3. The use of QCMD as an alternative method to identify sAPP α and sAPP β binding partners.	125
5.4. The investigation of calsyntenins 1 and 3 as potential novel binding partners for sAPP α	133
5.5 Discussion.	137
5.5.1. The use of microbead-based affinity isolation to identify novel binding partners for sAPP α	137
5.5.2. The use of QCM-D-facilitated isolation to pull-down novel binding partners for sAPP α	139
5.5.3. The functions of calsyntenin-1 and calsyntenin-3.....	141
5.5.4. The loss of calsyntenin-3, but not calsyntenin-1, may interfere with the binding of sAPP α to SH-SY5Y cells.	143
5.6. Chapter summary.....	145
6. Discussion.....	146
6.1. The generation of physiologically relevant sAPP α and sAPP β for use in downstream experiments.....	146
6.2. The development of an assay to quantify the binding of sAPP α and sAPP β to neuronal cells.....	149
6.3. sAPP α significantly reduced ROS production in SH-SY5Y cells.....	150
6.4. sAPP α significantly increased the expression of pre-synaptic markers in iPSC-derived neurons.....	151
6.5. The use of a novel unbiased pulldown method to identify sAPP α binding partners.	152
6.6. The novel use of QCM-D as an unbiased method to identify receptors for an immobilised ligand.	154
6.7. Calsyntenin-3 was required for the normal binding of sAPP α to SH-SHY5Y cells.....	155
6.8. The potential interaction between calsyntenin-3 and sAPP α	156
6.9. Concluding remarks.....	158
7. Supplementary Figures and Tables.....	160
8. References	177

Word count: 48,353

List of Figures

Figure 1.1. The neuropathological hallmarks of AD	18
Figure 1.2. The structure of the APP ₆₉₅ protein	23
Figure 1.3. The reciprocal processing of the amyloid precursor protein by α -secretase or β -secretase	26
Figure 1.4. Examples of mutations in APP which alter A β production	28
Figure 1.5. Linear representation of sAPP α ₆₉₅ domains and amino acid numberings	37
Figure 1.6. The sites of sAPP α that bind to different receptor candidates	45
Figure 2.1. The process for purifying hexahistidine-tagged recombinant sAPP α or sAPP β from complex cell medium through immobilised metal affinity chromatography (IMAC)	53
Figure 2.2. A summary of the protocol which facilitated the isolation of binding partners for specific ligands immobilised on the surface of tosylactivated microbeads	59
Figure 3.1. Amino acid sequence alignment of the N-terminal His-tagged sAPP α ₆₉₅ and sAPP β ₆₉₅ with APP ₆₉₅	68
Figure 3.2. The purification of N-terminal His-tagged recombinant human sAPP α and sAPP β	70
Figure 3.3. Characterisation of recombinant human sAPP α and sAPP β through immunoblotting	71
Figure 3.4. The protein purified from HEK-sAPP α cells was identified as APP through GeLC-MS/MS	73
Figure 3.5. Spectra identified from sAPP α purification excised bands	75
Figure 3.6. Immunoblot comparison of lab purified sAPP α with commercial sAPP α	76
Figure 3.7. Analysis of purified sAPP α and sAPP β using multi-angle light scattering	77
Figure 3.8 Analysis of purified sAPP α using analytical ultracentrifugation	78

Figure 4.1. Generation and characterisation of iPSC-derived human cortical neurons	88
Figure 4.2. Recombinant sAPP α and sAPP β bind to iPSC-derived human neurons ...	91
Figure 4.3. sAPP α significantly increased the expression of synaptophysin in certain hiPSC-derived neuron inductions	93
Figure 4.4. sAPP α did not increase the expression of VGLUT1 in hiPSC-derived neurons	94
Figure 4.5. sAPP α did not increase the expression of PSD95 in hiPSC-derived neurons	95
Figure 4.6. Recombinant sAPP α bound to SH-SY5Y cells, but binding was significantly reduced by denaturation	97
Figure 4.7. sAPP α binds to SH-SY5Y cells more readily than sAPP β	99
Figure 4.8. Menadione induces the significant production of H ₂ O ₂ in SH-SY5Y and SH-PrP cells in a concentration-dependent manner	101
Figure 4.9. Pre-incubation of sAPP α reduces ROS production in a time-dependent manner	102
Figure 5.1. Validation of the microbead-based isolation assay in SH-SY5Y cells	116
Figure 5.2. Schematic of GeLC-MS/MS workflow following the isolation of binding partners	118
Figure 5.3. Detergent-free membrane enrichment from SH-SY5Y cell lysates	121
Figure 5.4. The capture of prey proteins from membrane-enriched SH-SY5Y lysate using sAPP α and sAPP β as bait proteins by QCM-D	123
Figure 5.5. The capture of prey proteins from membrane-enriched NB7 cell fraction using sAPP α and sAPP β as bait proteins by QCM-D	124
Figure 5.6. Knockdown of GABABR1 did not significantly reduce the binding of sAPP α to SH-SY5Y cells	129
Figure 5.7. Knockdown of calsyntenin-1 did not reduce the binding of sAPP α to SH-SY5Y cells	130

Figure 5.8. Knockdown of calsyntenin-3 significantly reduced the binding of sAPP α to SH-SY5Y cells	131
--	-----

List of Tables

Table 1.1. A summary of the characteristics and effects of sAPP α in the published literature	44
Table 2.1. List of antibodies used in this thesis	56
Table 2.2. Composition of the cytoskeletal stabilising buffers used in the tosylactivated microbead pulldown	58
Table 2.3. Recipes for iPSC-derived human neuron cortical media	61
Table 3.1. Spectral counts for GeLC-MS/MS analysis of the protein purified from HEK-sAPP α cells	74
Table 5.1. Comparison of the characteristics of each tosylactivated pulldown	118
Table 5.2. The calsyntenin family of proteins were identified as sAPP α and sAPP β -specific binding partners in SH-SY5Y cells	119
Table 5.3. The calsyntenin family of proteins were identified as sAPP α and sAPP β -specific binding partners in SH-SY5Y cells and NB7 cells by QCM-D-based isolation	126
Table 5.4. The calsyntenin family of proteins were identified as sAPP α and sAPP β -specific binding partners in hiPSC-derived cortical neurons by QCM-D-based isolation	127

List of abbreviations

$\alpha 3$ -NKA: $\alpha 3$ -Na, K-ATPase.

A β : Amyloid beta.

A β Os: Amyloid beta oligomers.

AD: Alzheimer's disease.

ADAM10: A disintegrin and metalloproteinase domain-containing protein 10.

AICD: APP intracellular domain.

AMP: Anti-microbial peptide.

APLP1: APP-like protein 1.

APLP2: APP-like protein 2.

APOE: Apolipoprotein E.

APP: Amyloid precursor protein.

BACE1: β -site APP cleaving enzyme 1.

CLSTN1: Calsyntenin-1.

CLSTN3: Calsyntenin-3.

CSF: Cerebrospinal fluid.

CTF α : C-terminal fragment alpha.

CTF β : C-terminal fragment beta.

DMEM: Dulbecco's modified Eagle's medium.

DPBS: Dulbecco's phosphate-buffered saline.

DTBP: Dimethyl 3,3'-dithiobispropionimidate.

EMA: European Medicines Agency.

FDA: U.S. Food and Drug Administration.

GABA $_B$ R1a: γ -aminobutyric acid type B receptor subunit 1a.

GeLC-MS/MS: Gel electrophoresis followed by liquid chromatography-tandem mass spectrometry.

HEK: Human embryonic kidney cells.

IMAC: Immobilised Metal Affinity Chromatography.

iPSC: Induced pluripotent stem-cell.

JNK: c-Jun N-terminal kinase.

KPI: Kunitz-protease inhibitor.

LTP: Long term potentiation.

MCI: Mild cognitive impairment.

MSN: Medium spiny neuron.

NICE: UK National Institute for Health and Care Excellence.

NMDA: N-methyl-D-aspartate.

p⁷⁵NTR: p75 neurotrophin receptor.

PCR: Polymerase chain reaction.

PI3K: Phosphoinositide 3-kinase.

RNS: Reactive nitrogen species.

ROS: Reactive oxygen species.

RT: Room temperature.

sAPP α : Soluble amyloid precursor protein alpha.

sAPP β : Soluble amyloid precursor protein beta.

SDS-PAGE: Sodium dodecyl sulphate-polyacrylamide gel electrophoresis.

SGL: Subgranular layer.

SNX17: Sorting nexin 17.

SOD: Superoxide dismutase.

SORLA: Sorting protein related receptor A.

SVZ: Subventricular zone.

QCM-D: Quartz crystal microbalance with dissipation monitoring.

X11L: X11-like protein.

Abstract

'Dementia and Alzheimer's disease' is the leading cause of death in the UK, so new therapeutic options are of critical importance. One possible therapeutic avenue could be to protect neurons from damage through the use of neuroprotective molecules. The initial cleavage of the amyloid precursor protein (APP) by either α - or β -secretase produces the soluble amyloid precursor protein alpha (sAPP α) or beta (sAPP β) fragments, respectively. sAPP α binds to neuronal cells in a receptor-dependent manner and is 100-times more neuroprotective than sAPP β , despite differing by just 16 amino acids at their C-termini. The receptor(s) to which sAPP α binds to facilitate neuroprotection are unknown. Therefore, the identification of new binding partners for sAPP α could have therapeutic relevance. This thesis used two unbiased receptor identification methods to identify sAPP α binding partners in neuronal cells.

HEK cell lines stably overexpressing His-tagged sAPP α and sAPP β were generated. Both recombinant proteins were purified and their identities were confirmed through immunoblotting and GeLC-MS/MS. sAPP α and sAPP β were shown to bind to induced pluripotent stem cell (iPSC)-derived neurons and SH-SY5Y cells. sAPP α increased the expression of synaptophysin in iPSC-derived neurons. Pre-treatment of SH-SY5Y cells with sAPP α significantly reduced the production of reactive oxygen species following toxic insult in a time-dependent manner. Calsyntenin-1 and calsyntenin-3, type-I transmembrane proteins expressed on the post-synaptic membrane of neurons, were identified in both unbiased receptor identification methods as novel binding partners for sAPP α . Knockdown of calsyntenin-1 did not affect the binding of sAPP α to SH-SY5Y cells; however, knockdown of calsyntenin-3 significantly reduced the binding of sAPP α to SH-SY5Y cells.

Overall, the work described in this thesis demonstrated the beneficial effects of sAPP α to reduce oxidative stress in neuronal cells *in vitro* and identified calsyntenin-3 as a novel binding partner which was required for the binding of sAPP α to neuronal cells. The identification of calsyntenin-1 and calsyntenin-3 as neuronal binding partners for sAPP α may provide new therapeutic targets for neurodegenerative diseases such as Alzheimer's disease.

Declaration

No portion of the work referred to in this thesis has been submitted in support of an application for another degree or qualification of this or any other university or other institute of learning.

Copyright statement

- i. The author of this thesis (including any appendices and/or schedules to this thesis) owns certain copyright or related rights in it (the “Copyright”) and they have given the University of Manchester certain rights to use such Copyright, including for administrative purposes.
- ii. Copies of this thesis, either in full or in extracts and whether in hard or electronic copy, may be made only in accordance with the Copyright, Designs and Patents Act 1988 (as amended) and regulations issued under it or, where appropriate, in accordance with licensing agreements which the University has from time to time. This page must form part of any such copies made.
- iii. The ownership of certain Copyright, patents, designs, trademarks and other intellectual property (the “Intellectual Property”) and any reproductions of copyright works in the thesis, for example graphs and Tables (“Reproductions”), which may be described in this thesis, may not be owned by the author and may be owned by third parties. Such Intellectual Property and Reproductions cannot and must not be made available for use without the prior written permission of the owner(s) of the relevant Intellectual Property and/or Reproductions.
- iv. Further information on the conditions under which disclosure, publication and commercialisation of this thesis, the Copyright and any Intellectual Property and/or Reproductions described in it may take place is available in the University IP Policy (see <http://documents.manchester.ac.uk/DocuInfo.aspx?DocID=2442> 0), in any relevant Thesis restriction declarations deposited in the University Library, the University Library’s regulations (see <http://www.library.manchester.ac.uk/about/regulations/>) and in the University’s policy on Presentation of Theses.

Acknowledgements

I would like to acknowledge and sincerely thank my primary supervisor Prof. Nigel Hooper, who guided me throughout the PhD process and helped push me to create the best PhD project I could. In addition, my sincere thanks to my co-supervisor Prof. Martin Humphries for his fantastic support and advice throughout.

I would like to thank everyone at the University of Manchester, past and present, for their help and for making this PhD an amazing experience. In particular, my thanks to the Hooper lab for being such a brilliant and supportive group. A huge thank you to Dr. Kate Fisher for her constant help, support and for our laughs together. I will miss our chats across the lab bench! My great thanks to Dr. Katherine Kellett, who was always there to help and taught me so many of the things I relied on throughout my PhD. My sincere thanks to Dr. Jon Humphries, who facilitated the receptor identification work, guided me so helpfully and was a great laugh. My huge thanks to Dr. Monica Seif, Dr. Kelsey Hanson, Dr. Nishtha Chandra, Alex Neve, Marlene Polleres, Dr. Geoff Potjewyd, Ernesto Zarate Aldrete, Dr. Sam Moxon, Dr. David Hicks and Dr. Sarah Ryan for their help and support throughout. Thanks to Dr. Tom Jowitt for performing the QCM-D experiments and thanks to Emma Jayne Keevil for her help with the mass spectrometry work.

Thank you to the MRC and, in particular, my sincere thanks to John and Janet Hartley, who made this PhD possible. It was an absolute pleasure to meet you and I hope to see you again soon. Thank you for your incredible support throughout, and for your support after the pandemic interrupted my progress. Please let me know if you are ever nearby, as I hope to see you again soon.

I would also like to thank my parents Alan and Eileen for their constant support, motivation and help throughout my PhD and my entire life. I would never have got to this stage without you. Thank you to my sister Hannah, who was always there with help, advice and to bring a smile to my face. Thanks to my brother-in-law Paul, a great friend and a great scientist who was always there for me. His stag do was a fantastic and memorable break from my final lab-work crunch. Thanks to my sister Sinead, her partner Ste, and little Cillian who has brought so much joy into all our lives. Becoming an uncle is a true highlight of my life! I would also like to thank Noreen Twomey and Kathleen Twomey, two amazing Irish inspirations who I carry with me everywhere and always.

Finally, I would like to acknowledge and thank my wife Freya, who's love and support I treasure. She was always there for me whenever I needed her and understood everything I went through, studying for her own PhD at the same time. Freya was always there to celebrate the highs and to pick me up when I was down. I can't wait spend the rest of our lives together as one big adventure.

Thank you.

1. Introduction

1.1. An introduction to dementia

Dementia is an umbrella term for a neurological condition which is characterised by progressive memory loss and reduced cognitive ability (Gauthier et al. 2021). Dementia often also presents with psychiatric conditions such as depression and delusion (Gauthier et al. 2021). There are many overlapping causes of dementia, each with different symptoms (Hyman et al. 2012). Although over 50 million people have been diagnosed with dementia globally, an estimated 75% of cases remain undiagnosed (Gauthier et al. 2021). The global prevalence of dementia is expected to triple by 2050, making it one of the greatest health challenges of our time (Gauthier et al. 2021). In the UK in 2013, approximately 1 in 14 of over 65s had dementia (Prince et al. 2014) and in September 2022, 'Dementia and Alzheimer's disease' had been the leading cause of death in the UK for 15 consecutive months (ONS 2022). Dementia places a huge burden, both economically and emotionally, on a patient's family, friends as well as national health services. In the United States in 2015, it was estimated that the presence of dementia added \$180,000 onto caring costs for a single patient across their lifetime (Jutkowitz et al. 2017). In addition, an estimated 86% of this extra cost was covered by unpaid carers (Jutkowitz et al. 2017). In England in 2015, dementia cost an estimated £24.2 billion annually, with 42% being covered by unpaid carers (Wittenberg et al. 2019). Social care costs from dementia were estimated to be three times greater than healthcare costs (Wittenberg et al. 2019). The costs associated with dementia increase significantly with disease severity, indicating that treatments to slow the onset or progression of dementia would significantly reduce care costs as well as being incredibly beneficial for the patient and their family (Wittenberg et al. 2019).

Age is the largest single risk factor for dementia and a major cause of the increase in global dementia prevalence is the globally ageing population (Gauthier et al. 2021). The strong link between age and dementia suggests that an accumulation of cellular damage over time, through mechanisms such as oxidative damage, likely plays a large role in neurodegeneration and dementia (Huang et al. 2016). The estimated survival time from dementia diagnosis depends on several factors. The overall estimated median survival time for patients over 65 who were diagnosed with dementia was 4.5 years, though this varied largely with factors like age of onset and co-morbidities (Xie et al. 2008). The median survival from patients diagnosed

between 65-69 was 10.5 years, down to just 3.8 years for patients diagnosed over 90 years (Xie et al. 2008).

A common misconception is that dementia is a natural part of ageing. In reality, dementia is caused by underlying neurodegenerative diseases, such as Alzheimer's disease (AD), dementia with Lewy bodies, vascular dementia, Parkinson's disease or a combination of several such diseases (WHO 2017). Multiple pathologies can overlap within the brain of a single dementia patient, complicating diagnosis and treatment (Arvanitakis et al. 2019). A definitive diagnosis of the underlying cause of dementia is often only possible post-mortem, leading to a high level of mis-diagnosis which could impact the efficacy of different treatments (Selvackadunco et al. 2019). In fact, Selvackadunco *et al.* (2019) found that 36% of dementia cases had a different post-mortem neuropathological diagnosis to their original clinical diagnosis (Selvackadunco et al. 2019). Therefore, not only new treatments but also new diagnostic tools are required to increase the efficacy of dementia therapies.

Dementia is preceded by an initial state of mental deterioration called mild cognitive impairment (MCI) (Roberts and Knopman 2013). However, not all MCI patients progress to dementia, and it is possible for MCI patients to return to normal cognitive ability. In one study, 16% of MCI patients returned to normal cognition within one year of initial MCI diagnosis, whilst 20% progressed to dementia (Roberts and Knopman 2013). The remaining patients had stable MCI during that one-year period (Roberts and Knopman 2013). The diagnostic term 'MCI' covers a broad spectrum of cognitive impairments, which could help to explain the variable progression rates to dementia (Roberts and Knopman 2013). However, patients that had previously recovered from MCI were significantly more likely to develop dementia in future (Roberts et al. 2014).

1.2. Alzheimer's disease

Alzheimer's disease is the most common cause of dementia, causing an estimated 60-70% of all cases (WHO 2017). In 2014, over 500,000 people were living with AD in the UK (Bature et al. 2017). Over 95% of AD cases occur over the age of 65 and these cases are termed 'sporadic' or 'late-onset' AD (Bature et al. 2017). Cases of AD which develop under the age of 65 are termed 'familial' or 'early-onset' and are likely to have an inherited genetic cause (Bature et al. 2017). Due to a lack of definitive laboratory tests or biomarkers to aid in clinical diagnosis, doctors often use mental tests to measure cognitive ability (Gauthier et al. 2021). Different

versions of the mini-mental state examination (MMSE) represent some of the most common diagnostic tools used (Folstein et al. 1975). The MMSE measures several areas of cognition through a variety of questions and tests to confirm cognitive impairment and to determine likely causes (Baek et al. 2016). The gold-standard for the definitive diagnosis of AD is through the post-mortem histological analysis of patient brain tissue to identify the neuropathological hallmarks of the disease (Figure 1.1), but intense research is ongoing in order to identify novel biomarkers and diagnostic methods in living patients (Karantzoulis and Galvin 2011; Selvackadunco et al. 2019). A number of blood-based biomarkers are currently in development to aid in early AD diagnosis, but none are regularly used clinically at this time (Teunissen et al. 2022).

1.2.1. The neuropathology of Alzheimer's disease

AD has two distinct pathological hallmarks which were first characterised by Dr. Alois Alzheimer and Oskar Fischer in 1907 (Figure 1.1) (Alzheimer 1907; Fischer 1907). During post-mortem analysis of a patient with progressively degenerating dementia, Dr. Alzheimer identified extracellular amyloid plaques and intracellular tangles in the patient's brain tissue (Alzheimer 1907; Stelzmann et al. 1995). Oskar Fischer also found similar extracellular 'neuritic plaques' in the brains of 12 patients out of 16 who died with senile dementia (Fischer 1907). In 1984, the protein responsible for forming the extracellular amyloid plaques was identified as amyloid- β (A β) (Glenner and Wong 1984). Two years later, the microtubule-associated protein tau was found to be the key component of the intracellular neurofibrillary tangles (Grundke-Iqbal et al. 1986).

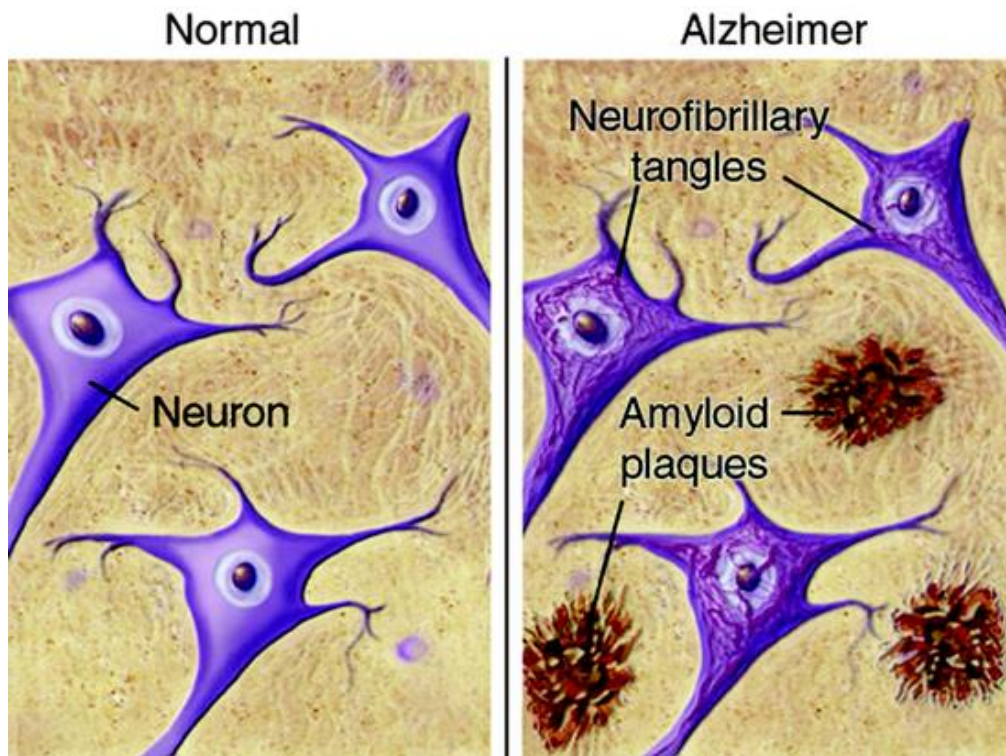


Figure 1.1. The neuropathological hallmarks of AD.

A healthy neuronal environment (left), contrasted with the neuropathology of Alzheimer's disease consisting of extracellular amyloid plaques and intracellular neurofibrillary tangles (right).

Figure reproduced without changes from Silbert 2007, with permission. Does statin use decrease the amount of Alzheimer disease pathology in the brain? Lisa C. Silbert
Neurology Aug 2007, 69 (9) E8-E11; DOI: 10.1212/01.wnl.0000280585.95661.1b. Available at: <https://n.neurology.org/content/69/9/E8>.

1.2.1. Hyperphosphorylated tau

Intracellular neurofibrillary tangles, present within neuronal cells in AD brains, are primarily composed of straight and paired helical filaments of hyperphosphorylated tau protein (Iqbal et al. 2010). The gene for tau is located on chromosome 17 and six human isoforms are produced through alternative splicing (Iqbal et al. 2010). The normal physiological function of tau is to promote and stabilise the assembly of tubulin into microtubules (Iqbal et al. 2010) and its activity is regulated by its phosphorylation state (Lindwall and Cole 1984). The phosphorylation of tau at different sites along the protein induces different effects on tau

activity; generally, an increase in phosphorylation reduces the microtubule-binding activity of tau and promotes self-aggregation (Gong and Iqbal 2008; Iqbal et al. 2010; Lindwall and Cole 1984). Consistent with this, the tau isolated from the aggregated neurofibrillary tangles of AD brains is up to four times more phosphorylated than from non-demented control brains (Gong and Iqbal 2008). As tau knockout mice are viable and have subtle deficits, such as muscle weakness and hyperactivity, the contribution of tau to AD is more likely to be a toxic gain-of-function resulting from its aggregation into tangles rather than a loss-of-function with regards to tau's role in microtubule regulation (Ikegami et al. 2000). Though certain types of dementia are caused by mutations in the tau gene, such as frontotemporal dementia with parkinsonism linked to chromosome 17 (Hutton et al. 1998), no mutations in tau have been shown to cause familial AD (Busche and Hyman 2020). Therefore, tau is not generally believed to be the primary cause of AD, though this is under constant debate (Busche and Hyman 2020). In contrast, there are strong genetic links between A β and AD, suggesting that A β is the initiator of the disease (Busche and Hyman 2020).

1.2.2. The normal physiological function of amyloid- β

A β is a 4.5 kDa protein derived from the amyloid precursor protein (APP), a larger protein of around 80 kDa (depending on the isoform) (Goldgaber et al. 1987; Kang et al. 1987; Robakis et al. 1987; Tanzi et al. 1987). A β exists in several isoforms of different lengths, but the most clinically relevant are A β_{40} and A β_{42} which consist of 40 and 42 amino acids, respectively (Jarrett et al. 1993). A β_{40} was shown to be required for neuronal viability and at low concentrations of around 0.1 nM A β had a neurotrophic effect on hippocampal neurons (Plant et al. 2003; Yankner et al. 1990). However, higher A β concentrations of over 100 nM were neurotoxic to hippocampal neurons (Yankner et al. 1990). Both the neurotrophic and neurotoxic effects were mapped to amino acids 25-35 of the A β protein (Yankner et al. 1990). These data suggested that A β has vital functions in normal physiology, but its accumulation over time or overproduction may lead to AD. The normal physiological function of A β is still emerging, though recent studies have shown it may function as an antimicrobial peptide (AMP) (Eimer et al. 2018; Kumar et al. 2016; Soscia et al. 2010). A β peptides undergo oligomerisation and fibrilisation which, although seen as detrimental in AD, was critical for the anti-microbial activity of A β against bacterial infections (Kumar et al. 2016). Synthetic A β_{40} and A β_{42} both had equivalent or greater antimicrobial activity against 7 of 12 tested

pathogens than LL-37, a known AMP (Soscia et al. 2010). In addition, AD human temporal lobe brain homogenates containing A β inhibited the growth of *Candida albicans* significantly more than control human temporal lobe brain tissue (Soscia et al. 2010). This effect was not seen with cerebellum brain tissue from the same AD patients, which typically has a lower A β load than the temporal lobe in AD (Soscia et al. 2010). Strikingly, immunodepletion of A β from the temporal lobe tissue samples removed the antimicrobial effect of the homogenates against *C. albicans* (Soscia et al. 2010). Synthetic A β_{42} had greater antimicrobial activity than synthetic A β_{40} against six of seven microorganisms, likely reflecting its increased aggregative ability (Soscia et al. 2010). Neither scrambled nor reverse A β_{42} exhibited any anti-microbial activity (Soscia et al. 2010). Thus, there is strong and growing evidence that A β may have important anti-microbial functions in the human brain (Soscia et al. 2010; Tharp and Sarkar 2013). Homologues of A β , the amyloid precursor protein it derives from and the β -secretase enzyme which produces it are conserved across vertebrates, suggesting functional importance (Tharp and Sarkar 2013). Intriguingly, several known amyloidoses are also caused by the deposition of amyloidogenic anti-microbial peptides, such as the aggregation of lactoferrin in corneal amyloidosis (Ando et al. 2002). Thus, it has been suggested that AD may actually be another AMP-derived amyloidosis (Kumar et al. 2016).

1.2.3. A β in Alzheimer's disease

Genetic evidence (explored further in Section 1.4) pointed to A β , rather than tau, as the primary cause of AD and led to the prominent amyloid cascade hypothesis (Hardy and Higgins 1992). The amyloid cascade hypothesis suggested that A β initiates a cascade of damaging processes which lead to neurodegeneration in AD (Hardy and Higgins 1992). *In vitro* studies have confirmed the neurotoxic effects of A β (Selkoe and Hardy 2016). Familial AD was also linked to mutations affecting the production of A β (Section 1.4), whereas no familial AD cases have been identified as being caused by mutations in tau (Murphy and LeVine 2010). Therefore, the majority of clinical trials have targeted A β in order to treat AD (Cummings et al. 2014).

The most prevalent and pathologically relevant forms of A β , A β_{40} and A β_{42} , vary at their C-termini, with A β_{40} being more prevalent but A β_{42} being more neurotoxic, aggregation prone and pathologically relevant (Iwatsubo et al. 1994; Jarrett et al. 1993). A β_{42} may nucleate the formation of new oligomers which the more abundant, but less amyloidogenic, A β_{40} can

aggregate onto, leading first to protofibrils and then to mature senile plaques (Iwatsubo et al. 1994). As such, an increase in the ratio of A β ₄₂ relative to A β ₄₀ is detrimental, demonstrated by genetic evidence showing that mutations which increase A β ₄₂ production are responsible for familial AD, such as the 'London' mutation (V642I, APP₆₉₅ numbering) (Section 1.4) (Bekris et al. 2010; Goate et al. 1991).

A β can aggregate into structures of many different sizes and solubilities, but the most toxic form of human A β is suggested to be the small, soluble, oligomeric form of the protein (Goure et al. 2014). A β oligomers exist as an intermediate structural form of the protein between the production of the monomer and its aggregation into the larger insoluble fibrils found in senile plaques (Goure et al. 2014). The exact definition of 'oligomeric' A β is variable between studies, but one review defined them as conformationally different from fibrils and consisting of at least a trimer of A β molecules (Sengupta et al. 2016). Oligomeric A β can damage neuronal cells in several ways. For example, oligomeric A β activated c-Jun N-terminal kinase (JNK), a kinase which phosphorylates tau, resulting in increased tau phosphorylation in human cells and in mice (Ferrari et al. 2003; Götz et al. 2001; Ma et al. 2009). Furthermore, A β stimulated the degradation of insulin receptor substrate-1, reducing insulin signalling and glucose metabolism in the brain, which are both characteristic of AD (Ma et al. 2009). A β oligomers (A β O) also inhibited the proteasome *in vitro* and *in vivo*, potentially exacerbating the aggregation of amyloid plaques and tau neurofibrillary tangles due to impaired protein degradation (Tseng et al. 2008). Soluble A β O may also facilitate the spread of amyloid throughout the brain (Sengupta et al. 2016). As certain A β O-mediated effects appear to be reversible upon oligomer removal, the aggregation of the oligomeric forms of A β into larger insoluble senile plaques could be a cellular defence mechanism to precipitate the most toxic, soluble oligomeric form of A β (Tanokashira et al. 2017). Interestingly, only humans, monkeys and apes appear to produce amyloidogenic A β or develop AD and, though mouse models are commonly used to study AD, wild-type mouse A β and tau proteins do not appear to readily aggregate to form plaques or neurofibrillary tangles in the same way, due to differences in their protein sequences (Drummond and Wisniewski 2017; Nitsche et al. 2021). Therefore, AD mouse models were generated to express human forms of the proteins (Drummond and Wisniewski 2017).

1.3. The amyloid precursor protein

A β is produced from a larger precursor protein called the amyloid precursor protein, or APP. APP is a type-I membrane protein that is expressed in a wide range of tissues, but it has gained particular attention for its role in neuronal cells as the precursor of A β (Selkoe et al. 1988). APP belongs to a family of homologous proteins in humans: APP, APP-like protein 1 (APLP1) and APP-like protein 2 (APLP2) (Tan and Gleeson 2019a). However, A β is only produced from the APP protein itself (Tan and Gleeson 2019a). The APP gene family is conserved across species, with *Drosophila* and *C. elegans* expressing the APP-related genes *APPL* and *APL-1* respectively (Daigle and Li 1993; Luo et al. 1990; Rosen et al. 1989).

The three major isoforms of APP are produced through the alternative splicing of exon 7, which codes for a Kunitz-protease inhibitor (KPI) domain, and exon 8, which includes an OX-2 homology sequence (Cappai 2014). The three isoforms are APP₆₉₅, which lacks both exons 7 and 8, APP₇₅₁, which lacks exon 8, and APP₇₇₀, which expresses all exons (Cappai 2014). APP₆₉₅ is the dominant neuronal isoform, whereas APP₇₅₁ and APP₇₇₀ are expressed to a greater degree in most other tissues (Kang and Müller-Hill 1990). APP has two rigidly folded extracellular domains, denoted E1 and E2, which are joined together by a flexible acidic domain (Figure 1.2) (Coburger et al. 2013). A flexible juxtamembrane region joins the E2 domain to the single-pass transmembrane helix followed by the APP intracellular domain (AICD) (Figure 1.2) (Coburger et al. 2013).

Knockout of APP alone did not cause a significant reduction in mouse viability or fertility, likely due to functional compensation by similar proteins such as APLP1 and APLP2; however, APP^{-/-} mice weighed around 20% less than wild-type mice (Zheng et al. 1995). APP knockout also impaired spatial learning (Müller et al. 1994), impaired long-term potentiation (Dawson et al. 1999), reduced hippocampal synaptic markers such as synaptophysin and MAP2 (Dawson et al. 1999; Seabrook et al. 1999), significantly elevated cerebral cortex copper levels (White et al. 1999) and increased hippocampal gliosis (Seabrook et al. 1999).

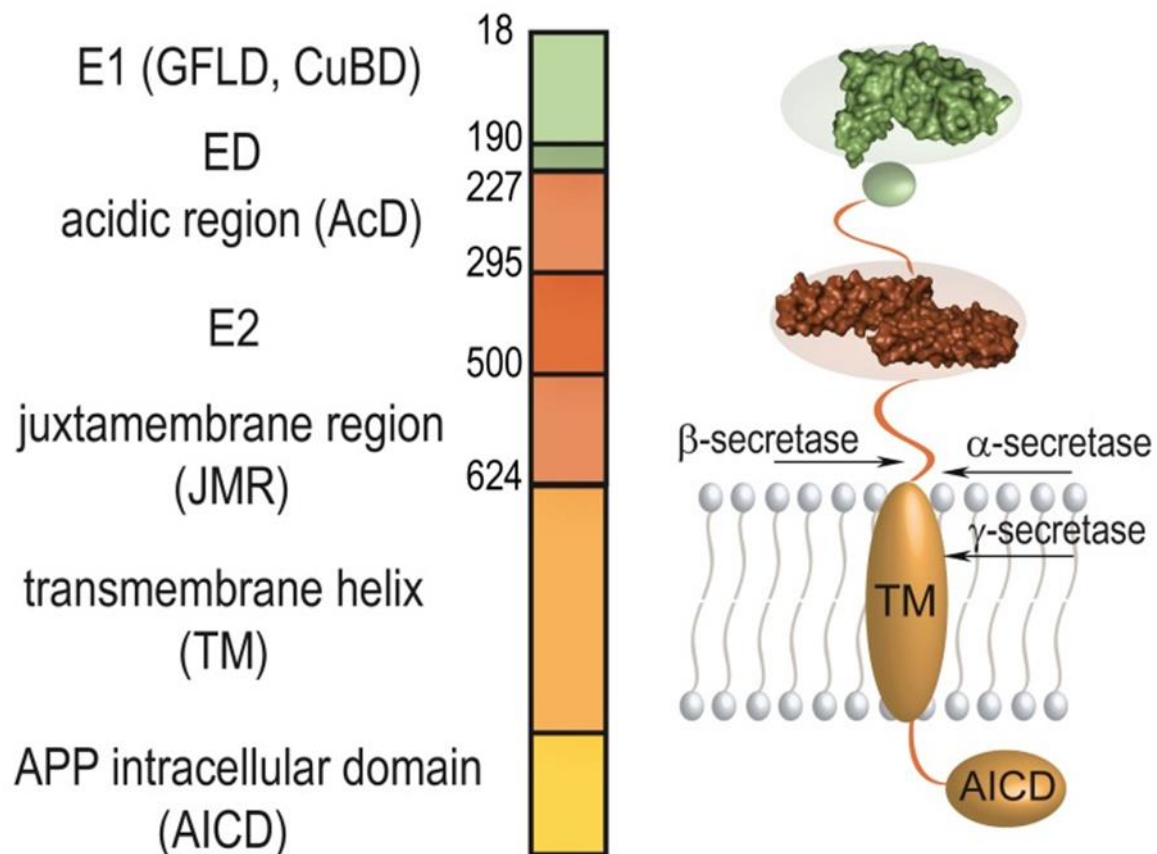


Figure 1.2. The structure of the APP₆₉₅ protein.

A linear and 3D representation of the amyloid precursor protein.

E1 = E1 domain of APP; GFLD = growth factor like domain; CuBD = copper binding domain; ED = extension domain; E2 = E2 domain of APP.

Figure adapted from PLOS ONE Coburger et al. 2013 with permissions under the CC BY 3.0 license, copyright 2013 (available at: <https://creativecommons.org/licenses/by/3.0/>).

Following its production, APP is transported to the plasma membrane where around 30% is cleaved by enzymes such as α -secretase within 10-20 minutes (Koo et al. 1996). Over half of cell surface APP may be endocytosed within 10 minutes and sorted into early endosomes (Koo et al. 1996), though other studies have suggested that 50% APP turnover from the cell surface requires around 60 minutes (Ring et al. 2007). Following endocytosis, a small amount of APP is recycled back to the plasma membrane from intracellular vesicles, but the majority of the remaining APP molecules are degraded inside lysosomes within 30 minutes (Kinoshita et al. 2003). APP has a cellular half-life of 30 minutes to one hour but one study suggested the

existence of separate, more stable pools of APP which are regulated differently and can remain at the cell surface for longer periods (Storey et al. 1999).

Post-translational modifications can affect protein stability, folding and activity (Ramazi and Zahiri 2021). APP undergoes several post-translational modifications such as phosphorylation (at sites such as Ser₁₉₈ and Ser₂₀₆) and O-glycosylation (at sites such as Thr₂₉₁ and Thr₂₉₂ and Thr₅₇₆), as well as N-glycosylation and sulphation (Perdivara et al. 2009). In particular, the O-glycosylation of Tyr₆₀₆, a site at the C-terminus of sAPP α and which is not present in sAPP β , could affect protein stability and receptor interaction (Halim et al. 2011; Madsen et al. 2020).

1.3.1. The reciprocal proteolytic processing of APP

APP can be cleaved in an amyloidogenic fashion by the β -secretase beta-site APP cleaving enzyme 1 (BACE1) between Met₅₉₆ and Asp₅₉₇ (APP₆₉₅ numbering) to generate soluble amyloid precursor protein beta (sAPP β) (Figure 1.3) (Kimura et al. 2016; Vassar et al. 1999). The function of sAPP β has not been extensively studied or characterised. One study suggested that the production of sAPP β is promoted by a scarcity of trophic factors, following which sAPP β is further cleaved by an unknown mechanism (Nikolaev et al. 2009). This led to an enhanced interaction between the N-terminal fragment of sAPP β and death receptor 6 (DR6), activating both caspase-3 and caspase-6 and leading to neurodegeneration (Nikolaev et al. 2009). Though this process may be beneficial during healthy development, it may become aberrantly activated during AD and promote neurodegeneration (Nikolaev et al. 2009). Following cleavage by BACE1, sAPP β is released extracellularly and the remaining membrane-bound Section, CTF β , can be cleaved by γ -secretase to generate A β (Figure 1.3) (Vassar et al. 1999). The γ -secretase complex is composed of nicastrin, pen-2, aph-1 and presenilin 1 or 2 (Edbauer et al. 2003; Kimberly et al. 2003). Mutations in presenilin, particularly presenilin 1, are the most common cause of familial AD (Zhang et al. 2011). Cleavage by BACE1 takes place optimally at an acidic pH of around 4.5 and occurs predominantly within intracellular compartments such as early endosomes and the trans-Golgi network (Kinoshita et al. 2003; Tan and Gleeson 2019a; Vassar et al. 1999). Within endosomal membranes, BACE1 localises to lipid rafts which are enriched in sphingolipids and cholesterol (Ehehalt et al. 2003; Yoon et al. 2007). BACE1 cleaves APP predominantly within lipid rafts at membranes, as a depletion of cholesterol significantly reduced A β (Ehehalt et al. 2003). Inhibition of endocytosis was also

shown to significantly reduce A β generation, demonstrating that BACE1 cleavage occurs predominantly intracellularly (Ehehalt et al. 2003).

A different, reciprocal pathway can result in APP being cleaved in a non-amyloidogenic fashion by the α -secretase 'a disintegrin and metalloproteinase domain-containing protein 10' (ADAM10) (Kuhn et al. 2010). ADAM10 cleaves APP between Lys₆₈₇ and Leu₆₈₈ (APP₆₉₅ numbering), between Lys₁₆ and Leu₁₇ of the A β sequence, which prevents the subsequent formation of A β (Kimura et al. 2016). The cleavage of APP by ADAM10 releases soluble amyloid precursor protein alpha (sAPP α) (Figure 1.3), a neuroprotective and neurotrophic protein explored in greater detail in Section 1.7. The remaining membrane-bound Section, CTF α , can then be cleaved by γ -secretase to generate the p3 protein (Figure 1.3) (Kuhn et al. 2010). The cleavage of APP by the non-amyloidogenic α -secretase is believed to occur predominantly at the plasma membrane (Parvathy et al. 1999). However, other studies have indicated that α -secretase may also compete with β -secretase for the cleavage of APP within the trans-Golgi network (Skovronsky et al. 2000; Tan and Gleeson 2019b). Nevertheless, the generally accepted view is that the α -secretase cleavage of APP occurs predominantly at the cell surface and the β -secretase cleavage of APP, which produces A β , occurs within intracellular vesicles such as early endosomes (Parvathy et al. 1999; Rajendran et al. 2006; Vassar et al. 1999; Zhang and Song 2013). As such, beneficial chaperone proteins have been identified which bind to APP to reduce BACE1 cleavage whilst APP is shuttled intracellularly (Araki et al. 2003). For example, the formation of an intracellular tripartite complex of X11-like protein (X11L), calsynenin-1 and APP significantly reduced A β ₄₀ production because of suppressed BACE1 cleavage (Araki et al. 2003).

The endocytosis of APP from the cell surface occurs through the binding of its C-terminal intracellular domain to endocytic adaptor proteins such as disabled-2 (Dab-2) and sorting nexin 17 (SNX17) (Lee et al. 2008). As such, overexpression of Dab-2 significantly increased APP endocytosis and significantly increased both A β ₄₀ and A β ₄₂ secretion (Lee et al. 2008). Dynamin is another protein involved in the endocytosis of cell surface proteins into clathrin-coated vesicles (Carey et al. 2005). HEK cells deficient in active dynamin had more cell surface APP and released significantly more sAPP α than wild-type HEK cells (Carey et al. 2005). A deficiency of dynamin also significantly decreased A β ₄₀ secretion (Carey et al. 2005). The importance of APP compartmentalisation is exemplified by the Arctic mutation (E693G),

which reduces cell surface APP by approximately 60% and causes familial AD (Sahlin et al. 2007). The change in APP localisation is likely responsible for the significant decrease in sAPP α and subsequent increase in A β in cells harbouring the Arctic mutation, as more APP molecules are available for intracellular BACE1 cleavage (Sahlin et al. 2007). In mouse models, deletion of the 15 amino acids containing the APP C-terminal YENPTY endocytic consensus sequence resulted in approximately 2.5 times higher APP cell surface expression and significantly reduced A β_{40} and A β_{42} levels *in vivo* (Ring et al. 2007). Therefore, an imbalance in the sub-cellular location of APP could promote the increased production of A β and contribute to AD pathogenesis.

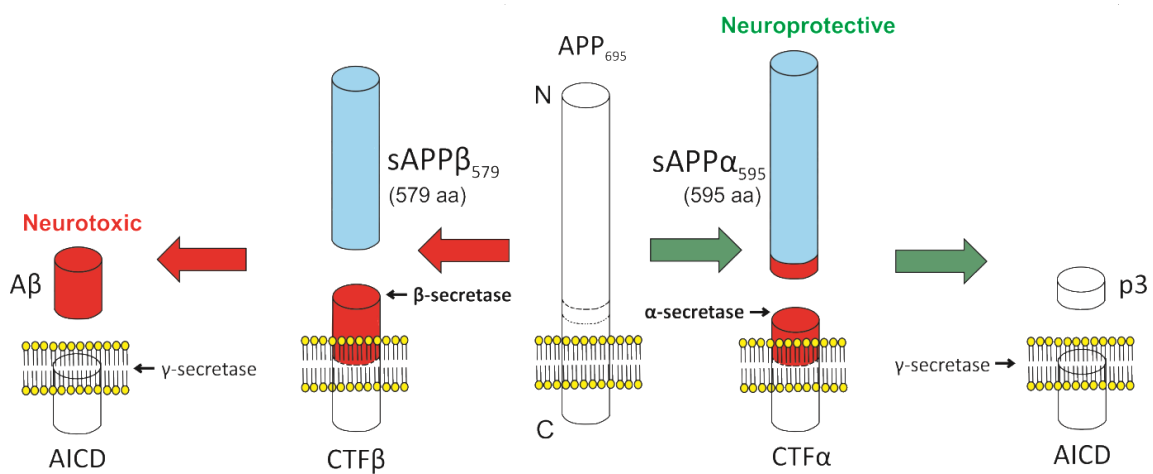


Figure 1.3. The reciprocal processing of the amyloid precursor protein by α -secretase or β -secretase.

APP can be cleaved either by the β -secretase BACE1 (red arrows) or by the α -secretase ADAM10 (green arrows) in a reciprocal cleavage pathway. Cleavage by ADAM10 produces soluble amyloid precursor protein alpha (sAPP α), a neuroprotective protein, and CTF α . CTF α can be further cleaved by γ -secretase to produce the p3 protein. Alternatively, APP can be cleaved by BACE1 to produce soluble amyloid precursor protein beta (sAPP β) and CTF β . CTF β can be further cleaved by γ -secretase to produce the neurotoxic A β protein (sequence highlighted in red), which is heavily implicated in AD.

1.4. Causes and risk factors of AD.

Less than 5% of cases of AD are classed as 'early-onset' and occur before the age of 65 (Bekris et al. 2010). Early-onset AD can also be called 'familial' AD, as it is often caused by autosomal

dominant heritable mutations which can help give insight into the mechanisms causing AD (Bekris et al. 2010). Mutations in *PSEN1*, a critical subunit of the γ -secretase which produces A β , are responsible for up to 80% of familial AD cases (Sun et al. 2017). Mutations in *PSEN2*, another component of the γ -secretase complex, cause around 5% of familial AD cases (Sun et al. 2017). These *PSEN* mutations primarily change the cleavage of APP so that either more amyloidogenic A β_{42} is produced relative to A β_{40} , or more total A β is produced (Bekris et al. 2010). Mutations in the *APP* gene itself also cause familial AD (Figure 1.4): the ‘Swedish’ mutation (K595N, M596L, APP₆₉₅ numbering) increases total A β production, whilst the ‘London’ mutation (V642I, APP₆₉₅ numbering) increases the ratio of A β_{42} relative to A β_{40} (Bekris et al. 2010; Goate et al. 1991; MacLeod et al. 2015; Mullan et al. 1992; Sun et al. 2017). Patients with Down syndrome, trisomy of chromosome 21, have an approximate 80% risk of developing early-onset AD (McCarron et al. 2014). This is likely due to an increased amount of A β , a cleavage product of the APP protein which is coded for by a gene on chromosome 21 (Bekris et al. 2010). Protective mutations also give insight into the mechanisms and main causes of AD. The ‘Icelandic’ mutation (A598T, APP₆₉₅ numbering) significantly reduces the β -secretase cleavage of APP, reducing A β_{40} and A β_{42} production by 40% and significantly protecting against AD (Figure 1.4) (Jonsson et al. 2012). Though these data suggest a clear causal link between A β and familial AD, it appears to be much more complicated in sporadic AD. Healthy non-demented individuals have been found with abundant brain amyloid- β deposition (Katzman et al. 1988), whilst many clinical trials targeting the production or clearance of A β have failed (Section 1.6). So, the exact causes and mechanisms behind sporadic AD remain unclear.

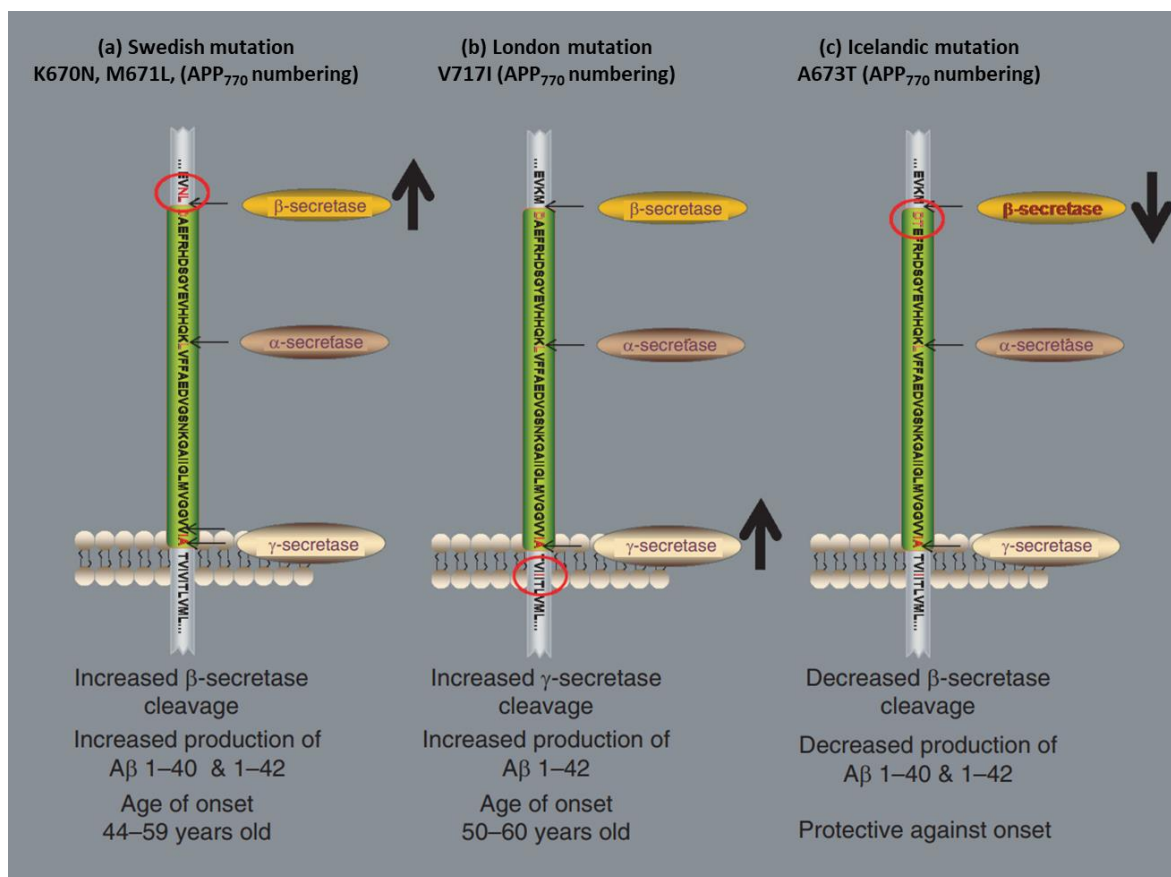


Figure 1.4. Examples of mutations in APP which alter $A\beta$ production.

Mutations in the APP gene which alter $A\beta$ production can cause or protect against familial AD. (a) The ‘Swedish’ mutation (K595N, M596L, APP₆₉₅ numbering) increases total $A\beta$ production. (b) The ‘London’ mutation (V642I, APP₆₉₅ numbering) increases the ratio of $A\beta_{42}$ relative to $A\beta_{40}$. (c) The ‘Icelandic’ mutation (A598T, APP₆₉₅ numbering) significantly reduces the production of both $A\beta_{40}$ and $A\beta_{42}$. Amino acid changes are highlighted in red. Black arrows denote whether the proteolytic cleavage of APP by that enzyme was increased or decreased by the mutation.

Figure adapted with changes from Future Science, MacLeod, R., Hillert, E. K., Cameron, R. T. and Baillie, G. S. (2015). with permissions under the CC BY 4.0 license (and disclaimer of warranties within).

The single greatest risk factor for sporadic AD is age and the risk of developing AD approximately doubles every 5 years over the age of 65 (Van Der Flier 2005). Females are at greater risk of AD, particularly at later ages, which may be linked to oestrogen signalling (Van Der Flier 2005). The largest genetic risk factor for sporadic AD is the apolipoprotein $\epsilon 4$ allele (Corder et al. 1993). Apolipoprotein E is a key component of CNS lipoproteins and one of the major transporters of cholesterol in the brain (Fernández-Calle et al. 2022). The brain contains around 20% of total bodily cholesterol and, as high cellular cholesterol may promote the amyloidogenic cleavage of APP by β -secretase within lipid rafts, the transport and regulation of cholesterol in neurons could play a key role in AD (Cho et al. 2019; Fernández-Calle et al. 2022). Indeed, some population studies have linked high cholesterol to increased AD risk, though uncertainty remains as to the exact risk contribution (Iwagami et al. 2021). Apolipoprotein E has three major isoforms: APOE2, APOE3 and APOE4, which result from polymorphisms in the *APOE* gene (Belloy et al. 2019). APOE3 is the most common isoform (Farrer et al. 1997). In the APOE4 isoform, two amino acid changes result in the formation of a salt bridge between the N-terminal and C-terminal domains (Belloy et al. 2019). Possession of two copies of the APOE4 allele (genotype $\epsilon 4/\epsilon 4$) increases the risk of developing sporadic AD by up to 12 times, whereas possession of one APOE4 allele increases the risk of developing sporadic AD by up to 4 times (Belloy et al. 2019; Farrer et al. 1997). In addition, carriers of APOE4 develop sporadic AD approximately 12 years younger than non-APOE4 carriers on average (Belloy et al. 2019). In contrast, the apolipoprotein $\epsilon 2$ allele (APOE2) exhibited a strong protective effect against sporadic AD (Farrer et al. 1997). Compared with $\epsilon 3/\epsilon 3$ genotypes, $\epsilon 2/\epsilon 2$ genotypes had a 40% lower risk of AD and a later age of onset (Belloy et al. 2019; Corder et al. 1994). As APOE does not pass the blood brain barrier, there are separate pools of CNS and peripheral APOE (Liu et al. 2012). Peripheral APOE is produced primarily by the liver whilst the CNS pool of APOE originates primarily from astrocytes and microglia (Liu et al. 2012; Nakai et al. 1996). Specifically, APOE is involved in the transport of astrocyte-secreted cholesterol into neurons, which could alter the β -secretase cleavage of APP within lipid rafts change the production of $A\beta$ (Wang et al. 2021). Healthy APOE may also play a role in the protection against oxidative damage, which is highly implicated in AD (Section 1.5) (Lauderback et al. 2002). $A\beta_{40}$ produced significantly more damaging reactive oxygen species (ROS) in synaptosomes from APOE knockout mice than wild-type mice (Keller et al. 2000). The activity of superoxide dismutase, an enzyme which neutralises ROS, was also reduced in APOE

knockout mice (Ramassamy et al. 2001). Mouse cortical synaptosomes expressing knocked-in human APOE4 were also significantly more vulnerable to A β ₄₂-induced oxidative stress than synaptosomes expressing human APOE2 or APOE3 (Lauderback et al. 2002). Therefore, APOE has a key role in several mechanisms which are linked to AD, though its exact mechanistic role in AD remains under investigation.

Another important contributor to dementia is diabetes (Zilkens et al. 2013). Type-2 diabetes, also called 'late-onset' diabetes, represents 90% of all diabetes cases and is characterised by hyperglycaemia, usually due to systemic resistance to insulin (Csajbók and Tamás 2016). Diabetes increases atherosclerosis and vascular damage (Paneni et al. 2013). One study found that pre-existing diabetes resulted in, on average, 2-years earlier dementia onset and a shorter survival time in dementia patients (Zilkens et al. 2013). In a population study, late-onset diabetes significantly increased the risk of all dementia by a factor of 1.66 (Leibson et al. 1997). In addition, the younger the age of type-2 diabetes onset, the higher the risk of dementia (Barbiellini Amidei et al. 2021). Infusion of insulin improved memory in non-APOE4 carrying AD patients but had no effect in AD patients carrying at least one APOE4 allele (Craft et al. 2000). Finally, insulin-degrading enzyme is one of the two major enzymes responsible for the degradation of extracellular A β , further linking the mechanisms of AD and diabetes (Qiu et al. 1998). In fact, the links between AD and diabetes are so strong that some groups have suggested that AD should be referred to as 'type-3 diabetes' (Steen et al. 2005). As such, the increasing rates of obesity and diabetes globally will also increase the risk of co-morbidities such as dementia (Zilkens et al. 2013).

1.5. Oxidative stress in AD

Oxidative molecules such as reactive oxygen species (ROS) are important in many healthy physiological processes, such as immune responses (Mittler 2017). However, oxidative stress occurs when the cellular balance between antioxidants and oxidants becomes weighted towards oxidants, leading to the damage of cellular components (Huang et al. 2016). This can occur either because of an increase in oxidants or a decrease in antioxidants (Huang et al. 2016). Oxidants are produced during normal metabolism and cellular activity such as respiration (Huang et al. 2016). Common examples of oxidants include 'radical' reactive oxygen species (ROS) such as the superoxide radical (O₂^{•-}) and 'non-radical' ROS such as hydrogen peroxide (H₂O₂) (Huang et al. 2016). Reactive nitrogen species are also potent

sources of physiological oxidative stress (Huang et al. 2016). The production of ROS such as H_2O_2 , $\text{O}_2^{\bullet-}$ and OH^{\bullet} is catalysed by metals such as iron and copper (Zhao and Zhao 2013). As a cellular defence mechanism, the highly oxidative superoxide radical, $\text{O}_2^{\bullet-}$, is reduced to the less toxic hydrogen peroxide (Zhao and Zhao 2013). However, hydrogen peroxide can itself form reactive hydroxyl radicals (OH^{\bullet}) (Zhao and Zhao 2013). Oxidative molecules such as ROS and RNS can damage biological molecules like lipids, nucleic acids and proteins through oxidation which alters their structure and function, leading to pathological dysfunction (Huang et al. 2016). Treatment of medium spiny neuron (MSN) neuroblastoma cells with H_2O_2 resulted in a 50% increase in ROS production and a 15% decrease in cell viability (Quiroz-Baez et al. 2009). As the brain has a high rate of respiration and oxygen consumption it is particularly exposed to oxidative stress (Huang et al. 2016). A number of antioxidant defences exist within cells to prevent oxidative damage, such as the enzyme superoxide dismutase (SOD) (Huang et al. 2016). SOD converts $\text{O}_2^{\bullet-}$ into H_2O_2 , which is less damaging (Huang et al. 2016).

The equilibrium between antioxidants and oxidants within cells is essential to prevent oxidative stress and functional impairment; however, during AD the balance is pushed towards oxidation (Huang et al. 2016). High levels of neuropathology in AD brains correlated with elevated levels of oxidatively damaged proteins, lipids and nucleic acids (Butterfield and Lauderback 2002; Cheignon et al. 2018). Metals catalyse the production of ROS, and the levels of metals such as copper and zinc can be three times higher in AD brains than healthy brains (Cheignon et al. 2018). In addition, metals such as iron and copper bind with high affinity to $\text{A}\beta$, facilitating the oxidation of molecules in proximity with $\text{A}\beta$ (Cheignon et al. 2018). One of the key mechanisms of $\text{A}\beta$ toxicity was demonstrated to be oxidative damage, as $\text{A}\beta$ treatment significantly increased H_2O_2 levels in cells whilst the addition of antioxidants prevented $\text{A}\beta$ -induced cell death (Behl et al. 1994). Similarly, lipid oxidation induced by $\text{A}\beta$ was prevented by the addition of antioxidants such as vitamin E (Behl et al. 1994). $\text{A}\beta$ oligomers ($\text{A}\beta\text{Os}$) increased ROS production in primary hippocampal neurons through the N-methyl-D-aspartate (NMDA) glutamate receptor (De Felice et al. 2007). Interestingly, memantine, a licensed therapy for AD, blocks NMDA receptors and was found to inhibit the ability of $\text{A}\beta\text{Os}$ to induce ROS in primary hippocampal neurons (De Felice et al. 2007). This could explain memantine's beneficial effect in AD patients. Treatment with H_2O_2 significantly

increased A β_{42} levels by 30% and concomitantly decreased total APP and sAPP α levels (Quiroz-Baez et al. 2009). Oxidative stress induced by H₂O₂ also significantly increased the expression of BACE1 (Quiroz-Baez et al. 2009). APOE status may also affect oxidative stress responses, as allele APOE4 was associated with significantly higher ROS formation than either APOE2 or APOE3 in response to A β_{42} treatment in mouse cortical synaptosomes (Lauderback et al. 2002). In addition, amyloid pathology itself may be driven by oxidative damage, as treatment of AD mice with the anti-inflammatory molecule curcumin significantly reduced oxidised protein markers, soluble A β levels and A β plaque burden (Lim et al. 2001). Therefore, oxidative stress may form a positive feedback loop in AD brains, with A β initiating a state of oxidative stress which causes oxidative damage that then drives further A β pathology. In summary, AD pathology is intrinsically linked to oxidative damage.

1.6. The failure of drug trials for AD

As AD is the greatest cause of dementia (WHO 2017), finding an effective disease-modifying treatment remains a major priority for researchers and pharmaceutical companies across the globe. Until late 2022, there had been no new licensed treatments for AD since memantine was licensed in 2003 (Cummings et al. 2014). For decades, the four major therapies licensed to help AD symptoms were: memantine, galantamine, rivastigmine and donepezil (Cummings et al. 2014). Memantine is an N-methyl-D-aspartate (NMDA) receptor blocker that reduced the glutaminergic excitotoxicity seen in AD (Parsons et al. 2013). Galantamine, rivastigmine and donepezil are all acetylcholinesterase inhibitors (AChEIs) (Parsons et al. 2013). Cholinergic neurons are lost in significant amounts in AD brains, leading to a reduction of up to 90% of the neurotransmitter acetylcholine (ACh) (Parsons et al. 2013). Loss of ACh correlates with cognitive decline in AD patients, so the three AChEIs prevent the breakdown of ACh by acetylcholinesterase in order to boost ACh quantities in the brain, which temporarily benefits cognition in AD patients (Parsons et al. 2013). However, all four of these therapies are purely symptomatic, as they do not treat the underlying cause of the disease (Parsons et al. 2013). Therefore, they do not slow neurodegeneration and become ineffective over time (Parsons et al. 2013).

Over 200 clinical trials of drugs to treat AD have taken place over recent decades, with the vast majority failing (Cummings et al. 2014). Many trials have targeted the A β peptide directly. One study found that active immunisation with A β_{42} itself could prevent or reverse AD

pathology in AD mice (Schenk et al. 1999). However, active immunisation using A β was not safely repeated in human trials, as a phase two trial of AN1792 (immunisation with full-length A β_{42}) in patients with mild-to-moderate AD as discontinued due to early reports of a significantly increased risk of meningoencephalitis (Orgogozo et al. 2003). One follow-up study of the patients who had been treated with AN1792 found that they had significantly lower mean A β load, but this did not improve overall survival or time to severe dementia (Holmes et al. 2008). However, there was a high variation in the antibody response and degree of plaque removal in patients immunised with AN1792, and a 15-year follow up study of AN1792 found that patients who had a large antibody response to AN1792 had significantly lower post-mortem plaque scores (Nicoll et al. 2019). Nevertheless, even patients with almost complete clearance of plaque load had still progressed to severe dementia prior to death (Nicoll et al. 2019). AN1792 is demonstrative of the many clinical trials performed with high initial hopes from *in vitro* and *in vivo* studies, which were later found to be ineffective or unsafe in human clinical trials at the stages of disease tested. One recent criticism of previous AD clinical trials was that they were tested in patients at too late a disease stage (Cummings et al. 2014).

However, in late 2022 and early 2023 two new therapies for AD were licensed by the US Food and Drug Administration (FDA): Aducanumab and Lecanemab (Mahase 2021b). Aducanumab, a monoclonal antibody targeting aggregated A β , was approved by the FDA through its accelerated drug approval pathway (Walsh et al. 2021). The FDA controversially approved aducanumab for treatment of people with mild AD; however, this decision was heavily criticised by some in the medical field as, quote, “probably the worst drug approval decision in recent US history” and led to three of the members of the FDA advisory panel resigning (Mahase 2021b). Indeed, both phase three trials for aducanumab were initially discontinued by Biogen due to preliminary analyses which suggested the treatment was ineffective (Knopman et al. 2021). However, 7 months later Biogen announced that subsequent analyses had shown that aducanumab was, in fact, effective at improving cognition and function (Knopman et al. 2021). In June 2021 aducanumab was licensed for use in the US by the FDA; however, it was not approved by the European Medicines Agency (EMA) (Mahase 2021a). The EMA cited a lack of evidence demonstrating efficacy, as well as safety concerns because 40% of high-dose recipients had experienced brain swelling or bleeding (Mahase 2021a). The FDA’s

decision to license aducanumab without the need for a new phase three trial was also criticised (Knopman et al. 2021).

Lecanemab, a monoclonal antibody against soluble A β protofibrils, significantly slowed cognitive decline in early AD patients by 27% in a phase three trial (van Dyck et al. 2023). Lecanemab was safer than aducanumab, with around 20% of lecanemab patients experiencing brain swelling or bleeding (Prillaman 2022). However, safety concerns remain as two patients died from “stroke-related complications” in the open-label extension trial for lecanemab (Prillaman 2022). Lecanemab was approved by the FDA in January 2023 and the sponsors have applied for marketing authorisation to the EMA (Larkin 2023; Mahase 2023; Reardon 2023).

However, even with the recent licensing of aducanumab and lecanemab, more AD therapies are needed. As demonstrated in previous clinical trials, A β -directed antibody therapies have been plagued by safety concerns in patients, so therapies targeting other mechanisms to slow cognitive and functional decline are crucial (Cummings et al. 2014). The efficacy of the newly licensed therapies has been called into question, and they are also very expensive. Aducanumab costs \$56,000 annually per patient and, in one study, was found to cost approximately \$383,030 per quality adjusted life year (QALY) gained compared to the current standard of care (Sinha and Barocas 2022). For comparison, the UK National Institute for Health and Care Excellence (NICE) considers a drug to be cost-effective if it costs under £30,000 per QALY gained (Gandjour 2020). In addition, since the current gold-standard method for attaining a definitive AD diagnosis is post-mortem tissue analysis, there is a real danger of misdiagnosis leading to patients with early stages of dementia caused by other diseases, such as vascular dementia or dementia with Lewy bodies, being wrongly subjected to A β -directed immunotherapies which would have no benefit yet pose significant safety risks (Selvackadunco et al. 2019). Therefore, treatments which could be beneficial across different causes of dementia, such as therapies which could improve neuronal resistance to damage, would be preferable.

Trials and studies for AD have also targeted other molecular mechanisms, such as the β -secretase and γ -secretase enzymes involved in the cleavage of APP to produce A β . As A β is believed to be the primary cause of AD, reducing its production through the inhibition of β -

secretase or γ -secretase was suggested as a therapeutic option to slow cognitive decline in AD (Zhao et al. 2020). However, to date, no β -secretase or γ -secretase inhibitors have been licensed, despite many clinical trials (Zhao et al. 2020). The first BACE1 inhibitor to move into a phase II/III clinical trial for mild-to-moderate AD was verubecestat (MK-8931), which reduced cerebrospinal fluid (CSF) A β levels by 94% (Zhao et al. 2020). However, the phase II/III clinical trial found no benefit to cognition, combined with higher rates of adverse reactions such as rash, weight loss and suicidal ideation (Egan et al. 2018). Due to this, the phase II/III clinical trial for verubecestat was prematurely halted in 2017 (Zhao et al. 2020). Similarly, there has been a lack of success using γ -secretase inhibitors to treat AD due to off-target toxicity and a lack of benefit to cognition (Zhao et al. 2020). Off-target toxicity is high due to the other substrates of γ -secretase being impacted by γ -secretase inhibition (Katoh 2020). For example, γ -secretase also cleaves Notch, a key transmembrane signalling protein which is dysregulated in many cancers (Katoh 2020). The γ -secretase inhibitor semagacestat (LY450139) failed in a large-scale phase III clinical trial due to no cognitive benefit but increased rates of skin cancer, infections and gastrointestinal symptoms (Doody et al. 2013). Therefore, β -secretase and γ -secretase are difficult pharmacological targets due to their high levels of off-target toxicity. They also appear to not have any benefit to cognition in mild-to-moderate AD patients, despite reducing A β . This mimics the A β immunotherapy AN1792, which significantly reduced A β in patient brains but did not affect rates of AD (Nicoll et al. 2019). Therefore, reducing A β load at late stages of AD may be ineffective, as extensive neurodegeneration has already occurred. However, early diagnosis of AD remains a problem. Therefore, early, possibly preventative treatment is also currently not possible. Thus, other treatment options could be preferable, such as utilising neuroprotective proteins like soluble amyloid precursor protein alpha (sAPP α) to reduce neuronal damage and slow neurodegeneration.

1.7. Soluble amyloid precursor protein (sAPP α).

The cleavage of APP by ADAM10 between Lys₆₁₂ and Leu₆₁₃ (APP₆₉₅ numbering) releases sAPP α ₆₉₅ extracellularly (Figure 1.3) (Kuhn et al. 2010). The C-terminus of sAPP α contains the first 16 amino acids of A β , which prevents the subsequent formation of A β (Figure 1.3) (Kuhn et al. 2010). The sAPP α molecule contains much of the overall APP sequence including the E1, acidic linker and E2 domains (Figure 1.5) (Reinhard et al. 2013). Several studies have

demonstrated neuroprotective and neurotrophic benefits of sAPP α both *in vitro* and *in vivo* (Hornsten et al. 2007; Ring et al. 2007). For example, genetic inactivation of *APL-1*, the sole gene related to *APP* in *C. elegans*, resulted in larval lethality (Hornsten et al. 2007). However, the neuronal expression of the extracellular domain of APL-1, representative of sAPP α , rescued the lethality of *APL-1* knockout (Hornsten et al. 2007). In fact, the E1 or E2 domain of APL-1 alone was sufficient to rescue the lethal effects of APL-1 inactivation (Hornsten et al. 2007). This demonstrated that vital functions of APL-1 were likely being facilitated by its secreted ectodomain. Therefore, some of the functions of APP in humans may also be facilitated by its cleavage product sAPP α . Similarly, knock-out of *APP* in mice caused significant deficits in long term potentiation (LTP), body weight and spatial learning (Ring et al. 2007). These deficits from *APP* knockout were either partially or completely rescued by knock-in of sAPP α (Ring et al. 2007). Studies like these suggest that some of the negative effects of APP knockout observed *in vitro* and *in vivo* could be due to the loss of sAPP α activity, rather than a loss of APP activity. sAPP α is of key interest in AD research because it has been shown to exhibit neuroprotective and neurotrophic activities (Corbett et al. 2018). The neuronal effects of sAPP α and its possible applications in AD treatment are discussed below.

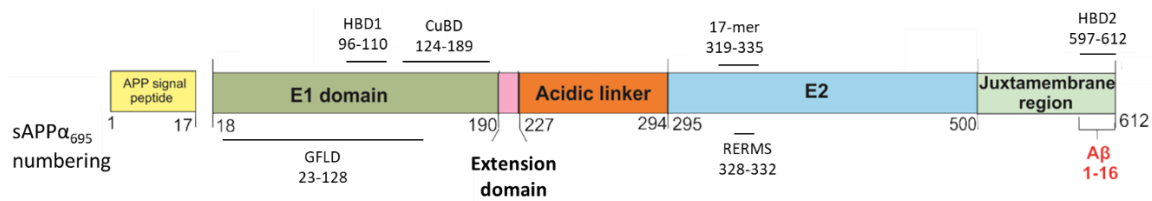


Figure 1.5. A linear representation of sAPP α_{695} domains with amino acid numberings.

Several known binding domains and regions of interest are highlighted. sAPP α_{695} numbering is shown. Precise domain numberings are still disputed within the literature. HBD = Heparin binding domain; CuBD = copper binding domain; GFLD = Growth factor like domain; RERMS and 17-mer = amino acid sequences (APP₃₂₈₋₃₃₂ and APP₃₁₉₋₃₃₅ respectively) which bound neuronal cells and promoted neurite outgrowth (Jin et al. 1994).

1.7.1. sAPP α improved neuronal survival in the presence of toxic levels of A β .

The exact mechanisms through which A β or tau cause neuronal death are varied and remain under investigation. Treatment of rat hippocampal neurons with 20 μ M A β_{40} for 4 days reduced cell survival to around 40% in a time- and concentration-dependent manner (Goodman and Mattson 1994). However, co-application of A β with 10 nM sAPP α_{695} or sAPP α_{751} significantly reduced the toxicity of A β and improved neuronal survival to around 75% in a concentration-dependent manner (Goodman and Mattson 1994). Another study showed that A β_{42} oligomers caused the death of between 25% and 40% of primary mouse cortical neurons (Dorard et al. 2018). However, co-incubation with 60 nM sAPP α reduced cell death from A β_{42} oligomers by over 95% (Dorard et al. 2018). These results were highly promising and highlighted the potential of sAPP α for the treatment of AD.

1.7.2. sAPP α protected neurons against glucose deprivation and glutamate excitotoxicity.

As early research progressed, studies began to identify the specific mechanisms through which A β induced neuronal cell death. One of the toxic effects of A β is the dysregulation of calcium homeostasis in neurons, leading to higher vulnerability to glutamate excitotoxicity (Arbel-Ornath et al. 2017; Mattson et al. 1992). Glutamate is the primary excitatory neurotransmitter in the brain, and the overstimulation of glutamate receptors can result in neuronal cell death through mechanisms involving calcium influx, oxidative stress and mitochondrial dysfunction (Armada-Moreira et al. 2020). This process is called excitotoxicity

(Armada-Moreira et al. 2020). The N-methyl-D-aspartate (NMDA) receptor is a key glutamate receptor which, when activated, increases the permeability of the cell membrane to calcium and results in calcium influx (Choi 1987; MacDermott et al. 1986). NMDA-receptor mediated calcium influx and excitotoxicity is implicated in many neurodegenerative diseases, including AD (Armada-Moreira et al. 2020). Treatment of rat primary hippocampal neurons with up to 500 μ M glutamate for 24 hours reduced survival in a concentration-dependent manner (Mattson et al. 1993). However, 24 hour pre-treatment with 10 nM sAPP α_{695} or sAPP α_{751} significantly increased neuronal survival in the presence of up to 200 μ M glutamate (Mattson et al. 1993). Linking excitotoxicity to AD, pre-treatment of rat hippocampal cell cultures with A β_{40} increased neuronal calcium sensitivity to glutamate, but this effect was reduced through co-application with 10 nM of sAPP α_{695} or sAPP α_{751} (Goodman and Mattson 1994). Therefore, sAPP α appeared to increase the resistance of neuronal cultures to glutamate excitotoxicity by increasing the threshold before which significant calcium influx occurred, combatting an important pathogenic mechanism in neurodegenerative diseases such as AD (Mattson et al. 1993).

Glucose deprivation of cultured neuronal cells resulted in cell damage and death within 30 hours (Mattson et al. 1993). Glucose deprivation appeared to particularly damage neurons, with less impact on glial cells (Monyer et al. 1989). Blockage of the N-methyl-D-aspartate (NMDA) receptor significantly improved mouse cortical neuronal survival from glucose deprivation, suggesting that neuronal damage through glucose deprivation may act through the activation of NMDA receptors and calcium influx (Monyer et al. 1989). Hypoglycaemia induced a significant increase in intracellular calcium in rat hippocampal neurons and the death of around 95% of cells within 20 hours (Cheng and Mattson 1992). However, rat hippocampal neurons grown in calcium-deficient media had significantly lower intracellular calcium in response to hypoglycaemia and exhibited approximately 90% survival after 20 hours of hypoglycaemic culture (Cheng and Mattson 1992). Therefore, an influx of calcium, linked to NMDA receptors, may be involved in neuronal death under hypoglycaemic conditions. 16 hours of pre-treatment with 10 nM sAPP α_{695} or sAPP α_{751} significantly increased the survival of cultured human cortical neurons, rat hippocampal neurons and rat cerebral cortex in hypoglycaemic conditions (Mattson et al. 1993). This effect was time-dependent and concentration-dependent (Mattson et al. 1993). Treatment with sAPP α_{695} or sAPP α_{751} rapidly

and significantly reduced intracellular calcium in cultured rat hippocampal neurons and human cortical neurons, within 1 min of application of 1 nM sAPP α , in a concentration-dependent manner (Mattson et al. 1993). Washing cells to remove sAPP α caused a swift increase in intraneuronal calcium concentration but the re-introduction of sAPP α significantly and rapidly reduced calcium concentration again (Mattson et al. 1993). The protective effect of sAPP α_{695} and sAPP α_{751} against hypoglycaemia-induced neuronal death was mapped to amino acids 444-592 (sAPP α_{695} numbering) (Mattson et al. 1993).

1.7.3. sAPP α protected neuronal cells against A β -induced oxidative stress and reduced A β and ptau levels.

Another mechanism by which A β causes neurotoxicity is through oxidative damage (Section 1.5) (Behl et al. 1994; De Felice et al. 2007). Incubation of A β_{40} with rat hippocampal neurons for 24 hours significantly increased levels of an oxidation marker by over 200% (Goodman and Mattson 1994). Co-treatment of A β with vitamin E, a potent antioxidant, abolished the oxidative effect of A β_{40} (Goodman and Mattson 1994). Co-treatment of A β with sAPP α_{695} or sAPP α_{751} also significantly reduced the oxidative effect of A β_{40} (Goodman and Mattson 1994). In a separate study, overexpression of sAPP α in APPswe/PS1dE9 AD mouse models significantly reduced soluble A β_{40} , A β_{42} and overall plaque load in the hippocampus and cortex (Fol et al. 2016). Overexpression of sAPP α in AD mice also significantly increased the expression of insulin degrading enzyme, a protease which degrades A β (Fol et al. 2016). sAPP α also inhibited the activity of GSK3 β , a serine/threonine kinase which promotes the hyperphosphorylation of tau, and AD mice overexpressing sAPP α exhibited reduced tau phosphorylation *in vivo* (Deng et al. 2015). Thus, sAPP α protected neurons against oxidative stress and reduced both A β levels and the hyperphosphorylation of tau, which are the two primary neuropathological hallmarks of AD.

Iron is raised in specific regions within aged brains and in many neurodegenerative diseases (including AD, Parkinson's disease, dementia with Lewy bodies and Huntington's disease) iron colocalises with protein inclusions present in the brain (Ndayisaba et al. 2019). As iron catalyses the production of ROS, it likely contributes to neurodegeneration (Zhao and Zhao 2013). Treatment with 10 μ M iron induced significant oxidative damage and cell death in rat hippocampal neurons (Goodman and Mattson 1994). However, treatment with 2 nM sAPP α_{695} and sAPP α_{751} significantly improved cell survival (Goodman and Mattson 1994). In

contrast, 20 μ M A β ₄₀ augmented the toxic oxidative effect of iron in neurons (Goodman and Mattson 1994). Therefore, the protective effect of sAPP α against iron-induced oxidative stress and the subsequent increase in neuronal survival could have therapeutic relevance for a range of different neurodegenerative diseases including AD (Goodman and Mattson 1994).

1.7.3. sAPP α is neurotrophic and stimulates neuronal growth.

sAPP α exhibits neurotrophic properties and several studies have noted its similarity with certain growth factors (Caillé et al. 2004; Dar and Glazner 2020; Rossjohn et al. 1999). Two weeks *in vivo* infusion of a 17 amino acid peptide, termed 17-mer and corresponding to Ala₃₁₉ to Met₃₃₅ of sAPP α ₆₉₅, significantly increased synaptic density in the frontoparietal cortex (but not the hippocampus) of rats (Roch et al. 1994). This increase in synaptic density was accompanied by a significant increase in memory retention in rats that did not have initial impaired learning (Roch et al. 1994). This increase in memory retention correlated significantly with a worsening in reversal learning, perhaps due to improved memory interfering with the learning of a new platform location (Roch et al. 1994). This study demonstrated that infusion of a peptide within sAPP α ₆₉₅ directly improved memory in rats *in vivo*. Addition of sAPP α ₆₉₅ also significantly increased the proliferation of rat neural stem cells in a concentration-dependent manner (Ohsawa et al. 1999). This effect on neural stem cell proliferation was blocked by the antibody 22C11, which binds to a region within amino acids 66-81 of sAPP α (Ohsawa et al. 1999). A 16-amino acid peptide containing amino acids 66-81 of sAPP α was also sufficient to significantly increase neural stem cell proliferation (Ohsawa et al. 1999).

Neurogenesis is reduced throughout adulthood, with reduced neural progenitor cells in the subventricular zone (SVZ) and subgranular layer (SGL), and this is linked to impaired learning and memory (Demars et al. 2013). APP and ADAM10 are highly expressed in the SVZ of adult mice (Demars et al. 2011). *In vivo*, sAPP α bound to cells specifically within the mouse subventricular zone and increased the proliferation of adult neural progenitor cells (Caillé et al. 2004). A separate study found that sAPP α (isoform not stated), injected intracerebroventricularly, significantly increased neural progenitor cell proliferation in the SVZ and SGL in mice of all ages (Demars et al. 2011; Demars et al. 2013). Interestingly, intracerebroventricular injection of sAPP β (isoform not stated) had the opposite effect, and significantly reduced the proliferation of neural progenitor cells in the SVZ and SGL (Demars

et al. 2013). Treatment with 1 to 5 nM sAPP α for 24 hours significantly increased neurite outgrowth in mouse primary cortical neurons (Hasebe et al. 2013), whilst treatment of B103 neuroblastoma cells with a 17-amino acid peptide corresponding to amino acids 319-335 of sAPP α_{695} significantly increased neurite number at concentrations above 4 nM (Jin et al. 1994). In summary, there is strong evidence that sAPP α promotes neuronal growth.

Plasma levels of sAPP α were found to be significantly elevated in patients with severe autism and aggression (Ray et al. 2011; Sokol et al. 2006). As sAPP α is neurotrophic, it was suggested that increased levels of sAPP α could contribute to the brain overgrowth linked to autism through the establishment of an anabolic brain environment (Ray et al. 2011; Sokol et al. 2006). This exemplifies the potential dangers of an over-stimulation of sAPP α activity, but also indicates the potentially beneficial neurotrophic properties of sAPP α (Blinkouskaya and Weickenmeier 2021). Increasing our understanding of the neurotrophic effects of sAPP α , such as the receptors with which sAPP α interacts, could elucidate viable mechanisms through which this anabolic brain environment could be utilised to combat the neuronal loss and brain atrophy seen in neurodegenerative diseases such as AD (Blinkouskaya and Weickenmeier 2021).

1.7.4. sAPP α enhanced memory and LTP.

sAPP α was demonstrated to improve memory and LTP *in vivo* (Tan et al. 2018). APP^{swe}/PS1^{dE9} AD mouse models exhibited significant impairments in hippocampal LTP, spatial memory and spatial learning but viral expression of sAPP α_{695} rescued those effects without improving underlying amyloid plaque pathology (Tan et al. 2018). Similarly, knockout of APP resulted in significant losses in spatial learning and LTP in mice but knock-in of sAPP α_{695} rescued those memory deficits (Ring et al. 2007). A third study found that overexpression of sAPP α in APP^{swe}/PS1^{dE9} AD mouse models rescued spatial memory but not spatial learning (Fol et al. 2016). Intracerebroventricular administration of sAPP α_{695} or sAPP α_{751} in mice significantly improved memory retention in object recognition tasks and significantly protected against memory deficits caused by the amnestic drug scopolamine (Meziane et al. 1998). sAPP α levels have been shown to correlate negatively with age in rats but correlate positively with cognitive ability and memory tasks (Anderson et al. 1999). A positive correlation was also found between CSF sAPP α levels and cognitive ability in neurological

tests in familial AD patients (Anderson et al. 1999). Therefore, sAPP α may have significant beneficial effects on cognition in both AD and non-AD subjects.

1.7.5. sAPP α protected neurons against proteasomal stress.

Proteasomal impairment has been linked to the neuropathology of neurodegenerative amyloidoses like AD, as proteins such as A β and tau aggregate rather than being degraded (Tseng et al. 2008). In fact, A β oligomers inhibited proteasomal activity and further enhanced the aggregation of A β and tau in a toxic positive feedback loop which likely occurs in the brains of AD patients (Tseng et al. 2008). The 20S proteasome inhibitor epoxomicin induces neuronal apoptosis *in vitro* due to impaired proteasomal activity (Copanaki et al. 2010). However, approximately 80 pM sAPP α , harvested from HEK cells overexpressing APP, significantly reduced cell-death and apoptosis markers following epoxomicin treatment in rat PC12 neuronal model cells (Copanaki et al. 2010). sAPP α decreased caspase-3 apoptotic activity in a concentration-dependent manner, whereas sAPP β had no effect (Copanaki et al. 2010). This protective effect of sAPP α was facilitated through the phosphoinositide 3-kinase (PI3K)/AKT pathway, which promotes cell survival and proliferation (Copanaki et al. 2010).

1.7.6. sAPP α is significantly more protective than sAPP β and therefore has higher therapeutic potential.

Fewer studies have investigated sAPP β than sAPP α , likely due to its reduced neuroprotective activity and therefore lower therapeutic potential (Chasseigneaux and Allinquant 2012; Furukawa et al. 1996). In a key study, sAPP α was found to be 100 times more potent than sAPP β at protecting against glutamate excitotoxicity, A β toxicity and glucose deprivation in rat hippocampal neurons (Furukawa et al. 1996). As sAPP α ₆₉₅ only differs from sAPP β ₆₉₅ by 16 amino acids at its C-terminus, the C-terminal region of sAPP α is likely crucial in facilitating this greater level of neuroprotection (Habib et al. 2017). Consistent with this hypothesis, a peptide composed of the twenty C-terminal amino acids of sAPP α (amino acids 591-612) was similarly protective as full-length sAPP α (Furukawa et al. 1996). Additionally, a peptide composed of sAPP α peptides 444-612 bound to rat hippocampal neurons to a greater degree than a peptide composed of sAPP α peptides 444-596, suggesting that sAPP α may bind to neurons with higher affinity than sAPP β as a result of the extra amino acids at its C-terminus, which could also explain the difference in their neuroprotective abilities (Furukawa et al. 1996). Pre-treatment with heparinase reduced the binding of sAPP α to rat hippocampal neurons and its

protective effect against excitotoxicity in a concentration-dependent manner, suggesting that the heparin-binding domain within amino acids 597-612 may play a critical role in sAPP α binding and neuroprotection (HBD2, Figure 1.5) (Furukawa et al. 1996). Crucially, the C-terminal heparin-binding domain is absent from sAPP β , which could explain why sAPP β cannot induce the same beneficial effects (Furukawa et al. 1996). However, 150 nM sAPP α ₆₉₅ and sAPP β ₆₉₅ both induced axon outgrowth to a similar degree in primary mouse cortical neurons, so they do share certain functions (Chasseigneaux et al. 2011). In summary, sAPP β was less protective than sAPP α and bound with lower affinity to neurons, but it remains comparatively understudied (Furukawa et al. 1996). There are also relatively few studies which include a direct comparison of the activity of sAPP α and sAPP β , making conclusions difficult (Chasseigneaux and Allinquant 2012). sAPP β may also have more unwanted deleterious effects, as sAPP α and sAPP β had opposite significant effects on the number of neural progenitor cell proliferation in the SVZ and SGL in mice (Demars et al. 2013). The higher therapeutic potential of sAPP α over sAPP β exemplifies why sAPP α was chosen as the focus of this project. Several examples of observed effects of sAPP α in the published literature are stated in Table 1.1.

Table 1.1 A summary of the characteristics and effects of sAPP α in the published literature

Protein isoform	Observed effect	Reference
'Secreted APP': sAPP α ₅₉₅ and sAPP α ₆₅₁ ; sAPP β ₅₇₉ and sAPP β ₆₃₅ , purified from HEK cells.	Significantly protected rat hippocampal neurons against A β -induced calcium elevation and oxidative damage.	(Goodman and Mattson 1994)
Total sAPP α	Significantly elevated in plasma samples of patients with severe autism, linked to excessive brain growth.	(Ray et al. 2011; Sokol et al. 2006)
sAPP α ₆₉₅ amino acids 319-335 named '17-mer'. Prokaryotic sAPP ₃₋₅₇₄	Significantly increased neurite number in B103 neuroblastoma cells.	(Jin et al. 1994)
Commercial sAPP α ₆₉₅ (Sigma)	Promoted neurite outgrowth by 18.7%.	(Hasebe et al. 2013)
sAPP α ₆₉₅ and sAPP α ₇₅₁	Intracerebral administration improved mouse long term memory retention in mice. Prevented scopolamine-induced learning defects.	(Meziane et al. 1998)
sAPP α ₆₉₅	Knock-in rescued hippocampal LTP deficits resulting from APP knockout.	(Ring et al. 2007)
sAPP α ₆₉₅	Overexpression in APPswe/PS1dE9 double transgenic AD mouse model rescued spatial memory deficits and significantly increased expression of insulin degrading enzyme, a protease which degrades A β .	(Fol et al. 2016)
Recombinant sAPP α , isoform not described	Significantly increased the inhibitory phosphorylation of GSK3 β in SHSY5Y cells, HeLa cells and tau hyperphosphorylation mouse models in a dose dependent manner.	(Deng et al. 2015)
Recombinant sAPP α , isoform not described	Significantly decreased tau phosphorylation, including in neuroblastoma cells over-expressing BACE1.	(Deng et al. 2015)

1.8. Known sAPP α receptors.

Due to the beneficial effects of sAPP α listed above (Section 1.7; Table 1.1), several studies have attempted to identify the receptors and mechanisms through which sAPP α exerts specific effects such as neurotrophy and neuroprotection (Dorard et al. 2018; Hasebe et al. 2013; Rice et al. 2019). Several studies have identified binding partners for sAPP α , including those responsible for facilitating beneficial neurotrophic processes such as neurite outgrowth, but none have yet identified the receptor responsible for facilitating the neuroprotective activity of sAPP α against damaging processes such as oxidative stress. Utilising the beneficial effects of sAPP α through stimulation of a specific receptor could be a promising alternative therapeutic option for AD (Habib et al. 2017). The main proteins which sAPP α has been shown to interact with sAPP α at the cell surface are discussed below.

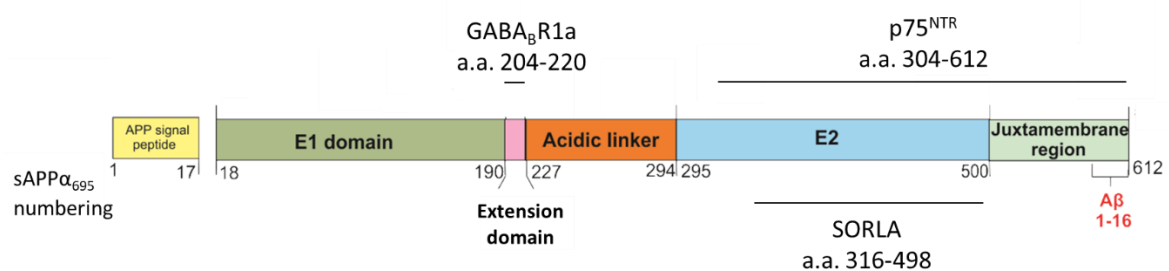


Figure 1.6. The sites within sAPP α that bind to different receptor candidates.

A map of the amino acid regions previously identified as being responsible for the binding of sAPP α to putative receptors. The potential binding site within APP for SORLA is also shown. The binding of α 3-NKA was not narrowed down to a specific region in sAPP α , so it is not shown.

1.8.1. p75 neurotrophin receptor.

sAPP α and sAPP β co-precipitated with human p75 neurotrophin receptor (p75^{NTR}) in targeted pull-down experiments (Hasebe et al. 2013). A C-terminal peptide composed of sAPP α amino acids 304-612 (C-sAPP α) also precipitated p75^{NTR}, suggesting the binding site was towards the C-terminus (Figure 1.6) (Hasebe et al. 2013). sAPP α , sAPP β and C-sAPP α all bound to the surface of COS-7 cells transfected to express p75^{NTR} on their cell surface, but not to wild-type cells (Hasebe et al. 2013). sAPP α bound with the highest affinity, with an EC₅₀ of 90 nM,

followed by sAPP β at 120 nM and finally C-sAPP α at 150 nM (Hasebe et al. 2013). Treatment with sAPP α for 24 hours significantly increased neurite outgrowth in mouse cortical neurons, but siRNA-mediated knockdown of p75^{NTR} abolished that effect (Hasebe et al. 2013). The induction of neurite outgrowth through the binding of sAPP α to p75^{NTR} was facilitated by protein kinase A (Hasebe et al. 2013). Together, the results from this study convincingly showed that p75^{NTR} acted as a cell surface receptor for sAPP α to promote neurite extension in cortical neurons. However, as sAPP β was also found to bind to p75^{NTR} with a similar affinity and produced a similar effect on neurite outgrowth, this receptor is unlikely to be responsible for the enhanced protective effects of sAPP α over sAPP β which could make sAPP α so therapeutically valuable (Hasebe et al. 2013).

1.8.2. SORLA and Sortilin.

Sorting protein related receptor A (SORLA) is a type I transmembrane protein that was shown to sequester APP in the Golgi, which reduced both ADAM10 and BACE1 cleavage and sAPP α , sAPP β and A β ₄₀ production (Andersen et al. 2005; Andersen et al. 2006). SORLA levels were found to be significantly lower in the grey matter of human AD frontal cortexes (Andersen et al. 2005). Knockout of SORLA in mice also significantly increased cortex A β ₄₀ and A β ₄₂ levels (Andersen et al. 2005). The binding site within APP for SORLA was suggested to be within amino acids 316-498 (APP₆₉₅ numbering), which is within the E2 domain (Figure 1.6) (Andersen et al. 2006). As sAPP α also contains that domain, it was suggested that SORLA may also bind to sAPP α (Andersen et al. 2006). In fact, a later study confirmed that transfection of HEK cells with SORLA, or a related protein called Sortilin, significantly increased the endocytosis of sAPP₇₅₁ (Gustafsen et al. 2013). SORLA appeared to shuttle sAPP α to the TGN, whereas sortilin shuttled it to lysosomes (Gustafsen et al. 2013). However, the functions of sAPP α binding to SORLA or sortilin remain unknown and the major apparent benefit of APP binding to SORLA, reduced BACE1 cleavage, would not impact sAPP α . Therefore, SORLA and Sortilin appear, at least for now, to have limited benefit regarding the neuroprotective actions of sAPP α . Their sequestration of APP could be beneficial to reduce APP cleavage by BACE1, but further study is required.

1.8.3. α 3-Na, K-ATPase.

Pulldown experiments using membrane-enriched cortico-hippocampal samples from mice followed by mass spectrometry identified α 3-Na, K-ATPase (α 3-NKA) as a potential interactor

for sAPP α_{695} -Fc (Dorard et al. 2018). This finding was confirmed in co-immunoprecipitation studies (Dorard et al. 2018). sAPP α bound to the cell surface of mouse cortical neurons rapidly, within 1 min of addition, and co-localised with $\alpha 3$ -NKA within 3 minutes (Dorard et al. 2018). Both knockdown and pharmacological inhibition of $\alpha 3$ -NKA in primary mouse cortical neurons significantly reduced the induction of neurite elongation by sAPP α (Dorard et al. 2018). However, knockdown or pharmacological inhibition of $\alpha 3$ -NKA did not reduce the neuroprotective ability of sAPP α to increase cell survival against oligomeric A β_{42} in mouse cortical neurons, suggesting a different receptor is responsible for facilitating sAPP α -mediated neuroprotection (Dorard et al. 2018). The binding site within sAPP α for $\alpha 3$ -NKA was not investigated, and sAPP β was not included in the study (Dorard et al. 2018).

1.8.4. GABA $_B$ R1a.

The γ -aminobutyric acid type B receptor subunit 1a (GABA $_B$ R1a) was identified as an interactor of sAPP α_{695} in synaptosome-enriched homogenates from rat brains through co-precipitation experiments (Rice et al. 2019). Specifically, sAPP α_{695} amino acids 204-220, within the extension domain of sAPP α (Figure 1.6), were identified as binding to the sushi-1 domain of GABA $_B$ R1a (Rice et al. 2019). The binding of sAPP α_{695} to GABA $_B$ R1a enhanced short term facilitation and inhibited the release of pre-synaptic vesicles (Rice et al. 2019). However, crucially, this study found no difference between sAPP α and sAPP β , meaning GABA $_B$ R1a is not responsible for the enhanced beneficial effects of sAPP α (Rice et al. 2019). The sAPP α protein used in the study was tagged at the C-terminus with a large Fc tag, which could have interfered with crucial C-terminal interactions which may have identified sAPP α -specific receptors (Rice et al. 2019). In addition, GABA $_B$ R1a was shown to reduce the cleavage of APP into A β (Dinamarca et al. 2019).

1.9. Thesis aims.

sAPP α induces a wide range of beneficial effects in neurons which have significant therapeutic potential in neurodegenerative diseases such as AD. However, the receptor through which sAPP α mediates its neuroprotective activity against oxidative stress, excitotoxicity and A β -induced neuronal death in humans remains unknown. GABA $_B$ R1a and p75^{NTR} exhibited no clear differences in the binding of sAPP α or sAPP β (Hasebe et al. 2013; Rice et al. 2019), meaning they are unlikely to contribute to the enhanced neuroprotective effect of sAPP α (Furukawa et al. 1996). In addition, $\alpha 3$ -NKA was demonstrated not to be responsible for

sAPP α -mediated neuroprotection (Dorard et al. 2018). Therefore, there were likely unidentified receptors which bound to sAPP α to mediate effects such as neuroprotection. As neuronal damage through mechanisms such as oxidative stress and excitotoxicity is known to play a critical role in the progression of AD (Cheignon et al. 2018), harnessing the neuroprotective effect of sAPP α could have great therapeutic potential. If the responsible receptor(s) were identified, stimulation of such specific receptors or its downstream signalling mechanisms could increase neuronal resistance to damage to slow or even stop neurodegeneration and cognitive decline in AD.

SH-SY5Y cells, a human neuroblastoma cell line, are commonly used to study neurodegenerative diseases in laboratories across the world because of their neuron-like characteristics, ease of culture and rapid growth rate (Slanzi et al. 2020). However, more physiologically accurate models of native human neurons are also available, such as iPSC-derived human cortical neurons (hiPSC-derived neurons), which derive from reprogrammed adult somatic cells (Slanzi et al. 2020). hiPSC-derived neurons provide a more physiologically accurate model of native patient neurons than immortalised cells do (Engle et al. 2018). However, hiPSC-derived neurons are fragile, challenging and time-consuming to culture, so they are not appropriate for use in all experiments (Engle et al. 2018). Therefore, experiments within this thesis used either SH-SY5Y cells or hiPSC-derived neurons where appropriate.

The main aim of this thesis was to perform unbiased screens to identify novel sAPP α binding partners in neuronal cells. This project utilised human N-terminally his-tagged recombinant sAPP α and repurposed methods previously used to successfully identify cell surface integrins using known ligands as bait (Jones et al. 2015). This was used in combination with a second, quartz crystal microbalance with dissipation monitoring (QCM-D) based, unbiased receptor isolation method. The *in vitro* effects and binding characteristics of sAPP α were studied using hiPSC-derived neurons and SH-SY5Y neuroblastoma cells. Identified receptors were validated through siRNA-mediated knockdown studies. Successful identification of novel sAPP α binding partners not only increased our understanding of the mechanisms of sAPP α but could also lead to novel potential therapeutic targets for a disease which is in critical need of safe and effective disease-modifying treatments.

2. Materials and Methods

2.1. Immortalised cell culture.

Human embryonic kidney 293 cells containing the T antigen (HEK293T) and SH-SY5Y human neuroblastoma cells were maintained in 75 cm² cell culture flasks (Thermo Scientific #132913) containing 10 mL Dulbecco's modified Eagle's medium (DMEM) supplemented with 10% (v/v) foetal bovine serum (FBS). Cells were incubated in a 5% CO₂ 37 °C humidified incubator. Upon reaching approximately 80-90% confluency, cells were passaged into new 75 cm² cell culture flasks (Thermo Scientific #132913). To passage, cells were detached using 10 mL Dulbecco's phosphate-buffered saline (DPBS) (- metals), centrifuged at 3000 rpm for 5 min, the supernatant discarded and the cell pellet resuspended in 10 mL DMEM+10% FBS (v/v) medium. For routine maintenance, 1 mL of the resuspended pellet was transferred into a fresh cell culture flask (Thermo Scientific #132913) containing 9 mL DMEM+10% FBS (v/v). When necessary, cells were counted using a Cell Countess II (ThermoFisher) and trypan blue stain according to the manufacturer's instructions. Cells were checked regularly for mycoplasma infection using the EZ-PCR mycoplasma test kit (Geneflow #K1-0210).

2.2. Construct generation and transfection into cells.

A pcDNA3.1+ plasmid encoding sAPP α ₆₉₅ under the transcriptional control of a 5' kozak enhancer sequence and with an N-terminal hexahistidine His-tag, positioned downstream of the APP signal peptide coding region, was provided by Dr. Kate Fisher at the start of the project. Dr. Kate Fisher also provided HEK cells which had been stably transfected with the sAPP α ₆₉₅ plasmid. A stop codon was introduced 48 nucleotides upstream of the 3' sAPP α stop codon using the Q5 site-directed mutagenesis kit (New England Biolabs, E0554S) (forward primer 5'-3': TAGGATGCAGAATTCCGACATG; reverse primer 5'-3': CATCTTCACTTCAGAGATC) to produce a plasmid coding for sAPP β ₆₉₅. Briefly, 12.5 μ L Q5 mastermix, 1.25 μ L F primer (10 μ M), 1.25 μ L R primer (10 μ M), 25 ng sAPP α template DNA in 1 μ L and 9 μ L DNase free H₂O were mixed and amplified through PCR. The PCR cycles were: 98 °C for 30 s; followed by 25 cycles of 98 °C for 10 s, 57 °C for 30 s, 72 °C for 240 s. 2 μ L PCR product was analysed through gel electrophoresis on a 1% agarose gel (0.01% SYBR Safe [v/v]) at 90V for 45 min. 1 μ L PCR product was ligated using KLD reaction mix (New England Biolabs M0554) according to the manufacturer's instructions. Briefly, 1 μ L PCR product, 5 μ L 2x KLD reaction buffer, 1 μ L 10x KLD enzyme and 3 μ L DNase free H₂O were mixed and incubated for 5 min at RT. 50 μ L

chemically competent *E. coli* cells were transformed with 5 μ L KLD reaction mix through heat shock (30 min on ice, heat shock 30 sec at 42 °C, recovery 3 min on ice, 1 h at 37 °C in SOC outgrowth medium). Transformed colonies were identified through overnight plating on LB agar plates containing 0.1 mg/ml ampicillin. Single colonies were selected and the plasmid was purified using the QIAprep Spin Miniprep kit (Qiagen 27104) according to the manufacturer's instructions. Eluted DNA was stored at -20 °C. Insertion of the stop codon was confirmed through analysis of the DNA sequence (sequencing performed by Eurofins Genomics). HEK293T cells were stably transfected with the plasmid encoding sAPP β ₆₉₅ through nucleofection according to the manufacturer's instructions (4D-Nucleofactor, Lonza). Transformed cells were selected with DMEM+10% FBS (v/v) containing 1 mg/ml geneticin. A plasmid map of sAPP α within pcDNA 3.1+ is presented in Supplementary Figure 7.4.

2.3. Purification of secreted hexahistidine-tagged recombinant sAPP α and sAPP β .

A protocol was developed for the purification of hexahistidine-tagged protein from cell medium using immobilised metal affinity chromatography (IMAC). The protocol is summarised in Figure 2.1. HEK cells, transfected to overexpress either sAPP α ₆₉₅ or sAPP β ₆₉₅, were grown to 100% confluency in four 500 cm² multilayer flasks (Thermo Scientific #132913) and, upon reaching confluence, were then incubated for 72 h in 60 mL OptiMEM medium (Gibco) per flask. The media was harvested and centrifuged for 5 min at 3000 rpm. The media was concentrated from a total of 240 mL to approximately 10 mL using several Vivaspin 20 10,000 MWCO centrifugal concentrators at 4 °C (Generon #VS2002) (Figure 2.1a). A sample of this media, termed 'input', was taken for analysis. The concentrated media sample was adjusted to a final concentration of 20 mM Tris pH 8, 300 mM NaCl and incubated with 200 μ L 50% slurry Nickel-NTA agarose (Qiagen) on a roller overnight at 4 °C (Figure 2.1b). The media was then centrifuged at 3000 rpm for 5 min (Figure 2.1c), the supernatant was removed and a sample was kept for analysis (termed 'unbound'). The nickel-NTA agarose was resuspended in 5 mL wash buffer 1 (20 mM Tris pH 8, 1 M NaCl) (Figure 2.1d), placed on a roller for 5 min at RT and centrifuged for 5 min at 3000 rpm (Figure 2.1e). The supernatant was removed (termed 'wash 1') and the nickel-NTA agarose was resuspended in 5 mL wash buffer 2 (20 mM Tris pH8, 300 mM NaCl, 10 mM imidazole). The sample was placed on a roller for 5 min at RT and centrifuged for 5 min at 3000 rpm. The supernatant was removed (termed 'wash 2') and the nickel-NTA agarose was resuspended in 2 mL wash buffer 3 (20 mM Tris pH

8, 300 mM NaCl, 20 mM imidazole). The nickel-NTA agarose was placed on a roller for 5 min at RT, centrifuged for 5 min at 3000 rpm and the supernatant removed (termed 'wash 3'). The nickel-NTA agarose was resuspended in 2 mL elution buffer (20 mM Tris pH 8, 300 mM NaCl, 500 mM imidazole) (Figure 2.1f) and incubated on a roller at RT for 10 min. The sample was centrifuged at 3000 rpm for 5 min (Figure 2.1g), the supernatant containing the purified protein was collected and a sample kept for analysis (termed 'elution 1'). All centrifugation steps were performed at 4 °C.

The purified protein sample was transferred to four Ultra-0.5 mL 10,000 MWCO centrifugal filter devices (Amicon) and centrifuged at 14,000 for 13 min. The flow through was removed, the 50 µL protein sample diluted in 450 µL DPBS and centrifuged again at 14,000 for 13 min. This buffer exchange process was performed a total of four times and the 200 µL protein sample was left concentrated following the fourth centrifugation step (Figure 2.1h). The concentration of purified protein was determined through a bicinchoninic acid assay using BSA (1 mg/mL) as a protein standard (Section 2.6).

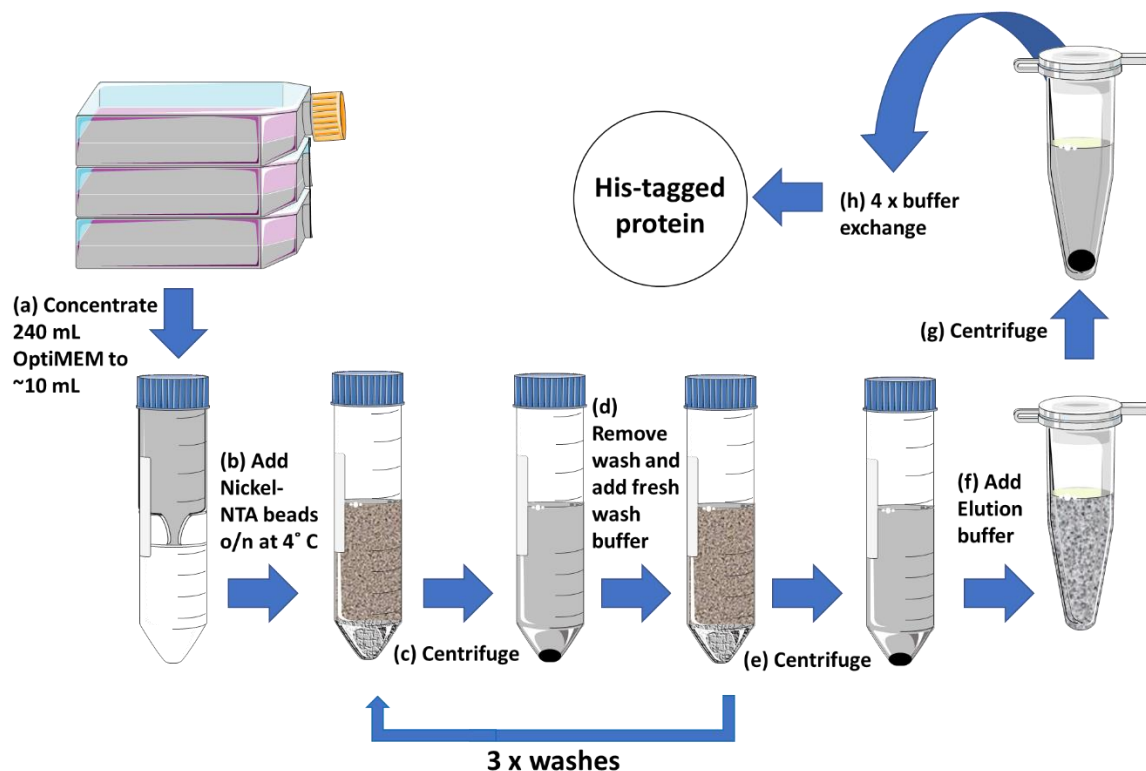


Figure 2.1. The process for purifying hexahistidine-tagged recombinant sAPP α or sAPP β from complex cell medium through immobilised metal affinity chromatography (IMAC).

(a) HEK cells, transfected to overexpress either sAPP α ₆₉₅ or sAPP β ₆₉₅, were grown to 100% confluency and incubated for 72 h in OptiMEM medium. The media was harvested, cell debris was removed through centrifugation and the media was concentrated from a total of 240 mL to approximately 10 mL through centrifugation. (b) The concentrated media sample was adjusted to a final concentration of 20 mM Tris pH 8, 300 mM NaCl and incubated with 50% slurry Nickel-NTA agarose (Qiagen) on a roller overnight at 4 °C. (c-e) The media was centrifuged and the supernatant removed. The nickel-NTA agarose was washed in wash buffers 1, 2 and 3. (f) The nickel-NTA agarose was resuspended in elution buffer and incubated on a roller at RT for 10 min. (g) The sample was centrifuged at 3000 rpm for 5 min and the supernatant containing the purified protein was removed. (h) Imidazole was removed through buffer exchange using DPBS and centrifugal filter devices.

2.4. Preparation of whole cell lysates.

1x10⁶ SH-SY5Y cells were seeded in 2 mL DMEM (containing 10% FBS) per well overnight in a 6 well plate. Cells were washed three times with 1 mL DPBS and incubated in 2 mL OptiMEM per well at 37 °C for 48 hours. Cells were washed three times with 1 mL ice-cold DPBS, scraped in 1 mL ice-cold RIPA lysis buffer (0.5% [w/v] sodium deoxycholate, 1% [v/v] Nonidet P-40, 50 mM Tris, 150 mM NaCl, pH 8, 4% [v/v] cOmplete EDTA-free protease inhibitor cocktail [Sigma #11873580001]), collected and incubated on ice for 30 min. Samples were centrifuged at 14,000 xg for 10 min at 4 °C and the supernatant was collected and stored at -20 °C until analysed.

2.5. Biophysical analysis of recombinant purified sAPP α and sAPP β .

The biophysical analysis of 100 μ g purified sAPP α and sAPP β was performed by Dr. Thomas Jowitt at the University of Manchester Biomolecular Analysis Facility. Protein oligomerisation was determined through multi-angle light scattering using a DAWN EOS 18-angle light scattering detector (Wyatt) and through analytical ultracentrifugation using an OptiMA XLA analytical ultracentrifuge (AUC) (Beckman Coulter). AUC sedimentation was performed at 230 nm and 40,000 rpm.

2.6. Bicinchoninic acid (BCA) assay.

Control samples (10 μ L total volume) of BSA (2-10 μ g/ μ L) were diluted in dH₂O and loaded in duplicate alongside a 10 μ L dH₂O blank control in a clear 96-well plate. Various volumes of experimental samples were diluted in dH₂O (10 μ L total volume) and loaded in duplicate. 200 μ L of a 1:50 mixture of 4% CuSO₄ (v/v) and BCA assay reagent A (ThermoFisher #23228) was added to each well, plates were sealed and then incubated for 20 min at 37 °C. Absorbance was read at 562 nm using an ELx800 microplate reader (BioTek). The mean protein concentration of each experimental sample was determined using a standard curve generated from the BSA control standards through Gen5 data analysis software (BioTek).

2.7. Sodium dodecyl sulphate polyacrylamide gel electrophoresis (SDS-PAGE).

Protein samples were diluted to the desired concentration in 1x loading buffer (100 mM Tris-HCl, 2% [w/v] SDS, 10% [v/v] glycerol, 100 mM DTT, 0.02% [w/v] bromophenol blue, pH 6.8) and heated at 95 °C for 5 min. Proteins were resolved through gel electrophoresis in 1.5 mm 10% Tris-Glycine polyacrylamide gels. A stacking gel of 3% Tris-Glycine polyacrylamide was used. PageRuler prestained protein ladder (ThermoFisher #26616), 10-180 kDa, was run

alongside samples to determine the molecular weight of protein bands. Electrophoresis was performed at 45 mA per gel for ~50 min using 1x Tris/Glycine/SDS protein electrophoresis buffer (25 mM Tris, 192 mM Glycine, 0.1% SDS [v/v], pH 8.3) (BioRad #1610772EDU). Electrophoresed SDS gels containing separated protein samples were either analysed through immunoblotting (Section 2.8) or stained with coomassie brilliant blue (Section 2.9).

2.8. Immunoblotting.

Electrophoresed SDS gels containing separated protein samples were transferred to Immuno-Blot PVDF membrane (BioRad #1620177), which had been pre-activated with a rinse in 100% methanol. Protein transfer was achieved via a wet-transfer system at 120 V for 80 min in transfer buffer (20% methanol [v/v], 150 mM Glycine, 20 mM Tris). The PVDF membrane was then blocked in 10 mL 5% (w/v) milk in DPBS containing 0.1% (v/v) Tween-20 (DPBST) for 1 h at RT, rinsed with DPBS and incubated with 5-10 mL primary antibody in 2% BSA (w/v) PBST overnight at 4 °C with rocking motion. A list of the antibodies and concentrations used are shown in Table 2.1. The membrane was washed in ~10 mL DPBST for 10 min at RT, followed by two washes in ~10 mL DPBS for 10 min each at RT. Washed PVDF membrane was incubated in 5-10 mL secondary antibody (horseradish peroxidase conjugate, Table 2.1) for 1 h at RT. The membrane was washed three times in ~10 mL DPBS for 10 min per wash and protein bands were visualised using the Pierce enhanced chemiluminescence detection system (ThermoFisher #32106) with a Syngene Gbox XT4. Data were analysed using GeneTools (Syngene). To control for protein loading, PVDF membranes were re-probed with 5-10 mL of antibody directed against β -actin (Table 2.1) and re-imaged.

Table 2.1. List of antibodies used in this thesis.

Antibody	Raised in	Source; catalogue no.	Concentration/dilution used
A β 1-16 (6E10)	Mouse	BioLegend; SIG-39320	0.25 $\mu\text{g/mL}$
APP 66-81 (22C11)	Mouse	Millipore; MAB348	0.5 $\mu\text{g/mL}$
sAPP β neoepitope (1A9)	Mouse	SmithKline Beecham Pharmaceuticals	1:2500
sAPP α neoepitope (2B3)	Mouse	Immuno-Biological Laboratories; 11088	1 $\mu\text{g/mL}$
Hexahistidine tag	Mouse	Abcam; ab18184	1 $\mu\text{g/mL}$
VGLUT1	Rabbit	Synaptic Systems; 135303	2 $\mu\text{g/mL}$
Synaptophysin	Rabbit	Abcam; ab68851	1:200
Anti-Mouse secondary HRP conjugated	Rabbit	Sigma-Aldrich; A9044	2.5–5 $\mu\text{g/mL}$
Anti-Rabbit secondary HRP conjugated	Goat	Invitrogen; A16096	0.25 $\mu\text{g/mL}$
PSD-95	Mouse	Abcam; ab2723	10 $\mu\text{g/mL}$
β -actin (AC-15)	Mouse	Abcam; ab6276	0.21–0.23 $\mu\text{g/mL}$
Calsyntenin-3	Rabbit	Proteintech; 13302-1-AP	1.5 $\mu\text{g/mL}$
MAP2	Chicken	Ab5392	1:10,000
Anti-Mouse IgG H&L Alexa Fluor 488 conjugated	Donkey	Abcam; ab150105	2 $\mu\text{g/mL}$
Anti-Rabbit IgG H&L Alexa Fluor 594 conjugated	Donkey	Abcam; ab150076	2 $\mu\text{g/mL}$
Anti-Chicken IgL H&L Alexa Fluor 647 conjugated	Goat	Invitrogen; A-21449	2 $\mu\text{g/mL}$
SATB2	Mouse	Abcam; ab51502	0.5 $\mu\text{g/mL}$
S100 β	Rabbit	ThermoFisher; BS-2015R	5 $\mu\text{g/mL}$
β III tubulin	Mouse	Elabscience; E-AB-20093	5 $\mu\text{g/mL}$
GFAP	Chicken	Abcam; ab4674	1:1000

2.9. Coomassie blue total protein gel stain.

Electrophoresed SDS gels containing separated protein samples were fully submerged in SimplyBlue SafeStain (Thermo LC6060) for at least 30 min at RT with gentle rocking, followed by overnight destaining in dH₂O at RT.

2.10. Bioinformatics.

Protein sequences were obtained from UniProt (available at www.uniprot.org). DNA sequence data provided by Eurofins Genomics were translated bioinformatically using ExPASy ProtParam (available at <https://web.expasy.org/protparam/>). Alignments were performed using Clustal Omega (available at www.ebi.ac.uk/tools/msa/clustalo).

2.11. The isolation of ligand-specific adhesion complexes using tosylactivated microbeads.

The following protocol is described in detail in Jones et al., 2015. The constituents of the required buffers are listed in Table 2.2. A summary of the protocol is shown in Figure 2.2. Approximately 5×10^7 beads per experimental condition were prepared. 125 μ L Tosylactivated M-450 microbeads (Invitrogen #14013) were washed with 125 μ L 0.1M sodium phosphate buffer pH 8 (0.1M PB) and incubated with sAPP α , sAPP β , OKT9 or TS216 so that 25 μ g of ligand was present per 5×10^7 beads at a final concentration of 200 μ g/mL. The coated beads were incubated at 1400 rpm at 25 °C for 15 min, followed by the addition of BSA to a final concentration of 0.5% (w/v). The coated beads were left incubating overnight at 1400 rpm, 25 °C. The coated beads were then magnetically separated, washed twice with 125 μ L 0.1% BSA (w/v) in DPBS (- metals) and incubated overnight in 125 μ L 0.2M Tris-HCl pH 8.5 containing 0.1% BSA (w/v) at 1400 rpm, 25 °C. The coated and blocked beads were then washed twice with 125 μ L DPBS (- metals) containing 0.1% BSA (w/v) and used immediately for receptor pulldown experiments.

SH-SY5Y neuroblastoma cells were passaged until approximately 1×10^8 cells were present per experimental condition on the day of the experiment. Cells were detached through incubation with DPBS (- metals) and counted using a Cell Countess II (ThermoFisher) with trypan blue stain. Detached cells were centrifuged at 3000 rpm for 5 min and resuspended to a final concentration of 1×10^7 cells/mL in DMEM-HEPES containing 0.2% BSA (w/v). Per condition, 1×10^8 cells were incubated with 5×10^7 coated beads to achieve a cell-to-bead ratio of 2:1. Beads and cells were incubated together for 30 min with gentle rotation at 70 rpm, 37 °C. Dimethyl 3,3'-dithiobispropionimide (DTBP) (ThermoFisher #20665) protein crosslinker

was then added to a final concentration of 3 mM followed by a further 30 min incubation at 70 rpm, 37 °C. Tris-HCl pH 8.5 was added to a final concentration of 20 mM for 3 min, followed by magnetic separation of beads and two washes with 5 mL cytoskeletal stabilising buffer (CSK⁻) containing 200 mM Tris (CSK⁻ with Tris) (Table 2.2). Beads were magnetically separated, resuspended in 2.5 mL CSK buffer containing 0.5% Triton X-100 (v/v) (CSK⁺) (Table 2.2) and sonicated using a Qsonica Sonicator Q700 (20% amplitude, 4 x 5 sec). Following sonication, beads were separated magnetically and washed four times with 5 mL CSK⁺. The beads were separated magnetically and incubated in 150 µL 2x loading buffer (200 mM Tris-HCl, 4% [w/v] SDS, 20% [v/v] glycerol, 200 mM DTT, 0.04% [w/v] bromophenol blue, pH 6.8) at 1400 rpm, 70 °C for 30 min followed by incubation at 1400 rpm, 95 °C for 5 min. Beads were magnetically separated, 100 µL of the supernatant was collected and stored at -80 °C until required for analysis.

Table 2.2. Composition of the cytoskeletal stabilising buffers used in the tosylactivated microbead pulldown.

Adapted from Jones, M. C., Humphries, J. D., Byron, A., Millon-Frémillon, A., Robertson, J., Paul, N. R., Ng, D. H. J., Askari, J. A. and Humphries, M. J. (2015) 'Isolation of integrin-based adhesion complexes', *Curr Protoc Cell Biol*, 66, pp. 9.8.1-9.8.15.

CSK ⁻	150 mM sucrose 500 mM NaCl 10 mM PIPES pH 6.8
CSK ⁻ with Tris	150 mM sucrose 500 mM NaCl 10 mM PIPES pH 6.8 200 mM Tris-HCl pH 8.5
CSK ⁺	150 mM sucrose 500 mM NaCl 10 mM PIPES pH 6.8 0.5% Triton X-100 (v/v) 1 x cOmplete mini protease inhibitor cocktail (#11836153001)

Abbreviations: CSK⁻, cytoskeletal stabilising buffer without Triton; CSK⁺, cytoskeletal stabilising buffer with Triton.

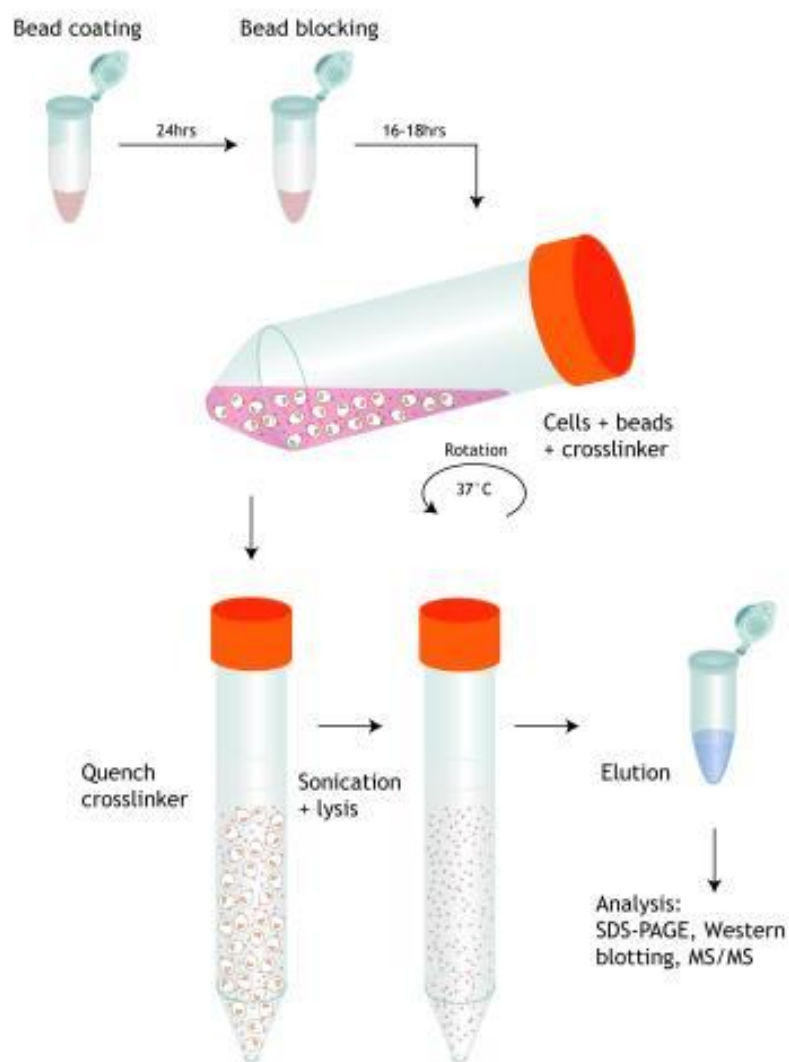


Figure 2.2. A summary of the protocol which facilitated the isolation of binding partners for specific ligands immobilised on the surface of tosylactivated microbeads.

Figure taken from Jones, M. C., Humphries, J. D., Byron, A., Millon-Frémillon, A., Robertson, J., Paul, N. R., Ng, D. H. J., Askari, J. A. and Humphries, M. J. (2015) 'Isolation of integrin-based adhesion complexes', *Curr Protoc Cell Biol*, 66, pp. 9.8.1-9.8.15.

2.12. GeLC-MS/MS analysis.

Liquid chromatography-tandem mass spectrometry (GeLC-MS/MS) analyses were performed by the Biological Mass Spectrometry (BioMS) Core Facility at the University of Manchester. Numbers shown in this thesis are total peptide counts, unless stated otherwise. Samples from microbead-based receptor pulldown (Section 2.11) or QCM-D based receptor pulldown (Section 2.21) experiments were heated at 95 °C for 5 min. Proteins were run into the top of a 1.5 mm 10% Tris-Glycine polyacrylamide gel via electrophoresis at 45 mA for 5 min using 1x Tris/Glycine/SDS protein electrophoresis buffer (25 mM Tris, 192 mM Glycine, 0.1% SDS [v/v], pH 8.3) (BioRad #1610772EDU).

Digestion

Bands of interest were excised from the gel and dehydrated using acetonitrile followed by vacuum centrifugation. Dried gel pieces were reduced with 10 mM dithiothreitol and alkylated with 55 mM iodoacetamide. Gel pieces were then washed alternately with 25 mM ammonium bicarbonate followed by acetonitrile. This was repeated, and the gel pieces dried by vacuum centrifugation. Samples were digested with trypsin overnight at 37 °C.

Mass Spectrometry

Orbitrap Elite machine

Digested samples were analysed by LC-MS/MS using an UltiMate® 3000 Rapid Separation LC (RSLC, Dionex Corporation, Sunnyvale, CA) coupled to an Orbitrap Elite (Thermo Fisher Scientific, Waltham, MA) mass spectrometer. Peptide mixtures were separated using a gradient from 92% A (0.1% FA in water) and 8% B (0.1% FA in acetonitrile) to 33% B, in 44 min at 300 nL/min, using a 75 mm x 250 µm i.d. 1.7 mM BEH C18, analytical column (Waters). Peptides were selected for fragmentation automatically by data dependant analysis.

QE HF machine

Digested samples were analysed by LC-MS/MS using an UltiMate® 3000 Rapid Separation LC (RSLC, Dionex Corporation, Sunnyvale, CA) coupled to a QE HF (Thermo Fisher Scientific, Waltham, MA) mass spectrometer. Mobile phase A was 0.1% formic acid in water and mobile phase B was 0.1% formic acid in acetonitrile and the column used was a 75 mm x 250 µm i.d. 1.7 mM CSH C18, analytical column (Waters).

A 1 μ L aliquot of the sample was transferred to a 5 μ L loop and loaded on to the column at a flow of 300 nL/min for 5 min at 5% B. The loop was then taken out of line and the flow was reduced from 300 nL/min to 200 nL/min in 0.5 min. Peptides were separated using a gradient that went from 5% to 18% B in 34.5 min, then from 18% to 27% B in 8 min and finally from 27% B to 60% B in 1 minute. The column is washed at 60% B for 3 min before re-equilibration to 5% B in 1 min. At 55 min the flow is increased to 300 nL/min until the end of the run at 60 min.

Mass spectrometry data was acquired in a data directed manner for 60 min in positive mode. Peptides were selected for fragmentation automatically by data dependant analysis on a basis of the top 12 peptides with m/z between 300 to 1750 Th and a charge state of 2, 3 or 4 with a dynamic exclusion set at 15 s. The MS Resolution was set at 120,000 with an AGC target of 3e6 and a maximum fill time set at 20 ms. The MS2 Resolution was set to 30,000, with an AGC target of 2e5, a maximum fill time of 45 ms, isolation window of 1.3 Th and a collision energy of 28.

Data Analysis

Data produced were searched using Mascot (Matrix Science UK), against the [Swissprot and TrEMBL] database with taxonomy of [human] selected. Data were validated using Scaffold (Proteome Software, Portland, OR).

2.13. The differentiation of induced pluripotent stem cells into cortical neurons.

The media used for iPSC-derived cortical neuronal differentiation are listed in Table 2.3. The protocol used was based on the study by Shi et al., (2012). A timeline of the workflow is shown in Figure 4.1. Human OX1-19 induced pluripotent stem cells (hiPSCs) (derived from a healthy male age 35-39 and provided to the Hooper lab by Sally Cowley [University of Oxford]) were passaged 2:1 in the presence of 10 μ M Rho kinase Y-27632 inhibitor (#ab120129) into a matrigel-coated well and incubated at 37 °C for 24 h. The medium was changed to neural induction medium (NIM) and the date was recorded as day 0. NIM was refreshed daily until day 12, when the cells were detached using 10% dispase II solution (v/v) (Gibco 17105041) and transferred to two wells of a 6-well plate pre-coated with 10 μ g/mL laminin (Sigma L2020). The cells were incubated overnight at 37 °C in neuronal maintenance medium (NMM) containing 20 ng/mL fibroblast growth factor (FGF). Following 4 days of FGF treatment, FGF

was withdrawn and cells were incubated in NMM alone. Upon the appearance of neuronal rosettes the cells were split 1:2 using dispase II, as previous. At approximately day 25, the cells were passaged to single cells accutase (Gibco A1110501) and transferred to new wells pre-coated with 10 µg/mL laminin (Sigma L2020). NMM was changed after 24 h and every subsequent 48 h. The cells were repeatedly passaged 1:2 upon confluence until day 35, when they were passaged for the final time into plates coated with 0.01% poly-L-ornithine solution (v/v) (Sigma P4957) to a density of 50-150,000 cells/cm². The NMM medium was changed every 3-4 days until the neurons were used for experiments at day 70+. The expression of cellular markers βIII tubulin, MAP2, SATB2, synaptophysin, S100B and GFAP were determined through immunofluorescence microscopy (Figure 4.1) (Section 2.19).

Table 2.3. Recipes for iPSC-derived human neuron cortical media.

<i>Reagent</i>	<i>Recipe</i>	<i>Volume/ concentration</i>	<i>Catalogue</i>
N2 medium	DMEM/F12 glutamax	500 mL	Life Tech 31331028
	1 x N-2 supplement	5 mL	Life Tech 17502048
	5 µg/mL insulin	0.25 mL	Sigma I9278
	200 mM L-glutamine	5.5 mL	Life Tech 25030024
	100 µM non-essential amino acids	5 mL	Life Tech 11140050
	100 µM 2-mercaptoethanol	0.1 mL	Life Tech 21985023
	Pen/Strep	2.5 mL	Life Tech 15140122
B27 medium	Neurobasal	500 mL	Life Tech 12348017
	1 x B27	10 mL	Life Tech 17504044
	200 mM L-glutamine	2.5 mL	Life Tech 25030024
	Pen/Strep	2.5 mL	Life Tech 15140122
Neural maintenance medium	1:1 mix of N2 and B27 media (+/-) Fibroblast Growth Factor	20 ng/mL	Merck-Millipore GF003
Neural induction medium	NMM	10 mL	
	SB431542	10 µM	R&D Systems #1614
	Dorsomorphin	1 µM	R&D Systems #3093

2.14. ROS assay.

H₂O₂ generation was measured using the ROS-Glo assay (Promega #G8820) according to the manufacturer's instructions. Briefly, 10,000 SH-SY5Y cells per well were seeded into a 96-well cell culture plate (ThermoFisher #165305) overnight in 100 μ L DMEM (10% FBS [v/v]), followed by one wash in 100 μ L DPBS and incubation in 80 μ L sAPP α or DPBS-only vector control in OptiMEM for 48 h at 37 °C. H₂O₂ substrate was added to a final concentration of 25 μ M for the final 6 h of the 48 h treatment. For the final 90 min of incubation, menadione (diluted in 100% ethanol) or a vehicle-only control were added at specified concentrations (μ M) in a final volume of 100 μ L. 50 μ L media from each well was transferred to a separate white opaque plate and mixed with 50 μ L ROS-Glo detection solution. The mixture was incubated for 20 min at RT in the dark, and luminescence was read using a Synergy HT microplate reader (BioTek).

2.15. Assessing the binding of sAPP α to human cells through immunoblotting.

SH-SY5Y cells or day 70+ iPSC-derived human cortical neurons, seeded in 6-well plate format as described previously (Section 2.4; Section 2.13), were incubated with 50 nM sAPP α or DPBS-only vector control in 500 μ L for specified times. The cells were washed three times with 1 mL DPBS, cell lysates were harvested (Section 2.4) and lysates analysed by SDS-PAGE (Section 2.7) followed by immunoblotting with a site-specific sAPP α neoepitope antibody (2B3) (Section 2.8). Bands were quantified using ImageJ and normalised against β -actin band intensity.

2.16. Assessing the binding of sAPP β to human cells through Mesoscale Discovery SH multiplex immunoassay.

SH-SY5Y cells or day 70+ iPSC-derived human cortical neurons, seeded in 6-well plate format as described previously (Section 2.4; Section 2.13), were incubated with 50 nM sAPP β or DPBS-only vector control in 500 μ L. The cells were washed three times with 1 mL DPBS and cell lysates were harvested (Section 2.4). The cell lysates were probed for sAPP β using the multiplex immunoassay sAPP β kit (mesoscale discovery) by Dr. Kate Fisher according to the manufacturer's instructions.

2.17. siRNA knockdown of calsyntenin-1, calsyntenin-3 and GABABR1.

1x10⁶ SH-SY5Y cells were seeded in 2 mL DMEM (containing 10% FBS [v/v]) in 6-well plates overnight. Cells were washed once in 1 mL OptiMEM and incubated in 500 μ L OptiMEM for

30 min at 37 °C. Gene-targeted siRNA (Ambion #439240) or control non-targeting (NT) siRNA (Invitrogen #4390843) were prepared according to the manufacturer's instructions in 1x siRNA buffer using nuclease-free water, mixed with Dharmafect 1 reagent to a final concentration of 50 nM siRNA and incubated for 15 min at RT. The siRNA sequence for calsyntenin-1 was 5' GGAACAACAGGAUUGAGUAtt 3' (sense) and for calsyntenin-3 was 5' GGAACAAAAGGAUCGAAUAtt 3' (sense). The GABABR1 siRNA used was Silencer Select #4392420 siRNA assay ID s5464 (ThermoFisher). The siRNA mixture was diluted 1:5 in DMEM containing 10% FBS (v/v) and 1 mL 50 nM siRNA was added to cells for 48 hr. Whole cell lysates were collected (as described in Section 2.4) and gene expression was quantified by Dr. Kate Fisher through real-time qPCR (RT-qPCR) (Section 2.18).

2.18. RT-qPCR.

Following siRNA-mediated gene knockdown, total RNA was extracted using the RNeasy kit (Qiagen #74004) according to the manufacturer's instructions. cDNA was synthesised using the iScript cDNA Synthesis kit (BioRad #1708890) according to the manufacturer's instructions. Gene expression levels were measured through RT-qPCR using the SYBR Green method. The primer sequences for GABA_BR1a were F: 5' ACAAGGGGCTGCTGCTGCTG 3' and R: 5' GATAGCCATGCCCCACGGCCC 3'. The primer sequences for calsyntenin-1 were F: 5' CATCCAGGCCTATGATTGTGG 3' and R: 5' TACTCATTACGTCGTTTACC 3'. The primer sequences for RPL13 were F: 5' TCAAAGCCTTCGCTAGTCTCC 3' and R: 5' GGCTCTTTTTGCCGTATGC 3'. Reaction mixtures containing 50 ng cDNA, 200 µM dNTPs, 1x SYBR Green, 200 nM forward primer and 200 nM reverse primer were amplified in triplicate using a QuantStudio 3 thermal cycler (Applied Biosystems). The qPCR cycle parameters were 50 °C for 2 min, 95 °C for 10 min; followed by 40 cycles of 95 °C for 15 s and 60 °C for 1 min; followed by 95 °C for 15 s and finally 60 °C for 15 s. Gene expression was normalised against RPL13 reference gene expression. Gene expression in the NT sample was set as 100%.

2.19. Immunofluorescence microscopy.

5,000 SH-SY5Y cells in 50 µL DMEM (+10% FBS) were seeded for 3 h onto coverslips in a 24-well plate format, followed by incubation in 1 mL DMEM (+10% FBS). Seeding with iPSC-derived neurons was performed as previously described (section 2.13). When confluent, coverslips were washed three times with 300 µL DPBS and fixed with 300 µL 4% paraformaldehyde (v/v) for 10 min at RT. Coverslips were then washed three times with 300

μL DPBS and permeabilised using 300 μL DPBS containing 0.2% Triton X100 (v/v) for 4 min at RT. Coverslips were washed twice with 300 μL and incubated in 300 μL 10% Donkey serum (v/v) in DPBS for 3 h at RT. Coverslips were transferred to a moist chamber and incubated with 60 μL primary antibody overnight at RT. Coverslips were washed three times with 300 μL DPBS and incubated with fluorescently-conjugated secondary antibody in 300 μL 10% Donkey serum (v/v) for 1 h (Table 2.1). Coverslips were washed twice with 300 μL DPBS and once with 300 μL dH₂O. Coverslips were allowed to dry and mounted onto slides using a drop of ProLong Gold Antifade Mountant with DAPI (Invitrogen #P36931). A Z-stack of images were captured at 60x using an Olympus IX83 inverted microscope with MetaMorph and DeltaVision software using the appropriate wavelengths for the secondary antibodies. Images were processed using ImageJ (<http://imagej.net/Fiji/Downloads>).

2.20. Detergent-free membrane enrichment.

Cells were scraped from three confluent 75 cm² cell culture flasks (Thermo Scientific #132913) in 1 mL ice-cold DPBS containing 1x protease inhibitor cocktail cOmplete EDTA-free protease inhibitor cocktail (Sigma #11873580001). The sample was sonicated using a Qsonica Sonicator Q700 (20% amplitude, 3 x 5 sec). Nuclei and large debris were removed through centrifugation at 800 xg for 10 min. The pellet was discarded and the supernatant was centrifuged (22,000 xg for 30 min at 4°C). The supernatant, containing the cytosolic fraction, was retained. The pellet, containing the membrane fraction, was resuspended in 200 μL DPBS containing 1x PIC (Sigma #11873580001).

2.21. Quartz Crystal Microbalance with Dissipation Monitoring

Bilayers of 1-palmitoyl-2-oleoyl-sn-glycero-3-phosphocholine (POPC) were produced with head group-functionalised lipid (1,2-dipalmitoyl-sn-glycero-3-phosphoethanolamine-N-(cap biotinyl) (Biotinyl Cap PE). Below is described the preparation of a 5-mol% head group-functionalised lipid layer.

Multilamellar vesicles preparation

10 mg/mL POPC stock suspension of lyophilised POPC within a glass bijoux with air tight lid dissolved in 1 mL chloroform and 1 mg/mL head-group functionalised lipid stock suspension of lyophilised Biotinyl Cap PE within a glass bijoux with air tight lid was dissolved in 1 mL chloroform and swirled to homogenise.

A molar 5% biotinylated biotinyl cap PE lipids was made (95% POPC) and chloroform removed under a continuous gentle nitrogen stream to produce a thin lipid film ensuring all chloroform was removed by drying under vacuum overnight.

Lipids were rehydrated in 1 mL 0.2 μ M filtered 10 mM HEPES, 150 mM NaCl, 2 mM CaCl₂, pH 7.4 (final molar concentration of 1.3 mM) and incubated at room temperature for a minimum of 30 min before sonicating with a tip sonicator 14-Hz 12 second intervals on ice. Unilamellar vesicle size was determined using DLS prior to using (vesicles under 80 nm).

QCM-D sensors (SiO₂) were sonicated in 2% SDS (w/v) for approximately 15 min to remove bound particles before being rinsed both sides with copious amounts of ultrapure water then ethanol and dried under a nitrogen stream to ensure no streaks were present.

Sensors were placed in a UV Ozone cleaner for 30 mins and used immediately.

Lipid bilayer formation using QCM-D

0.2 mM unilamellar lipid solution was used for bilayer deposition. ~200 μ L of sample in the calcium containing buffer was injected over the sensor. Fully formed bilayers should produce final frequency and dissipation values of approximately -25 Hz and 0.1×10^{-6} , respectively.

Once bilayer formed and signals had stabilised, running buffer was used to flush through the system to ensure removal of free lipid (approximately 10 mins).

10 μ g/mL avidin/streptavidin solution was injected over the surface (200 μ L) for 10 min until a saturated layer had formed, followed by a wash of the surface with buffer. This surface was ready for addition of biotinylated molecules to be adhered to the streptavidin.

Capture of ligands to the surface and identification of binders

Purified recombinant sAPP α or sAPP β samples were flowed over the surface until a saturated level was formed, followed by the desired cell lysate. The lysate was flowed at a constant rate of 5 μ L/min for 20 min. Immediately following this there was a 1 min buffer wash to ensure all non-bound material was washed from the flow-cell, and the chip was recovered. The lipid-layer was collected using 25 μ L 2% SDS gel loading buffer. The sample was then analysed through GeLC-M/MS.

2.22. Statistics.

GraphPad Prism 7 (version 7.04) was used to perform all statistical tests and a normal distribution was assumed for all sample populations. A value of $p < 0.05$ was considered statistically significant. For experiments with more than one independent variable, a one-way ANOVA with Tukey's multiple comparison test was performed. For experiments with one independent variable, an unpaired t-test with Welch's correction was performed. All error bars represent standard deviation from the mean, unless otherwise indicated.

3. The purification and biophysical characterisation of recombinant soluble amyloid precursor proteins alpha and beta

3.1. Introduction.

Many of the known functions of APP may be exerted by its secreted cleavage products sAPP α or sAPP β , rather than the full-length protein itself (Dawkins and Small 2014). Cleavage of the transmembrane protein APP₆₉₅ by ADAM10 between Lys₆₁₂ and Leu₆₁₃ results in the extracellular release of sAPP α ₆₉₅ (Kuhn et al. 2010). Cleavage by BACE1 between Met₅₉₆ and Asp₅₉₇ results in the extracellular release of sAPP β ₆₉₅ (Kimura et al. 2016; Vassar et al. 1999). sAPP α was found to protect against excitotoxicity, A β toxicity and glucose deprivation 100 times more effectively than sAPP β (Furukawa *et al.*, 1996). However, the molecular mechanisms and receptor interactions through which sAPP α exerted its enhanced protective effects were unknown. In addition, the causes of the critical functional differences between sAPP α and sAPP β were also unknown. For example, knock-in of sAPP α rescued APP/APLP2 double knockout postnatal lethality in the majority of mice (Weyer et al. 2011), whereas sAPP β knock-in did not (Li et al. 2010). A peptide consisting solely of those C-terminal 16 amino acids of sAPP α , which sAPP β lacks, was sufficient to rescue long-term potentiation deficits in APP/APLP2 double knockout mice, whilst full-length sAPP β had no effect (Richter et al. 2018). Therefore, it was hypothesised that the C-terminal sequence was critical in the different effects of the two proteins, perhaps by facilitating interaction with different receptors. Identification of the receptor(s) responsible for the protective effect of sAPP α could help discover new treatment options for neurodegenerative diseases. Therefore, in this study, sAPP β was included for comparison with sAPP α in the receptor identification experiments because binding partners isolated using sAPP β may not be responsible for the specific neuroprotective and neurotrophic effects of sAPP α . However, there is also the potential that sAPP α and sAPP β bind to the same receptor yet exert different effects or with different affinities.

Due to the C-terminus being the sole difference between the two proteins, a hexahistidine tag (added to facilitate protein purification) was added at the N-terminus, downstream of the signal peptide, to prevent functional disruption. The identities of the purified proteins were confirmed through immunoblotting and GeLC-MS/MS. The biophysical characteristics of each

protein were assessed, which demonstrated high solubility and little aggregation. Producing the proteins in human cells ensured that appropriate physiological post-translational modifications (PTMs) would be present, which could be relevant for protein stability and receptor interaction (Madsen et al. 2020). Similar previous receptor studies of sAPP α all either used C-terminally tagged protein or protein produced in *E. coli* (Dorard et al. 2018; Hasebe et al. 2013; Rice et al. 2019). Rice et al (2019) also used an Fc tag at the C-terminus, which is much larger than a His-tag and therefore more likely to interfere with protein function. To date, no study had used N-terminal hexahistidine tagged sAPP α and sAPP β produced in human cells, in combination with two different unbiased receptor identification methods, to identify and compare novel binding partners in human cells.

3.1.1. Chapter aims.

To isolate potential binding partners and characterise the effect of human sAPP α and sAPP β *in vitro*, large quantities of each protein would be required. Additionally, both the sAPP α and sAPP β proteins available commercially were produced in *E. coli*, meaning they lacked potentially important post-translational modifications found on the eukaryotic proteins. Because of this, it was decided to produce both sAPP α and sAPP β to allow sufficient production of human proteins with the appropriate post-translational modifications and to minimise potential supply disruptions. These proteins were referred to as 'in-house' proteins. Therefore, the aims of this chapter were to:

- Generate HEK cells overexpressing N-terminal His-tagged recombinant sAPP α and sAPP β .
- Confirm overexpression and secretion of sAPP α and sAPP β in each respective HEK cell line.
- Purify each His-tagged protein from the complex HEK cell medium under non-denaturing conditions.
- Confirm the identities of in-house His-tagged proteins as sAPP α and sAPP β .
- Compare in-house sAPP α with commercially acquired sAPP α .
- Analyse the biophysical characteristics of in-house sAPP α and sAPP β .

3.2. Generation of recombinant plasmids coding for sAPP α or sAPP β with N-terminal His-tags.

The three major alternatively spliced isoforms of APP are APP₆₉₅, APP₇₅₁ and APP₇₇₀. A Kunitz protease inhibitor domain is present in both APP₇₅₁ and APP₇₇₀, whilst APP₇₇₀ also contains an additional OX-2 antigen domain (Cappai 2014). As APP₆₉₅ is the dominant neuronal isoform (Kang et al. 1987; Rohan de Silva et al. 1997), the DNA sequence of sAPP α deriving from human APP₆₉₅, with an additional N-terminal hexahistidine tag, was engineered to be overexpressed in human cells.

A plasmid coding for human sAPP α ₆₉₅ under the control of kozak enhancer sequence was available in the lab, provided by Dr. Kate Fisher. To produce it, briefly, a stop codon had been inserted into an APP₆₉₅ plasmid through site directed mutagenesis between codons 612 and 613, which is the ADAM10 cleavage site. A tag of six histidine residues and a glycine-serine-glycine spacer sequence were added through site-directed mutagenesis immediately following the N-terminal signal peptide. Following amplification through *E. coli*, the plasmids were sequence verified, translated using ExPASy Translate (<https://web.expasy.org/translate/>) and aligned to the known APP₆₉₅ amino acid sequence (Figure 3.1). Sequencing and alignment confirmed successful insertion of a hexahistidine-tag and spacer sequence between the APP signal peptide and the N-terminus of the mature sAPP α protein. The sequence alignment also confirmed insertion of a stop codon between codons 612 and 613 of the APP sequence, confirming the production of a plasmid encoding N-terminal hexahistidine sAPP α ₆₉₅.

To produce a plasmid encoding sAPP β ₆₉₅, a stop codon was inserted immediately after the β -secretase cleavage site of the sAPP α ₆₉₅ plasmid sequence, between APP codons 596 and 597. Following amplification through *E. coli*, the sAPP β ₆₉₅ plasmid was purified and sequence verified. The DNA sequence was translated and aligned to the APP₆₉₅ and sAPP α ₆₉₅ plasmid sequences (Figure 3.1). Translated sequence alignment confirmed successful insertion of a stop codon at the desired position, between APP codons 596 and 597, resulting in a plasmid encoding sAPP β ₆₉₅ with an N-terminal hexahistidine tag and spacer sequence. sAPP sequences were placed downstream of a kozak consensus sequence to enhance translation. Thus, these data showed successful generation of recombinant plasmids for both recombinant sAPP α ₆₉₅ and sAPP β ₆₉₅, hereafter simply referred to as sAPP α and sAPP β .

APP	MLPGLALLLLAAWTARA-----LEVPTDGNAGLLAEPQIAMFCGRLLNMHMNVQNGK	51
r_sAPP α	MLPGLALLLLAAWTARAHHHHHGSGLLEVPTDGNAGLLAEPQIAMFCGRLLNMHMNVQNGK	60
r_sAPP β	MLPGLALLLLAAWTARAHHHHHGSGLLEVPTDGNAGLLAEPQIAMFCGRLLNMHMNVQNGK	60

APP	WSDSPSGTKTCIDTKEGILQYCQEVPELQITNVVEANQPVTIQNWCKRGRKQCKTHPHF	111
r_sAPP α	WSDSPSGTKTCIDTKEGILQYCQEVPELQITNVVEANQPVTIQNWCKRGRKQCKTHPHF	120
r_sAPP β	WSDSPSGTKTCIDTKEGILQYCQEVPELQITNVVEANQPVTIQNWCKRGRKQCKTHPHF	120

APP	VIPYRCLVGEFVSDALLVPDKCKFLHQERMDVCETHLHWHTVAKETCSEKSTNLHDYGML	171
r_sAPP α	VIPYRCLVGEFVSDALLVPDKCKFLHQERMDVCETHLHWHTVAKETCSEKSTNLHDYGML	180
r_sAPP β	VIPYRCLVGEFVSDALLVPDKCKFLHQERMDVCETHLHWHTVAKETCSEKSTNLHDYGML	180

APP	LPCGIDKFRGVEFVCCPLAEESDNVDSADAEEDSDVWVGADTDYADGSEDKVVEVAEE	231
r_sAPP α	LPCGIDKFRGVEFVCCPLAEESDNVDSADAEEDSDVWVGADTDYADGSEDKVVEVAEE	240
r_sAPP β	LPCGIDKFRGVEFVCCPLAEESDNVDSADAEEDSDVWVGADTDYADGSEDKVVEVAEE	240

APP	EEVAEVEEEEEADDEDEDGDEVEEEAEPEYEEATERTTSIATTTTTTTESVEEVVRVPT	291
r_sAPP α	EEVAEVEEEEEADDEDEDGDEVEEEAEPEYEEATERTTSIATTTTTTTESVEEVVRVPT	300
r_sAPP β	EEVAEVEEEEEADDEDEDGDEVEEEAEPEYEEATERTTSIATTTTTTTESVEEVVRVPT	300

APP	TAASTPDAVDKYLETPGDENEHAHFQKAKERLEAKHRERMSQVMREWEAEERQAKNLPKA	351
r_sAPP α	TAASTPDAVDKYLETPGDENEHAHFQKAKERLEAKHRERMSQVMREWEAEERQAKNLPKA	360
r_sAPP β	TAASTPDAVDKYLETPGDENEHAHFQKAKERLEAKHRERMSQVMREWEAEERQAKNLPKA	360

APP	DKKAVIQHFQEKVESLEQEAANERQQQLVETHMARVEAMLNDRRLALENYITALQAVPPR	411
r_sAPP α	DKKAVIQHFQEKVESLEQEAANERQQQLVETHMARVEAMLNDRRLALENYITALQAVPPR	420
r_sAPP β	DKKAVIQHFQEKVESLEQEAANERQQQLVETHMARVEAMLNDRRLALENYITALQAVPPR	420

APP	PRHVFNMLKKYVRAEQKDRQHTLKHFEHVRMVDPKKAAQIRSQVMTHLRVIYERMNQSL	471
r_sAPP α	PRHVFNMLKKYVRAEQKDRQHTLKHFEHVRMVDPKKAAQIRSQVMTHLRVIYERMNQSL	480
r_sAPP β	PRHVFNMLKKYVRAEQKDRQHTLKHFEHVRMVDPKKAAQIRSQVMTHLRVIYERMNQSL	480

APP	LLYNVPAVAEEIQDEVDELLQKEQNYSDDLANMISEPRISYGNDAIMPSTETKTTVEL	531
r_sAPP α	LLYNVPAVAEEIQDEVDELLQKEQNYSDDLANMISEPRISYGNDAIMPSTETKTTVEL	540
r_sAPP β	LLYNVPAVAEEIQDEVDELLQKEQNYSDDLANMISEPRISYGNDAIMPSTETKTTVEL	540

APP	LPVNGEFSLDDLQPWHSFGADSVPAANTENEVEPVDARPAADRGLTTRPGSGLTNIKTEEI	591
r_sAPP α	LPVNGEFSLDDLQPWHSFGADSVPAANTENEVEPVDARPAADRGLTTRPGSGLTNIKTEEI	600
r_sAPP β	LPVNGEFSLDDLQPWHSFGADSVPAANTENEVEPVDARPAADRGLTTRPGSGLTNIKTEEI	600

APP	SEVKMDAEFRHDSGYEVHHQKLVFFAEDVGSNKGAIIGLMVGGVV	651
r_sAPP α	SEVKMDAEFRHDSGYEVHHQKLVFFAEDVGSNKGAIIGLMVGGVV	621
r_sAPP β	SEVKM-----	605

APP	QYTSIHGGVVEVDAAVTPEERHLSKMQQNGYENPTYKFFEQMQN	695
r_sAPP α	-----	621
r_sAPP β	-----	605





 = Signal peptide
 = 6x His tag
 = Glycine spacer
 * = Consensus between three amino acid sequences
 " = Consensus between two amino acid sequences
 - = No open reading frame
 = Amyloid- β sequence

Figure 3.1. Amino acid sequence alignment of the N-terminal His-tagged sAPP α ₆₉₅ and sAPP β ₆₉₅ with APP₆₉₅.

A pcDNA3.1 plasmid encoding sAPP α ₆₉₅ under the transcriptional control of a 5' kozak enhancer sequence and with an N-terminal (Figure legend continues on following page)

(continuation of Figure 3.1 legend) hexahistidine His-tag, positioned downstream of the APP signal peptide coding region, was generated by Dr. Kate Fisher. To produce a plasmid encoding sAPP β ₆₉₅, a stop codon was introduced 48 nucleotides upstream of the 3' sAPP α stop codon through site directed mutagenesis. Insertion of the stop codon was confirmed through analysis of the plasmid DNA sequence (performed by Eurofins Genomics). DNA sequence data were translated using ExPASy, available at: <https://www.expasy.org/>. Alignment against the APP₆₉₅ sequence was performed using Clustal Omega, available at <https://www.ebi.ac.uk/Tools/msa/clustalo/>.

APP, amyloid precursor protein; r_sAPP α , recombinant sAPP α ; r_sAPP β , recombinant sAPP β . The sAPP α plasmid and DNA sequence data were generated and provided by Dr. Kate Fisher. The APP₆₉₅ amino acid sequence was obtained from Uniprot (available at <https://www.uniprot.org/>).

3.3. Expression and purification of recombinant his-tagged sAPP α and sAPP β .

Due to the potential importance of eukaryotic PTMs in the function of sAPP α and sAPP β , recombinant plasmids encoding human sAPP α and sAPP β were stably transfected into HEK293 cells rather than a prokaryotic cell line. The resulting cell lines were referred to as 'HEK-sAPP α ' and 'HEK-sAPP β ' cells, respectively.

The expression of sAPP α and sAPP β in the HEK-sAPP α and HEK-sAPP β cell lines, respectively, was confirmed through immunoblotting. Transfection greatly increased the secretion of either sAPP α or sAPP β from each respective cell line compared to untransfected HEK cells (Figure 3.2a). Following this, a protocol was optimised for the non-denaturing purification of His-tagged secreted proteins from the HEK cell conditioned medium through immobilised metal affinity chromatography (IMAC) using Ni-NTA resin (Figure 3.2b, Figure 3.2c). Samples were taken at each relevant point of the purification process and analysed by SDS-PAGE and coomassie staining (Figure 3.2b, Figure 3.2c). The protocol successfully purified sAPP α (Figure 3.2b) and sAPP β (Figure 3.2c) to a high degree of purity. This purification process yielded approximately 0.6 mg/mL in 200 μ L of sAPP α , and 1.2 mg/mL in 200 μ L of sAPP β per experiment.

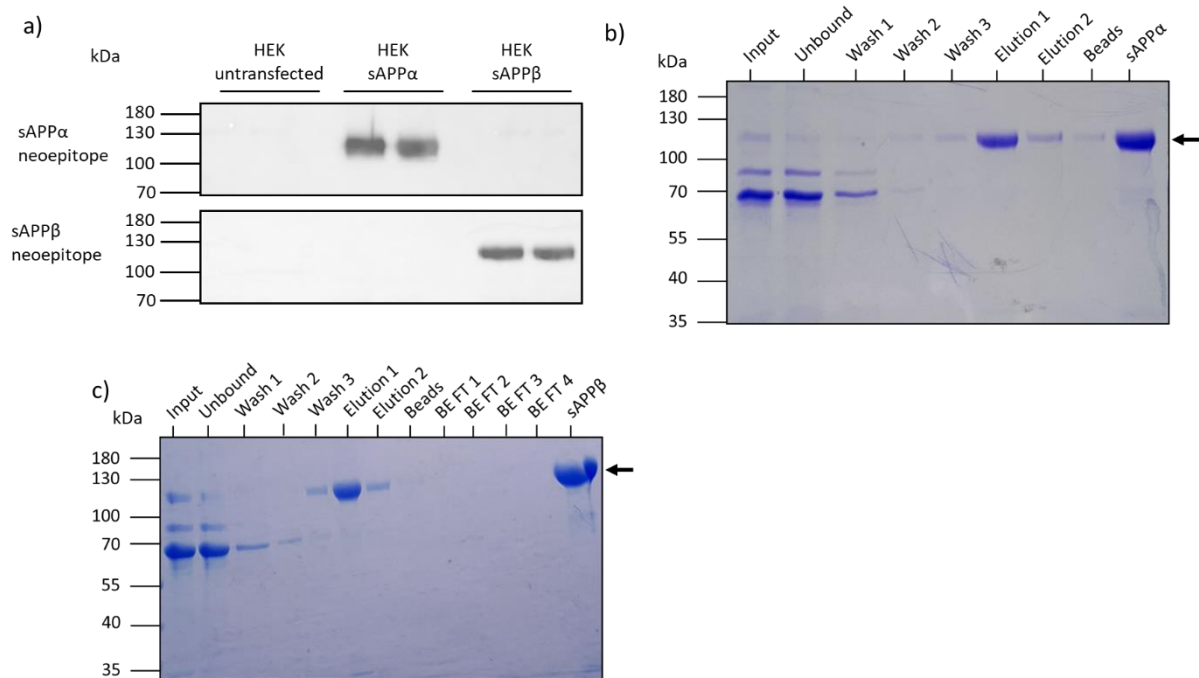


Figure 3.2. The purification of N-terminal His-tagged recombinant human sAPPα and sAPPβ from HEK cells.

(a) HEK293 cells, either untransfected or stably transfected with the cDNA encoding His-tagged sAPPα or His-tagged sAPPβ, were incubated in OptiMEM medium for 72 h at 37 °C. Total medium was harvested and 30 µg total protein was analysed through immunoblotting using either an antibody directed against the human sAPPα neoepitope (2B3) or the human sAPPβ neoepitope (1A9), as indicated. Technical replicates from each respective flask were loaded in duplicate. (b) A representative gel image from a single sAPPα purification. (c) A representative gel image from a single sAPPβ purification. Extra lanes were included to determine protein loss during buffer exchange (buffer exchange flow throughs 'BE FT' 1-4). Black arrows indicate the desired recombinant protein.

The proteins purified from the HEK-sAPP α and HEK-sAPP β cell lines through IMAC were confirmed as sAPP α and sAPP β , respectively, through immunoblotting with site-specific antibodies (Figure 3.3) and GeLC-MS/MS (Figure 3.4; Table 3.1). An antibody specifically directed against the neoepitope formed on the C-terminus of sAPP α following cleavage by ADAM10 successfully recognised the protein purified from HEK-sAPP α cells, but not the protein purified from HEK-sAPP β cells (Figure 3.3a). Similarly, an antibody (6E10) directed against APP 599-604, an epitope present in sAPP α but not sAPP β , only recognised the protein purified from HEK-sAPP α cells (Figure 3.3b). Conversely, antibodies directed against the neoepitope formed on the C-terminus of sAPP β following cleavage by BACE1 only recognised the protein purified from HEK-sAPP β cells (Figure 3.3c). Both purified sAPP α and sAPP β were recognised by an antibody directed towards the N-terminus of APP (amino acids 66-81) with a slight molecular weight shift visible between the two proteins (Figure 3.3d), consistent with sAPP β being 16 amino acids smaller than sAPP α . These results confirmed that the identities of the proteins overexpressed and purified from the two HEK cell lines were sAPP α and sAPP β .

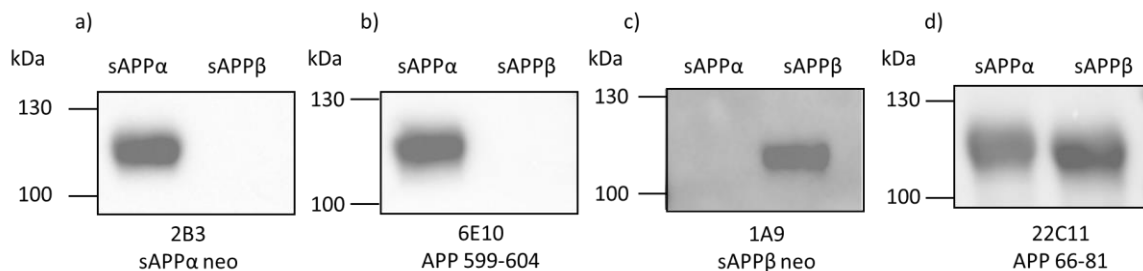


Figure 3.3. Characterisation of recombinant human sAPP α and sAPP β through immunoblotting.

Immunoblot analysis of protein purified from the conditioned medium of HEK-sAPP α and HEK-sAPP β cells. Samples were subjected to SDS-PAGE and immunoblotting. The membranes were incubated with the indicated primary antibodies (a) sAPP α C-terminal neoepitope (2B3); (b) APP 599-604 (6E10) (c) sAPP β C-terminal neoepitope (1A9); (d) APP 66-81 (22C11) and imaged using the Pierce enhanced chemiluminescence detection system. 0.5 μ g of purified protein was loaded per lane.

Samples from the IMAC purification of conditioned medium from HEK-sAPP α cells samples were interrogated further through SDS-PAGE and GeLC-MS/MS. Samples from a single sAPP α purification were analysed through SDS-PAGE with coomassie blue staining (Figure 3.4). Four protein bands of interest were excised and their protein components were identified through GeLC-MS/MS (Figure 3.4; Table 3.1). The band predicted to contain purified sAPP α was analysed (Figure 3.4a, band B), along with the band of corresponding molecular weight from the pre-purification 'input' lane (Figure 3.4a, band A). Band A was identified as 'APP' and contained peptide spectra located within the KPI and OX-2 domains present in APP and sAPP α / β derived from the APP₇₅₁ and APP₇₇₀ isoforms, likely due to the production of endogenous APP and sAPP α / β in HEK cells (Figure 3.4 band A; Figure 3.5a). However, the protein purified by IMAC did not contain any peptide spectra within the KPI and OX-2 domains, indicating that only the His-tagged sAPP α ₆₉₅ isoform was purified as desired (Figure 3.4 band B; Figure 3.5b). Band D was also of interest because it persisted following the IMAC purification process, so it and the corresponding band in the input medium (band C) were also analysed by GeLC-MS/MS. Band D was identified as a mid-to-C terminal fragment of APP; likely a fragment of His-tagged sAPP α that was purified due to its overexpression in the cell line (Table 3.1; Figure 3.5c). The corresponding band from the 'input' pre-purification lane did not identify APP, though this could be due to the presence of other proteins masking the low spectral count of the APP fragment (Figure 3.4 band C; Table 3.1).

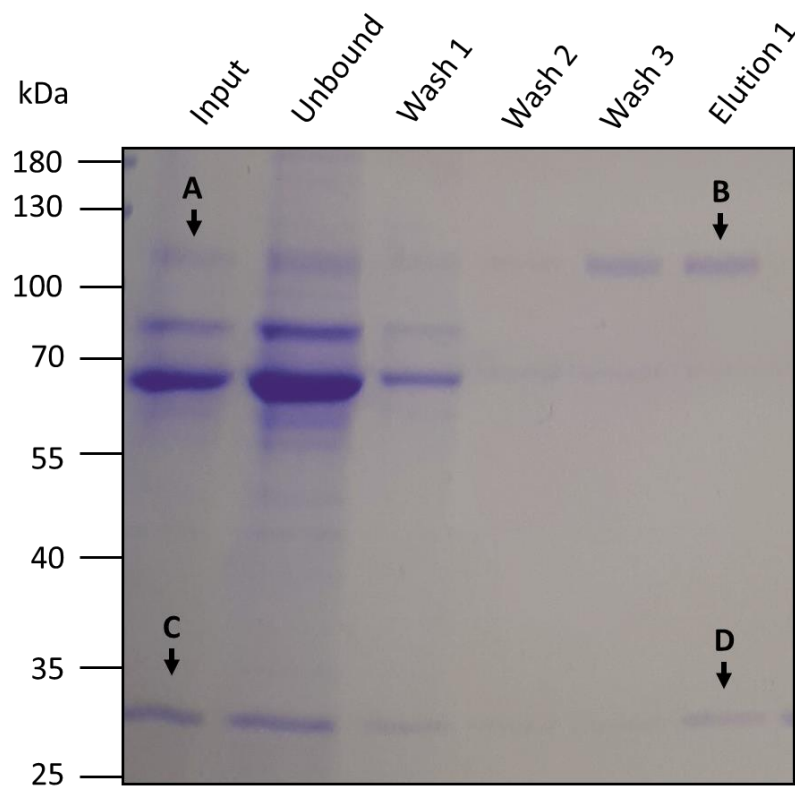


Figure 3.4. The protein purified from HEK-sAPP α cells was identified as APP through GeLC-MS/MS.

Conditioned medium from HEK cells expressing sAPP α was harvested over a 72 h period and His-tagged protein was purified through IMAC (Section 2.3). Samples were subjected to SDS-PAGE and the gel was stained with coomassie blue. Bands A-D were excised from the gel and their protein components were interrogated through GeLC-MS/MS (Table 3.1), performed by the BioMS core facility at the University of Manchester.

Table 3.1. Spectral counts for GeLC-MS/MS analysis of the protein purified from HEK-sAPP α cells.

Conditioned medium from HEK cells expressing sAPP α was harvested over a 72 h period and His-tagged protein was purified using IMAC (Section 2.3). Samples were subjected to SDS-PAGE and the gel was stained with coomassie blue. Bands A-D were excised from the gel and protein identities interrogated through GeLC-MS/MS (Figure 3.4), performed by the BioMS core facility at the University of Manchester. GeLC-MS/MS results were processed and viewed using Scaffold (99.9% protein threshold, 80% peptide threshold, min #2 peptides). Numbers shown correspond to total spectral counts for each excised protein band.

Protein identity	Protein band (total spectral counts)			
	A	B	C	D
APP (Homo sapiens)	110	118	0	6

(a) Band A

11 exclusive unique peptides, 19 exclusive unique spectra, 110 total spectra, 125/770 amino acids (16% coverage)

MLPGLALLLLAAWTARALEVFTDGNAGLLAE PQIAMFCGR LNMHNMVQNGK **TPDPFSGTK** 60
 TCIDTKEGILQYQCEVYPQLQITNVVEANQPVTIQNWCKRGRKQCKTHPHFVIPYR **CLVG** 120
 EFVSDALLVPDKCKFLHQERMDVCETHLHWHTVAKETCSEKSTNLHDYGMLPCGIDKFR 180
 GVEFVCCPLAEESDNVDSADAEEDSDVWVGADTDYADGSEDKVVEVAEEEEVAEVEE 240
 EADDDDEDDGDEVEEEAEFPYEATERITTSIATTTTTTSVEEVV **REVCSEQAETGPG** 300
 RAMISRWFVDVTEGK **APFFYGGCGGNRNNFDTEEYCMVCGSAMSQSLLKTTQEPLARD** 360
 FV **KLPTTA**ASTPDAVDKYLETPGDENEHAFQKAKERLEAKHRERMSQVMR **QWEEAERQA** 420
 KNLPKADKKAIVQHFOEK **ESLTCFAANR**QQLVETHMAR **YAMINR**RRLALENYITAL 480
 QAVPRPRHVFNM LKKYVRAEQKDRQHTLKHFEHVRMVDPKKAAQIRSQVMTHLRVIYER 540
 MNQSLSLLYNVPFAVEEIQDEVDLLQK **QNYSDVPLANNHSEPRISTYGNKALMPSLT** 600
ITIVLELLPVNGEFSDDLQFWHSFGADSVFANTENEVEFVDARPAADRGILTRPGSGLTN 660
 IKTEEISEVQM **DAEFRHDSGYEVHHQ**KLVFFAEDVGSNGKAIIGLMVGGVVIATVIVITL 720
 VMLKKKQYTSIHGGVVEVDRAVTPEERHLSKMQQNGYENPTYKFFEQMQN 770

(b) Band B

9 exclusive unique peptides, 17 exclusive unique spectra, 118 total spectra, 99/770 amino acids (13% coverage)

MLPGLALLLLAAWTARALEVFTDGNAGLLAE PQIAMFCGR LNMHNMVQNGK **TPDPFSGTK** 60
 TCIDTKEGILQYQCEVYPQLQITNVVEANQPVTIQNWCKRGRKQCKTHPHFVIPYR **CLVG** 120
 EFVSDALLVPDKCKFLHQERMDVCETHLHWHTVAKETCSEKSTNLHDYGMLPCGIDKFR 180
 GVEFVCCPLAEESDNVDSADAEEDSDVWVGADTDYADGSEDKVVEVAEEEEVAEVEE 240
 EADDDDEDDGDEVEEEAEFPYEATERITTSIATTTTTTSVEEVV **REVCSEQAETGPG** 300
 RAMISRWFVDVTEGKAPFFYGGCGGNRNNFDTEEYCMVCGSAMSQSLLKTTQEPLARD 360
 FV **KLPTTA**ASTPDAVDKYLETPGDENEHAFQKAKERLEAKHRERMSQVMR **QWEEAERQA** 420
 KNLPKADKKAIVQHFOEK **ESLTCFAANR**QQLVETHMAR **YAMINR**RRLALENYITAL 480
 QAVPRPRHVFNM LKKYVRAEQKDRQHTLKHFEHVRMVDPKKAAQIRSQVMTHLRVIYER 540
 MNQSLSLLYNVPFAVEEIQDEVDLLQK **QNYSDVPLANNHSEPRISTYGNKALMPSLT** 600
ITIVLELLPVNGEFSDDLQFWHSFGADSVFANTENEVEFVDARPAADRGILTRPGSGLTN 660
 IKTEEISEVQM **DAEFRHDSGYEVHHQ**KLVFFAEDVGSNGKAIIGLMVGGVVIATVIVITL 720
 VMLKKKQYTSIHGGVVEVDRAVTPEERHLSKMQQNGYENPTYKFFEQMQN 770

(c) Band D

3 exclusive unique peptides, 5 exclusive unique spectra, 6 total spectra, 45/770 amino acids (6% coverage)

MLPGLALLLLAAWTARALEVFTDGNAGLLAE PQIAMFCGR LNMHNMVQNGK **TPDPFSGTK** 60
 TCIDTKEGILQYQCEVYPQLQITNVVEANQPVTIQNWCKRGRKQCKTHPHFVIPYR **CLVG** 120
 EFVSDALLVPDKCKFLHQERMDVCETHLHWHTVAKETCSEKSTNLHDYGMLPCGIDKFR 180
 GVEFVCCPLAEESDNVDSADAEEDSDVWVGADTDYADGSEDKVVEVAEEEEVAEVEE 240
 EADDDDEDDGDEVEEEAEFPYEATERITTSIATTTTTTSVEEVV **REVCSEQAETGPG** 300
 RAMISRWFVDVTEGKAPFFYGGCGGNRNNFDTEEYCMVCGSAMSQSLLKTTQEPLARD 360
 FV **KLPTTA**ASTPDAVDKYLETPGDENEHAFQKAKERLEAKHRERMSQVMR **QWEEAERQA** 420
 KNLPKADKKAIVQHFOEK **ESLTCFAANR**QQLVETHMAR **YAMINR**RRLALENYITAL 480
 QAVPRPRHVFNM LKKYVRAEQKDRQHTLKHFEHVRMVDPKKAAQIRSQVMTHLRVIYER 540
 MNQSLSLLYNVPFAVEEIQDEVDLLQK **QNYSDVPLANNHSEPRISTYGNKALMPSLT** 600
ITIVLELLPVNGEFSDDLQFWHSFGADSVFANTENEVEFVDARPAADRGILTRPGSGLTN 660
 IKTEEISEVQM **DAEFRHDSGYEVHHQ**KLVFFAEDVGSNGKAIIGLMVGGVVIATVIVITL 720
 VMLKKKQYTSIHGGVVEVDRAVTPEERHLSKMQQNGYENPTYKFFEQMQN 770

Figure 3.5. Spectra identified from sAPP α purification excised bands.

Conditioned medium from HEK cells expressing sAPP α was harvested and His-tagged protein was purified through IMAC (Section 2.3). Samples were subjected to SDS-PAGE and the gel was stained with coomassie blue. Bands of interest (Figure 3.4) were excised from the gel and protein identities were interrogated through GeLC-MS/MS (Table 3.1). GeLC-MS/MS results were processed and viewed using Scaffold (99.9% protein threshold, 80% peptide threshold, min #2 peptides) for (a) band A; (b) band B; (c) band D. Identified peptide spectra are highlighted in green within the APP₇₇₀ sequence. The KPI and OX-2 domains, which are not present in sAPP α ₆₉₅, are surrounded by a black box. The final 16 amino acids of sAPP α (A β 1-16) are shown in red font. The signal peptide, not present in mature sAPP α , is highlighted in yellow.

3.4. Immunoblot comparison of the purified sAPP α with commercial sAPP α .

The sAPP α produced and purified in the lab was compared to N-terminal His-tagged sAPP α purchased commercially (Sigma #S9564) through immunoblotting (Figure 3.6). Both proteins were recognised by an N-terminal region antibody (APP 66-81), but there was a slight molecular weight shift between them (Figure 3.6a). This shift in molecular weight could be due to the presence of human PTMs on the sAPP α purified in the lab, as it was produced in HEK cells rather than in *E. coli*. There was also a discrepancy in band intensity, despite equal protein loading. The antibody directed against APP 599-604 (6E10), near the C-terminus of sAPP α , had an even larger discrepancy in band intensity between the two proteins (Figure 3.6b). Finally, there was almost no relative staining of commercial sAPP α with the C-terminal neoepitope antibody (2B3) (Figure 3.6c), though a band in the commercial sAPP α lane became visible with a longer exposure time. These results suggested that the C-terminal end of the commercial protein may have been acted on by carboxypeptidases and further highlighted the potential superior characteristics of the in-house lab sAPP α .

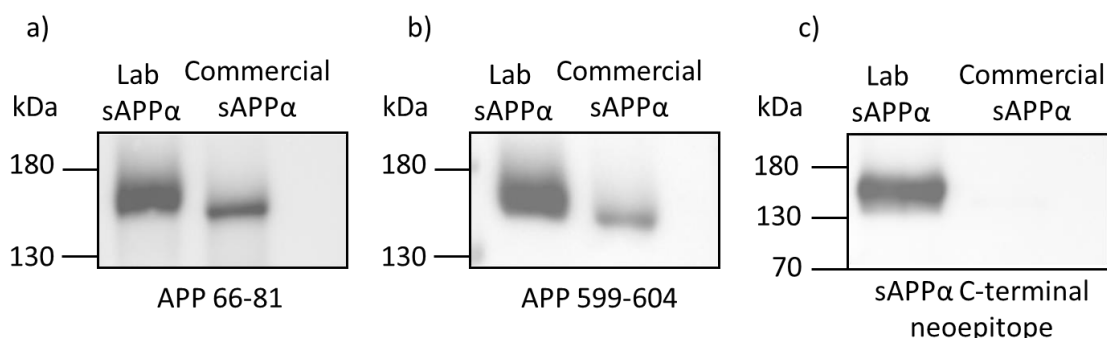


Figure 3.6. Immunoblot comparison of lab purified sAPP α with commercial sAPP α .

Lab purified sAPP α and commercial sAPP α (Sigma #S9564) were subjected to SDS-PAGE and immunoblotting. 0.5 μ g total protein was loaded per lane. The membranes were incubated in different primary antibodies: (a) APP 66-81 (22C11); (b) APP 599-604 (6E10); (c) sAPP α C-terminal neoepitope (2B3).

3.5. Biophysical analysis of lab purified sAPP α and sAPP β .

The biophysical characteristics of the lab-purified sAPP α and sAPP β , such as protein solubility and aggregation, were analysed through multi-angle light scattering (MALS) (Figure 3.7). Light scattering (LS) (red) indicated with aggregated protein and the refractive index (dRI) (blue)

indicated soluble protein. The UV (green) trace indicated the total protein present in each fraction. The vast majority of both sAPP α and sAPP β UV traces overlayed with the dRI curve, showing that both proteins were predominantly soluble and did not form aggregates in solution (Figure 3.7).

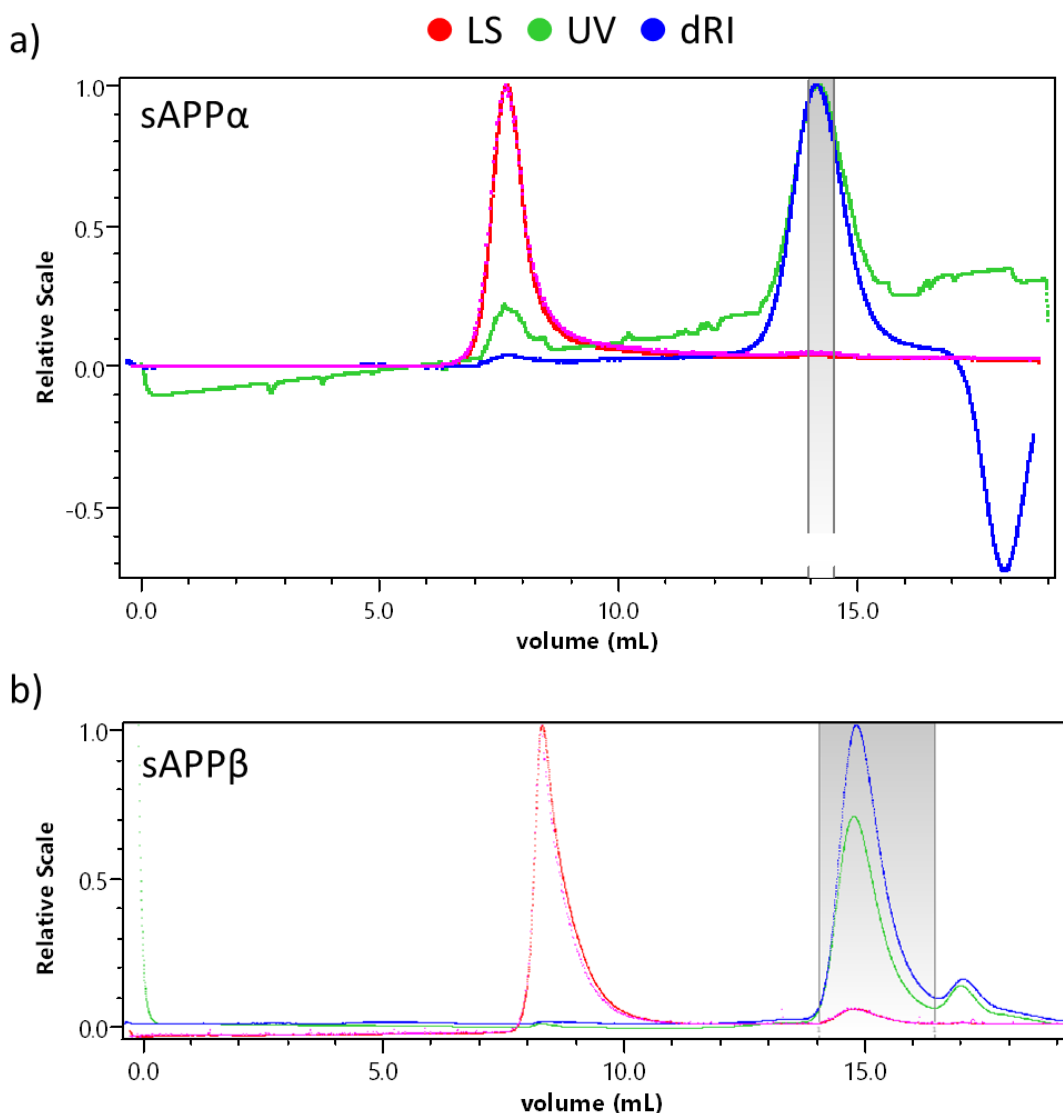


Figure 3.7. Analysis of purified sAPP α and sAPP β using multi-angle light scattering.

Multi-angle light scattering analysis was performed by Dr. Thomas Jowitt at the University of Manchester Biomolecular Analysis Facility using a DAWN EOS 18-angle light scattering detector (Wyatt) (a) MALS analysis of recombinant sAPP α . (b) MALS analysis of recombinant sAPP β . LS = light scattering; UV = absorbance at 280 nm; dRI = differential refractive index. The predominantly soluble protein fraction is highlighted in dark blue. Axes were re-labelled for clarity of presentation.

Further biophysical analysis of sAPP α , the main protein of interest for this study, was performed through analytical centrifugation (AUC) (Figure 3.8). The sigmoidal nature and distinct boundaries of the sedimentation curves indicated a highly pure protein sample (Figure 3.8a). A single sedimentation coefficient peak indicated that the vast majority of sAPP α was homogenous in solution, as different aggregates would have given several defined peaks (Figure 3.8b).

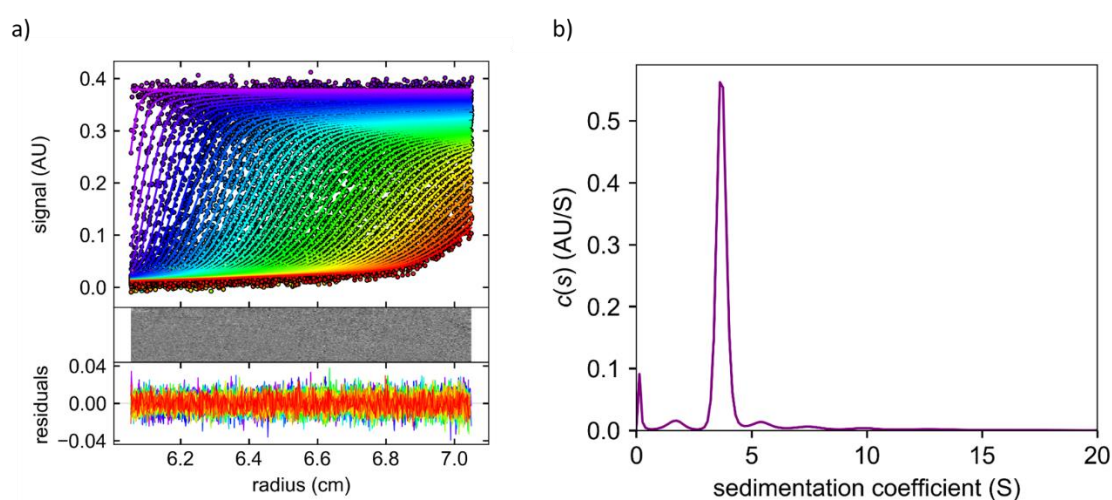


Figure 3.8. Analysis of purified sAPP α using analytical ultracentrifugation.

Analytical ultracentrifugation was performed by Dr. Thomas Jowitt at the University of Manchester Biomolecular Analysis Facility. Sedimentation was performed with a purified sample of 100 μ g sAPP α and a wavelength of 230 nm at 40,000 rpm using an OptiMA XLA analytical ultracentrifuge (Beckman Coulter).

3.6. Discussion.

This chapter describes the production and purification of sAPP α and sAPP β from human cells for use in downstream functional assays and unbiased receptor identification experiments.

3.6.1. Generation of HEK293 cell lines overexpressing N-terminal hexahistidine tagged sAPP α or sAPP β .

Certain previous studies, such as (Rice et al. 2019), used sAPP α produced in *E. coli* for receptor identification experiments. Whilst the use of *E. coli* has benefits, such as the rapid production of large amounts of protein, there are also limitations. For example, proteins produced in *E. coli* lack potentially important eukaryotic (PTMs) (Tan et al. 2021). Several phosphorylation sites (Ser₁₉₈ and Ser₂₀₆) and O-glycosylation sites (Thr₂₉₁, Thr₂₉₂ and Thr₅₇₆) have been identified in sAPP α and sAPP β *in vitro* (Perdivara et al. 2009). At least two further N-glycosylation sites have also been predicted in both proteins (Asn₄₆₇ and Asn₄₉₆) (Yazaki et al. 1996). Additional sites have been identified in human samples such as Tyr₆₀₆, which lies within the sAPP α -specific C-terminal 16 amino acid region, which was O-glycosylated in human CSF samples (Halim et al. 2011). Though PTMs were found not to be necessary for the promotion of axon outgrowth by either sAPP α or sAPP β (Chasseigneaux et al. 2011), O-glycosylation is known to potentially modulate protein stability and receptor interaction and so could be critical for other functions (Madsen et al. 2020). Thus, the sAPP α -specific O-glycosylation site of Tyr₅₈₉ could contribute to sAPP α -specific effects. Therefore, producing a protein with physiologically accurate PTMs could be critically important to protein activity and therefore receptor identification in human cells. Therefore, human His-tagged sAPP α and sAPP β were produced and purified using HEK cells.

Because the C-terminus appears critical in the enhanced neuroprotective activity of sAPP α over sAPP β (Richter et al. 2018), it was hypothesised that the C-terminus may play a crucial role in binding to the unknown neuroprotective receptor. Thus, a hexahistidine tag was attached at the N-terminus to prevent possible interference with neuroprotective activity and receptor binding at the C-terminus. A previous study identified GABA_BR₁ as an sAPP α receptor in synaptosomes (Rice et al. 2019), however it used sAPP α with a large C-terminal Fc tag which could have impacted important C-terminal interactions. The study which identified p75^{NTR} as a receptor used mouse sAPP α rather than the human sAPP α sequence (Hasebe et al. 2013). Human sAPP α differs from mouse sAPP α at several sites, including three amino acid changes

within the A β 1-16 sequence specific to sAPP α over sAPP β (sAPP α 601 R->G, 606 Y->F and 609 H->R) (Xu et al. 2015). These amino acids changes at the mouse sAPP α C-terminus could impact the protein activity or receptor binding which facilitates the greater level of neuroprotection by sAPP α over sAPP β (Furukawa et al. 1996). Thus, we hypothesised that previous studies, though the use of C-terminally tagged sAPP α , mouse sAPP α or protein produced in *E. coli*, may not have facilitated the optimal identification of receptors responsible for the neuroprotective actions of sAPP α . Therefore, we used sAPP α produced in human cells and tagged at the N-terminus with a small hexahistidine tag.

DNA sequence verification and translation using online tools confirmed successful generation of both sAPP α and sAPP β encoding plasmids with N-terminal hexahistidine tags and glycine-serine-glycine spacers (Figure 3.1). The DNA sequences encoding sAPP α and sAPP β were positioned downstream of a kozak enhancer sequence to increase protein production. Comparison of media samples between HEK-untransfected, HEK-sAPP α and HEK-sAPP β cells confirmed a large increase in the secretion of each specific protein following transfection (Figure 3.2a).

3.6.2. IMAC-facilitated purification of hexahistidine tagged sAPP α and sAPP β .

The hexahistidine tag facilitated protein purification through IMAC. IMAC was chosen due to its non-denaturing conditions, ensuring the maintenance of correct protein folding and function (Hemdan et al. 1989). Following protein elution the imidazole, which is toxic and would also interfere with the BCA protein assay used to measure protein concentration, was replaced with DPBS using centrifugal concentrators which allowed buffer exchange but retained the protein sample. DPBS was chosen because the pH was more basic than the predicted isoelectric point of recombinant sAPP α (theoretical isoelectric point = 4.74) (<https://web.expasy.org/protparam>), which should result in high solubility (Zayas 1997). This high level of solubility was confirmed through biophysical analyses of purified sAPP α and sAPP β (Figures 3.7 and 3.8).

Protein identities were confirmed through immunoblotting with site-specific antibodies and GeLC-MS/MS (Figures 3.3, 3.4 and 3.5; Table 3.1). Hexahistidine sAPP α and sAPP β had predicted molecular weights of around 68.7 kDa and 66.8 kDa respectively, however they migrated on SDS-PAGE at much higher molecular due to their elongated nature and PTMs (Gralle et al. 2002). Immunoblotting confirmed that each purified protein bound their

respective highly specific neoepitope antibodies, giving strong evidence of their identity (Figure 3.3). The slight molecular weight shift seen between the two proteins suggested that the purified sAPP α was slightly larger than sAPP β , as expected due to the extra 16 amino acids (Figure 3.3d). The use of an antibody with an epitope towards the N-terminus (22C11) and C-terminal antibodies indicated that the full-length proteins were present.

GeLC-MS/MS results showed the presence of endogenous untagged APP/sAPP of larger isoforms (likely 751 and 770 isoforms) expressed by the HEK cells prior to purification, due to the presence of spectra identified within the KPI/OX-2 domains (Figure 3.5a, black boxes). However, no spectra were identified within the KPI or OX-2 domains in the purified protein band (Figure 3.5b) suggesting that only the His-tagged sAPP α_{695} isoform was purified, as desired. Identified fragments were distributed across the sAPP α sequence and no spectra were identified outside of the sAPP α sequence within APP. Interestingly, the same fragments were identified, apart from spectra within the KPI/OX-2 domain, between bands A and B. This could indicate that those specific spectra were the most stable peptide fragments generated through this specific GeLC-MS/MS method and therefore most likely to be identified. These data provided strong evidence that the purified 110 kDa 'band B' was hexahistidine-tagged sAPP α_{695} , as it survived the purification process and did not contain any spectra from within the KPI/OX-2 domains. Interestingly no spectra from APP were identified in band C (Table 3.1), however a small number of spectra from APP were identified in band D (Table 3.1; Figure 3.5c). The ~30 kDa band visible post-purification was identified as a fragment of APP/sAPP, though it was unexpectedly C-terminal (away from the hexahistidine tag) rather than N-terminal. This fragment could therefore not contain the His-tag as it is not large enough when considering the location of the spectra identified (Figure 3.5c). It may have associated with the full-length His-tagged protein and therefore bound to the Ni-NTA column indirectly, surviving the purification process until eluted and separated through SDS-PAGE. It was decided that the smaller fragment was unlikely to cause problems with receptor identification, as the amount of the fragment was often low relative to the amount of full-length protein (Figure 3.2c+d).

3.6.3. Comparison of lab-produced and commercially-acquired sAPP α .

The slight molecular weight shift seen between the in-house and commercial proteins (Figure 3.6a) is likely due to a lack of eukaryotic PTMs on the commercial protein. There is also an

indication of possible carboxypeptidase action at the C-terminus of the commercial sAPP α , as it was recognised to a much lesser degree by the site-specific sAPP α neoepitope antibody (2B3) (Figure 3.6c). Finally, though the same amount of total protein was loaded per lane, the bands for lab-produced sAPP α were more intense which suggested a purer sample. These results demonstrated that the in-house sAPP α was likely superior to the commercially available sAPP α for the purposes of this study.

3.6.4. Biophysical analyses of sAPP α and sAPP β confirmed expected solubilities and lack of aggregation.

Following the successful purification and identification of sAPP α and sAPP β , the final important step in protein production and validation was the verification of solubility and lack of aggregation or precipitation prior to downstream experiments. The small UV peak (green) which correlated with the light scattering peak (red) showed that a small amount of sAPP α aggregated; however, the much larger UV peak which correlated with the refractive index peak (blue) demonstrated that most of the protein was soluble (Figure 3.7a). Similar biophysical characteristics were found with sAPP β , which exhibited even less aggregation (Figure 3.7b). As sAPP α was the main protein of interest, it was further interrogated biophysically through AUC. AUC analysis showed a highly pure and homogenous protein sample, as shown by sigmoidal curves with distinct boundaries (Figure 3.8a). Sedimentation analysis showed that the protein was homogenous in solution, as a single main peak was resolved. A non-homogenous protein with several different aggregates would have resolved into several different peaks. Taken together, these biophysical analyses confirmed high solubility and a lack of aggregation for the purified sAPP α and sAPP β , as desired.

3.7. Chapter summary

This chapter demonstrated the robust production and purification of highly soluble recombinant N-terminal hexahistidine tagged sAPP α and sAPP β from human HEK cells. This resulted in the reliable production of physiologically relevant sAPP α and sAPP β for use in downstream experiments investigating protein activity and protein interactions.

- HEK293 cells were transfected with plasmids encoding N-terminal His-tagged sAPP α and sAPP β under the transcriptional control of a 5' kozak enhancer sequence.

- Overexpression and secretion of sAPP α and sAPP β in each respective HEK cell line was demonstrated, confirming successful plasmid transfection.
- Each His-tagged protein was successfully purified from the complex HEK cell medium under non-denaturing conditions.
- The identity of each purified protein was confirmed as sAPP α or sAPP β through immunoblotting and GeLC-MS/MS.
- In-house sAPP α was compared with commercially acquired sAPP α and found to be likely superior for the purposes of this study.
- Biophysical analyses of in-house sAPP α and sAPP β demonstrated protein solubility. sAPP α was found to be highly homogenous in solution.

4. The binding and protective effects of soluble APP to neuronal cells

4.1. Introduction.

The lack of success in clinical trials for disease-modifying AD treatments has emphasised the need for novel therapies and drug targets (Cummings et al. 2014). The ongoing loss of neurons in AD results in progressive cognitive decline (Arendt et al. 2015). For example, compared with healthy aged brains, the mean number of neurons in the nucleus basalis of Meynert (a major source of cholinergic neurons into the cerebral cortex) was 33% lower in mild dementia, 61% lower in moderate dementia and 83% lower in severe dementia (Arendt et al. 2015). Synaptic loss correlates with cognitive decline in AD and, more specifically, pre-synaptic markers appear to be more affected than post-synaptic markers (de Wilde et al. 2016). The correlation between synaptic loss and cognitive decline was particularly pronounced in the hippocampus (de Wilde et al. 2016). The loss of hippocampal synaptophysin, a presynaptic vesicle protein and marker of synaptic density (Roch et al. 1994), correlated directly with cognitive decline in AD (Sze et al. 1997). Similarly, the loss of the presynaptic vesicular glutamate transporter VGLUT1 also correlated with the progression of cognitive decline in AD (Kashani et al. 2008). Thirdly, the level of the post-synaptic scaffold protein PSD95 was also significantly reduced in an age-dependent manner in the apical dendrites of the hippocampus, known for excitatory synapses, in the 5xFAD mouse model (Shao et al. 2011). Therefore, increasing neuron density and specifically synaptic density with neurotrophic molecules could help to slow cognitive decline in AD. sAPP α has been shown to promote neurotrophism (Habib et al. 2017). Three days of subcutaneous infusion with amino acids 319-336 of sAPP α ₆₉₅ significantly increased the number of presynaptic terminals, marked by synaptophysin immunoreactivity, in the frontoparietal cortex of rats (Roch et al. 1994). This resulted in significantly improved memory retention in a subset of aged rats (Roch et al. 1994), demonstrating a direct link between sAPP α treatment and improvements in memory *in vivo*. Thus, sAPP α could potentially slow synaptic loss in AD and therefore the associated cognitive decline.

Another mechanism through which neurons are damaged during neurodegeneration is oxidative stress (Huang et al. 2016). The brain has a high oxygen consumption rate, which

results in the production of a large amount of ROS, and therefore it is exposed to high levels of oxidative stress throughout an individual's lifespan (Huang et al. 2016). In fact, the free radical theory of ageing suggested that aged tissues progressively accumulated oxidatively damaged molecules over time, leading to adverse alterations in cell structure and function (Huang et al. 2016). This effect could be particularly pronounced in neurons, which are generally considered to be post-mitotic, terminally differentiated cells that would therefore accumulate oxidatively-damaged molecules (Aranda-Anzaldo 2012). Oxidative stress is one of the key mechanisms of neuronal damage in neurodegenerative diseases such as AD, and is linked with both A β and tau accumulation (Huang et al. 2016). Consistently, markers of oxidative stress were increased in AD brains compared to healthy controls (Butterfield and Lauderback 2002; Mandal et al. 2012). A β increased the generation of ROS in astrocytes (Abramov et al. 2004) and ROS such as H₂O₂ may also contribute to the aggregation of A β (Dyrks et al. 1993), which could lead to a toxic positive feedback loop. H₂O₂ also reduced neuron viability by 50% within 3 h (Whittemore et al. 1995). sAPP α has been shown in previous studies to protect against oxidative stress (Goodman and Mattson 1994). For example, incubation of cultured neurons with sAPP α for 24 h significantly reduced the generation of ROS upon treatment with A β oligomers (A β Os) (Goodman and Mattson 1994). In contrast, sAPP β was shown to be 100-times less neuroprotective than sAPP α (Furukawa et al. 1996). If such a protective effect of sAPP α against oxidative stress could be harnessed, it could help protect against neuronal damage and therefore slow cognitive decline in neurodegenerative diseases such as AD.

Chapter 3 demonstrated the successful production and purification of human hexahistidine-tagged sAPP α and sAPP β . Following this, it was important to confirm that purified sAPP α bound to cells and exhibited effects consistent with the published literature. The ability to produce both sAPP α and sAPP β also allowed for a direct comparison of both proteins, to investigate the possible causes for the enhanced protective effect of sAPP α (Goodman and Mattson 1994). Therefore, this chapter investigated several potential effects of sAPP α and, where possible, compared sAPP α and sAPP β using hiPSC-derived cortical neurons and immortalised neuroblastoma cells. The effects of sAPP α have only been directly compared with sAPP β in a small number of studies (Chasseigneaux et al. 2011; Furukawa et al. 1996).

4.1.1. Chapter aims.

The aims of this chapter were to:

- Generate and characterise iPSC-derived human cortical neurons.
- Demonstrate that sAPP α and sAPP β bind effectively to iPSC-derived human cortical neurons.
- Compare the effects of sAPP α and sAPP β on the expression of synaptic proteins in iPSC-derived human cortical neurons.
- Demonstrate that sAPP α and sAPP β bind to neuroblastoma cells. Determine whether successful binding is specific to the active form of the protein. Compare the binding properties, such as effective concentration and speed of binding, of sAPP α with sAPP β .
- Investigate the neuroprotective ability of sAPP α to reduce the generation of reactive oxygen species in neuroblastoma cells following chemical insult.

4.2. The generation of iPSC-derived human neurons.

iPSC-derived human cortical neurons were differentiated from OX1-19 human induced pluripotent stem cells following an established protocol (Section 2.13) (Figure 4.1a) (Shi et al. 2012). Briefly, human OX1-19 iPSCs were passaged in the presence of Rho kinase inhibitor, followed by incubation in neural induction medium until day 12 (Figure 4.1a). Then, cells were passaged and incubated in neuronal maintenance medium (NMM) containing FGF for 4 days (Figure 4.1a). The FGF was removed and cells were incubated in NMM until the appearance of neuronal rosettes, at which point they were passaged and incubated in NMM until day 35. Finally, the cells were passaged for the last time and fed with NMM as required until at least day 70, when they were ready for experimental use. A summary of the iPSC-derived neuron differentiation workflow is shown in Figure 4.1a. Following differentiation, the expression of the various cell markers was investigated through immunofluorescence microscopy (Figure 4.1b, 4.1c). S100B is primarily an astrocyte and oligodendrocyte marker, whilst GFAP is widely used as a marker of activated astrocytes (Du et al. 2021; Jurga et al. 2021). β III tubulin and MAP2 are markers of neuronal differentiation (Person et al. 2017; Soltani et al. 2005). SATB2 is a neuronal marker which binds DNA (Alcamo et al. 2008). Synaptophysin confirms the presence of nerve terminals and has previously been used to measure synaptic density (Dawson et al. 1999; Sze et al. 1997; Togo et al. 2021). Therefore, following the differentiation protocol, iPSC-derived neurons were generated as shown by the high expression of β III tubulin, MAP2 and SATB2 (Figure 4.1). Nerve terminals were formed, as demonstrated by the expression of synaptophysin (Figure 4.1b). However, other cells were also present, including astrocytes as shown by the positive GFAP staining (Figure 4.1b).

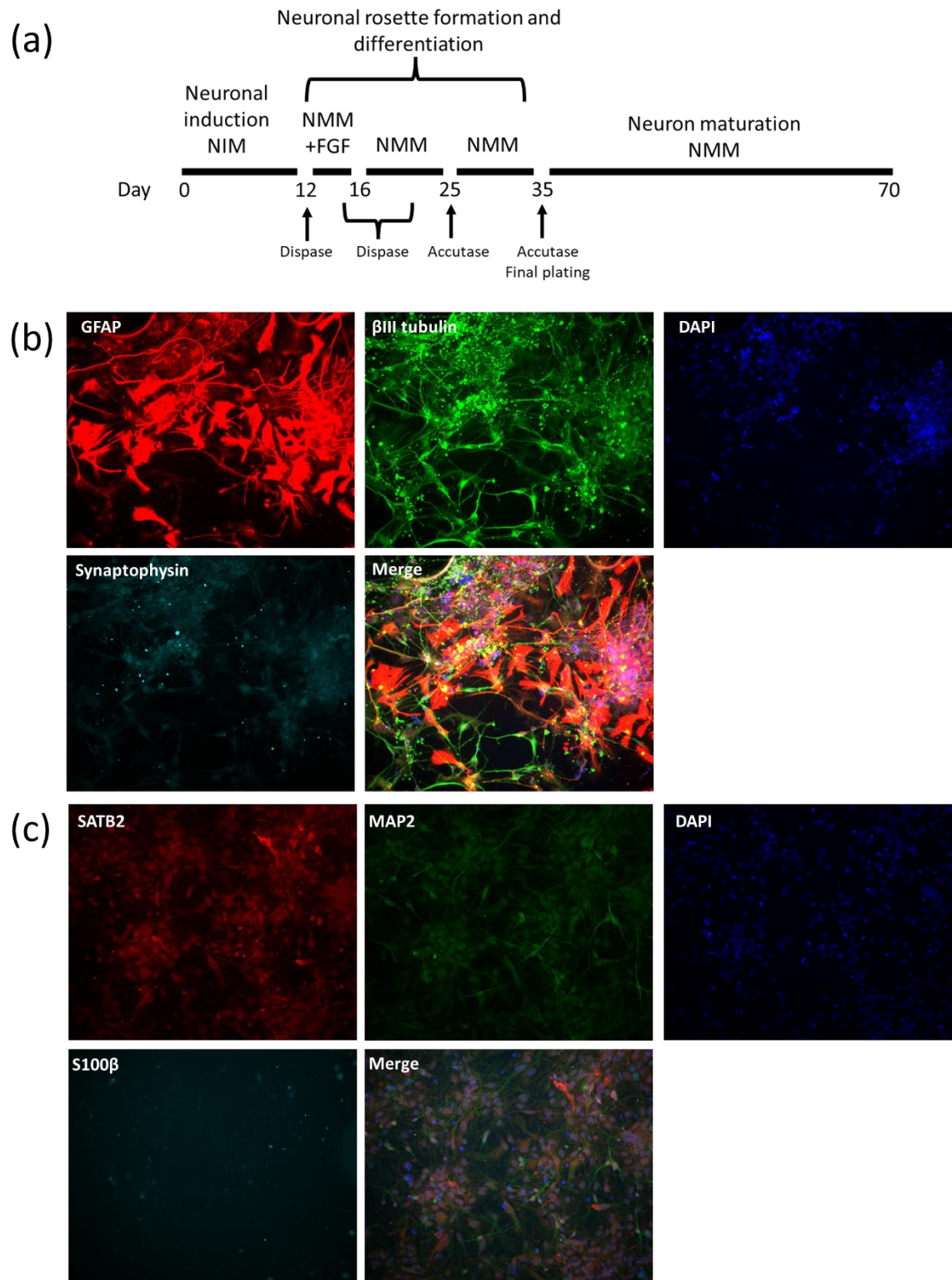


Figure 4.1. Generation and characterisation of iPSC-derived human cortical neurons.

(a) A summary of the workflow to generate hiPSC-derived cortical neurons from OX1-19 hiPSCs. Human OX1-19 iPSCs were passaged 2:1 in the presence of Rock Y-27632 inhibitor (#ab120129) into a single matrigel (Figure legend continues on following page)

(continuation of Figure 4.1 legend) coated well for 24 h. The medium was changed to neural induction medium (NIM) and the date recorded as day 0. NIM was refreshed daily until day 12, when the cells were detached using 10% dispase solution (v/v) and transferred plates previously coated with 1 ml 0.01% poly-L-ornithine solution (v/v) (Sigma P4957). The cells were incubated in neuronal maintenance medium (NMM) containing 20 ng/mL FGF for 4 days. FGF was then withdrawn and cells were incubated in NMM alone. Upon the appearance of neuronal rosettes, the cells were split 1:2 using dispase. At approximately day 25, the cells were passaged to single cells using accutase (Gibco A1110501), transferred to new wells coated using 10 µg/mL laminin (Sigma L2020) and incubated in NMM. The cells were passaged 1:2 upon confluence until day 35, when they were passaged for the final time into plates coated with 0.01% poly-L-ornithine solution (v/v) (Sigma P4957) to a density of 50-150,000 cells/cm². Cells were incubated in NMM until the neurons were used for experiments at day 70+. NMM was changed as required. (b) Day 93 iPSC-derived neurons were fixed in 4% PFA (v/v) and probed for GFAP, β III tubulin and synaptophysin. Cells were imaged using an Olympus IX83 inverted microscope and images were processed using ImageJ (false coloured). (c) Day 93 iPSC-derived neurons were fixed in 4% PFA (v/v) and probed for SATB2, MAP2 and S100 β . Cells were imaged using an Olympus IX83 inverted microscope at 60x magnification with Metamorph and Deltavision software. The imaging settings were as follows: GFAP, 300 ms exposure; β III 300 ms exposure; DAPI, 150 ms exposure; Synaptophysin, 100 ms exposure; SATB2, 150 ms exposure; MAP2, 300 ms exposure; DAPI, 150 ms exposure; S100 β , 100 ms exposure. Images were processed using ImageJ (false coloured).

4.3. Investigation of the binding of purified sAPP α and sAPP β to iPSC-derived human cortical neurons.

Prior to assessing the effects of sAPP α and sAPP β , the binding of each protein to hiPSC-derived neurons cells was investigated using a novel binding assay. First, various concentrations of purified sAPP α were incubated with iPSC-derived neurons. The cells were then washed and cell lysates were collected. The lysates were probed through immunoblotting using a specific sAPP α neoepitope antibody to detect sAPP α that had bound to the neurons and been retained. Concentrations of sAPP α above 30 nM were detected as binding to iPSC-derived neurons in this assay (Figure 4.2a). As sAPP α bound to iPSC-derived neurons within 30 min, the speed of binding was further interrogated. Purified recombinant sAPP α was incubated with iPSC-derived neurons for various times (Figure 4.2b). sAPP α bound rapidly to the neurons, within 10 min of administration (Figure 4.2b). These results demonstrated that recombinant sAPP α bound to iPSC-derived human neurons rapidly and at nanomolar concentrations. sAPP β was not able to be visualised through immunoblotting using the protocol develop for sAPP α , possibly due to the lower sensitivity of the sAPP β neoepitope antibody (1A9), so neuron lysates treated with sAPP β were analysed through a more sensitive multiplex immunoassay (Mesoscale Discovery) using an sAPP β -specific probe (Figure 4.2c). The immunoassay analysis established that sAPP β bound to the neurons (Figure 4.2c). Following this, the effects of sAPP α and sAPP β on hiPSC-derived neurons were investigated.

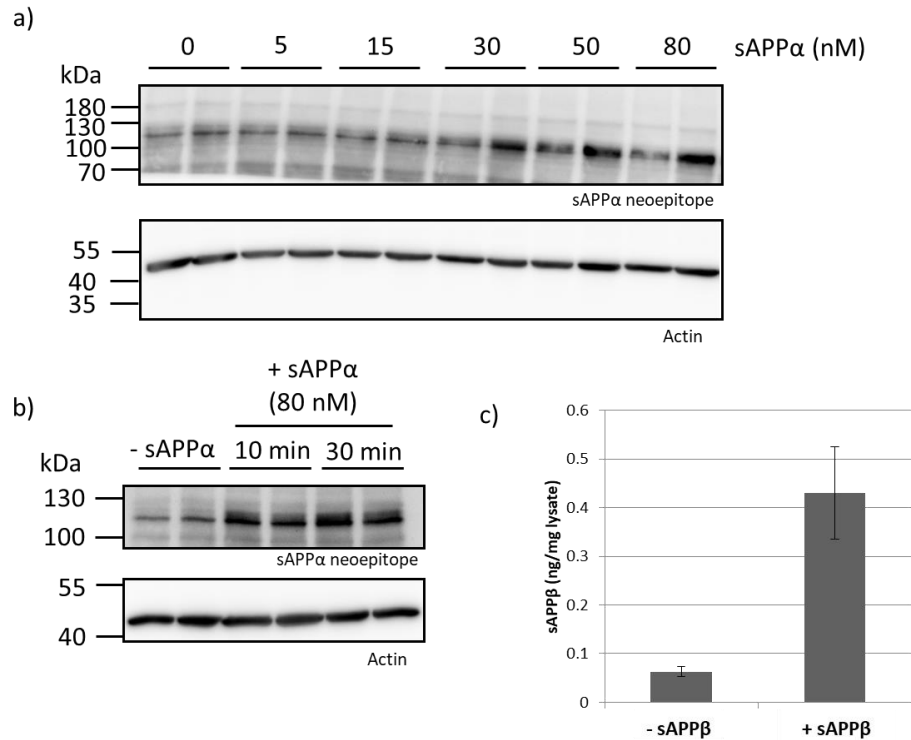


Figure 4.2. Recombinant sAPPα and sAPPβ bind to iPSC-derived human neurons.

(a) hiPSC-derived cortical neurons were incubated with purified recombinant sAPPα at the concentrations indicated for 30 min at 37 °C. The neurons were washed three times in DPBS, followed by lysate harvesting. Whole cell lysate (30 µg total protein) was loaded per lane in SDS-PAGE. Proteins were transferred to PVDF membrane and probed using the sAPPα neoepitope antibody (2B3). The membrane was re-probed for Actin. (b) hiPSC-derived cortical neurons were incubated with 80 nM sAPPα for 10 or 30 min alongside a vehicle control (-sAPPα). Three washes in DPBS were followed by lysate collection. 30 µg total lysate was loaded per lane in SDS-PAGE. Proteins were transferred to PVDF membrane and probed using a highly specific sAPPα neoepitope antibody. The membrane was re-probed for Actin. (c) 80 nM sAPPβ in OptiMEM was incubated with hiPSC-derived cortical neurons for 30 min. The neurons were washed three times in DPBS, followed by lysate harvesting. The presence of sAPPβ in the lysates was determined by Dr. Kate Fisher through multiplex immunoassay (mesoscale discovery) using an sAPPβ-specific probe (n = 4 per condition). Lysates were diluted 3:1 prior to analysis and the data was normalised to total protein amount. Error bars represent standard error of the mean.

4.4. Comparison of the effect of sAPP α and sAPP β on synaptic protein expression.

To measure and compare the effects of sAPP α and sAPP β on the expression of synaptic proteins *in vitro*, iPSC-derived human cortical neurons were incubated with either sAPP α , sAPP β or a vehicle control for 48 h. A total of three neuronal inductions were analysed with two wells per treatment condition. The concentrations of sAPP α or sAPP β used were either 15 nM or 50 nM. The cells were then harvested, lysates were prepared the expression of the synaptic proteins synaptophysin (Figure 4.3), VGLUT1 (Figure 4.4) and PSD95 (Figure 4.5) were investigated through immunoblotting. There was variability in the effect of sAPP α on synaptophysin expression between the three different inductions. In induction 3, 15 nM sAPP α significantly increased synaptophysin expression compared with the vehicle control ($p = 0.0201$), whilst 15 nM sAPP β had no significant effect ($p = 0.3614$) (Figure 4.3c; supplementary Table 7.4). 50 nM sAPP α also had no effect compared with vehicle in induction 3 ($p = >0.999$), so the observed effect on synaptophysin expression was specific to the lower dose of sAPP α (supplementary Table 7.4). There was no significant effect of any treatment compared to the vehicle control in the other two inductions (supplementary Tables 6.2; 6.3), and the effect on synaptophysin expression was just below significance when the data from all inductions were combined (Figure 4.3d; $p = 0.0869$, supplementary Table 7.1).

The expression of the pre-synaptic vesicle glutamate transporter protein VGLUT1 was also measured following the incubation of neurons with either sAPP α or sAPP β at concentrations of 15 nM or 50 nM for 48 h (Figure 4.4). There were no significant differences in the expression of VGLUT1 compared to the vehicle control following any of the treatments in induction 1, induction 2 or induction 3 (supplementary Tables 7.6-7.8). There was no significant effect compared to the vehicle control on VGLUT1 expression when all data was normalised and combined (Figure 4.4; $p = 0.9993$, supplementary Table 7.5).

Finally, the expression of PSD95 was measured through immunoblotting following 48 h incubation with either sAPP α or sAPP β at concentrations of 15 nM or 50 nM (Figure 4.5). One-way ANOVA analysis found no significant difference in PSD95 expression following any treatment compared to the vehicle control in any of the individual inductions (supplementary Tables 7.9-11) or when all inductions were combined ($p = 0.2302$, supplementary Table 7.12).

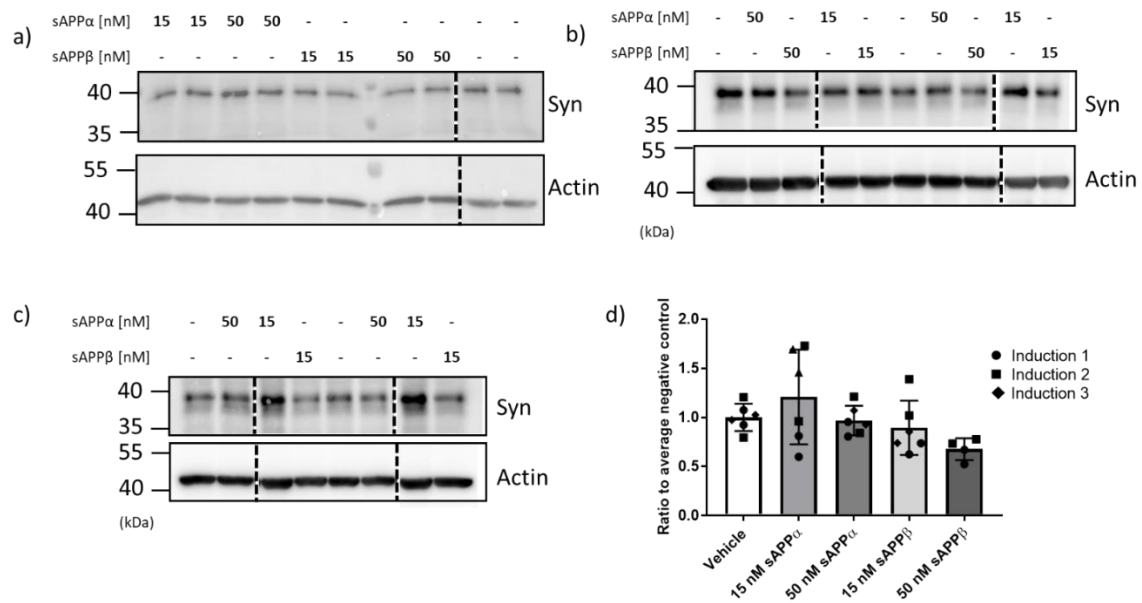


Figure 4.3. sAPPα significantly increased the expression of synaptophysin in certain hiPSC-derived neuron inductions.

hiPSC-derived cortical neurons were grown to day 73 and incubated with sAPPα or sAPPβ at concentrations of 15 nM or 50 nM for 48 h in NMM. Cells were washed three times in DPBS (+ metals), lysates were collected and subjected to SDS-PAGE with 30 µg total protein loaded per lane. Proteins were transferred to PVDF membrane and probed with anti-synaptophysin antibody (Table 2.1). Membranes were washed, blocked with 5% milk (w/v) and re-probed with anti-actin antibody. All lanes within each panel are from the same blot image, at the same brightness and contrast (full blots shown in supplementary Figure 7.1), but irrelevant lanes were removed for clarity of presentation. Dotted lines denote where irrelevant lanes were removed. Three inductions were used, with two wells of neurons per induction. (a) Induction 1; (b) Induction 2; (c) Induction 3. (d) Quantification of all inductions combined. Error bars represent standard deviation. Band intensity was quantified using ImageJ, normalised against actin and made relative to the mean expression of synaptophysin in the vehicle control. Statistics were performed using a one-way ANOVA with Tukey's post-hoc test in GraphPad Prism 7. Neurons treated with 50 nM sAPPβ for induction 3 were infected and so were not used. Synaptophysin estimated molecular weight = 34-39 kDa.

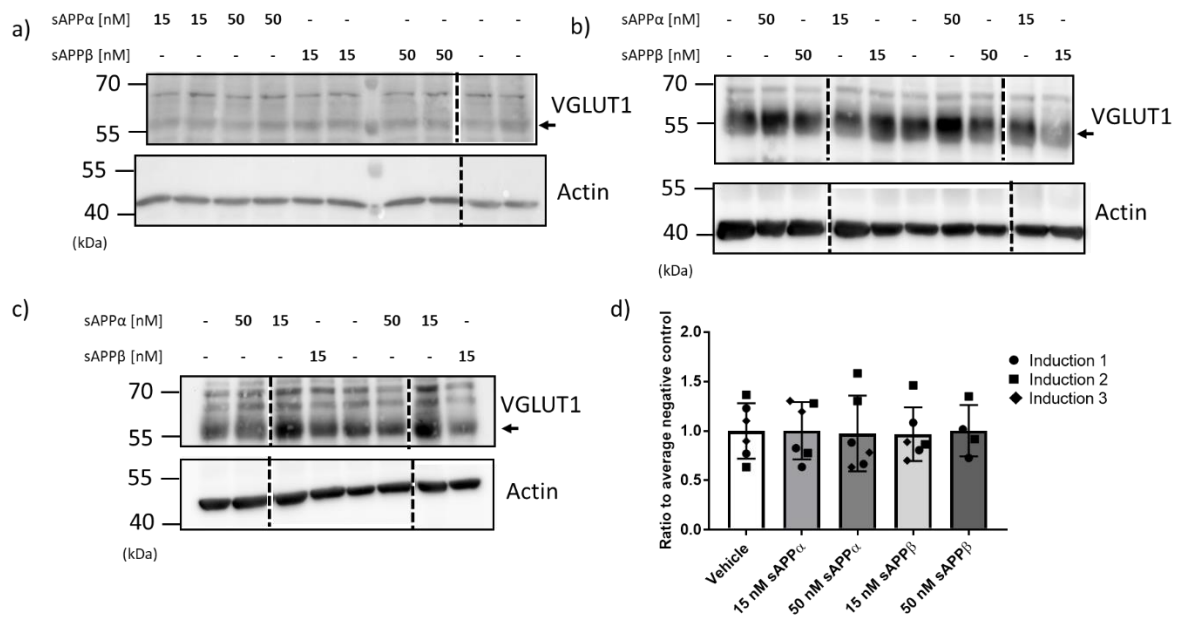


Figure 4.4. sAPPα did not increase the expression of VGLUT1 in hiPSC-derived neurons.

hiPSC-derived cortical neurons were grown to day 73 and incubated with sAPPα or sAPPβ at concentrations of 15 nM or 50 nM for 48 h in NMM. Cells were washed three times in DPBS (+ metals), lysates were collected and subjected to SDS-PAGE with 30 µg total protein loaded per lane. Proteins were transferred to PVDF membrane and probed with anti-VGLUT1 antibody (Table 2.1). Membranes were washed, blocked with 5% milk (w/v) and re-probed with anti-actin antibody. All lanes within each panel are from the same blot image, at the same brightness and contrast (full blots shown in supplementary Figure 7.2), but irrelevant lanes were removed for clarity of presentation. Dotted lines denote where irrelevant lanes were removed. Three inductions were used, with two wells of neurons per induction. (a) Induction 1; (b) Induction 2; (c) Induction 3. (d) Quantification of all inductions combined. Error bars represent standard deviation. Band intensity was quantified using ImageJ, normalised against actin and made relative to the mean expression of VGLUT1 in the vehicle control. Statistics were performed using a one-way ANOVA with Tukey's post-hoc test in GraphPad Prism 7. Neurons treated with 50 nM sAPPβ for induction 3 were infected and so were not used. VGLUT1 estimated molecular weight = 62 kDa.

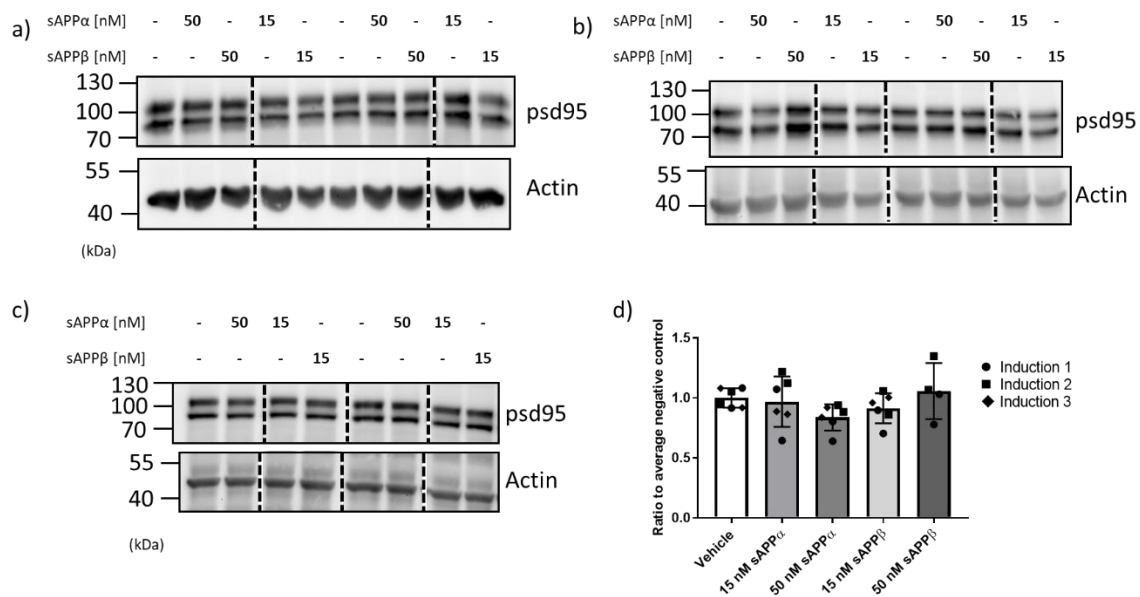


Figure 4.5. sAPPα did not increase the expression of PSD95 in hiPSC-derived neurons.

hiPSC-derived cortical neurons were grown to day 73 and incubated with sAPPα or sAPPβ at concentrations of 15 nM or 50 nM for 48 h in NMM. Cells were washed three times in DPBS (+ metals), lysates were collected and subjected to SDS-PAGE with 30 µg total protein loaded per lane. Proteins were transferred to PVDF membrane and probed with anti-PSD95 antibody (Table 2.1). Membranes were washed, blocked with 5% milk (w/v) and re-probed with anti-actin antibody. All lanes within each panel are from the same blot image, at the same brightness and contrast (full blots shown in supplementary Figure 7.3), but irrelevant lanes were removed for clarity of presentation. Dotted lines denote where irrelevant lanes were removed. Three inductions were used, with two wells of neurons per induction. (a) Induction 1; (b) Induction 2; (c) Induction 3. (d) Quantification of all inductions combined. Error bars represent standard deviation. Band intensity was quantified using ImageJ, normalised against actin and made relative to the mean expression of PSD95 in the vehicle control. Statistics were performed using a one-way ANOVA with Tukey's post-hoc test in GraphPad Prism 7. Neurons treated with 50 nM sAPPβ for induction 3 were infected and so were not used. PSD95 estimated molecular weight = 95 kDa.

4.5. Demonstration of the binding of purified sAPP α and sAPP β to immortalised SH-SY5Y cells.

Prior to the characterisation and receptor identification studies using SH-SY5Y cells, it was necessary to determine that the recombinant purified sAPP α and sAPP β proteins bound to the cell line. The same protocol that was used to identify the binding of sAPP α to iPSC-derived neurons through immunoblotting (Section 4.3) was used here. Briefly, SH-SY5Y cells were incubated with sAPP α at 37 °C, followed by three washes. Then, lysates were collected and probed specifically for sAPP α through immunoblotting with a neoepitope-specific antibody (2B3). First, increasing concentrations of sAPP α , up to 80 nM, were incubated with SH-SY5Y cells for 30 min at 37 °C. Concentrations of sAPP α as low as 15 nM could be visualised as binding to SH-SY5Y cells in this assay (Figure 4.6a). sAPP α bound to cells in a dose dependent manner, with a large increase in the binding of sAPP α at 80 nM (Figure 4.6a). Following determination that concentrations as low as 15 nM of sAPP α visibly bound to SH-SY5Y cells within 30 min at 37 °C, the required incubation time was further investigated. 80 nM sAPP α was incubated with cells at 37 °C for various lengths of time between 5 min and 30 min, as indicated. sAPP α was shown to bind to SH-SY5Y cells within 5 min of application (Figure 4.6b). To determine whether the binding visualised by this assay was specific to the active form of sAPP α , rather than a result of non-specific binding, a sample of sAPP α was boiled for 30 min prior to dilution and incubation with cells. The boiled, denatured sAPP α had a significantly reduced ability to bind to cells compared with the native protein (Figure 4.6c).

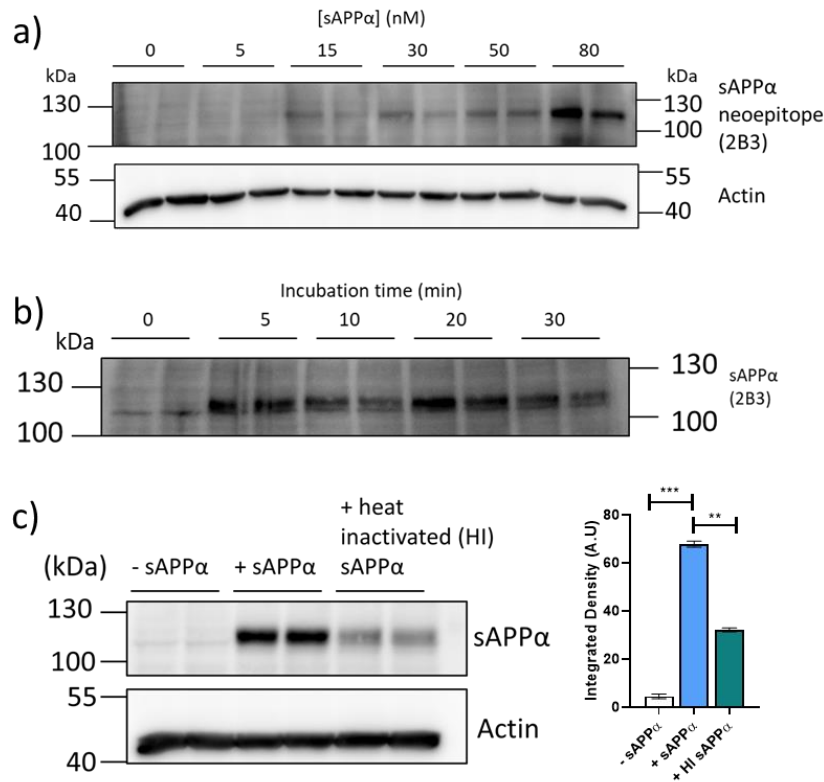


Figure 4.6. Recombinant sAPPα bound to SH-SY5Y cells, but binding was significantly reduced by denaturation.

(a) SH-SY5Y cells were incubated with purified recombinant sAPPα at the concentrations indicated for 30 min at 37 °C, along with a vehicle control (0 nM). The cells were washed three times in DPBS, followed by lysate harvesting. 30 µg whole cell lysate was loaded per lane in SDS-PAGE. Proteins were transferred to PVDF membrane and probed using the sAPPα neoepitope antibody (2B3). The membrane was re-probed for Actin. (b) SH-SY5Y cells were incubated with 80 nM sAPPα for various lengths of time (min), as indicated, along with a vehicle control (-sAPPα). Three washes in DPBS were followed by lysate collection. 30 µg total lysate was loaded per lane in SDS-PAGE. Gels were transferred to PVDF membrane and probed using the sAPPα neoepitope antibody (2B3). (c) sAPPα was either denatured through boiling or left in its native form prior to dilution to 50 nM in OptiMEM. 50 nM sAPPα was then incubated with SH-SY5Y cells for 30 min at 37 °C. The cells were washed three times in DPBS, followed by lysate harvesting. 30 µg whole cell lysate was loaded per lane in SDS-PAGE. Proteins were transferred to PVDF membrane and probed using the sAPPα neoepitope antibody (2B3). The membrane was re-probed for Actin. Band intensity was quantified using ImageJ (quantification shown to the right), with error bars representing standard deviation (n = 2). Statistics were performed using a one-way ANOVA with Tukey's post-hoc test in GraphPad Prism 7.

The assay developed to measure the binding of sAPP α to SH-SY5Y cells (Figure 4.6) was also used to compare the binding of sAPP α and sAPP β to cells. SH-SY5Y cells were incubated with sAPP α or sAPP β for 30 min and immunoblot analysis was performed using an N-terminal APP antibody (22C11) which would recognise sAPP α , sAPP β , and APP (Figure 4.7). SH-SY5Y cells treated with sAPP α had significantly higher mean 22C11 band intensity, by a factor of approximately 2.91, than cells treated with vehicle (Figure 4.7b; supplementary Table 7.13). sAPP β treatment also increased mean 22C11 band intensity, but to a lesser factor of approximately 1.46 and not significantly ($p = 0.1567$) (Figure 4.7b; supplementary Table 7.13). When probed with highly specific neoepitope antibodies, sAPP β was not visualised binding to the cells (Figure 4.7c), whereas sAPP α was (Figure 4.6). Taken together, these data suggested that sAPP α bound more effectively to SH-SY5Y cells than sAPP β under the conditions tested in this assay. As sAPP β was not able to be visualised through immunoblotting using its neoepitope antibody using this protocol (Figure 4.7c), the binding of sAPP β was investigated using a more sensitive multiplex immunoassay (MesoScale Discovery) using an sAPP β -specific kit. Analysis of whole cell neuron lysates incubated with sAPP β using the multiplex immunoassay demonstrated that addition of sAPP β to SH-SY5Y cells significantly increased the mean intensity of sAPP β -specific antibody by approximately 2.83 times (Figure 4.7d).

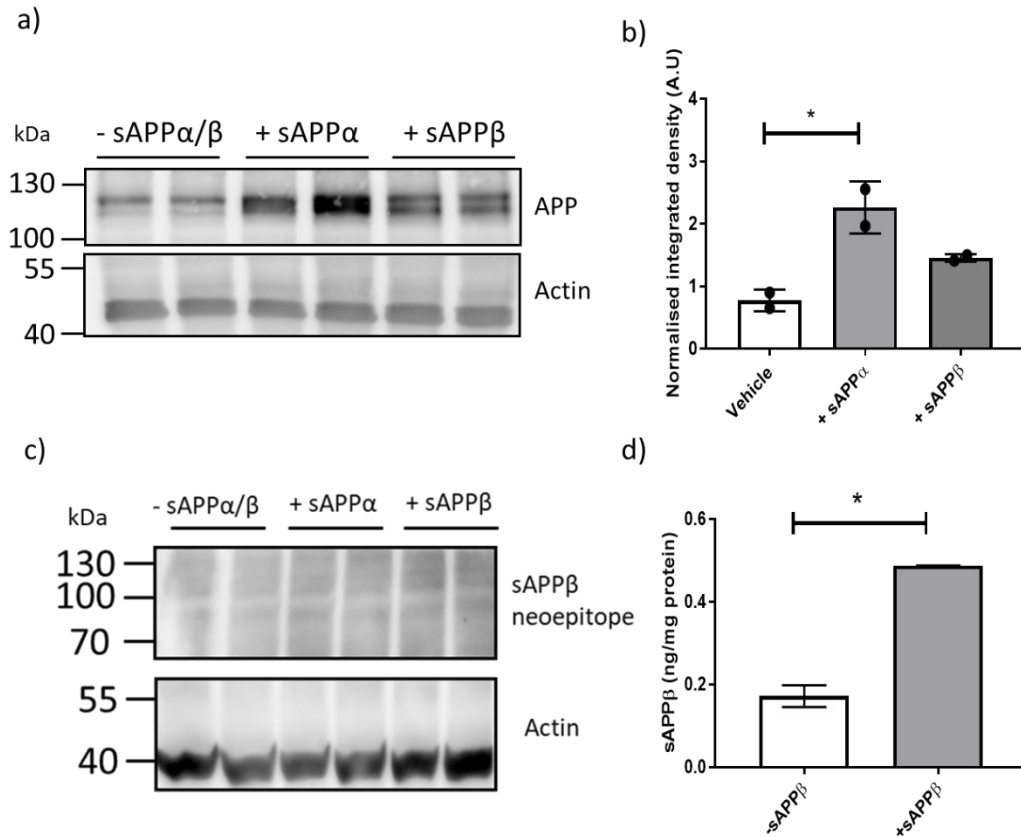


Figure 4.7. sAPPα binds to SH-SY5Y cells more readily than sAPPβ.

(a) SH-SY5Y cells were incubated with 50 nM sAPPα, sAPPβ or vehicle control in OptiMEM for 30 min at 37 °C. The cells were washed three times in DPBS, followed by lysate harvesting. 30 µg total protein was loaded per lane in SDS-PAGE. Proteins were transferred to PVDF membrane and probed using the N-terminal APP antibody 22C11 (APP amino acids 66-81). The membrane was re-probed for Actin. (b) The intensity of bands from panel (a), normalised against actin, were quantified using ImageJ. Both bands in each single lane were quantified together. Error bars show standard deviation (n = 2). Statistics were performed using a one-way ANOVA with Tukey's post-hoc test in GraphPad Prism 7. * = p<0.05. (c) 50 nM sAPPα or sAPPβ or vehicle control in OptiMEM were incubated with SH-SY5Y cells for 30 min. Three washes in PBS (+ metals) were followed by lysate collection. 30 µg total lysate was loaded per lane in SDS-PAGE. Proteins were transferred to PVDF membrane and probed using an sAPPβ specific neo-epitope antibody (1A9). Each membrane was re-probed for Actin. (d) The binding of 80 nM sAPPβ to SH-SY5Y cells was analysed by Dr. Kate Fisher through multiplex immunoassay (mesoscale discovery) using an sAPPβ-specific kit. Lysates were diluted 3:1 prior to analysis and data was normalised to total protein amount. Error bars represent standard error of the mean (n = 2 per condition). Statistics were performed using an unpaired t-test with Welch's correction in GraphPad Prism 7. * = p<0.05.

4.6. sAPP α reduced oxidative stress in SH-SY5Y cells.

Oxidative stress, a key driver of AD pathology, is caused by damaging oxidative molecules such as the ROS H_2O_2 (Huang et al. 2016). sAPP α has been shown to protect against oxidative stress in neurons (Goodman and Mattson 1994). Additionally, stimulation of ADAM10 activity in SH-SY5Y cells overexpressing the prion protein (SH-PrP) reduced the generation of ROS by A β Os (Jarosz-Griffiths et al. 2019). Here, the neuroprotective effect of sAPP α on H_2O_2 production by the redox-cycler menadione was investigated using SH-SY5Y and SH-PrP cells. First, the concentration of menadione required to induce significant H_2O_2 production was determined in both SH-SY5Y (Figure 4.8a) and SH-PrP (Figure 4.8b) cells. Cells were incubated in OptiMEM for 48 h before menadione was added to final concentrations of between 1 μM and 100 μM . (Figure 4.8). The generation of the ROS H_2O_2 was measured using the ROS-GLO kit following the manufacturer's instructions. In SH-SY5Y cells, menadione upwards from 5 μM significantly increased mean H_2O_2 generation in a concentration-dependent manner (Figure 4.8a). 10 μM menadione increased mean H_2O_2 production by a factor of approximately 5.17, whilst 100 μM menadione increased mean H_2O_2 production by a factor of approximately 12.30 (Figure 4.8a). A similar effect of menadione was seen in SH-PrP cells, where 10 μM menadione increased H_2O_2 production by a factor of approximately 7.14 (Figure 4.8b). For downstream studies, 10 μM menadione was chosen to induce a significant but potentially reversible ROS response.

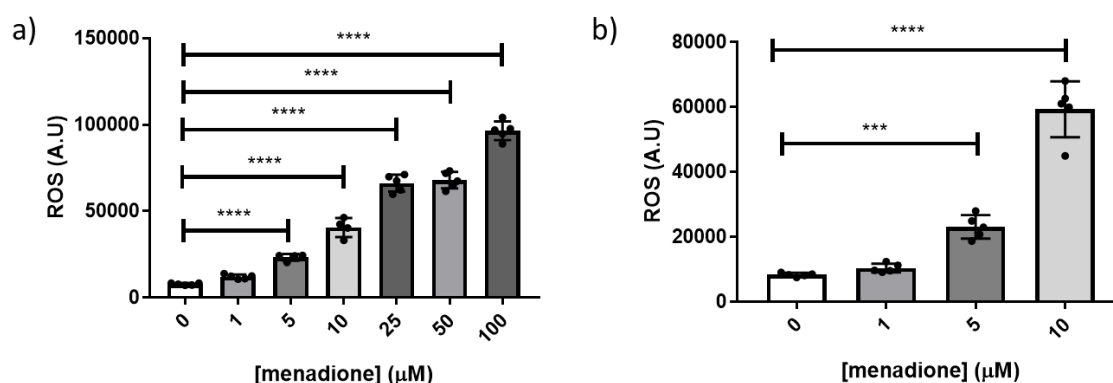


Figure 4.8. Menadione induces the significant production of H₂O₂ in SH-SY5Y and SH-PrP cells in a concentration-dependent manner.

(a) SH-SY5Y or (b) SH-PrP cells were seeded in 96 well plates overnight, followed by 48 h incubation in OptiMEM. Various concentrations of menadione, as indicated, were added for 90 min and the generation of H₂O₂ measured using the ROS-GLO kit according to the manufacturer's instructions. Data was analysed with a one-way ANOVA with Tukey's multiple comparison test, n = 4-5 wells per condition. PrP, overexpressing prion protein.

Following the finding that menadione significantly increased H₂O₂ generation in a dose-dependent manner, the protective effect of sAPPα was investigated. SH-SY5Y cells were incubated with 5, 15 or 50 nM sAPPα for 4, 24 or 48 h. Following this, 10 μM menadione was added and the production of ROS was measured (Figure 4.9). 10 μM menadione significantly increased mean H₂O₂ generation by a factor of approximately 4.74, compared to the vehicle control, in SH-SY5Y cells (Figure 4.9a-c). Pre-incubation with 5 nM sAPPα significantly decreased mean H₂O₂ generation by menadione in the SH-SY5Y cells in a time-dependent manner by approximately 15%, 38% and 45% at 4 h, 24 h and 48 h timepoints, respectively (Figure 4.9a). Similarly, pre-incubation with 15 nM sAPPα for 24 h and 48 h significantly reduced mean H₂O₂ production by menadione by approximately 30% and 45%, respectively, in a time-dependent manner (Figure 4.9b). Finally, pre-incubation with 50 nM sAPPα for 4, 24 and 48 h also significantly reduced mean H₂O₂ production by menadione by approximately 27%, 13% and 56%, respectively (Figure 4.9c).

A similar effect of sAPPα was observed in SH-PrP cells, though to a lesser degree (Figure 4.9d-f). 10 μM menadione significantly increased mean H₂O₂ generation, compared to its vehicle

control, by a factor of approximately 4.09 (Figure 4.9d-f). 48 h incubation of 5 nM sAPP α significantly reduced mean H₂O₂ generation by menadione by approximately 31% (Figure 4.9d). Similarly, 24 h incubation of 15 nM sAPP α significantly reduced mean H₂O₂ generation by menadione by approximately 23% (Figure 4.9e). Finally, 48 h incubation of 50 nM sAPP α significantly reduced mean H₂O₂ generation by menadione by approximately 21% (Figure 4.9f). Taken together, these results demonstrated that pre-incubation with sAPP α significantly reduced the generation of H₂O₂ by menadione in both SH-SY5Y and SH-PrP cells. These data demonstrated the ability of sAPP α to reduce oxidative stress in neuronal cells.

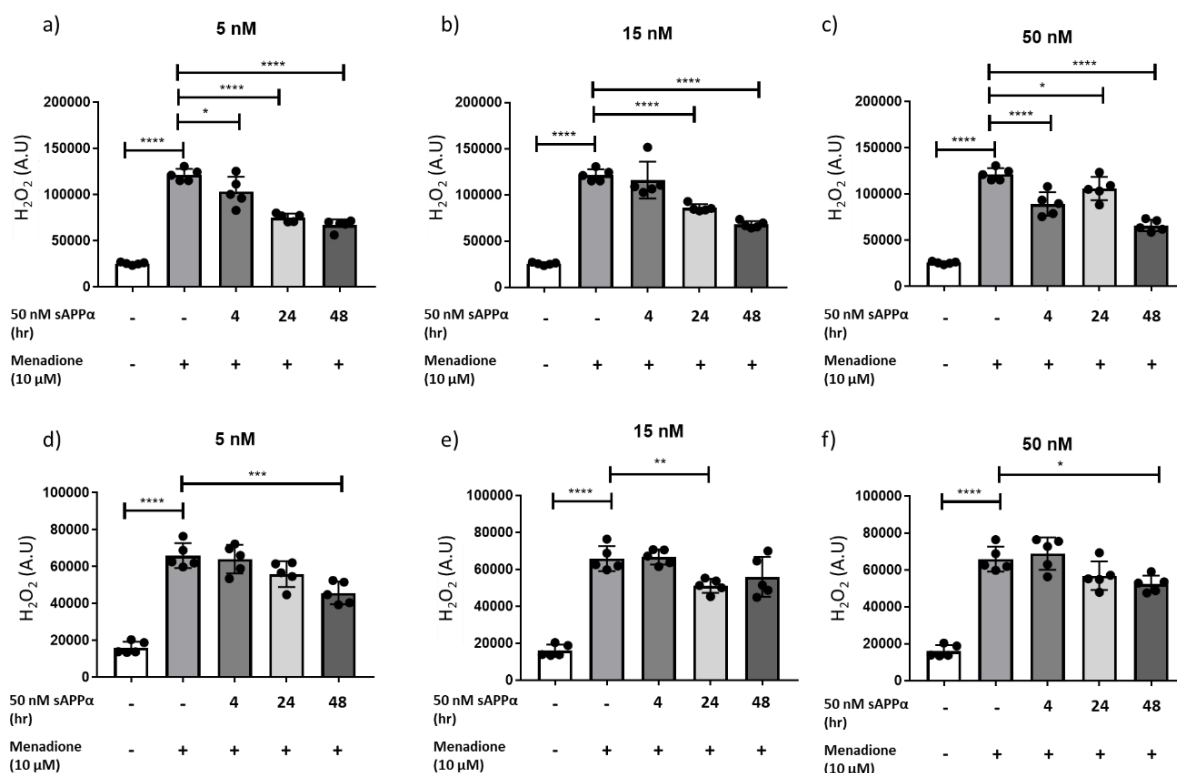


Figure 4.9. Pre-incubation of sAPPα reduces ROS production in a time-dependent manner.

SH-SY5Y (a-c) and SH-PrP cells (d-f) were seeded in 96 well plates overnight. sAPPα was then incubated with cells for timepoints of either 4 h, 24 h or 48 h at concentrations of 5 nM, 15 nM or 50 nM. 10 μM menadione were added for the final 90 min of sAPPα incubation and the level of H₂O₂ was measured using the ROS-GLO kit according to the manufacturer's instructions. Statistics were performed using a one-way ANOVA with Tukey's multiple comparison test. N = 5 wells per condition. PrP, overexpressing prion protein.

4.7. Discussion

This chapter described efforts to characterise the activity of the recombinant sAPP α and sAPP β purified in chapter 3. The binding of sAPP α and sAPP β to both SH-SY5Y cells and iPSC-derived neurons was demonstrated. 15 nM sAPP α , but not sAPP β , significantly increased the expression of synaptophysin in one induction of iPSC-neurons and almost reached significance when all inductions were combined. sAPP α was also shown to significantly reduce H₂O₂ generation in SH-SY5Y and SH-PrP cells in a time-dependent manner. These data demonstrated the potential enhanced neurotrophic effect of sAPP α over sAPP β and demonstrated the neuroprotective activity of sAPP α against ROS. Such activities could be highly beneficial in the treatment of neurodegenerative diseases.

4.7.1. The interaction between sAPP α , sAPP β and iPSC-derived human cortical neurons

Prior to investigating and comparing the effects of sAPP α or sAPP β on synaptic protein expression, the binding of both proteins to iPSC-derived neurons was investigated. These initial experiments also allowed the optimisation of appropriate concentrations and incubation times for later experiments. Firstly, iPSC-derived cortical neurons were generated using an established protocol (Figure 4.1a) (Shi et al. 2012) and the expression of the neuronal differentiation markers MAP2, β III tubulin, synaptophysin and SATB2 was confirmed by immunofluorescence microscopy (Figure 4.1b, 4.1c). iPSC-derived neurons were used in this thesis because some studies consider them to be a more physiologically similar model of the native neurons within patients than undifferentiated immortalised cells are (Engle et al. 2018; Lopes et al. 2017). One study found that large proportions of iPSC-derived cortical neurons expressed genes associated with synaptic function, NMDA receptor genes and over 90% of cells tested expressed neuronal-specific markers such as MAP2 (Handel et al. 2016). The expression of the neuronal marker MAP2 was similarly confirmed in iPSC-derived neurons in figure 4.1 of this thesis. In addition, OX1-19 iPSC cell lines were readily available in the Hooper lab, along with extensive experience of performing neuronal differentiation. However, one negative of iPSC-derived neurons is they can have a high degree of variation between inductions, and particularly between stem cells sourced from different donors with distinct genetic backgrounds, potentially leading to variable results (Schwartzentruber et al. 2018). In addition, some studies suggested that iPSC-derived neurons were more similar in gene expression to foetal neurons rather than adult neurons (Handel et al. 2016). However, the

use of iPSC-derived neurons in this thesis provided an interesting comparator to immortalised SH-SY5Y cells to validate the reliability of results in later chapters, when data derived from the two cell types were compared. Unlike hiPSC-derived neurons, undifferentiated SH-SY5Y cells have a high proliferative rate (Lopes et al. 2017), are variable in electrophysiological activity (Santillo et al. 2014) and are generally considered to be a less accurate neuronal model (Engle et al. 2018). However, in some cases SH-SY5Y cells are preferable because hiPSC-derived neurons are much more fragile, challenging and time-consuming to culture, meaning hiPSC-derived neurons are not always appropriate for high-throughput studies or studies requiring large amounts of cellular material.

Another cell model which could have been used was differentiated SH-SY5Y cells, which possess a more mature neuronal phenotype than undifferentiated SH-SY5Y cells (Kovalevich and Langford 2013). Future experiments could repeat or build on the experiments listed in this discussion using differentiated cells. However, the use of iPSC-derived human neurons in this thesis provided a different model and somewhat mitigated the lack of differentiated immortalised cells.

Following confirmation of the expression of neuronal differentiation markers in iPSC-derived human neurons, the binding of sAPP α to the neurons was investigated. Previous studies reported sAPP α activity at nanomolar concentrations such as 10-40 nM (Goodman and Mattson 1994), 1-100 nM (Mattson et al. 1993) and 10 nM (Claasen et al. 2009). Thus, a range of concentrations ranging from 5 nM to 80 nM sAPP α were incubated with iPSC-derived neurons for 30 min at 37 °C. Concentrations of 30 nM sAPP α and above resulted in visible sAPP α binding when probed through immunoblotting using a neoepitope antibody (2B3) (Figure 4.2a). There was a degree of variation in the sAPP α band intensity between the wells of each condition above 30 nM, perhaps due to slight differences in cell composition between wells during neuronal differentiation (Figure 4.2a). Concentrations of sAPP α below 30 nM may also have bound to iPSC-derived cortical neurons, but this binding could have been below the detection limit of the sAPP α neoepitope antibody used in this assay. However, these data indicated that sAPP α bound to hiPSC-derived neurons visibly at concentrations of 30 nM and above. This was consistent with previous studies, which demonstrated sAPP α activity on cells at a variety of concentrations between 1 nM and 100 nM (Dorard et al. 2018; Furukawa et al. 1996; Goodman and Mattson 1994; Mattson et al. 1993).

Following determination that sAPP α bound to hiPSC-derived neurons at concentrations comparable to previous studies, the time required for sAPP α to bind to the neurons was also investigated. 80 nM sAPP α bound rapidly to neurons, within 10 min, which was the shortest timepoint tested (Figure 4.2b). This rapid binding of sAPP α to cells was consistent with a previous study, which showed binding by 1 min (Dorard et al. 2018). Similar experiments were performed with sAPP β for comparison; however, no sAPP β binding was visualised through this immunoblotting assay using the sAPP β neoepitope antibody (Figure 4.7c). This could be attributed to sAPP β having a lower binding ability to cells, or the specific sAPP β neoepitope antibody (1A9) having a lower sensitivity than the sAPP α neoepitope antibody (2B3) in the immunoblotting assay. To confirm that sAPP β also bound to neurons, prior to downstream experiments, hiPSC-derived neurons were treated with 80 nM sAPP β and the resulting lysates were probed using a multiplex immunoassay (Figure 4.2c). The immunoassay was a more sensitive method to detect an increase in sAPP β compared to the vehicle control, if binding had occurred. Analysis through the multiplex immunoassay confirmed that sAPP β bound to iPSC-derived neurons (Figure 4.2c).

Previous studies found that sAPP α increased the expression of synaptic markers such as synaptophysin *in vivo* (Roch et al. 1994). sAPP α was also suggested to be more neurotrophic than sAPP β with regards to inducing axon outgrowth (Chasseigneaux et al. 2011). A direct comparison of sAPP α and sAPP β on synaptic protein expression in neurons had not previously been performed. The loss of synaptophysin and VGLUT1 were shown to correlate significantly with cognitive decline in AD, so increasing their expression levels could be therapeutically beneficial (Kashani et al. 2008; Sze et al. 1997). APP and sAPP α were previously shown to accumulate at presynaptic terminals, suggesting a role in synapse function (Buxbaum et al. 1998). Injection of 500 nM of a peptide containing the C-terminal 17 amino acids of sAPP α , absent from sAPP β , led to a significant increase in synaptophysin-like immunoreactivity in a rabbit spinal cord ischaemia model (Bowes et al. 1994). Subcutaneous infusion of a different peptide, consisting of sAPP α ₆₉₅ amino acids 319-335 called '17-mer', significantly increased synaptophysin immunoreactivity in rat frontoparietal cortexes (Roch et al. 1994). Therefore, the effect of sAPP α or sAPP β on the expression of the pre-synaptic markers synaptophysin, VGLUT1 and the post-synaptic marker PSD95 in hiPSC-derived neurons was investigated.

Three different inductions of hiPSC-derived neurons were used, with two biological replicate wells per treatment condition. First, the effect of sAPP α or sAPP β on the expression of synaptophysin was measured. There was a large degree of variation between different inductions of iPSC-derived neurons. 15 nM sAPP α had a significant effect on synaptophysin expression in the third induction of neurons compared to the vehicle control, whilst 15 nM sAPP β had no significant effect (Figure 4.3c). This supported data in the literature showing enhanced neurotrophic effects of sAPP α relative to sAPP β (Bowes et al. 1994; Chasseigneaux et al. 2011). Interestingly, 50 nM sAPP α had no effect on the expression of synaptophysin in induction 3 neurons (Figure 4.3c), so the effect was specific to the lower 15 nM dose. However, neither sAPP α nor sAPP β had a significant effect on the expression of synaptophysin in the other two inductions of neurons, but the effect of sAPP α was close to significance when all inductions were combined ($p = 0.0869$). No significant effect of sAPP α or sAPP β was found on the expression of either VGLUT1 or PSD95 in any induction. As synaptophysin expression was previously used as a marker of synaptic density (Roch et al., 1994), the data in this chapter potentially support a neurotrophic effect of sAPP α . However, this effect was only observed clearly in one induction of neurons. This variation between neuronal inductions could be due to the growth of different cell populations following the 70-day differentiation protocol. For example, inductions 1 and 2 could have had a higher proportion of non-neuronal cells differentiate from the OX1-19 iPSC precursors, leading to lower synaptic density and therefore a reduced effect of sAPP α . Thus, further investigation of the effect of sAPP α in iPSC-derived neurons is required. Future work should repeat this experiment to determine whether the observed effect of sAPP α on synaptophysin expression in iPSC-derived neurons is accurate and replicable.

4.7.2. The interaction between sAPP α , sAPP β and SH-SY5Y neuroblastoma cells

While hiPSC-derived neurons are more physiologically accurate models of human neurons, immortalised cells offer a more high-throughput and faster method of measuring cellular effects. Thus, the binding of sAPP α and sAPP β to SH-SY5Y immortalised cells was investigated and compared. A range of concentrations between 5 nM and 80 nM sAPP α were added to cells to test binding ability through immunoblotting. Concentrations of 15 nM sAPP α and above were visualised binding to SH-SY5Y cells using this protocol (Figure 4.6a). Following this, the speed of binding of sAPP α to the cells was also assessed, which determined that 80 nM

sAPP α bound within 5 min of application, which was the shortest timepoint tested (Figure 4.6b). These findings were consistent with previous studies demonstrating rapid binding of sAPP α to cells at nanomolar concentrations (Dorard et al. 2018; Mattson et al. 1993). Following these results, the effect of protein denaturation through boiling on the binding of sAPP α to SH-SY5Y cells was investigated and compared to that of native sAPP α . Boiling sAPP α for 30 min significantly reduced the amount of binding to SH-SY5Y cells (Figure 4.6c). This finding confirmed that native protein folding was required for the successful binding of sAPP α to SH-SY5Y cells. These data suggested that the binding of sAPP α to SH-SY5Y cells was facilitated through an interaction which required correct protein folding, such as binding to a receptor at the cell surface.

Following demonstration of the binding of sAPP α to SH-SY5Y cells, a comparison of the binding ability of sAPP α was compared with the binding ability of sAPP β . The use of the 22C11 antibody, which has an epitope in the N-terminal region of APP, allowed for a direct comparison of the binding of sAPP α and sAPP β . Addition of 50 nM sAPP α significantly increased the intensity of 22C11 staining, whereas addition of 50 nM sAPP β did not (Figure 4.7a). The staining of 22C11 was slightly increased following sAPP β incubation, possibly indicating a smaller amount of binding relative to sAPP α (Figure 4.7b). These results suggested that sAPP α bound more readily to SH-SY5Y cells than sAPP β . However, a future experiment could probe equal amounts of purified sAPP α and sAPP β with 22C11 to confirm that they are recognised to the same degree by the antibody. In addition, the statistical power of the experiment was limited due to the low n number, so future studies could repeat this experiment with higher n numbers. Some limited previous data in the literature suggested that sAPP α bound more readily to receptors than sAPP β , with one study showing that mouse sAPP α bound to mouse p75^{NTR} with a half maximal effective concentration (EC₅₀) of 90 nM, whereas mouse sAPP β had a higher EC₅₀ of 120 nM (Hasebe et al. 2013). The increased binding of sAPP α to cells over sAPP β shown in Figure 4.7a, along with limited data from the literature, suggested that some of the enhanced neuroprotective and neurotrophic effects of sAPP α compared with sAPP β could be due to the increased ability of sAPP α to bind to neuronal cells (Chasseigneaux and Allinquant 2012). The data suggesting differences in the binding abilities of sAPP α and sAPP β further justified the placement of the hexahistidine tag

at the N-terminus of recombinant sAPP α in chapter 3, to minimise its interference with C-terminal activity and potential sAPP α -specific interactions.

In addition to the novel binding assay, other assays were also considered to identify and quantify the binding of sAPP α or sAPP β to cells *in vitro*. One possible alternative assay was immunofluorescence microscopy using specific sAPP α , sAPP β or His-tag antibodies following the addition of sAPP α or sAPP β to live cells. This assay was repeatedly attempted, but the antibodies had excessive background fluorescence such that no binding could be discerned. Due to this, one strength of the novel immunoblotting binding assay was the clear difference between untreated and treated cells following the addition of sAPP α or sAPP β due to low levels of background staining. However, one strength of immunofluorescence microscopy over the novel immunoblotting binding assay would have been the ability to visualise the location of sAPP α or sAPP β at the cell surface and within cells, along with the potential for co-staining for candidate receptors to investigate ligand-receptor co-localisation which would indicate protein interactions. One weakness of the novel immunoblotting binding assay was that the higher levels of sAPP α or sAPP β staining did not necessarily indicate binding but could reflect higher levels of endogenous protein production following the addition of sAPP α or sAPP β to cells. The use of a His-tag antibody in immunoblotting could be used in future experiments to show that any staining visualised is caused by exogenous recombinant His-tagged protein and not due to higher levels of endogenously produced protein.

As the addition of 50 nM sAPP β for 30 min did not significantly increase the band intensity of APP in SH-SY5Y cell lysates, as detected by immunoblotting, a different approach was used to demonstrate the binding of sAPP β to SH-SY5Y cells prior to receptor pulldown studies (chapter 5). The sAPP β specific neoepitope antibody was not sensitive enough to visualise the retention of sAPP β in SH-SY5Y lysates through immunoblotting (Figure 4.7c). Therefore, a more sensitive multiplex immunoassay was used to determine whether sAPP β bound to SH-SY5Y cells. Multiplex immunoassay analysis of whole cell lysate from SH-SY5Y cells incubated with sAPP β , using an sAPP β -specific immunoassay probe, indicated that sAPP β bound successfully to the SH-SY5Y cells (Figure 4.7d). The statistical power of this experiment was low, due to the use of duplicates, and could be improved with the use of triplicates in future. However, the effect was strong enough to reach statistical significance with an n number of just two.

Previous studies touted the neuroprotective activity of sAPP α as a potential mechanism to reduce neurodegeneration (Fol et al. 2016; Goodman and Mattson 1994). If the protective effect of sAPP α could be harnessed, it could help protect neurons from oxidative stress to reduce neuronal damage and therefore cognitive decline. Several studies have linked oxidative stress to AD, and sAPP α to neuroprotective effects (Goodman and Mattson 1994; Huang et al. 2016). Mechanisms such as excitotoxicity, oxidative stress and proteasomal stress are key drivers of AD pathology (Section 1.5) (Copanaki et al. 2010; Furukawa et al. 1996). Treatment of hippocampal neurons with 10 nM sAPP α_{695} for 24 h significantly attenuated A β_{42} -induced ROS production (Goodman and Mattson 1994). Pre-treatment of rat PC12 immortalised cells with 25 nM and 50 nM sAPP α also significantly protected against apoptosis from proteasomal stress in a concentration dependent manner (Copanaki et al. 2010). 50 nM sAPP β had no protective effect against proteasomal-stress induced apoptosis, demonstrating a critical difference between the neuroprotective abilities of sAPP α and sAPP β (Copanaki et al. 2010). sAPP α also provided 100-times greater protection of hippocampal neurons against cell death induced by A β toxicity, excitotoxicity and glucose deprivation compared with sAPP β (Furukawa *et al.*, 1996). Treatment with 1 nM sAPP α significantly reduced hippocampal cell death due to NMDA excitotoxicity (Ryan et al. 2013). Overexpression of APP significantly reduced the production of H₂O₂ from rotenone in SH-SY5Y cells (Cimdins et al. 2019). The overexpression of APP would consequently lead to increased secretion of sAPP α , which could have been responsible for the reduced production of H₂O₂ from rotenone (Cimdins et al. 2019). Building on such previous data in the literature, the ability of recombinant sAPP α to reduce H₂O₂ production from menadione in SH-SY5Y cells was investigated.

The protective effect of sAPP α against oxidative stress was determined using an assay which measured the production of H₂O₂, a long-lived ROS (Huang, Zhang and Chen, 2016). SH-SY5Y cells, rather than hiPSC-derived cortical neurons, were chosen to measure sAPP α -mediated neuroprotection because cell density was a critical variable in the ROS-GLO assay. SH-SY5Y cells exhibit less variation in cell number between wells because they are experimented on within 72 h of seeding, whereas hiPSC-derived neurons necessitate 40 days of maturation. Post-experiment cell density quantification was unreliable because the cells detached very easily following the ROS-GLO assay. As a result, SH-SY5Y cells were determined to be a more

appropriate model for use with the ROS assay. A previous study demonstrated that treatment with A β O significantly increased ROS production in SH-PrP cells (Jarosz-Griffiths et al. 2019). However, this increase in ROS was ablated through stimulation of ADAM10 activity. Whilst the authors attributed this effect to ADAM10-mediated cleavage of the prion protein from the surface of cells and subsequently reduced A β O binding, the reduced ROS could also have been contributed to by increased sAPP α production due to increased ADAM10 activity (Jarosz-Griffiths et al. 2019). Therefore, SH-PrP cells were also included to investigate the protective effects of sAPP α .

To stimulate the production of H₂O₂ and therefore induce oxidative stress, SH-SY5Y cells were incubated with menadione. Menadione is a potent generator of ROS in cells through redox cycling (Criddle et al. 2006). Incubation with menadione significantly increased H₂O₂ generation in SH-SY5Y cells (Figure 4.8a) and SH-PrP cells (Figure 4.8b) in a concentration dependent manner. 10 μ M menadione was chosen for later experiments as it was one of the lower concentrations that still provided a significant and robust ROS response. It was deemed important not to overload the cells with high concentrations of menadione, so that its effect on ROS production was still reversible. Following this, the putative protective effect of sAPP α pre-treatment on ROS production was investigated. The incubation time of sAPP α treatment appeared to be more important than sAPP α concentration, with time-dependent reductions in H₂O₂ production at 5 nM, 15 nM and 50 nM sAPP α concentrations. This is consistent with a study which found that sAPP α induced gene expression changes in a time-dependent manner, including activating the transcription factors of protective immediate early genes and the enhanced activation of NF κ B, which may be involved in neuroprotection in AD (Guo et al. 1998; Ryan et al. 2013). Similar results were seen in SH-PrP cells (Figure 4.9d-f), but sAPP α appeared to have a reduced effect in those cells compared to SH-SY5Y cells. As APP is known to bind to the prion protein, sAPP α could also bind in a similar manner due to its large sequence overlap with APP (Bai et al. 2008). Therefore, the over-expression of the prion protein on the surface of SH-PrP cells may have competed for the binding of sAPP α with the receptor(s) responsible for the facilitating the reduction in H₂O₂, which would reduce the protective effect of sAPP α in SH-PrP cells relative to wild-type SH-SY5Y cells (as seen in Figure 4.9). The ROS experiment was also attempted with sAPP β , but the assay was repeatedly unsuccessful. ROS assays can be troublesome to perform, due to the transient and extremely

reactive nature of ROS (Pavelescu 2015). Future work should repeat this ROS experiment to directly compare the protective effects of sAPP α and sAPP β on H₂O₂ production. In summary, sAPP α significantly reduced ROS production in a time-dependent manner in both SH-SY5Y cells and SH-PrP cells, demonstrating its possible therapeutic potential to reduce neuronal oxidative stress in neurodegenerative diseases.

4.8. Chapter summary

The data in this chapter demonstrated that the recombinant sAPP α and sAPP β proteins purified in chapter 3 bound to both hiPSC-derived cortical neurons and SH-SY5Y cells. The binding of sAPP α was rapid, within 5 min and 10 min of application to SH-SY5Y cells and hiPSC-derived neurons respectively (the shortest timepoints tested in both cases). sAPP α also bound to both cell types at nanomolar concentrations. These results were consistent with previous studies (Dorard et al. 2018; Mattson et al. 1993). The binding of sAPP α to SH-SY5Y cells was significantly reduced by heat denaturation. sAPP α bound more readily to SH-SY5Y cells than sAPP β when measured with an N-terminal APP antibody through immunoblotting. 15 nM sAPP α significantly increased the expression of synaptophysin in one induction of hiPSC-derived neurons, indicating a potential beneficial neurotrophic effect at synapses, whilst 15 nM sAPP β had no significant effect. Pre-incubation of SH-SY5Y cells and SH-PrP cells with sAPP α was shown to be neuroprotective and significantly reduced H₂O₂ production from menadione in a time-dependent manner. Together, these results demonstrated the neuroprotective and potentially neurotrophic effects of sAPP α and validated the biological activity of the sAPP α purified in chapter 3.

5. The unbiased identification of sAPP α and sAPP β binding partners

5.1. Introduction.

5.1.1. Putative sAPP α and sAPP β receptors.

The reciprocal cleavage of APP by α -secretase or β -secretase produces sAPP α or sAPP β , respectively (Kuhn et al. 2010; Vassar et al. 1999). In the β -secretase cleavage pathway, downstream cleavage by γ -secretase releases the neurotoxic A β protein, which is heavily implicated in AD (Chow et al. 2010). Conversely, following its release through α -secretase cleavage of APP, sAPP α has a range of protective effects on neuronal cells, such as protection against A β -induced oxidative stress (Goodman and Mattson 1994), enhancement of synaptic growth (Roch et al. 1994) and protection against A β -induced neuronal cell death (Furukawa et al. 1996). Strikingly, sAPP α is around 50- to 100-times more neuroprotective than sAPP β , despite only possessing an extra 16 amino acids at its C-terminus (Chasseigneaux and Allinquant 2012; Furukawa et al. 1996). sAPP β is less well-studied than sAPP α , likely due to its decreased neuroprotective effect and therefore reduced clinical potential (Chasseigneaux and Allinquant 2012). To facilitate its enhanced neuroprotective properties relative to sAPP β , we hypothesised that sAPP α may bind to a different receptor, or bind to cells with a higher affinity, because of its different C-terminus. Due to its reduced protectivity, sAPP β was chosen as a control protein for receptor identification experiments aiming to identify receptors responsible for sAPP α -specific protective effects. The identification of receptor(s) which are responsible for protective effects of sAPP α could translate into clinical benefits. The responsible receptor(s) could be targeted pharmacologically, with the aim of harnessing precise beneficial properties of sAPP α and minimising off-target toxicity.

Several studies have attempted to identify the cell surface neuronal receptors that mediate the neuroprotective and neurotrophic effects of sAPP α , though fewer have investigated and compared sAPP α and sAPP β directly (Dorard et al. 2018; Hasebe et al. 2013; Rice et al. 2019). The binding of sAPP α to p75 neurotrophin receptor (p75^{NTR}) stimulated neurite outgrowth in cultured mouse cortical neurons, an effect that was lost following p75^{NTR} knockdown (Hasebe et al. 2013). sAPP β also bound to p75^{NTR}, but the effect of sAPP β on neurite outgrowth was not tested (Hasebe et al. 2013). In a separate study, the binding of sAPP α to the $\alpha 3$ subunit of Na⁺/K⁺-ATPase ($\alpha 3$ -NKA) promoted axonal outgrowth in mouse primary cortical neurons,

but was not responsible for sAPP α -induced protection against A β neurotoxicity (Dorard et al. 2018). Neither the binding of sAPP β to the α 3-NKA nor its effect on axonal outgrowth were investigated (Dorard et al. 2018). Affinity purification pulldowns using rat synaptosome extracts, followed by mass spectrometric analysis, identified the γ -aminobutyric acid type B receptor subunit 1a (GABA $_B$ R1a) as a potential receptor for sAPP α (Rice et al. 2019). The binding of sAPP α to GABA $_B$ R1a enhanced short-term facilitation and modulated the release of pre-synaptic vesicles (Rice et al. 2019). However, sAPP β bound to the same receptor and exerted the same effects as sAPP α (Rice et al. 2019). The role of GABA $_B$ R1a in sAPP α -mediated protection against neurotoxicity was not investigated (Rice et al. 2019). In summary, though several cell surface binding partners have been identified for sAPP α , no study has yet identified the receptor(s) or mechanism(s) through which sAPP α protects neuronal cells from oxidative stress or protects against A β -induced neurotoxicity. Identifying novel receptors that may be responsible for such protective effects could provide clinical benefits to treat neurodegenerative conditions.

5.1.2. Microbead-based receptor identification methods.

The identification of receptor-ligand interactions is central to the understanding of biological processes. The strength and time of ligand-receptor interactions can vary widely (Lim et al. 2021), so different receptor isolation techniques may be appropriate for different interactions. Co-immunoprecipitation, which involves the coupling of a 'bait' protein of interest to an antibody (usually immobilised on beads), is a common technique for isolating protein interactors (Lim et al. 2021). Proteins that interact with the bait are pulled down and referred to as 'prey' (Lim et al. 2021). However, these experiments often isolate prey from cell lysates, which is not an accurate representation of how those proteins may come into contact in their native cellular environments. Protein interactions or structures could also be interfered with by detergents, such as those used to harvest cell lysates, meaning some protein interactions could be lost or changed (Lim et al. 2021). Furthermore, the aberrant binding of solubilised proteins within lysates to the bait or the microbeads themselves can result in the isolation of non-specific associations (Jones et al. 2015). As previous sAPP α receptor identification studies had used conventional co-immunoprecipitation methods with cell extracts (Rice et al. 2019), novel methods were used in this study to identify new interactions.

One way to overcome limitations of conventional co-immunoprecipitation using cell extracts was to use a method compatible with live cells to capture receptor-ligand interactions in their native environment. One such method, outlined by Jones et al., 2015, was originally designed for the isolation of integrin adhesion complexes. This method not only facilitated the capture of receptors from live cells in their native environment using bait proteins adhered to magnetic beads, but also removed cell body and cytoplasmic proteins prior to mass spectrometric analysis to highlight membrane prey proteins of interest (Jones et al. 2015). The use of protein crosslinkers also allowed for the stabilisation and identification of transient or weaker interactions, which may be of interest (Jones et al. 2015). This method was compatible with a wide range of cell lines that could survive suspension for short periods and be grown in large quantities. The inclusion of a positive control, such as beads coated with a specific antibody, was recommended to allow for the identification and removal of non-specific background prey proteins from consideration (Jones et al. 2015). Following the isolation of prey proteins using the microbead-based method, the successful pull-down of positive control prey could be verified by western blotting. For example, a bead coated with an antibody directed against the transferrin receptor (TFR) should isolate the TFR protein from cells in order to indicate a successful isolation experiment. GeLC-MS/MS analysis of each bait sample would identify a list of prey proteins, which would be analysed to identify proteins of interest.

5.1.3. QCM-D-based receptor identification methods.

Another method to identify protein interactions is quartz crystal microbalance with dissipation monitoring (QCM-D). QCM-D detects mass changes taking place on a sensor surface and also measures the viscoelastic properties of the surface-adhering layer (Dixon 2008). QCM-D allows for the measurement of protein interactions in real-time, such as the interaction between an immobilised bait protein on a sensor chip with prey proteins within cell lysates. The resonance frequency of a piezoelectric chip (f) changes following the adsorption of molecules onto its surface (Dixon 2008). A change in resonance frequency (Δf) indicates the adherence of molecules to the QCM-D chip. By coating the chip with a bait protein, it is possible to measure the binding of prey proteins to bait proteins of interest (Peh et al. 2007). The inclusion of dissipation monitoring (D) enables the measurement of viscoelastic molecules such as proteins, liquid lysates and lipid bilayers on the surface of the

chip, which have different vibrative properties than solid substances (Dixon 2008). Therefore, simultaneous recording of changes in dissipation (ΔD) and changes in resonant frequency (Δf) can show the adsorption of prey to the QCM-D chip. The QCM-D chip can then be stripped of bait and prey proteins and proteins of interest identified through GeLC-MS/MS.

5.1.4. Chapter aims.

This chapter aimed to isolate, identify and compare the binding partners of sAPP α and sAPP β in neuronal cells. Two unbiased receptor identification methods were used in combination with purified recombinant hexahistidine sAPP α and sAPP β . Following isolation, prey proteins were identified using GeLC-MS/MS. The identified prey proteins from each method were cross-referenced and potential receptors of interest were knocked down to investigate their role in the binding of sAPP α to cells.

Therefore, the aims of this chapter were to:

- Use a microbead-based isolation method, followed by GeLC-MS/MS, to isolate and identify sAPP α and sAPP β binding partners.
- Use QCM-D as an affinity purification method, followed by GeLC-MS/MS, to isolate and identify sAPP α and sAPP β binding partners.
- Compare the sAPP α and sAPP β binding partners isolated using the microbead and QCM-D methods, identifying any proteins isolated by both methods.
- Investigate the role of identified potential receptor(s) in the binding of sAPP α to cells.

5.2. The microbead-based identification of sAPP α and sAPP β binding partners.

To identify neuronal proteins that interact with sAPP α and sAPP β , three microbead-based affinity isolation experiments were performed using live SH-SY5Y cells. These were based on a published protocol for the isolation of protein binding partners using ligand-coated magnetic microbeads (Jones et al. 2015). The protocol was adapted for use with SH-SY5Y cells and sAPP α and sAPP β (Figure 5.1a). To confirm that both sAPP α and sAPP β successfully coated the microbeads as bait, each protein was incubated with tosylactivated microbeads (Section 2.11). Following washing and magnetic separation, any retained bait protein was eluted and analysed by immunoblotting (Figure 5.1b). Both sAPP α and sAPP β were eluted from the beads, demonstrating that they bound to the magnetic microbeads as bait and were retained through the washing steps (Figure 5.1b).

The compatibility of the microbead-based pulldown experiment with neuronal SH-SY5Y cells was then tested. Tosylactivated beads were coated either with anti-integrin β 1 antibody, anti-TFR antibody, sAPP α or sAPP β (Figure 5.1c). The coated beads were then incubated with cells and prey proteins were subsequently isolated. Isolated bait-prey complexes were separated, eluted and analysed by immunoblotting (Figure 5.1c). Immunoblot analysis of SH-SY5Y whole cell lysate confirmed that integrin β 1 and TFR were expressed by the SH-SY5Y cell line (Figure 5.1c, 'WCL' lane). The integrin β 1 antibody bait specifically isolated the larger mature molecular weight species of integrin β 1 from SH-SY5Y cells, but not the lower molecular weight intracellular precursor form (Koivisto et al. 1994) (Figure 5.1c). Integrin β 1 was not isolated by any other ligand (Figure 5.1c). Similarly, only the tosylactivated beads coated with the TFR antibody specifically isolated the TFR protein as prey from SH-SY5Y cells (Figure 5.1c).

These results demonstrated that the microbead-based affinity isolation protocol was able to isolate specific and relevant prey proteins from SH-SY5Y cells using specific bait proteins. The data also demonstrated that the conditions of the pull-down were appropriate for the preferential isolation of cell surface proteins, rather than cytosolic proteins, through the isolation of the cell surface, mature form of integrin β 1 alone (Figure 5.1c). This was advantageous for the desired isolation of cell surface receptors for sAPP α and sAPP β .

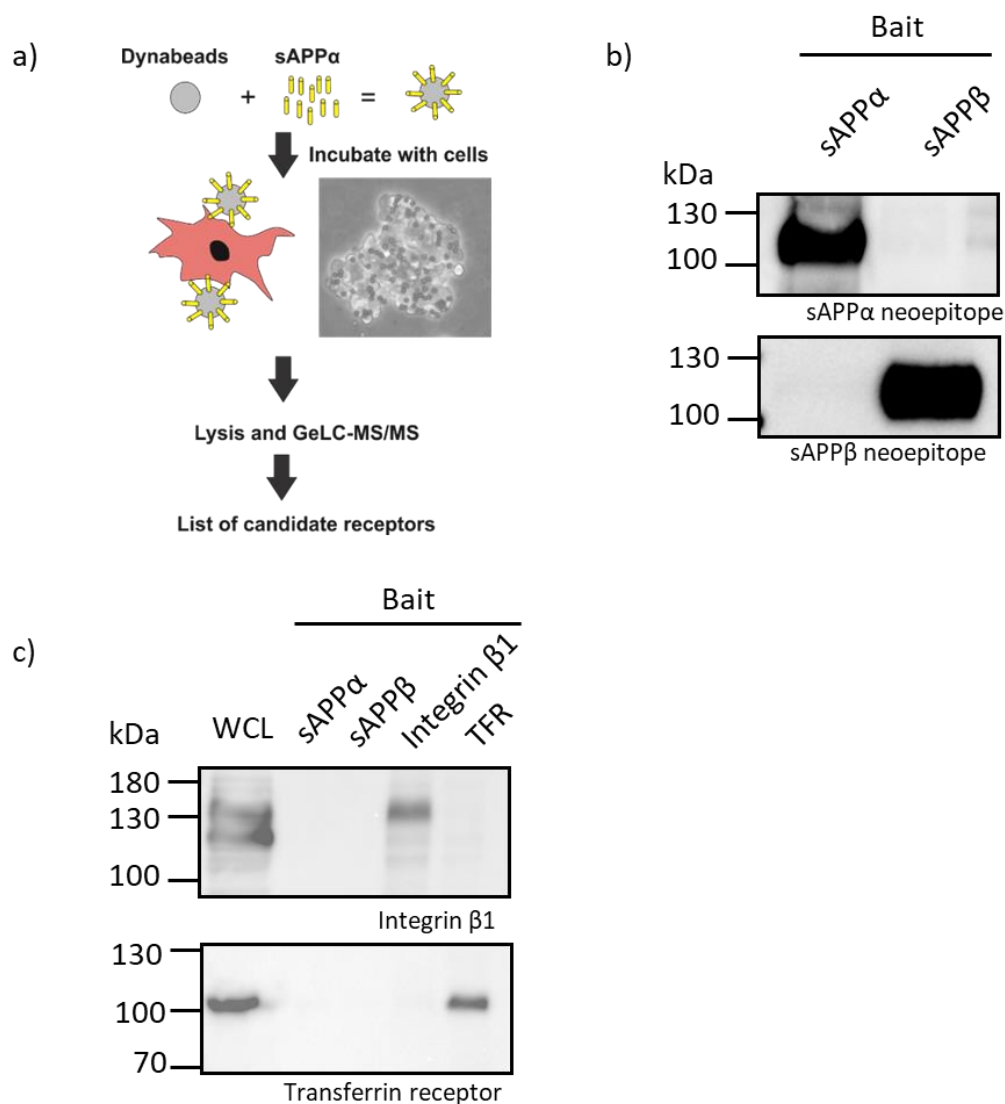


Figure 5.1. Validation of the microbead-based isolation assay in SH-SY5Y cells.

(a) Workflow of the microbead-based isolation protocol. (b) Immunoblots of sAPPα or sAPPβ bait eluted from tosylactivated microbeads. sAPPα or sAPPβ were incubated with tosylactivated microbeads according to the manufacturer's instructions, washed, and then heated to 95 °C in reducing sample buffer. Eluted samples were probed with the indicated antibody (sAPPα neopeptide - 2B3; sAPPβ neopeptide - 1A9). (c) Immunoblots of prey samples isolated from SH-SY5Y cells with specific bait proteins (sAPPα, sAPPβ, integrin β1 antibody [TS2/16], transferrin receptor antibody [OKT9]) using the microbead-based isolation protocol (Jones et al. 2015). Immunoblots were probed with the indicated antibody: Integrin β1 (TS2/16); Transferrin receptor, (OKT9). WCL = SH-SY5Y whole cell lysate, loaded for comparison.

Following the successful isolation of integrin $\beta 1$ and the TFR from SH-SY5Y cells using their respective antibodies as bait (Figure 5.1c), three larger-scale microbead-based affinity isolation experiments were performed to isolate sAPP α or sAPP β binding partners from SH-SY5Y cells. The antibody directed against the TFR was included as a positive control bait. The conditions of the three isolation experiments are listed in Table 5.1. Following the affinity isolation experiment, the prey proteins were identified using GeLC-MS/MS (workflow summarised in Figure 5.2). The full lists of all identified proteins for each bait protein are available as supplementary data (<https://doi.org/10.48420/22337503>). The first two pulldowns, when data was merged, identified a total of 1,294 proteins. The third pulldown identified a total of 1,395 proteins. In every pulldown, the microbeads coated with an antibody directed against the TFR successfully isolated the TFR from SH-SY5Y cells (Table 5.2). The TFR was only identified as prey in samples which used the TFR antibody as bait (Table 5.2). Each list was analysed for potential cell surface proteins of interest that were enriched in the sAPP α pulldown samples (Table 5.2). 'APP', which represented sAPP α and sAPP β in the swissprot trembl database, was identified specifically in the sAPP α and sAPP β bait samples (Table 5.2). The proteins identified in the TFR sample, except TFR itself, were considered to represent background proteins. The data were filtered manually through a review of the lists for proteins enriched in the sAPP α or sAPP β bait sample and lacking peptides in the TFR bait sample. Preference was given to cell-surface proteins as potential receptors and proteins particularly enriched in sAPP α bait samples. One family of isolated prey proteins was of particular interest: the type-I neuronal membrane proteins called calsyntenins (also called alcadeins). Calsyntenin-1 was identified as prey in two pulldown experiments with sAPP α as bait (Table 5.2) and two pulldown experiments with sAPP β as bait (Table 5.2). Calsyntenin-2 was identified as prey in two pulldowns using sAPP α as bait (Table 5.2) and one pulldown using sAPP β as bait (Table 5.2). Calsyntenin-3 was identified with a relatively high total spectral count in all three pulldowns using sAPP α as bait (Table 5.2) and with a lower spectral count in one pulldown using sAPP β as bait (Table 5.2). No calsyntenins were identified in the samples using the TFR antibody as bait, demonstrating that their isolations were specific to sAPP α and sAPP β .

Table 5.1. Comparison of the characteristics of each pulldown performed.

Pulldown #	Approximate number of microbeads	Approximate number of cells per bait	Amount of each bait used (μg)	Mass spectrometer used
1	2×10^7	4×10^7	10	Orbitrap
2	3×10^7	9×10^7	15	Orbitrap
3	3.95×10^7	7.9×10^7	19.75	Thermo QE HF

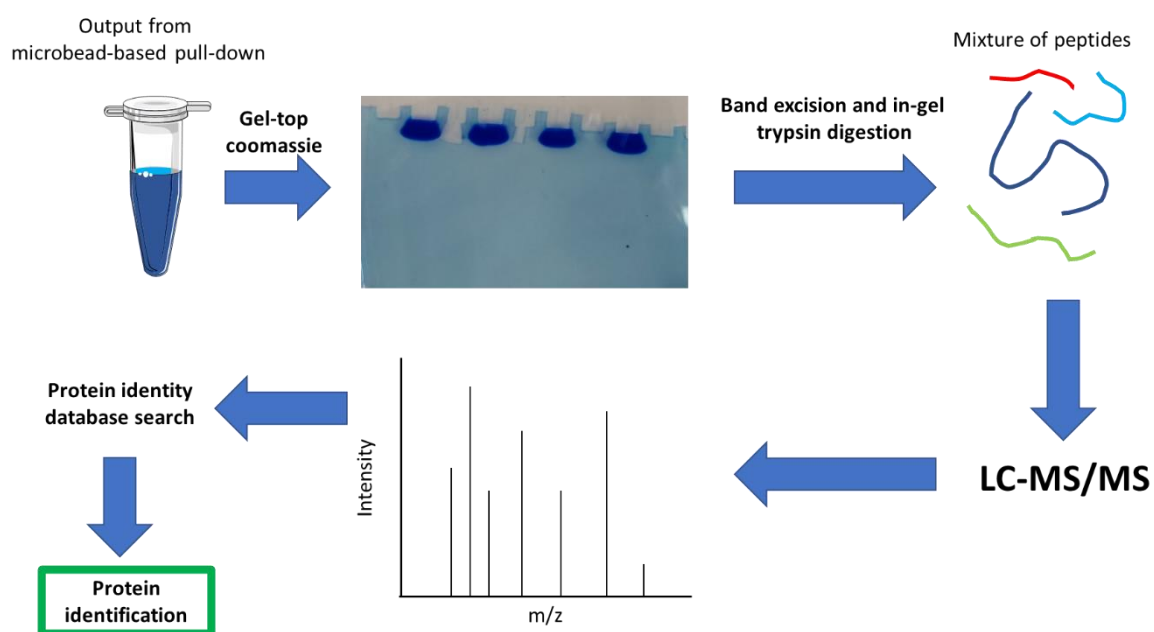


Figure 5.2 Schematic of GeLC-MS/MS workflow following the isolation of binding partners.

Adapted from (Dupree et al. 2020).

Table 5.2. The calsyntenin family of proteins were identified as sAPP α and sAPP β -specific binding partners in SH-SY5Y cells.

Tosylactivated dynabeads were coated with specified bait proteins and incubated with SH-SY5Y cells. Following incubation, bait-prey complexes were cross-linked, separated magnetically, washed, and lysed through sonication as described in the materials and methods (Section 2.11). Ligand-receptor adhesion complexes were eluted from the beads and analysed through GeLC-MS/MS by the University of Manchester BioMS core facility and lists of identified proteins were generated. Candidate sAPP α binding partners were considered if they were identified in the sAPP α pulldown, but not in the transferrin receptor antibody, and were expressed on the cell surface. Data for pulldowns 1 and 2 were generated using a Orbitrap Elite (ThermoFisher Scientific) mass spectrometer. Data for pulldown 3 were generated using a Thermo QE HF with U3000 nanoUPLC mass spectrometer. Numbers shown are total spectrum counts from three pulldowns. Data from pulldowns 1 and 2 were merged in Scaffold. Data from pulldown 3 was analysed separately. The full Tables of identified proteins are available as supplementary data. Pulldowns 1 and 2 - Protein Threshold: 99%; Min # of peptides: 2; Peptide threshold: 90%; Database: Swissprot trembl. Species: Human. Pulldown 3 - Min # peptides: 2; Database: Swissprot trembl. Species: Human. Full data can be found at <https://doi.org/10.48420/22337503>.

	Bait	TFR Ab			sAPP α			sAPP β		
	Pulldown #	1	2	3	1	2	3	1	2	3
Identity of prey protein	Transferrin receptor	24	15	105	0	0	0	0	0	0
	APP	0	0	0	37	23	81	57	31	73
	Calsyntenin-1	0	0	0	0	5	2	2	2	0
	Calsyntenin-2	0	0	0	0	2	3	3	0	0
	Calsyntenin-3	0	0	0	8	8	11	0	3	0
	Clusterin	0	0	0	2	3	4	4	0	4
	Nidogen	0	0	0	4	11	4	7	0	8
	Hemopexin	0	0	0	10	7	2	0	0	0
	Serine/threonine-protein phosphatase PP1-beta catalytic subunit	0	0	13	11	7	12	12	9	13

5.3. The use of QCMD as an alternative method to identify sAPP α and sAPP β binding partners.

As an alternative approach to the microbead-based method, QCM-D was used to isolate potential binding partners for sAPP α and sAPP β . QCM-D experiments were performed using cell lysates from immortalised SH-SY5Y cells, immortalised NB7 neuroblastoma cells and hiPSC-derived cortical neurons. As the aim of this chapter was to identify cell surface receptors, the lysate samples from NB7 cells and SH-SY5Y cells were first subjected to detergent-free membrane fractionation to enrich for membrane proteins prior to QCM-D-based isolation (Figure 5.3). First, the success of membrane fractionation was assessed by immunoblotting (Figure 5.3). The TFR was chosen as a membrane protein marker (Figure 5.3a) and β III tubulin was chosen as a cytosolic protein marker (Figure 5.3b). Following detergent-free membrane fractionation, the TFR was enriched in the membrane fraction (Figure 5.3a, arrow) and β III tubulin was enriched in the cytosolic fraction (Figure 5.3b, arrow).

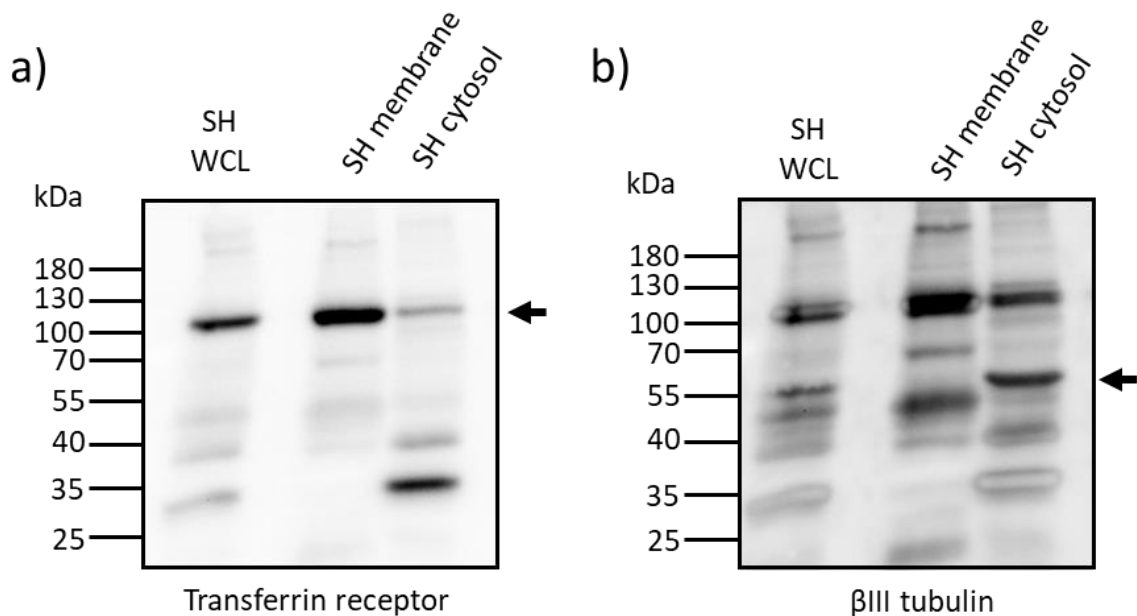


Figure 5.3. Detergent-free membrane enrichment from SH-SY5Y cell lysates.

Immunoblots of SH-SY5Y (SH) whole cell lysate (WCL), a membrane-enriched fraction and a cytosol-enriched fraction. Lysates were collected from SH-SY5Y cells in a detergent-free environment. Membrane fractionation was achieved by high-speed centrifugation (22,000 xg, 30 min, 4 °C). Immunoblots were initially probed with an antibody directed against (a) the transferrin receptor and the membrane was reprobed with an antibody directed against (b) β III tubulin. Arrows denote protein bands corresponding to (a) the TFR (predicted 84 kDa) and (b) β III tubulin (predicted 55 kDa).

Following confirmation of successful membrane fractionation, the membrane-enriched fraction was used for QCM-D-based isolation experiments. The membrane-enriched fraction from an additional human neuroblastoma cell line, NB7, was also included. Following the establishment of a streptavidin-coated lipid bilayer on the QCM-D chips (Figure 5.4a, Figure 5.4b), demonstrated by alterations in frequency and dissipation measurements, biotinylated sAPP α and sAPP β protein samples were added to act as bait proteins. The addition of sAPP α (Figure 5.4c) and sAPP β (Figure 5.4d) caused alterations in f and D , indicating adherence of the bait proteins to the QCM-D chip. Following this, the membrane-enriched lysate fractions were incubated with the bait-covered QCM-D chips to pull down binding partners for sAPP α or sAPP β . The addition of the SH-SY5Y membrane-enriched fraction caused alterations in the f and D traces, indicating adherence of prey proteins within the sample to the sAPP α (Figure 5.4e) or sAPP β (Figure 5.4f) immobilised bait proteins. Similar results to those described above were obtained using membrane-enriched fractions harvested from NB7 neuroblastoma cells to isolate sAPP α and sAPP β binding partners (Figure 5.5).

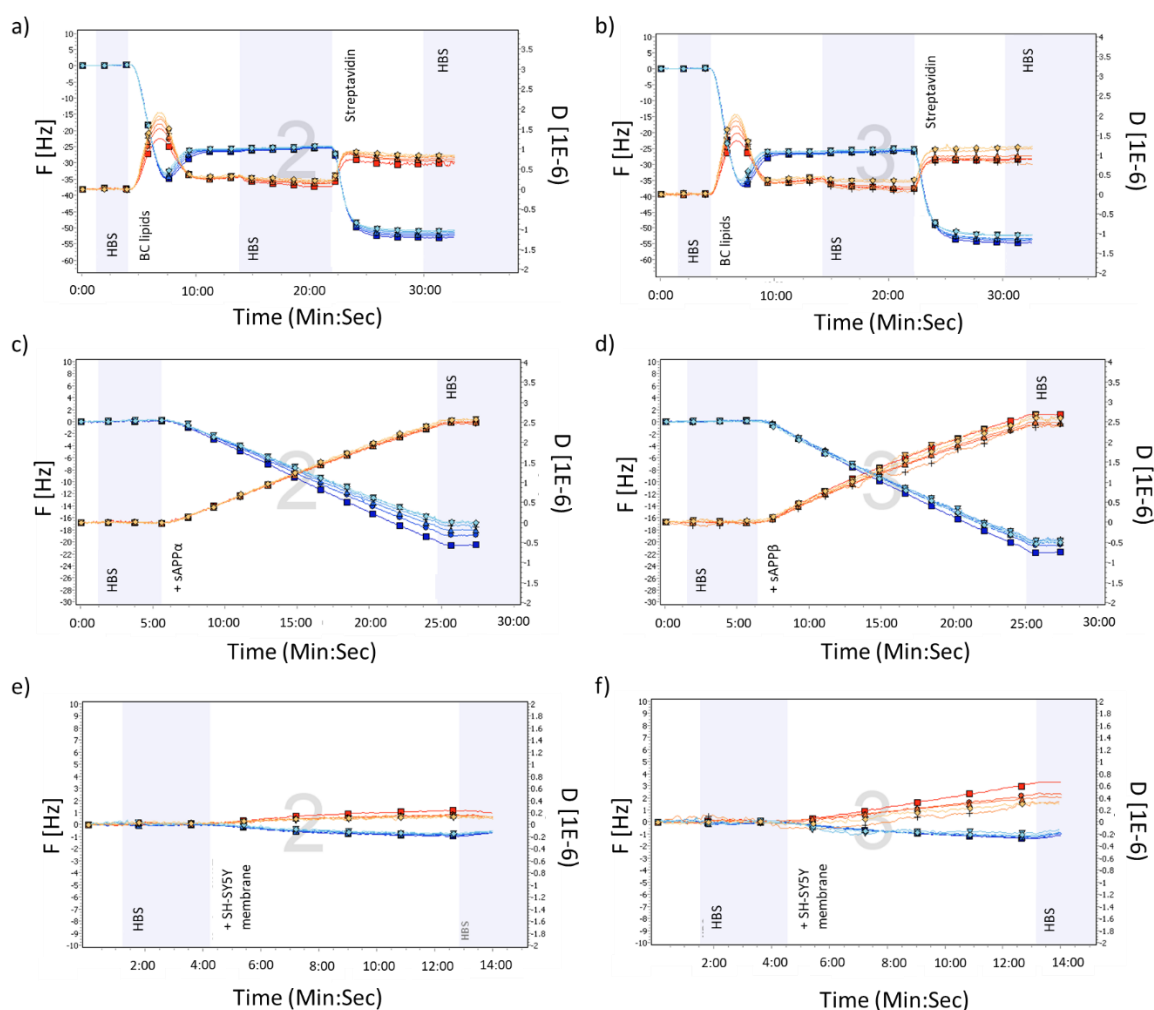


Figure 5.4. The capture of prey proteins from membrane-enriched SH-SY5Y lysate using sAPP α and sAPP β as bait proteins by QCM-D.

Changes in frequency and dissipation measurements indicate adherence to the QCM-D chip. (a), (b) Changes in frequency and dissipation measurements following the addition of lipid vesicles on the surface of the chip, forming a lipid bilayer, followed by the addition of streptavidin. (c) Biotinylated sAPP α was added to the chip, followed by (e) membrane-enriched SH-SY5Y cell fraction. (d) Biotinylated sAPP β was added to the chip, followed by (f) membrane-enriched SH-SY5Y cell fraction. F [Hz], frequency (blue); D [1E-6], dissipation (red).

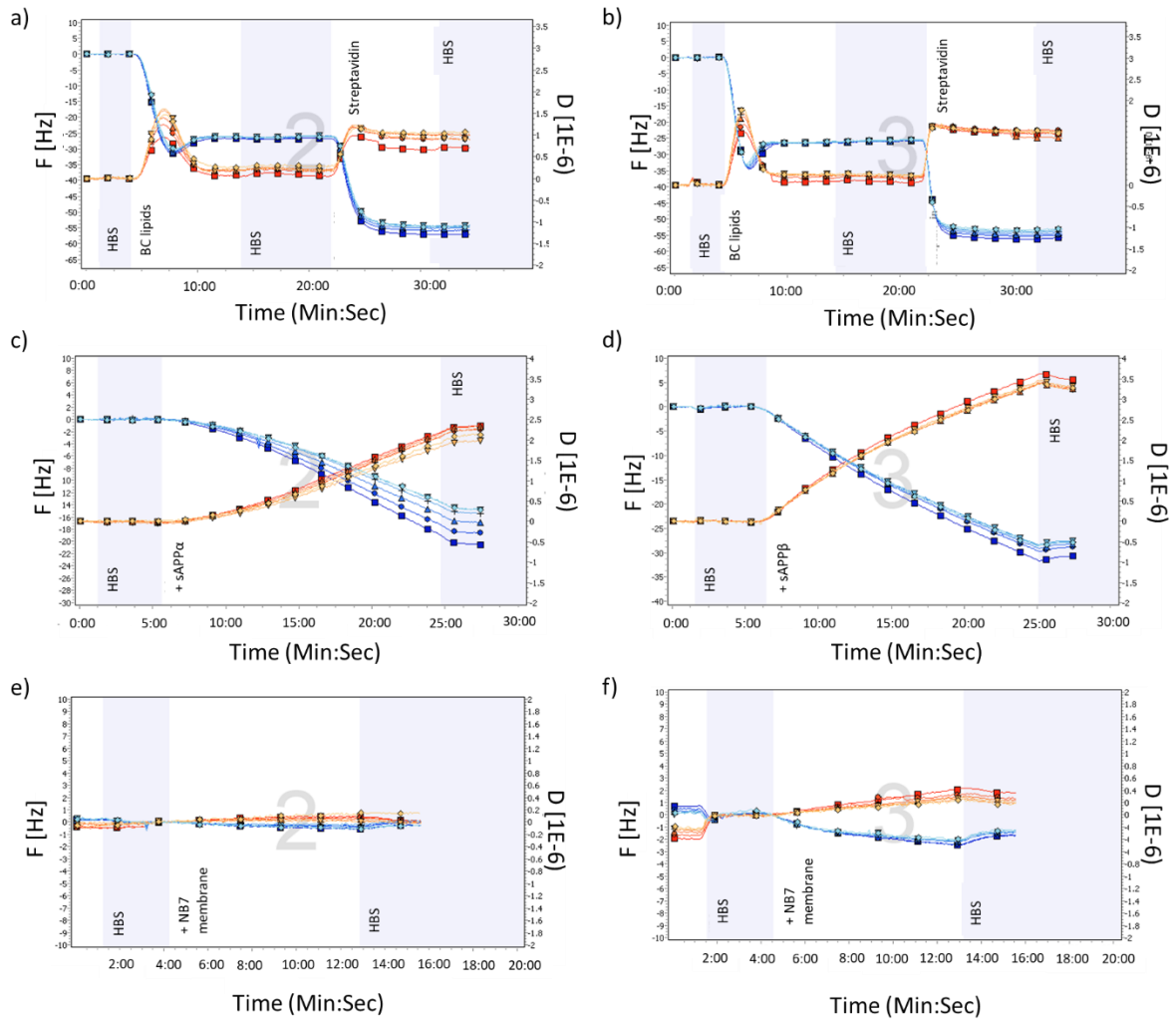


Figure 5.5. The capture of prey proteins from membrane-enriched NB7 cell fraction using sAPPα and sAPPβ as bait proteins by QCM-D.

Changes in frequency and dissipation measurements indicate adherence to the QCM-D chip. (a), (b) Changes in frequency and dissipation measurements following the addition of lipid vesicles on the surface of the chip, forming a lipid bilayer, followed by the addition of streptavidin. (c) Biotinylated sAPPα was added to the chip, followed by (e) membrane-enriched NB7 cell fraction. (d) Biotinylated sAPPβ was added to the chip, followed by (f) membrane-enriched NB7 cell fraction. F [Hz], frequency (blue); D [1E-6], dissipation (red).

Following the QCM-D-mediated isolation of prey proteins using sAPP α or sAPP β from SH-SY5Y and NB7 membrane-enriched lysates, the adhered bait and prey proteins were stripped from the QCM-D chip and their identities interrogated through GeLC-MS/MS (Table 5.3). The protein 'APP' represents the sAPP α and sAPP β bait in the swissprot trembl database (Table 5.3). Calsyntenin-1 was isolated specifically with sAPP α bait, but not sAPP β bait, from the membrane-enriched fraction of both SH-SY5Y cells and NB7 cells (Table 5.3). By contrast, calsyntenin-3 was isolated specifically with sAPP β bait, but not sAPP α , from the membrane-enriched fractions of both cell types (Table 5.3). However, only a single peptide spectrum of calsyntenin-3 was identified using sAPP β .

To isolate sAPP α and sAPP β binding partners in a more physiologically accurate model of human neurons, the QCM-D-mediated isolation experiment was repeated using whole cell lysate derived from hiPSC-derived neurons. A negative control chip, without bait, was also included. Adhered proteins were again stripped from the QCM-D chip and identified using GeLC-MS/MS. 'APP' was identified in the sAPP α and sAPP β bait samples, but not the negative control bait sample (Table 5.4). Calsyntenins-1 and -3 were identified in both sAPP α and sAPP β bait samples, but not the negative control bait sample (Table 5.4).

Table 5.3 The calsyntenin family of proteins were identified as sAPP α and sAPP β -specific binding partners in SH-SY5Y cells and NB7 cells by QCM-D-based isolation.

Following QCM-D-based ligand isolation, the QCM-D chips were stripped with reducing sample buffer and analysed by GeLC-MS/MS, performed by the University of Manchester BioMS core facility using an Orbitrap Elite (ThermoFisher Scientific) mass spectrometer. A list of candidate receptors was generated. Candidate binding partners were included if they (i) were identified in the sAPP α pulldown but not in the sAPP β pulldown and were expressed on the cell surface or (ii) were identified as candidate receptors in the microbead-based pulldown (Table 5.2). Data shown are total spectrum counts. The full list of identified proteins is available as supplementary). Min # peptides: 1. Database: Swissprot trembl. Species: Human. Full data can be found at <https://doi.org/10.48420/22337503>.

	Bait:	sAPP α		sAPP β	
	Cell sample:	SH membrane	NB7 membrane	SH membrane	NB7 membrane
Identity of prey protein	APP	3	4	14	11
	Calsyntenin-1	3	4	0	0
	Calsyntenin-3	0	0	1	1
	Clusterin	0	1	0	0
	cDNA FLJ57622, highly similar to Clusterin	2	0	1	0
	Nidogen	0	0	0	0
	Hemopexin	0	0	0	0
	Serine/threonine protein phosphatase PP1-beta catalytic subunit	0	0	0	0

Table 5.4. The calsyntenin family of proteins were identified as sAPP α and sAPP β -specific binding partners in hiPSC-derived cortical neurons by QCM-D-based isolation.

QCM-D-based receptor isolation was performed using whole cell lysate from hiPSC-derived cortical neurons. Following this, the QCM-D chips were stripped with reducing sample buffer and analysed by GeLC-MS/MS performed by the University of Manchester BioMS core facility using an Orbitrap Elite (ThermoFisher Scientific) mass spectrometer. A list of candidate receptors was generated. Candidate binding partners were included if they (i) were expressed on the cell surface and identified with the sAPP α bait but not with the negative control bait or (ii) were identified as candidate receptors in the microbead-based pulldown (Table 5.2). Data shown are total spectrum counts. The full list of identified proteins is available as supplementary data. Protein threshold: 99.0%; Min # peptides: 1; Peptide Threshold: 95%. Database: Swissprot trembl. Species: Human. Full data can be found at <https://doi.org/10.48420/22337503>.

		Bait		
		None	sAPP α	sAPP β
Identity of prey protein	APP	0	22	26
	Calsyntenin-1	0	2	4
	Calsyntenin-3	0	1	1
	Clusterin	1	2	2
	Nidogen	0	1	4
	Hemopexin	0	0	0
	Serine/threonine-protein phosphatase PP1-beta catalytic subunit	0	2	1

5.4. The investigation of calsyntenins 1 and 3 as potential novel binding partners for sAPP α .

Following the identification of calsyntenin-1 and calsyntenin-3 as potential novel binding partners of sAPP α through both microbead-based and QCM-D based receptor isolation studies, their roles in the binding of sAPP α to SH-SY5Y cells was investigated. GABABR1, a previously identified sAPP α receptor which facilitated sAPP α binding when expressed in HEK cells (Rice et al. 2019), was included as a known receptor for comparison. The assay for investigating the binding of sAPP α to SH-SY5Y cells was validated in chapter 4 (Figure 4.6). First, the effect of knockdown of GABABR1 on the binding of sAPP α to SH-SY5Y cells was investigated (Figure 5.6). GABABR1 gene expression was reduced by approximately 70% by siRNA knockdown (Figure 5.6a). The knockdown of GABABR1 did not significantly reduce the binding of sAPP α to SH-SY5Y cells (Figure 5.6b, 5.6c). Secondly, the importance of calsyntenin-1 in the binding of sAPP α to SH-SY5Y cells was investigated (Figure 5.7). Calsyntenin-1 gene expression was also reduced by approximately 70% by siRNA knockdown (Figure 5.7a). The knockdown of calsyntenin-1 did not significantly reduce the binding of sAPP α to SH-SY5Y cells (Figure 5.7b, 5.7c). Finally, the importance of calsyntenin-3 in the binding of sAPP α to SH-SY5Y cells was investigated (Figure 5.8). The ability to knockdown calsyntenin-3 through siRNA was tested by immunoblotting and confirmed (Figure 5.8a). Knockdown significantly reduced calsyntenin-3 expression by approximately 70% (Figure 5.8c). Following this, knockdown of calsyntenin-3 significantly reduced the mean intensity of sAPP α -specific antibody staining by approximately 35% in SH-SY5Y cells treated with sAPP α (Figure 5.8b, 5.8d).

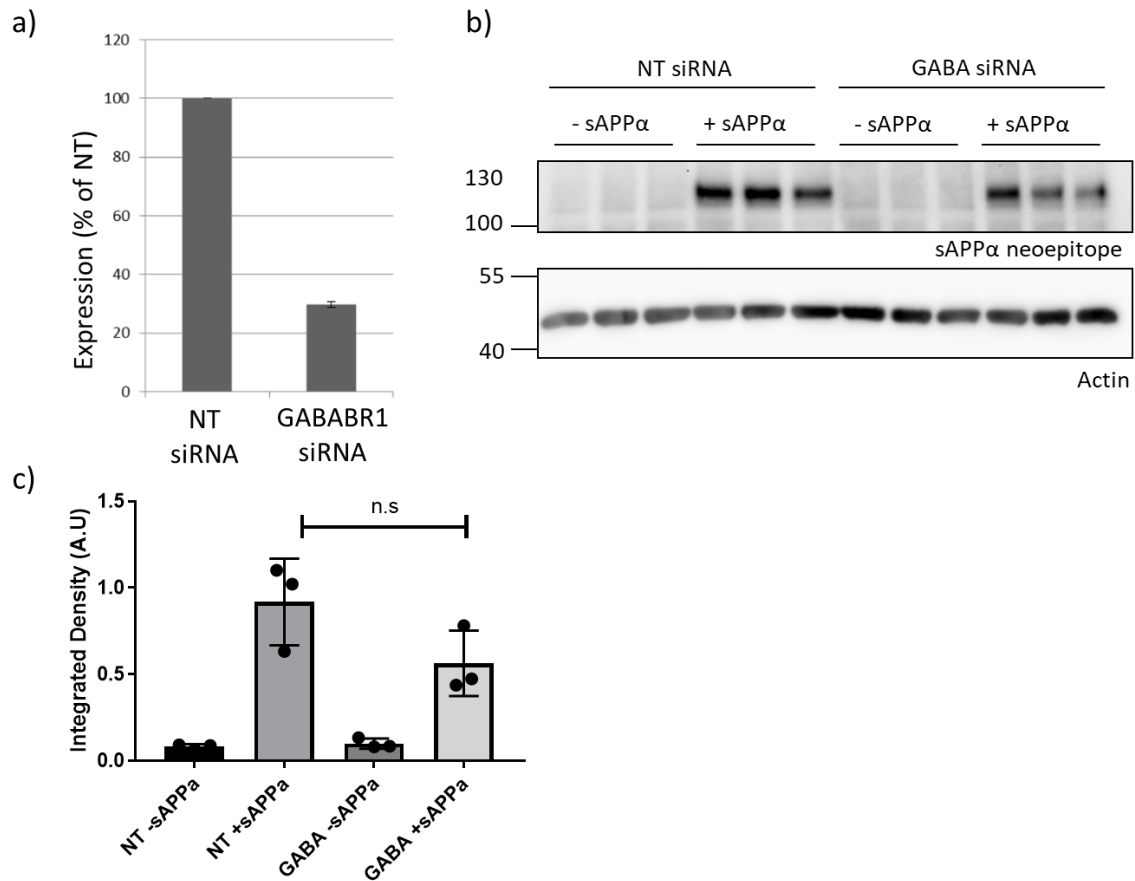


Figure 5.6. Knockdown of GABABR1 did not significantly reduce the binding of sAPPα to SH-SY5Y cells.

SH-SY5Y cells were incubated with either GABABR1 siRNA or non-targeting (NT) siRNA for 48 h. (a) Whole cell lysates were collected and GABABR1 gene expression was quantified by qPCR. GABABR1 gene expression in the NT sample was set to 100%. N = 3 wells of cells per siRNA. (b) DPBS vehicle control (- sAPPα) or 50 nM sAPPα (+ sAPPα) were incubated with cells for 5 min. The cells were washed three times in DPBS, followed by lysate collection. Lysate (30 µg protein) was analysed by immunoblotting using the sAPPα neoepitope antibody (2B3). The membrane was re-probed for actin. (c) Quantification of immunoblot band intensity of sAPPα, normalised against actin. A one-way ANOVA with Tukey's post-hoc test was performed with GraphPad Prism.

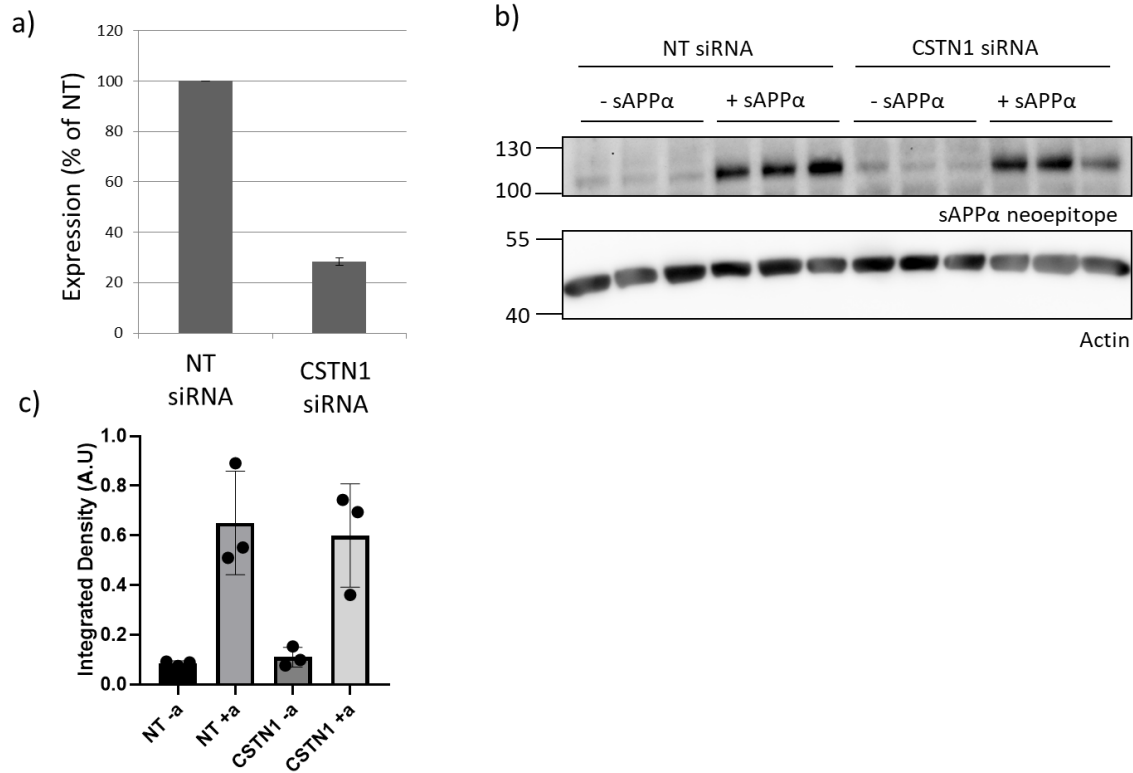


Figure 5.7. Knockdown of calsyntenin-1 did not reduce the binding of sAPPα to SH-SY5Y cells.

SH-SY5Y cells were incubated with either calsyntenin-1 siRNA or non-targeting (NT) siRNA for 48 h. (a) Whole cell lysates were collected and calsyntenin-1 gene expression was quantified by qPCR. Calsyntenin-1 gene expression in the NT sample was set to 100%. N = 3 wells of cells per siRNA. (b) DPBS vehicle control (- sAPPα) or 50 nM sAPPα (+ sAPPα) were incubated with cells for 5 min. The cells were washed three times in DPBS, followed by lysate collection. Lysate (30 µg protein) was analysed by immunoblotting using the sAPPα neoepitope antibody (2B3). The membrane was re-probed for actin. (c) Quantification of immunoblot band intensity of sAPPα, normalised against actin. A one-way ANOVA with Tukey's post-hoc test was performed with GraphPad Prism.

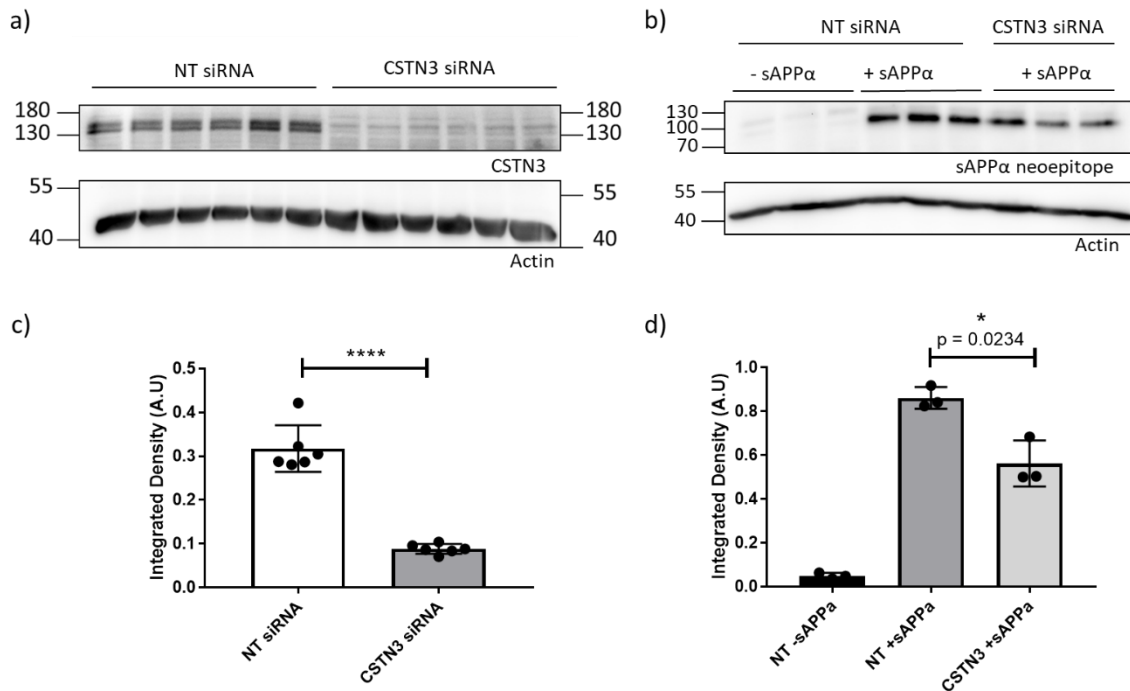


Figure 5.8. Knockdown of calsyntenin-3 significantly reduced the binding of sAPPα to SH-SY5Y cells.

SH-SY5Y cells were incubated with either calsyntenin-3 siRNA or non-targeting (NT) siRNA for 48 h. (a) Whole cell lysates were collected, and calsyntenin-3 expression was determined by immunoblotting. (b) DPBS vehicle control (- sAPPα) or 50 nM sAPPα (+ sAPPα) were incubated with cells for 5 min. The cells were washed three times in DPBS, followed by lysate collection. Lysate (30 µg protein) was analysed by immunoblotting using the sAPPα neoepitope antibody (2B3). The membrane was re-probed for actin. (c) Quantification of immunoblot band intensity of Calsyntenin-3 from the panel above, normalised against actin. An unpaired t-test with Welch's correction was performed with GraphPad Prism. (d) Quantification of immunoblot band intensity of sAPPα from the panel above, normalised against actin. A one-way ANOVA with Tukey's post-hoc test was performed with GraphPad Prism.

5.5 Discussion.

In this chapter, calsyntenin-1 and calsyntenin-3 were identified as potential novel binding partners of sAPP α in both immortalised cells and hiPSC-derived human cortical neurons using two distinct unbiased receptor identification methods. Knockdown of calsyntenin-3, but not calsyntenin-1 or the known receptor GABABR1, significantly reduced the binding of sAPP α to SH-SY5Y cells. These data implicate calsyntenin-1 and, particularly, calsyntenin-3 as potential novel binding partners of sAPP α and justify future investigations into their roles and molecular interactions.

5.5.1. The use of microbead-based affinity isolation to identify novel binding partners for sAPP α .

Several potential binding partners were identified for sAPP α and sAPP β through the microbead-based isolation experiments, such as calsyntenin-1, calsyntenin-2, calsyntenin-3, clusterin, nidogen, hemopexin and the serine/threonine-protein phosphatase PP1-beta catalytic subunit (table 5.2). Hemopexin was only identified in sAPP α bait samples and therefore had evidence as an sAPP α -specific interactor (table 5.2). Hemopexin has previously been linked to the mechanisms of ADs because of its role as an iron/heme-binding protein and the role of iron and oxidative stress in AD (Ashraf et al. 2020; Cheignon et al. 2018) (discussed in Section 1.5). However, hemopexin was deemed unlikely to be a plasma membrane receptor for sAPP α due to its lack of expression at the cell surface and its secretion (Ashraf et al. 2020).

Another protein identified as a potential sAPP α binding partner was Nidogen (table 5.2). Nidogen is a key component of the basement membranes and helps to stabilise the extracellular matrix (Reed et al. 2019). Nidogen could play a role in AD due to its position within the extracellular matrix of compartments such as the blood-brain barrier; however, as nidogen is predominantly secreted, it was viewed as unlikely to be a cell-surface receptor candidate for sAPP α in neurons (Reed et al. 2019).

A third candidate protein identified in the microbead-based pulldowns was clusterin (table 5.2). Clusterin is a secreted lipid transport protein which has been strongly implicated in AD in past studies (Foster et al. 2019). In fact, following *APOE* and *BIN1*, polymorphisms in the clusterin gene *CLU* were ranked in one study as the third greatest risk factor for late onset AD (Foster et al. 2019). Therefore, it is intriguing that clusterin was identified as a possible

interactor of sAPP α , as clusterin has previously been shown to bind to A β and APP (Foster et al. 2019; Wang et al. 2019). However, as clusterin is predominantly secreted protein with a role in lipid transport, it was not considered a strong candidate for a neuronal cell-surface receptor for sAPP α (Foster et al. 2019).

Serine/threonine-protein phosphatases have been implicated in AD due to the dysregulation of tau phosphorylation, highlighting the identification of serine/threonine-protein phosphatase PP1-beta catalytic subunit in the pulldowns as interesting, but its lack of expression at the cell surface indicated that the protein was unlikely to be an sAPP α membrane receptor (Braithwaite et al. 2012).

Finally, the particular enrichment of calsyntenin-3 in sAPP α samples compared to sAPP β samples, the localisation of calsyntenins at cell membranes and the robust evidence in the literature demonstrating interactions between APP, A β and the calsyntenin family of proteins placed them and, particularly, calsyntenin-3 as the primary receptor candidates in this thesis. Though there were existing links with A β and APP, calsyntenin-1 and calsyntenin-3 had not previously been identified as interacting with sAPP α or sAPP β , perhaps reflecting the novel methodology used in this thesis. Live human cells were used in combination with an N-terminally his-tagged bait protein, whereas previous sAPP α receptor identification studies have used synaptosome extract (Rice et al. 2019), a suspected receptor protein itself in a directed co-immunoprecipitation with sAPP α (Hasebe et al. 2013) or cortico-hippocampal mouse membrane extract (Dorard et al. 2018). One study also used mouse sAPP α , rather than the human sAPP α used in this study (Hasebe et al. 2013). Another strength of the present study was the use of human cells, whereas the three previous studies aimed at identifying potential sAPP α binding partners used extracts from rats or mice (Dorard et al. 2018; Hasebe et al. 2013; Rice et al. 2019). The use of human cells in this thesis thus increased the relevance of any identified receptor(s) as potential pharmacological targets in Alzheimer Disease patients.

Many techniques are available to identify protein binding partners *in vitro*, with each having its own strengths and limitations. Example methods include co-immunoprecipitation-based assays (Lim et al. 2021), microbead-based adhesion complex affinity isolation assays (Jones et al. 2015) and proximity-based labelling assays (Trinkle-Mulcahy 2019). The choice of microbead-based method for receptor identification was made for several reasons. Firstly,

the microbead-based protocol for the isolation of cell surface binding partners using bait ligands was developed by members of the supervisory team, so experience with the method was readily available (Jones et al. 2015). Secondly, the chosen microbead-based method used live human cells, allowing for the capture of the binding partners of sAPP α and sAPP β in their native environment rather than in cell lysates. In contrast, Rice *et al.*, 2019 used rat synaptosome extracts, enriching for synaptic prey proteins but potentially missing other prey proteins. Thirdly, as sAPP α is up to 100 times more neuroprotective than sAPP β (Furukawa et al. 1996), we hypothesised that the C-terminus was critical in its neuroprotective effect. Therefore, to facilitate protein purification, we tagged sAPP α and sAPP β with a small hexahistidine tag at the N-terminus to minimise interference with receptor binding at the C-terminus. The use of tosylactivated microbeads also ensured that the bait proteins were immobilised on microbeads in many different orientations, exposing various binding sites to potential prey proteins. In contrast, Rice *et al.*, 2019 used a C-terminal Fc-tag to immobilise sAPP α to beads via its C-terminus, potentially preventing C-terminal bait-prey interactions and subsequent isolation. Finally, the microbead-based isolation of the mature form of integrin β 1, but not the intracellular precursor form of the protein, during optimisation (Figure 5.1c) demonstrated the preferential isolation of cell surface prey proteins using this method (Koivisto et al. 1994; Yu et al. 2005). One limitation of the microbead-based assay was that hiPSC-derived cortical neurons, a more physiologically accurate model of neurons than SH-SY5Y cells (Engle et al. 2018), were not compatible with the assay. As a result, the more proliferative and hardier SH-SY5Y immortalised cell line was chosen for microbead-based isolation experiments.

5.5.2. The use of QCM-D-facilitated isolation to pull-down novel binding partners for sAPP α .

In addition to the microbead-based receptor identification method, QCM-D was chosen as an additional unbiased method to isolate the binding partners of sAPP α and sAPP β . Prey proteins within the membrane-enriched lysates rapidly adhered to the sAPP α or sAPP β coated chips in both cell lines, as shown by divergences in Δf and ΔD (Figures 5.4, 5.5). Following QCM-D-based isolation, adhered proteins were eluted and GeLC-MS/MS analysis was performed to identify potential binding partners. 'APP', which represented the sAPP α or sAPP β bait protein in the swissprot trembl database, confirmed the retention of each bait protein (Table 5.3). Calsyntenin-1 was identified as sAPP α -specific in both SH-SY5Y and NB7 membrane-enriched

fractions (Table 5.3). Calsyntenin-3 was identified as sAPP β -specific; however, only a single peptide spectrum was identified in the sAPP β bait sample. The lack of calsyntenin-3 in the sAPP α bait sample could be a result of the low amount of cellular material used in the QCM-D experiment, which was a limitation of this assay. In addition to the use of immortalised cell membrane fraction, the QCM-D-based isolation method allowed the use of whole cell hiPSC-derived cortical neuron lysate, which are more accurate neuronal model cells (Engle et al. 2018) (Table 5.4). In hiPSC-derived neurons, calsyntenin-1 and calsyntenin-3 were isolated by both sAPP α and sAPP β , but not by the uncoated negative control chip (Table 5.4). The use of hiPSC-derived neuron lysate further validated the identification of calsyntenin-1 and calsyntenin-3 as potential binding partners of sAPP α .

QCM-D is commonly used to monitor the adherence of molecules to substances coating a piezoelectric chip (Dixon 2008). Following the adherence of prey proteins within cell lysates to the sAPP α or sAPP β bait proteins coating the chip, the prey and bait proteins were stripped from the chip and identified by GeLC-MS/MS. QCM-D had previously been used to measure and compare the strength of known protein-protein interactions (Peh et al. 2007). QCM-D-based isolation required cell lysate rather than live cells, which provided an excellent contrast to the live-cell microbead method. Whole cell lysates were fractionated in detergent-free conditions to enrich for membrane proteins and enhance the isolation of potential cell surface receptors. A lack of detergent during cell lysate harvesting was necessary to avoid disruption of the lipid bilayer coating the QCM-D chip, upon which sAPP α or sAPP β were immobilised. Another benefit of QCM-D was that it allowed real-time measurement of the rapid interaction between bait and prey proteins.

Both microbead based and QCM-D-based receptor-isolation methods identified calsyntenins 1 and 3 as sAPP α and sAPP β binding partners using live human cells and human cell lysates. The use of two highly different isolation methods increased confidence in the accuracy of the isolated interaction between calsyntenins and sAPP α . No previously identified receptors, such as GABA $_B$ R1a (Rice et al. 2019), α 3-NKA (Dorard et al. 2018) or p75^{NTR} (Hasebe et al. 2013), were isolated in any of the pulldown methods used in this study, further reinforcing the novelty of the approaches used in this thesis.

5.5.3. The functions of calsyntenin-1 and calsyntenin-3.

Calsyntenin-1 (also known as alcadein- α) and calsyntenin-3 (also known as alcadein- β) are type-I transmembrane proteins, belonging to the cadherin superfamily of proteins, which are predominantly expressed in the brain within the post-synaptic membrane of neurons (Hintsch et al. 2002). Calsyntenin-1 was found to form a tripartite complex with APP and X11L, which reduced the β -secretase cleavage of APP and therefore decreased A β production (Araki et al. 2003). Knockdown of calsyntenin-1 disrupted the axonal transport of APP and significantly increased the β -secretase cleavage of APP in rat cortical neurons *in vitro* (Vagnoni et al. 2012). Therefore, there are existing links between APP, which shares much of its sequence with sAPP α , and calsyntenin-1. Calsyntenin-1 also has links to memory and synaptic function. The shed ectodomain of CASY-1, the sole *C. elegans* orthologue of the calsyntenin family, was found to be required for several types of learning (Ikeda et al. 2008). The CASY-1 study noted the similarity that the shed ectodomain of APP (sAPP α) was also able to rescue the learning deficits of APP knockout in mice (Ikeda et al. 2008). In fact, the CASY-1 study from 2008 explicitly suggested: “it may turn out that the cleaved ectodomains of calsyntenin and APP act in concert or in parallel to modulate learning and memory” (Ikeda et al. 2008), a hypothesis which is supported by the findings in this thesis. Calsyntenin-1 co-accumulated with APP within dystrophic neurites surrounding A β plaques in human AD brain samples (Araki et al. 2003). Knockout of calsyntenin-1 significantly increased β -secretase cleavage of APP in mice *in vivo* and significantly increased A β plaque density in APP transgenic AD mice (Gotoh et al. 2020). Calsyntenin-1 expression is also significantly reduced in human AD brains (Vagnoni et al. 2012) and in the cerebrospinal fluid of AD patients prior to clinical symptoms (Lleó et al. 2019). In summary, calsyntenin-1 likely binds to APP in a tripartite complex with X11L, which prevents the β -secretase cleavage of intracellular APP. The complex is then trafficked along the axon towards its functional destination. Loss of calsyntenin-1 thus increases the amount of free APP to undergo β -secretase cleavage, increasing A β production. As sAPP α contains the majority of the APP sequence, it follows that sAPP α may also interact with calsyntenin-1. In addition, calsyntenin-1 already has strong links to learning, memory and AD.

The calsyntenin family of proteins undergo regulated intramembrane proteolysis in a remarkably similar way to APP. Calsyntenins are first cleaved by ADAM10 or ADAM17, the

APP α -secretases, followed by a presenilin-dependent γ -secretase to release an intracellular domain (Hata et al. 2009). Therefore, perturbations in β -secretase or γ -secretase cleavage will also affect calsyntenin processing and function, potentially contributing to neuronal dysfunction.

Two forms of calsyntenin-3 have been identified previously: one neuronal-specific form called calsyntenin-3 α and one identified in adipocytes called calsyntenin-3 β (Zeng et al. 2019). For simplicity, the neuronal-specific calsyntenin-3 α will, from here, be referred to as calsyntenin-3. Calsyntenin-3 is a synaptic organising molecule which enhances pre-synaptic differentiation through trans-synaptic interaction with both α - and β -neurexins on the pre-synaptic membrane (Kim et al. 2020; Pettem et al. 2013). There is conflicting data within the literature as to whether calsyntenin-3 physically binds to α - and β -neurexins directly or whether they interact functionally, but not physically (Kim et al. 2020; Um et al. 2014). Knockout of calsyntenin-3 in mice significantly reduced both excitatory and inhibitory synaptic density and compromised synaptic transmission *in vivo* (Pettem et al. 2013). However, a separate study only saw an effect of calsyntenin-3 in excitatory neurons (Um et al. 2014). In another study, the individual knockdown of each calsyntenin isoform had no effect on synaptic density in cultured neurons; however, synaptic density was significantly reduced when all three calsyntenin isoforms were knocked-down, suggesting that the different calsyntenin isoforms may provide a level of functional redundancy for each other (Um et al. 2014).

Calsyntenin-1 and calsyntenin-3, but not calsyntenin-2, were identified as *in vivo* APP interactors in an immunoprecipitation experiment using mice (Bai et al. 2008). This study provided the only previous direct link in the literature between calsyntenin-3 and APP, but it was not explored further (Bai et al. 2008). Interestingly, the same study also identified GABA_BR1a, later identified as a synaptic receptor for sAPP α , as an *in vivo* APP interactor (Bai et al. 2008; Rice et al. 2019). Therefore, previously identified APP interactors may also be relevant binding partners of sAPP α . This thesis produced similar results, repeatedly isolating calsyntenin-1 and calsyntenin-3 as sAPP α binding partners through microbead-based and QCM-D receptor identification experiments. No previous study had identified a direct experimental link between either calsyntenin-1 or calsyntenin-3 and sAPP α or sAPP β .

5.5.4. The loss of calsyntenin-3, but not calsyntenin-1, may interfere with the binding of sAPP α to SH-SY5Y cells.

The roles of calsyntenin-1 and calsyntenin-3 in the binding of sAPP α to immortalised cells was tested (Figures 5.7 and 5.8) using a method optimised earlier in this thesis (Section 4.5). GABABR1, which was previously identified as a cell surface receptor for sAPP α (Rice et al. 2019), was also included as a known sAPP α receptor for comparison (Figure 5.6). Previously, the transfection and expression of GABA_BR1a in HEK cells was shown to facilitate the binding of sAPP α to the cell surface (Rice et al. 2019). Therefore, we hypothesised that the knockdown of total GABABR1 would reduce the binding of sAPP α in SH-SY5Y cells (Figure 5.6). An approximate 70% reduction in GABABR1 gene expression, quantified by qPCR (Figure 5.6a), did not lead to a significant reduction in the binding of sAPP α to SH-SY5Y cells (Figure 5.6b, 5.6c). This could be explained by other receptors, such as α 3-NKA (Dorard et al. 2018) or p75^{NTR} (Hasebe et al. 2013), providing a level of redundancy which may compensate for the loss of GABABR1 in SH-SY5Y cells. Nevertheless, there was a small reduction in sAPP α binding following GABABR1 knockdown (Figure 5.6).

Next, the effect of calsyntenin-1 knockdown on the binding of sAPP α to SH-SY5Y cells was investigated (Figure 5.7). An approximate 70% reduction in calsyntenin-1 gene expression was confirmed by qPCR (Figure 5.7a). The knockdown of calsyntenin-1 did not affect the binding of sAPP α to the cells (Figure 5.7b, 5.7c), which suggested that calsyntenin-1 was not critical for the binding of sAPP α to SH-SY5Y cells. However, as shown with the lack of a significant effect on binding following GABABR1 knockdown, this result does not discount the hypothesis that calsyntenin-1 has a role in sAPP α action. Finally, the role of calsyntenin-3 in the binding of sAPP α to SH-SY5Y cells was investigated (Figure 5.8). The knockdown of calsyntenin-3, confirmed by immunoblotting (Figure 5.8a, 5.8c), led to a significant decrease in the binding of sAPP α to SH-SY5Y cells (Figure 5.8b, 5.8d). These data indicate that calsyntenin-3 plays a role in the binding of sAPP α to SH-SY5Y cells, which is a novel finding.

Future work could investigate whether the knockdown of calsyntenin-3 reduces the binding of sAPP β to SH-SY5Y cells, to determine whether the effect is sAPP α -specific. Calsyntenin-3 has several overlapping functions with sAPP α , which could be explained by their possible interaction. Calsyntenin-3, a post-synaptic transmembrane protein, promoted the development of excitatory and inhibitory pre-synapses through interaction with both α - and

β -neurexins, increasing synaptic density (Kim et al. 2020; Pettem et al. 2013). Similarly, sAPP α incubation was also shown to increase pre-synaptic density *in vivo* and sAPP α was found to bind to β -neurexins (Cvetkovska et al. 2022; Roch et al. 1994). Therefore, if sAPP α does interact with calsyntenin-3, as this chapter suggests, some of the synaptogenic activities of sAPP α may be facilitated via interaction with calsyntenin-3 to induce downstream synaptogenic signalling. As APP is known to form a tripartite complex with calsyntenin-1 and X11L, perhaps sAPP α could facilitate the binding of calsyntenin-3 and neurexins through the formation of a similar complex. This could help explain why some studies identify direct interactions between calsyntenin-3 and neurexins and other studies refute this (Kim et al. 2020; Um et al. 2014). However, further study is required to confirm the interaction between sAPP α and calsyntenin-3 and to determine what effects are facilitated by such an interaction. Future work could also determine the effect of calsyntenin-1 or calsyntenin-3 knockdown on the neuroprotective activities of sAPP α , such as the protection against oxidative stress and the protection against A β neurotoxicity. A double knockdown of calsyntenin-1 and calsyntenin-3 could be performed to determine if there is an additive effect due to a reduction in receptor redundancy. Further investigation of the calsyntenins as potential binding partners for sAPP α would increase our understanding of synaptic processes and could open new therapeutic targets for neurodegenerative diseases.

5.6. Chapter summary.

The data in this chapter identified calsyntenin-1 and calsyntenin-3 as potential binding partners for sAPP α in neuronal cells using two distinct unbiased receptor isolation methods. Knockdown of calsyntenin-3 significantly reduced the ability of sAPP α to bind to SH-SY5Y cells. Together, these results justify further investigation into the roles of calsyntenin-1 and calsyntenin-3 as sAPP α binding partners.

- A microbead-based isolation method, followed by GeLC-MS/MS, identified calsyntenin-1, calsyntenin-2 and calsyntenin-3 as novel sAPP α and sAPP β binding partners using live SH-SY5Y cells.
- A QCM-D-based isolation method, followed by GeLC-MS/MS, also identified calsyntenin-1 and calsyntenin-3 as sAPP α or sAPP β binding partners in SH-SH5Y and NB7 neuronal cells. Calsyntenin-1 and calsyntenin-3 were also identified as an sAPP α and sAPP β binding partner in hiPSC-derived cortical neurons.
- Knockdown of GABABR1, a known sAPP α receptor, had no significant effect on the binding of sAPP α to SH-SY5Y cells.
- Knockdown of calsyntenin-1 had no significant effect on the binding of sAPP α to SH-SY5Y cells.
- Knockdown of calsyntenin-3 significantly reduced the binding of sAPP α to SH-SY5Y cells.

6. Discussion

Dementia is currently the leading cause of death in the UK (ONS 2022). The need for new disease-modifying treatments for Alzheimer's disease necessitates the identification of novel therapeutic targets. The identification of mechanisms through which neuroprotective molecules protect neurons from cellular damage could elucidate new pharmacological options to treat neurodegenerative diseases. One neuroprotective molecule of interest was sAPP α , which protected neurons against multiple forms of cellular damage and promoted neuronal growth (Habib et al. 2017) (Section 1.7). However, despite several previous attempts to identify the receptors which mediate the effects of sAPP α , the mechanism through which sAPP α reduced oxidative stress and protected neurons against A β -induced neurotoxicity remained elusive (Dorard et al. 2018; Hasebe et al. 2013; Rice et al. 2019). This thesis aimed to identify novel sAPP α binding partners using two unbiased receptor identification methods. HEK cells secreting large quantities of N-terminal hexahistidine-tagged sAPP α and sAPP β were generated and each protein was purified under non-denaturing conditions. sAPP α significantly reduced ROS generation in neuroblastoma cells following toxic insult in a time-dependent manner and increased the expression of synaptophysin across three iPSC-derived neuron inductions close to significance. Crucially, calsyntenin-1 and calsyntenin-3 were identified through two different unbiased receptor identification methods as novel potential binding partners for sAPP α in human neuronal cells. Furthermore, calsyntenin-3 was shown to have a significant role in the binding of sAPP α to SH-SY5Y cells. Overall, this work further demonstrated the beneficial effects of sAPP α and identified novel interactions between sAPP α and calsyntenin-1 and calsyntenin-3. Discussed in this chapter are the implications for these data in the wider field of AD research, as well as limitations and suggestions for future work.

6.1. The generation of physiologically relevant sAPP α and sAPP β for use in downstream experiments.

Previous studies identified receptors responsible for facilitating neurotrophic and synaptic effects of sAPP α (Dorard et al. 2018; Hasebe et al. 2013; Rice et al. 2019), but failed to identify the receptor(s) responsible for facilitating the neuroprotective effect of sAPP α against oxidative stress and A β -toxicity. Therefore, it was hypothesised that there were unidentified

receptors responsible for mediating those neuroprotective effects and that previous studies may have missed binding partners due to flaws with their experimental models, which this thesis aimed to resolve.

Several previous receptor pulldown studies used sAPP α produced in *E. coli* (Dorard et al. 2018; Hasebe et al. 2013). Whilst protein synthesis in *E. coli* can allow for production in higher quantities, the purified protein would lack any mammalian post-translational modifications. The post-translational modification of APP, described in Section 1.3, could affect protein stability, receptor interaction and therefore subsequent receptor isolation (Tan et al. 2021). Thus, proteins produced in mammalian cells are the most appropriate for use in receptor isolation studies using human cells. This thesis addressed these concerns through the expression of sAPP α and sAPP β in HEK cells (chapter 3), which ensured that the proteins would have the appropriate mammalian post-translational modifications and thus maximum physiological relevance (Tan et al. 2021).

In addition, several previous receptor identification studies used sAPP α tagged at its C-terminus (Dorard et al. 2018; Rice et al. 2019). The C-terminus of sAPP α is hypothesised to be critical in the enhanced neuroprotective effect of sAPP α over sAPP β , likely due to differential receptor binding (Furukawa et al. 1996). Therefore, the tagging of sAPP α at the C-terminus in previous studies, particularly with a large Fc tag (Dorard et al. 2018; Rice et al. 2019), may have prevented important receptors from interacting with the C-terminal region of sAPP α and being isolated and identified. Supporting this, though Rice et al. (2019) compared both sAPP α and sAPP β , the study identified GABA $_B$ R1a as interacting with a region common to both sAPP α and sAPP β . Therefore, GABA $_B$ R1a is unlikely to be responsible for the enhanced effect of sAPP α over sAPP β . Their lack of identification of sAPP α -specific proteins could be because the large Fc tag at the C-terminus may have blocked C-terminal interactions. The use of large C-terminal tags may also contribute to the absence of receptors responsible for sAPP α -mediated neuroprotection in the literature. In this thesis, to ensure the availability of the C-terminus of sAPP α to potential receptors, a much smaller hexahistidine tag was placed at the N-terminus. The data presented in chapter 3 demonstrated the insertion of a hexahistidine tag at the N-terminus of each sAPP sequence and the insertion of a stop codon at the ADAM10 or BACE1 cleavage site in sAPP α and sAPP β plasmids, respectively (Figure 3.1). The hexahistidine tag was inserted immediately downstream of the APP signal peptide, which is

removed during APP membrane translocation and is not present in the secreted sAPP α or sAPP β protein (Hegde and Bernstein 2006). Immunoblotting data, using highly specific neoepitope antibodies for the C-terminus of sAPP α and sAPP β , demonstrated the production and secretion of large quantities of sAPP α or sAPP β from HEK cells with intact C-termini (Figure 3.3). Both sAPP α and sAPP β were purified successfully, to a high purity, through IMAC via their N-terminal hexahistidine tags (Figure 3.2). The IMAC purification of tagged sAPP α was similar in principle to the purification of sAPP α in other studies. Rice et al (2019) generated HEK cells which secreted large amounts of sAPP α -Fc protein into OptiMEM and purified the protein via the C-terminal Fc tag through affinity chromatography using protein-G plus agarose. Dorard et al (2018) generated sAPP α -Fc plasmids in monkey COS cells and purified the protein via the Fc tag using protein-A Sepharose. Hasebe et al (2013) used the commercial N-terminal His-tagged sAPP α , produced in *E. coli*, which therefore lacked mammalian post-translational modifications. The sAPP α produced and used in this thesis should therefore allow for the isolation of C-terminal sAPP α interactions more optimally than any previous sAPP α study. Previous studies also switched between using sAPP α -Fc and recombinant commercial N-terminally His-tagged sAPP α for different experiments within the same study, including the use of mouse sAPP α in some cases (Dorard et al. 2018; Hasebe et al. 2013). In contrast, all relevant experiments within this thesis used human sAPP α from the same source.

Mass spectrometric analysis of sAPP α from transfected HEK cell media demonstrated the removal of larger sAPP isoforms containing the KPI/OX-2 domains following IMAC purification, showing that only the sAPP α_{695} isoform was being purified via its N-terminal hexahistidine tag as desired (Figure 3.5). The sAPP α purified in this thesis was compared with commercially available sAPP α through immunoblotting. Interestingly, commercially acquired sAPP α (Sigma #S9564) appeared to have reduced immunoblot staining across all tested sAPP α antibody epitopes, with almost no staining occurring with the neoepitope C-terminal antibody compared to the lab-produced sAPP α , despite equal protein loading (Figure 3.6). This could indicate a lower purity of the commercial protein and possible carboxy-peptidase action at the C-terminus. This further highlighted the superiority of the recombinant sAPP α used in this thesis over the commercially-acquired protein used in other studies (Dorard et al. 2018; Hasebe et al. 2013).

Prior to downstream experiments, the biophysical characteristics of the recombinant sAPP α and sAPP β proteins, such as solubility, were investigated. The biophysical characteristics of sAPP α and sAPP β had not been studied in any previous receptor identification experiment. Biophysical analysis confirmed that sAPP α and sAPP β were both highly soluble proteins and had a low level of aggregation under the conditions used for purification (Figure 3.7).

6.2. The development of an assay to quantify the binding of sAPP α and sAPP β to neuronal cells.

sAPP α is a neuroprotective and neurotrophic protein (Habib et al. 2017). In chapter 4 of this thesis, the effects of the sAPP α on human cells were investigated. iPSC-derived neurons were generated according to the protocol established by Shi, Kirwan and Livesey (2012) (Figure 4.1a). Neuronal differentiation was confirmed through immunofluorescence microscopy demonstrating the expression of β III tubulin, SATB2 and MAP2 neuronal markers (Figure 4.1b, 4.1c). iPSC-derived neurons also expressed synaptophysin, demonstrating the formation of synapses (Figure 4.1c). However, the assay also co-stained for the astrocyte marker GFAP and the astrocytic and oligodendrocyte marker S100 β . Staining for S100 β was present, but there was a clear presence of cells staining strongly for GFAP, indicating the presence of astrocytes within the iPSC-derived neuron culture (Figure 4.1b). This demonstrates a limitation of using iPSC-derived neurons, as other cell types can differentiate from the OX1-19 iPSC precursors. However, as astrocytes are also present in the human brain, the co-culture could be seen as more representative of a patient brain than neurons alone. In summary, the differentiation of iPSC-derived neurons was confirmed through the expression of neuronal markers, but other cell types such as astrocytes were also present.

The binding of sAPP α to the cell surface has been previously demonstrated through immunofluorescent microscopy (Dorard et al. 2018; Hasebe et al. 2013; Rice et al. 2019). However, immunofluorescence microscopy was not successful in this thesis due to high levels of background fluorescence (data not shown). Therefore, a novel method for detecting the binding of sAPP α and sAPP β to the cell surface was developed which utilised immunoblotting. Previous studies have demonstrated sAPP α activity at concentrations ranging between 1 nM and 100 nM (Section 1.7) (Dorard et al. 2018; Goodman and Mattson 1994; Hasebe et al. 2013; Mattson et al. 1993). Thus, concentrations between 5 nM and 80 nM were tested in the novel binding assay with iPSC-derived human neurons (Figure 4.2) and SH-SY5Y cells

(Figure 4.6). Despite a degree of variation between wells of the iPSC-derived neurons, the binding of sAPP α was visible at concentrations above 30 nM in iPSC-derived neurons and at concentrations above 15 nM SH-SY5Y cells using this assay. One limitation of this assay was that the antibody specific for the neoepitope of sAPP β (1A9) did not have a high enough sensitivity to identify sAPP β at the concentrations used (Figure 4.7), so a more sensitive multiplex immunoassay was used to determine sAPP β binding. The binding of sAPP β to iPSC-derived neurons was successfully demonstrated through this assay, confirming the successful binding of both recombinant sAPP α and sAPP β proteins to human cells.

Previous studies had also demonstrated the rapid nature of the binding of sAPP α to cells, which occurred within minutes (Dorard et al. 2018; Mattson et al. 1993). The data presented in in chapter 5 also confirmed the rapid binding of recombinant sAPP α to iPSC-derived neurons within 10 minutes (Figure 4.2) and to SH-SY5Y cells within 5 minutes (Figure 4.6). Therefore, the recombinant sAPP α protein purified in chapter 3 bound at similar concentrations and at similar rates as in previous studies within the literature. Crucially, the binding of sAPP α was shown to be significantly reduced by heat denaturation, demonstrating that the binding was dependent on correct protein folding (Figure 4.6.). When sAPP α and sAPP β were compared directly using an antibody which recognised an N-terminal epitope on both proteins (22C11), more sAPP α bound than sAPP β (Figure 4.7). This may suggest that sAPP β had a lower affinity for the cell surface than sAPP α , which is supported by previous data in the literature (Furukawa et al. 1996; Hasebe et al. 2013).

6.3. sAPP α significantly reduced ROS production in SH-SY5Y cells

Oxidative stress is a major mechanism through which neuronal cells are damaged in AD (Tönnies and Trushina 2017; Zhao and Zhao 2013). sAPP α was previously shown to reduce the generation of ROS and therefore protect against oxidative stress (Goodman and Mattson 1994). This effect could be therapeutically beneficial to reduce neuronal damage and neurodegeneration in diseases such as AD. However, the receptor and mechanism mediating the protection against oxidative stress by sAPP α was unknown. In chapter 4 of this thesis, the protective effect of sAPP α against ROS production in SH-SY5Y wild-type cells was investigated. As the toxic activity of A β oligomers has been linked to the prion protein and ADAM10 stimulation was beneficial in those cells, the protective effect of sAPP α on ROS generation in SH-SY5Y cells overexpressing the prion protein was also investigated. The addition of

menadione significantly increased ROS production in a concentration-dependent manner, however pre-treatment with sAPP α significantly reduced the ROS production in a time-dependent manner (Figures 4.8, 4.9). A similar effect was seen in SH-SY5Y cells overexpressing the prion protein (Figure 4.9). These data supported studies in the literature showing neuroprotective effects of sAPP α against A β oligomer-induced ROS (Goodman and Mattson 1994). One limitation of these results was the lack of a direct comparison of sAPP α with sAPP β in their effects on ROS production, due to difficulties encountered with the ROS assay. The ROS assay could also be attempted with more relevant neuronal models, such as primary neurons or iPSC-derived neurons. However, difficulties may be encountered with cell fragility. Future work could directly compare the neuroprotective effects of sAPP α and sAPP β against ROS production, including in different cell types such as iPSC-derived neurons, which has not been previously studied.

6.4. sAPP α significantly increased the expression of pre-synaptic markers in iPSC-derived neurons.

Aside from protection against oxidative stress, another of the beneficial effects of sAPP α are its neurotrophic effects. Previous studies showed that sAPP α significantly increased synaptic density, measured through synaptic markers such as synaptophysin (Roch et al. 1994). Treatment with sAPP α also significantly increased neurite outgrowth in mouse primary cortical neurons (Hasebe et al. 2013). In this thesis, the neurotrophic effect of sAPP α on the expression of the pre-synaptic markers synaptophysin and VGLUT1 and the post-synaptic marker PSD95 was investigated. Synaptic markers such as these have been used in previous studies to quantify synaptic density, and the loss of synaptophysin and VGLUT1 from AD brains correlated significantly with cognitive decline (Kashani et al. 2008; Roch et al. 1994; Sze et al. 1997). Three different iPSC-derived neuron inductions were used. In one induction, pre-treatment with 15 nM sAPP α , but not 15 nM sAPP β , clearly and significantly increased synaptophysin expression (Figure 4.3c); however, when analysed across all inductions, sAPP α did not significantly affect the expression of synaptophysin. A larger degree of variation is expected when using iPSC-derived neurons compared to immortalised cells due to their extensive differentiation protocol and long maturation time. This can mean that separate differentiations, and even technical replicates within a single differentiation, may develop differently with different amounts of contaminating non-neuronal cells (Volpato and Webber

2020). The differences in the response to sAPP α treatment on synaptophysin expression between differentiations could indicate a higher presence of non-neuronal cells in the less-responsive inductions, or a particularly high number of sensitive neurons and synapses in induction 3. The significant increase in synaptophysin expression in induction 3 was consistent with previous studies which demonstrated a similar neurotrophic effect of sAPP α in mice *in vivo* (Roch et al. 1994). As the loss of synaptophysin from AD brains correlates significantly with cognitive decline, the possible effect of sAPP α to increase synaptophysin expression could be therapeutically beneficial (Sze et al. 1997). There was no significant effect of sAPP α on the expression of VGLUT1 or PSD95 in iPSC-derived neurons. Future work could repeat this experiment, with the aim of reducing variation and interrogating the promising neurotrophic result.

6.5. The use of a novel unbiased pulldown method to identify sAPP α binding partners.

Chapter 4 of this thesis demonstrated the rapid binding of recombinant sAPP α to cells at nanomolar concentrations along with protective activities consistent with previous studies in the literature (Goodman and Mattson 1994). Following these results, recombinant sAPP α and sAPP β were used as bait in three unbiased receptor pulldown experiments to identify novel candidate binding partners using tosylactivated microbeads. The aim of chapter 5 was to identify novel binding partners which could be responsible for unattributed beneficial effects of sAPP α , such as its protection against oxidative stress and A β -induced cell death (Goodman and Mattson 1994).

Several previous studies used immunoprecipitation-based approaches to identify sAPP α binding partners from cell extracts (Dorard et al. 2018; Hasebe et al. 2013; Rice et al. 2019). For example, Rice et al (2019) performed affinity purification from rat synaptosome extracts using sAPP α ₆₉₅ with a C-terminal Fc tag covalently linked to protein-G plus agarose resin. The use of rat synaptosome-enriched extract was due to their interest in synaptic sAPP α protein interactions. However, this enrichment for synaptic proteins may have prevented the identification of important non-synaptic protein interactions. As such, a pulldown which utilised living neuronal cells could provide a more relevant model to investigate the interactions of sAPP α with neuronal cells in its native physiological environment.

In chapter 5 of this thesis, a pulldown method with living human cells was used to identify sAPP α binding partners using tosylactivated microbeads. This method had been developed

by the Humphries lab at the University of Manchester for the ligand-specific isolation of cell surface receptors (Jones et al. 2015). The use of this method allowed for the novel capture of sAPP α interactions with the cell surface of human SH-SY5Y cells in their native environment. Tosylactivated microbeads would immobilise sAPP α molecules through a wide range of sites via sulfhydryl and primary amino groups, which would facilitate the exposure of a many potential receptor binding sites.

First, the novel microbead-based isolation method was optimised for use with SH-SY5Y cells, as this thesis was the first time SH-SY5Y cells had been used with this method. sAPP α and sAPP β both successfully coated tosylactivated microbeads and survived washing steps (Figure 5.1). Bait antibodies directed against integrin β 1 and the transferrin receptor successfully isolated the transferrin receptor protein and integrin β 1 proteins as prey from SH-SY5Y cells (Figure 5.1). Interestingly, only the larger molecular weight isoform of integrin β 1 was isolated as prey from the SH-SY5Y cells, which represented the mature cell surface isoform (Sørensen et al. 2015) (Figure 5.1). These data showed that the conditions were optimised for the preferential isolation of cell surface proteins from SH-SY5Y cells. Whilst previous studies directed their pulldown efforts towards certain cell compartments such as synaptosomes (Rice et al. 2019) or specific candidate receptors themselves, such as p75^{NTR} (Hasebe et al. 2013), this thesis attempted to identify novel candidate binding partners for sAPP α using live cells in an undirected and unbiased manner.

sAPP α and sAPP β were coated onto tosylactivated microbeads and used to isolate prey proteins from SH-SY5Y cells using the protocol established by Jones et al., (2015). A positive control transferrin receptor antibody bait was also included. Following the receptor isolation experiment, GeLC-MS/MS was used to identify components isolated by the sAPP α bait in comparison to control baits. Previous studies had used MALDI-TOF MS/MS (Dorard et al. 2018) or LC-MS/MS (Rice et al., 2019). GeLC-MS/MS was used in this thesis as it allowed for the removal of molecules which could have interfered with the analysis by mass spectrometry, such as buffers and salts, and was the standard protein identification method offered by the BioMS core facility at the University of Manchester (Piersma et al. 2013). However, GeLC-MS/MS can also result in the loss of some peptides during extraction from the gel compared to MALDI-TOF MS/MS or LC-MS/MS approaches (Dzieciatkowska et al. 2014). Three separate pulldowns were performed, with two using a less sensitive Orbitrap

Elite mass spectrometry machine and the third using the more sensitive QE mass spectrometry machine. Calsyntenin-3 was specifically isolated by sAPP α in three pulldowns and by sAPP β in one pulldown. Though total spectral counts are not fully quantitative, the higher total spectrum counts for calsyntenin-3 in the sAPP α samples gave more confidence in its identification as a binding partner than in the single sAPP β pulldown. Calsyntenin-1 was also isolated specifically by sAPP α and sAPP β , with spectral counts being relatively similar between the two bait proteins. In each repeat, the transferrin receptor antibody bait also isolated the transferrin receptor as prey from SH-SY5Y cells, which validated each pulldown. Interestingly, no previously identified sAPP α receptors, such as GABA $_B$ R1a (Rice et al. 2019), α 3-NKA (Dorard et al. 2018) or p75^{NTR} (Hasebe et al. 2013), were isolated in any of the receptor isolation experiments in this thesis. This could be because the tosylactivated microbead method exposed different receptors and binding partners to sAPP α than the methods used in other papers and could highlight the novelty of the approach used in this thesis. One limitation of this pulldown experiment was the lack of a negative control, so future experiments could include beads blocked with BSA alone. However, comparison with the list of proteins isolated using the transferrin receptor proved sufficient to identify calsyntenin-1 and calsyntenin-3 as sAPP α binding partners.

6.6. The novel use of QCM-D as an unbiased method to identify receptors for an immobilised ligand.

All previous studies investigating sAPP α binding partners used a single bead-based receptor identification method (Dorard et al. 2018; Hasebe et al. 2013; Rice et al. 2019). However, a second receptor identification method was used in this thesis, to investigate potential sAPP α binding partners more thoroughly and to give greater confidence in the results. Proximity-labelling approaches were attempted, but repeated cloning efforts to produce sAPP α joined to an APEX2 labelling molecule were unsuccessful. This thesis therefore utilised QCM-D, which measures the adherence of molecules to the surface of a chip in a label-free real-time manner, as an additional method to identify sAPP α binding partners (Section 5.3). Biotinylated sAPP α was immobilised in random orientations onto a streptavidin-coated lipid bilayer on the surface of the QCM-D chip (Section 5.3). As this thesis was primarily focused on identifying cell surface receptors, whole cell lysates harvested from SH-SY5Y cells and NB7 cells were subjected to detergent-free membrane fractionation to enrich each cell extract for

membrane proteins. The use of membrane-enriched cell lysates mirrored the study by Rice et al (2019), which utilised synaptosome-enriched extracts due to their interest in synaptic receptors. The QCM-D-mediated approach also facilitated the use of lysates from iPSC-derived neurons, as live iPSC-derived neurons were not compatible with the tosylactivated-microbead method due to their fragility. QCM-D-mediated isolation, followed by GeLC-MS/MS, again identified calsyntenin-1 and calsyntenin-3 as potential binding partners for sAPP α . Calsyntenin-3 was not identified in sAPP α bait samples in immortalised cells, perhaps due to the low spectral counts generated by this method because of less cellular material (Table 5.3). Calsyntenin-1 was identified as an sAPP α -specific binding partner in immortalised cells (Table 5.3). In iPSC-derived neuron extract, calsyntenin-3 was identified in both sAPP α and sAPP β bait samples with one spectral count (Table 5.4) (Engle et al. 2018). Calsyntenin-1 was identified in both sAPP α and sAPP β bait samples for iPSC-derived neurons (Table 5.4). If this experiment were to be repeated in future, a negative control of uncoated QCM-D chip should be included for the QCM-D isolation experiment using immortalised cells, similar to how a negative control chip was included in the iPSC-derived neuron QCM-D isolation experiment.

In summary, tosylactivated microbead-based isolation and QCM-D-based isolation, two very different receptor identification methods which utilised live cells and membrane-enriched cell lysates respectively, both identified calsyntenin-1 and calsyntenin-3 as potential sAPP α binding partners in human cells. Though comparisons are somewhat difficult due to the different mass spectrometry machines used and the different experimental parameters, Rice et al. (2019) identified GABA B 1a as an sAPP α interactor with initial total spectral counts of 5-10 spectra, similar to the number of spectra identified for sAPP α in this thesis for calsyntenin-3 from the tosylactivated microbead pulldown experiments. The identification of novel binding partners for sAPP α supports the original thesis hypothesis that there were unidentified sAPP α receptors which could have a role in the activity of sAPP α .

6.7. Calsyntenin-3 was required for the normal binding of sAPP α to SH-SH5Y cells.

Following the robust identification of calsyntenin-1 and calsyntenin-3 as potential binding partners for sAPP α , their roles in the binding of sAPP α to immortalised cells was investigated. GABA B 1, which was identified as an sAPP α binding partner in a previous study (Rice et al. 2019), was included as a positive control. Each protein of interest was knocked down through

siRNA gene silencing and the effect on the binding of sAPP α was measured through immunoblotting. The data in this thesis demonstrated that knockdown of calsyntenin-1 did not affect the binding of sAPP α to SH-SY5Y cells (Figure 5.7). The knockdown of GABA $_B$ R1 reduced sAPP α binding, but not significantly (Figure 5.6). Strikingly, the knockdown of calsyntenin-3 significantly reduced the binding of sAPP α (Figure 5.8). These data suggested that calsyntenin-3 may have a larger role in the binding of sAPP α to SH-SY5Y cells than GABA $_B$ R1, a known sAPP α receptor (Rice et al. 2019), and validated the results of the receptor identification experiments.

6.8. The potential interaction between calsyntenin-3 and sAPP α .

Calsyntenin-1 and calsyntenin-3 are type I transmembrane proteins predominantly expressed on the post-synaptic membrane of neuronal cells (Hintsch et al. 2002). Calsyntenin-1 has been previously shown to form a tripartite complex with APP and X11-L to reduce A β production (Araki et al. 2003). As sAPP α contains most of the APP sequence, it follows that sAPP α may also bind to calsyntenin-1 in a similar manner to APP. This is supported by previous studies which suggested that some functions of APP may be performed by sAPP α (Hornsten et al. 2007; Ring et al. 2007), that calsyntenins may be required for certain types of learning (Ikeda et al. 2008) and that calsyntenin-1 is significantly reduced in AD brains (Vagnoni et al. 2012). Therefore, there are already existing links in the literature between calsyntenin-1, APP and memory. However, this thesis was the first to identify a potential molecular link between sAPP α and calsyntenin-1.

Calsyntenin-3 is relatively understudied in comparison to calsyntenin-1. Calsyntenin-3 promoted the differentiation of synapses (Pettem et al. 2013), which could correlate with the known synaptic activity of sAPP α , such as the increase in markers of synaptic density such as synaptophysin (Section 4.4; Roch et al., 1994). Interestingly, one previous *in vivo* study identified calsyntenin-1, calsyntenin-3, and GABA $_B$ R1a as interactors of APP in mice (Bai et al. 2008). However, in the study by Bai et al (2008), no further investigation into calsyntenin-1 or calsyntenin-3 was performed. Similar to calsyntenin-1, a C-terminal fragment of calsyntenin-3 was found to accumulate around A β plaques in dystrophic neurites in both AD mouse models and AD patient brain samples (Uchida et al. 2013). Overexpression of calsyntenin-3 significantly accelerated the death of cultured rat cortical neurons from serum starvation (Uchida et al. 2013). Treatment of rat cortical neurons with A β ₁₋₄₂ significantly increased the

expression of calsyntenin-3, down-regulated calsyntenin-2 and did not alter calsyntenin-1 (Uchida et al. 2011). Compared to wild-type mice, calsyntenin-3 gene expression was also significantly up-regulated in AD mouse models with the Swedish mutation, whilst the expression of calsyntenin-1 and calsyntenin-2 were unchanged (Uchida et al. 2011). Interestingly, GABABR1a was also found to associate with APP and one of calsyntenin-1 or calsyntenin-3 through affinity purification experiments, suggesting a potential interaction between the three proteins (Dinamarca et al. 2019).

This thesis was the first study to identify an interaction between calsyntenin-3 and sAPP α or sAPP β , and the first to demonstrate that calsyntenin-3 may be critical for the binding of sAPP α to SH-SY5Y cells (Section 5.4). Future studies could investigate whether calsyntenin-3 is required for the binding of sAPP β to neuronal cells.

The exact nature of the interaction between sAPP α and calsyntenin-3 is unclear. Calsyntenin-3, expressed on the post-synaptic membrane, interacted with neuexins on the pre-synaptic membrane to induce synaptic differentiation (Pettem et al. 2013). Loss of calsyntenin-3 significantly reduced synaptic density in mice (Pettem et al. 2013). However, there are conflicting reports within the literature as to whether calsyntenin-3 interacted physically with neuexins or not (Kim et al. 2020; Um et al. 2014). This conflicting data in the literature, combined with the data in this thesis, could suggest that sAPP α facilitates the binding of neuexins and calsyntenin-3 in a similar way to the tripartite complex of calsyntenin-1, APP and X11-L. This could explain why some studies find a physical interaction between neuexins and calsyntenin-3 while others do not, if the interaction depended on the presence of sAPP α (Kim et al. 2020; Um et al. 2014). This could also explain some of the neurotrophic effects of sAPP α at the synapse, as the interaction between calsyntenin-3 and neuexin induces synaptic differentiation (Kim et al. 2020; Um et al. 2014). However, this is purely a speculative hypothesis at present. Future work should aim to identify the exact role calsyntenin-3 plays in the binding of sAPP α to human cells and determine its role in mediating sAPP α activity. Future work could investigate the co-localisation of sAPP α and calsyntenin-1 or calsyntenin-3 through confocal immunofluorescence microscopy. In addition, a future study could investigate whether knockdown of calsyntenin-3 or calsyntenin-1 impacted the protective effect of sAPP α against A β -induced cell death (Furukawa et al. 1996). These findings would

further interrogate the therapeutic potential of calsyntenin-1 and calsyntenin-3 and their roles in neurodegeneration.

6.9. Concluding remarks.

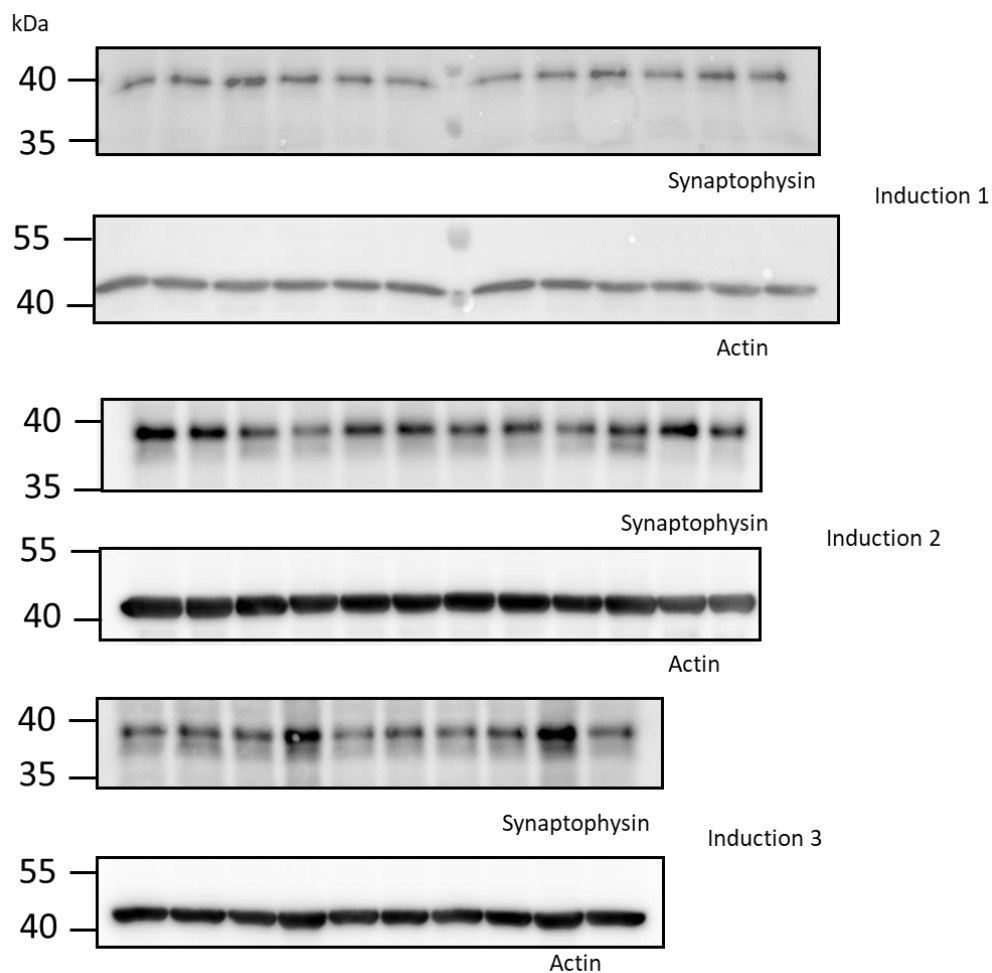
As dementia emerges as the largest cause of death globally, new therapeutic avenues are desperately needed. Alzheimer's disease is the greatest cause of dementia, but other diseases such as vascular dementia or dementia with Lewy bodies also contribute heavily to disease burden. Successful treatment is complicated by overlapping pathologies often occurring within individual patients and difficulties in achieving an accurate diagnosis (Hyman et al. 2012; Selvackadunco et al. 2019). Therefore, the development of therapeutic strategies which could be effective against several causes of dementia, such as harnessing neuroprotective molecules to increase neuronal resistance to cellular damage, is a crucial area of research. sAPP α has been shown to protect neurons against oxidative damage, a critical neurodegenerative mechanism in dementia (Goodman and Mattson 1994). sAPP α also promoted neuronal growth and improved memory (Hasebe et al. 2013; Ohsawa et al. 1999; Roch et al. 1994). These characteristics demonstrate the therapeutic potential of sAPP α for treating a wide range of neurodegenerative diseases. However, sAPP α can have detrimental effects, so knowledge of the specific receptors and mechanisms through which it acts is crucial to avoid off-target toxicity in patients. Prior to this thesis, previous studies had identified receptors responsible for synaptic modulation (Rice et al. 2019) and the promotion of neurite outgrowth (Dorard et al. 2018; Hasebe et al. 2013). However, no study had identified the receptor(s) which facilitated other sAPP α effects such as the protection against oxidative stress. Therefore, it was hypothesised that there remained unidentified sAPP α receptors which could have high therapeutic potential.

The data presented in this thesis demonstrated that sAPP α has a significant protective effect against oxidative stress in human cells and may increase the expression of synaptophysin in iPSC-derived neurons. This thesis identified calsyntenin-1 and calsyntenin-3 as novel binding partners for sAPP α using two different unbiased receptor identification methods. Calsyntenin-3 was shown to have a significant role in facilitating the binding of sAPP α to human neuronal cells. Following on from these findings, future work could characterise the exact nature of the interaction between calsyntenin-3 and sAPP α . The identification of novel binding partners for sAPP α in this thesis demonstrated the lack of knowledge and

understanding of the mechanisms by which sAPP α acts and highlighted its potential as a therapeutic option for dementia that requires further investigation.

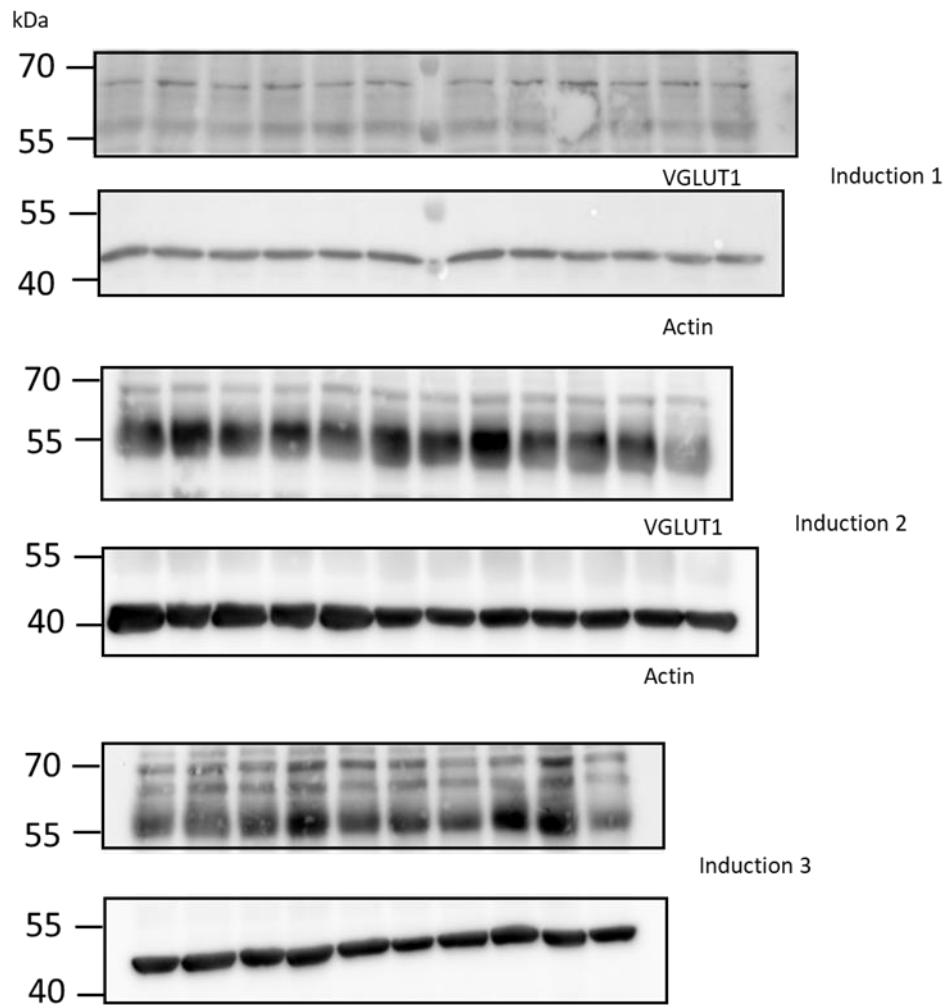
7. Supplementary Figures and Tables

Full mass spectrometry data can be found at <https://doi.org/10.48420/22337503>.

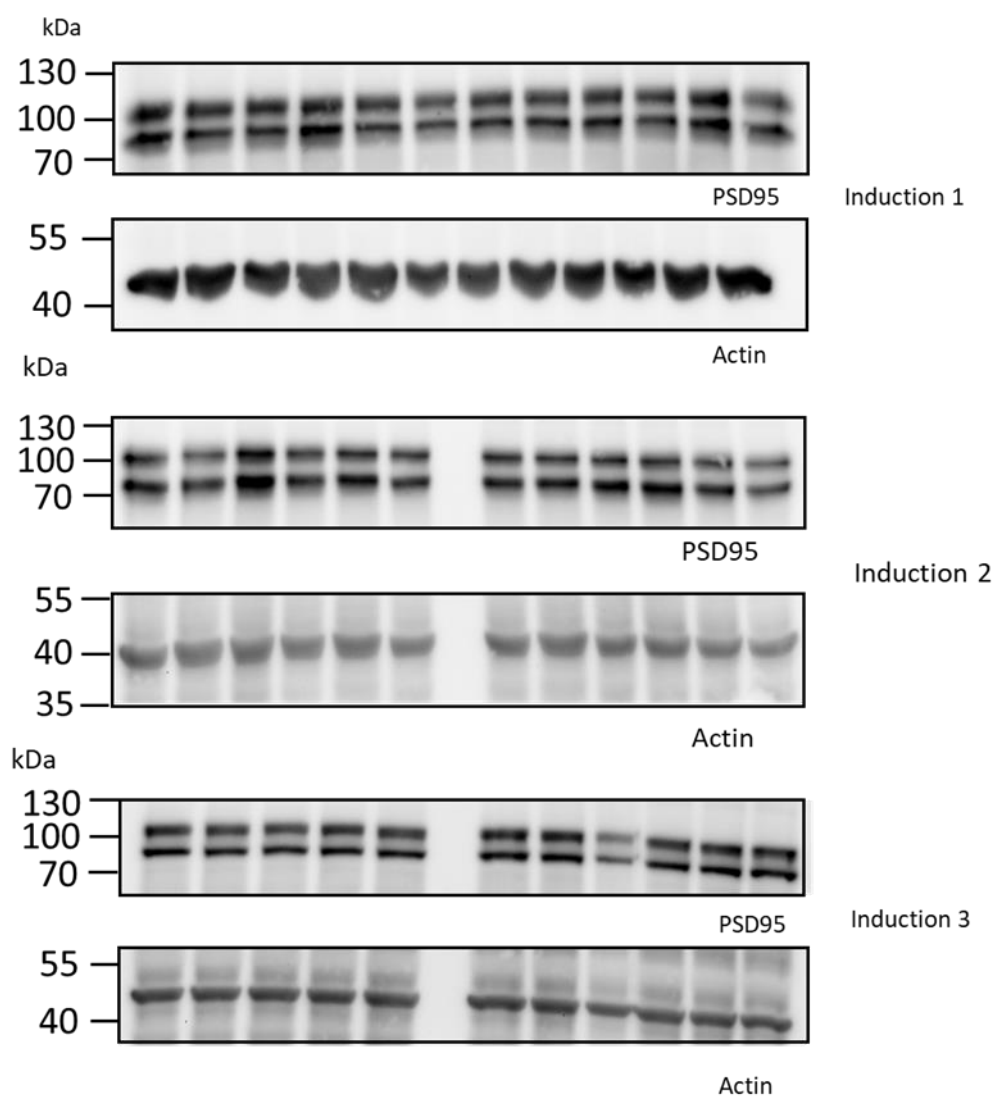


Supplementary Figure 7.1. Full blots of the effect of sAPP α and sAPP β on the expression of synaptophysin in iPSC-derived human neurons.

Linked to Figure 4.3.



Supplementary Figure 7.2. Full blots of the effect of sAPP α and sAPP β on the expression of VGLUT1 in iPSC-derived human neurons.
Linked to Figure 4.4.



Supplementary Figure 7.3. Full blots of the effect of sAPP α and sAPP β on the expression of PSD95 in iPSC-derived human neurons.

Linked to Figure 4.5.



Supplementary Figure 7.4. Plasmid map of sAPP α

Plasmid map of sAPP α in the pcDNA3.1+ plasmid. AmpR, ampicillin resistance; CMV, cytomegalovirus; Lac, lactose. Imaged using SnapGene Viewer.

Supplementary Table 7.1. One-way ANOVA results for synaptophysin expression (all inductions combined). Tukey's multiple comparison's test was used to compare all conditions to the vehicle negative control. Blots shown in Figure 4.3a-c.

ANOVA Table	SS	DF	MS	F (DFn, DFd)	P value
Treatment (between columns)	0.7252	4	0.1813	F (4, 23) = 2.324	P=0.0869
Residual (within columns)	1.794	23	0.078		
Total	2.519	27			

Tukey's multiple comparisons test	Mean Diff.	95.00% CI of diff.	Adjusted P Value
Vehicle vs. 15 nM sAPP α	-0.2086	-0.6853 to 0.268	0.6975
Vehicle vs. 50 nM sAPP α	0.03159	-0.4451 to 0.5082	0.9996
Vehicle vs. 15 nM sAPP β	0.1058	-0.3708 to 0.5825	0.9637
Vehicle vs. 50 nM sAPP β	0.3231	-0.2098 to 0.856	0.4017
15 nM sAPP α vs. 50 nM sAPP α	0.2402	-0.2365 to 0.7169	0.5791
15 nM sAPP α vs. 15 nM sAPP β	0.3145	-0.1622 to 0.7911	0.3207
15 nM sAPP α vs. 50 nM sAPP β	0.5317	-0.001194 to 1.065	0.0507
50 nM sAPP α vs. 15 nM sAPP β	0.07426	-0.4024 to 0.5509	0.9901
50 nM sAPP α vs. 50 nM sAPP β	0.2915	-0.2414 to 0.8244	0.5020
15 nM sAPP β vs. 50 nM sAPP β	0.2173	-0.3157 to 0.7502	0.7485

Supplementary Table 7.2. One-way ANOVA results for synaptophysin expression (induction 1 alone).

Tukey's multiple comparison's test was used to compare all conditions to the vehicle negative control. Blot shown in Figure 4.3a.

ANOVA Table	SS	DF	MS	F (DFn, DFd)	P value
Treatment (between columns)	0.2139	4	0.05348	F (4, 5) = 4.289	P=0.0710
Residual (within columns)	0.06234	5	0.01247		
Total	0.2762	9			

Tukey's multiple comparisons test	Mean Diff.	95.00% CI of diff.	Adjusted Value	P
Vehicle vs. 15 nM sAPP α	0.2953	-0.1527 to 0.7432	0.1959	
Vehicle vs. 50 nM sAPP α	0.1199	-0.3281 to 0.5678	0.8134	
Vehicle vs. 15 nM sAPP β	0.3194	-0.1285 to 0.7674	0.1564	
Vehicle vs. 50 nM sAPP β	0.4023	-0.04559 to 0.8503	0.0739	
15 nM sAPP α vs. 50 nM sAPP α	-0.1754	-0.6233 to 0.2725	0.5677	
15 nM sAPP α vs. 15 nM sAPP β	0.02415	-0.4238 to 0.4721	0.9993	
15 nM sAPP α vs. 50 nM sAPP β	0.1071	-0.3409 to 0.555	0.8628	
50 nM sAPP α vs. 15 nM sAPP β	0.1995	-0.2484 to 0.6475	0.4670	
50 nM sAPP α vs. 50 nM sAPP β	0.2825	-0.1655 to 0.7304	0.2208	
15 nM sAPP β vs. 50 nM sAPP β	0.08291	-0.365 to 0.5309	0.9369	

Supplementary Table 7.3. One-way ANOVA results for synaptophysin expression (induction 2 alone).

Tukey's multiple comparison's test was used to compare all conditions to the vehicle negative control. Blot shown in Figure 4.3b.

ANOVA Table	SS	DF	MS	F (DFn, DFd)	P value
Treatment (between columns)	0.3984	4	0.09959	F (4, 5) = 0.9612	P=0.5014
Residual (within columns)	0.518	5	0.1036		
Total	0.9164	9			

Tukey's multiple comparisons test	Mean Diff.	95.00% CI of diff.	Adjusted P Value
Vehicle vs. 15 nM sAPP α	-0.3452	-1.636 to 0.9461	0.8140
Vehicle vs. 50 nM sAPP α	-0.02568	-1.317 to 1.266	>0.9999
Vehicle vs. 15 nM sAPP β	-0.2047	-1.496 to 1.087	0.9622
Vehicle vs. 50 nM sAPP β	0.2439	-1.047 to 1.535	0.9327
15 nM sAPP α vs. 50 nM sAPP α	0.3195	-0.9718 to 1.611	0.8489
15 nM sAPP α vs. 15 nM sAPP β	0.1404	-1.151 to 1.432	0.9902
15 nM sAPP α vs. 50 nM sAPP β	0.589	-0.7022 to 1.88	0.4484
50 nM sAPP α vs. 15 nM sAPP β	-0.179	-1.47 to 1.112	0.9763
50 nM sAPP α vs. 50 nM sAPP β	0.2696	-1.022 to 1.561	0.9079
15 nM sAPP β vs. 50 nM sAPP β	0.4486	-0.8426 to 1.74	0.6561

Supplementary Table 7.4. One-way ANOVA results for synaptophysin expression (induction 3 alone).

Tukey's multiple comparison's test was used to compare all conditions to the vehicle negative control. Blot shown in Figure 4.3c.

ANOVA Table	SS	DF	MS	F (DFn, DFd)	P value
Treatment (between columns)	0.6763	3	0.2254	F (3, 4) = 19.35	*P=0.0076
Residual (within columns)	0.0466	4	0.01165		
Total	0.7229	7			

Tukey's multiple comparisons test	Mean Diff.	95.00% CI of diff.	Adjusted Value	P
Vehicle vs. 15 nM sAPP α	-0.576	-1.015 to -0.1366	*0.0201	
Vehicle vs. 50 nM sAPP α	0.0005595	-0.4388 to 0.4399	>0.9999	
Vehicle vs. 15 nM sAPP β	0.2028	-0.2365 to 0.6422	0.3614	
15 nM sAPP α vs. 50 nM sAPP α	0.5765	0.1371 to 1.016	*0.0200	
15 nM sAPP α vs. 15 nM sAPP β	0.7788	0.3394 to 1.218	**0.0068	
50 nM sAPP α vs. 15 nM sAPP β	0.2023	-0.2371 to 0.6416	0.3632	

Supplementary Table 7.5. One-way ANOVA results for VGLUT1 expression (all inductions combined).

Tukey's multiple comparison's test was used to compare all conditions to the vehicle negative control. Blots shown in Figure 4.4a-c.

ANOVA Table	SS	DF	MS	F (DFn, DFd)	P value
Treatment (between columns)	0.006596	4	0.001649	F (4, 23) = 0.01787	P=0.9993
Residual (within columns)	2.122	23	0.09226		
Total	2.129	27			

Tukey's multiple comparisons test	Mean Diff.	95.00% CI of diff.	Adjusted Value	P
Vehicle vs. 15 nM sAPP α	-0.002798	-0.5212 to 0.5156	>0.9999	
Vehicle vs. 50 nM sAPP α	0.02506	-0.4933 to 0.5435	0.9999	
Vehicle vs. 15 nM sAPP β	0.03267	-0.4857 to 0.5511	0.9997	
Vehicle vs. 50 nM sAPP β	-0.002478	-0.5821 to 0.5771	>0.9999	
15 nM sAPP α vs. 50 nM sAPP α	0.02786	-0.4905 to 0.5463	0.9998	
15 nM sAPP α vs. 15 nM sAPP β	0.03547	-0.4829 to 0.5539	0.9996	
15 nM sAPP α vs. 50 nM sAPP β	0.0003195	-0.5793 to 0.5799	>0.9999	
50 nM sAPP α vs. 15 nM sAPP β	0.00761	-0.5108 to 0.526	>0.9999	
50 nM sAPP α vs. 50 nM sAPP β	-0.02754	-0.6071 to 0.552	>0.9999	
15 nM sAPP β vs. 50 nM sAPP β	-0.03515	-0.6147 to 0.5444	0.9997	

Supplementary Table 7.6. One-way ANOVA results for VGLUT1 expression (induction 1 alone).

Tukey's multiple comparison's test was used to compare all conditions to the vehicle negative control. Blot shown in Figure 4.3a.

ANOVA Table	SS	DF	MS	F (DFn, DFd)	P value
Treatment (between columns)	0.1018	4	0.02544	F (4, 5) = 0.5595	P=0.7032
Residual (within columns)	0.2273	5	0.04547		
Total	0.3291	9			

Tukey's multiple comparisons test	Mean Diff.	95.00% CI of diff.	Adjusted P Value
Vehicle vs. 15 nM sAPP α	0.269	-0.5864 to 1.124	0.7230
Vehicle vs. 50 nM sAPP α	0.2258	-0.6296 to 1.081	0.8200
Vehicle vs. 15 nM sAPP β	0.05491	-0.8005 to 0.9103	0.9987
Vehicle vs. 50 nM sAPP β	0.1279	-0.7275 to 0.9832	0.9691
15 nM sAPP α vs. 50 nM sAPP α	-0.04316	-0.8985 to 0.8122	0.9995
15 nM sAPP α vs. 15 nM sAPP β	-0.2141	-1.069 to 0.6413	0.8441
15 nM sAPP α vs. 50 nM sAPP β	-0.1411	-0.9965 to 0.7143	0.9568
50 nM sAPP α vs. 15 nM sAPP β	-0.1709	-1.026 to 0.6845	0.9196
50 nM sAPP α vs. 50 nM sAPP β	-0.09794	-0.9533 to 0.7574	0.9881
15 nM sAPP β vs. 50 nM sAPP β	0.07295	-0.7824 to 0.9283	0.9961

Supplementary Table 7.7. One-way ANOVA results for VGLUT1 expression (induction 2 alone).

Tukey's multiple comparison's test was used to compare all conditions to the vehicle negative control. Blot shown in Figure 4.4b.

ANOVA Table	SS	DF	MS	F (DFn, DFd)	P value
Treatment (between columns)	0.2466	4	0.06165	F (4, 5) = 0.4375	P=0.7783
Residual (within columns)	0.7046	5	0.1409		
Total	0.9512	9			

Tukey's multiple comparisons test	Mean Diff.	95.00% CI of diff.	Adjusted Value	P
Vehicle vs. 15 nM sAPP α	-0.02735	-1.533 to 1.479	>0.9999	
Vehicle vs. 50 nM sAPP α	-0.4422	-1.948 to 1.064	0.7642	
Vehicle vs. 15 nM sAPP β	-0.1619	-1.668 to 1.344	0.9906	
Vehicle vs. 50 nM sAPP β	-0.1328	-1.639 to 1.373	0.9955	
15 nM sAPP α vs. 50 nM sAPP α	-0.4148	-1.921 to 1.091	0.7989	
15 nM sAPP α vs. 15 nM sAPP β	-0.1346	-1.64 to 1.371	0.9953	
15 nM sAPP α vs. 50 nM sAPP β	-0.1055	-1.611 to 1.4	0.9981	
50 nM sAPP α vs. 15 nM sAPP β	0.2803	-1.226 to 1.786	0.9358	
50 nM sAPP α vs. 50 nM sAPP β	0.3094	-1.197 to 1.815	0.9123	
15 nM sAPP β vs. 50 nM sAPP β	0.0291	-1.477 to 1.535	>0.9999	

Supplementary Table 7.8. One-way ANOVA results for VGLUT1 expression (induction 3 alone).

Tukey's multiple comparison's test was used to compare all conditions to the vehicle negative control. Blot shown in Figure 4.4c.

ANOVA Table	SS	DF	MS	F (DFn, DFd)	P value
Treatment (between columns)	0.3487	3	0.1162	F (3, 4) = 8.364	*P=0.0338
Residual (within columns)	0.05559	4	0.0139		
Total	0.4043	7			

Tukey's multiple comparisons test	Mean Diff.	95.00% CI of diff.	Adjusted P Value
Vehicle vs. 15 nM sAPP α	-0.25	-0.7299 to 0.2299	0.2865
Vehicle vs. 50 nM sAPP α	0.2916	-0.1883 to 0.7715	0.2039
Vehicle vs. 15 nM sAPP β	0.205	-0.2749 to 0.6849	0.4125
15 nM sAPP α vs. 50 nM sAPP α	0.5416	0.06168 to 1.021	*0.0336
15 nM sAPP α vs. 15 nM sAPP β	0.455	-0.02486 to 0.9349	0.0592
50 nM sAPP α vs. 15 nM sAPP β	-0.08654	-0.5664 to 0.3934	0.8791

Supplementary Table 7.9. One-way ANOVA results for PSD95 expression (all inductions combined).

Tukey's multiple comparison's test was used to compare all conditions to the vehicle negative control. Blots shown in Figure 4.5a-c.

ANOVA Table	SS	DF	MS	F (DFn, DFd)	P value
Treatment (between columns)	0.1461	4	0.03653	F (4, 23) = 1.517	P=0.2302
Residual (within columns)	0.5538	23	0.02408		
Total	0.7	27			

Tukey's multiple comparisons test	Mean Diff.	95.00% CI of diff.	Adjusted P Value
Vehicle vs. 15 nM sAPP α	0.03087	-0.234 to 0.2957	0.9967
Vehicle vs. 50 nM sAPP α	0.1619	-0.103 to 0.4267	0.3938
Vehicle vs. 15 nM sAPP β	0.08561	-0.1792 to 0.3504	0.8718
Vehicle vs. 50 nM sAPP β	-0.05757	-0.3537 to 0.2385	0.9775
15 nM sAPP α vs. 50 nM sAPP α	0.131	-0.1338 to 0.3958	0.5958
15 nM sAPP α vs. 15 nM sAPP β	0.05474	-0.2101 to 0.3196	0.9719
15 nM sAPP α vs. 50 nM sAPP β	-0.08844	-0.3845 to 0.2077	0.9003
50 nM sAPP α vs. 15 nM sAPP β	-0.07626	-0.3411 to 0.1886	0.9115
50 nM sAPP α vs. 50 nM sAPP β	-0.2194	-0.5155 to 0.07665	0.2185
15 nM sAPP β vs. 50 nM sAPP β	-0.1432	-0.4393 to 0.1529	0.6158

Supplementary Table 7.10. One-way ANOVA results for PSD95 expression (induction 1 alone).

Tukey's multiple comparison's test was used to compare all conditions to the vehicle negative control. Blot shown in Figure 4.5a.

ANOVA Table	SS	DF	MS	F (DFn, DFd)	P value
Treatment (between columns)	0.08791	4	0.02198	F (4, 5) = 0.6465	P=0.6533
Residual (within columns)	0.17	5	0.03399		
Total	0.2579	9			

Tukey's multiple comparisons test	Mean Diff.	95.00% CI of diff.	Adjusted P Value
Vehicle vs. 15 nM sAPP α	0.1407	-0.5989 to 0.8803	0.9311
Vehicle vs. 50 nM sAPP α	0.2773	-0.4623 to 1.017	0.6006
Vehicle vs. 15 nM sAPP β	0.1987	-0.5409 to 0.9383	0.8115
Vehicle vs. 50 nM sAPP β	0.09434	-0.6453 to 0.834	0.9824
15 nM sAPP α vs. 50 nM sAPP α	0.1366	-0.6031 to 0.8762	0.9374
15 nM sAPP α vs. 15 nM sAPP β	0.05798	-0.6816 to 0.7976	0.9971
15 nM sAPP α vs. 50 nM sAPP β	-0.04638	-0.786 to 0.6932	0.9988
50 nM sAPP α vs. 15 nM sAPP β	-0.07859	-0.8182 to 0.661	0.9910
50 nM sAPP α vs. 50 nM sAPP β	-0.1829	-0.9226 to 0.5567	0.8491
15 nM sAPP β vs. 50 nM sAPP β	-0.1044	-0.844 to 0.6353	0.9748

Supplementary Table 7.11. One-way ANOVA results for PSD95 expression (induction 2 alone).

Tukey's multiple comparison's test was used to compare all conditions to the vehicle negative control. Blot shown in Figure 4.5b.

ANOVA Table	SS	DF	MS	F (DFn, DFd)	P value
Treatment (between columns)	0.1403	4	0.03508	F (4, 5) = 2.494	P=0.1716
Residual (within columns)	0.07032	5	0.01406		
Total	0.2107	9			

Tukey's multiple comparisons test	Mean Diff.	95.00% CI of diff.	Adjusted P Value
Vehicle vs. 15 nM sAPP α	-0.1722	-0.6479 to 0.3036	0.6268
Vehicle vs. 50 nM sAPP α	0.08837	-0.3874 to 0.5641	0.9362
Vehicle vs. 15 nM sAPP β	0.04033	-0.4354 to 0.5161	0.9961
Vehicle vs. 50 nM sAPP β	-0.2095	-0.6852 to 0.2663	0.4761
15 nM sAPP α vs. 50 nM sAPP α	0.2605	-0.2152 to 0.7363	0.3116
15 nM sAPP α vs. 15 nM sAPP β	0.2125	-0.2632 to 0.6882	0.4649
15 nM sAPP α vs. 50 nM sAPP β	-0.03731	-0.5131 to 0.4384	0.9971
50 nM sAPP α vs. 15 nM sAPP β	-0.04804	-0.5238 to 0.4277	0.9925
50 nM sAPP α vs. 50 nM sAPP β	-0.2978	-0.7736 to 0.1779	0.2250
15 nM sAPP β vs. 50 nM sAPP β	-0.2498	-0.7256 to 0.2259	0.3416

Supplementary Table 7.12. One-way ANOVA results for PSD95 expression (induction 3 alone).

Tukey's multiple comparison's test was used to compare all conditions to the vehicle negative control. Blot shown in Figure 4.5c.

ANOVA Table	SS	DF	MS	F (DFn, DFd)	P value
Treatment (between columns)	0.02592	3	0.008641	F (3, 4) = 1.983	P=0.2588
Residual (within columns)	0.01743	4	0.004358		
Total	0.04336	7			

Tukey's multiple comparisons test	Mean Diff.	95.00% CI of diff.	Adjusted Value	P
Vehicle vs. 15 nM sAPP α	0.1241	-0.1447 to 0.3928	0.3614	
Vehicle vs. 50 nM sAPP α	0.12	-0.1488 to 0.3887	0.3833	
Vehicle vs. 15 nM sAPP β	0.01781	-0.2509 to 0.2866	0.9921	
15 nM sAPP α vs. 50 nM sAPP α	-0.004096	-0.2728 to 0.2646	0.9999	
15 nM sAPP α vs. 15 nM sAPP β	-0.1063	-0.375 to 0.1625	0.4651	
50 nM sAPP α vs. 15 nM sAPP β	-0.1022	-0.3709 to 0.1666	0.4919	

Supplementary Table 7.13. One-way ANOVA results for sAPP α vs sAPP β SH-SY5Y binding intensity (22C11).

Tukey's multiple comparison's test was used to compare all conditions to the vehicle negative control. Blot shown in Figure 4.7a.

ANOVA Table	SS	DF	MS	F (DFn, DFd)	P value
Treatment (between columns)	2.215	2	1.107	F (2, 3) = 15.94	P=0.0252
Residual (within columns)	0.2084	3	0.06948		
Total	2.423	5			

Tukey's multiple comparisons test	Mean Diff.	95.00% CI of diff.	Adjusted Value	P
Vehicle vs. + sAPP α	-1.487	-2.588 to -0.385	0.0224	
Vehicle vs. + sAPP β	-0.6814	-1.783 to 0.4201	0.1567	
+ sAPP α vs. + sAPP β	0.8051	-0.2964 to 1.907	0.1082	

8. References

- Abramov AY, Canevari L, Duchen MR. 2004. Beta-amyloid peptides induce mitochondrial dysfunction and oxidative stress in astrocytes and death of neurons through activation of nadph oxidase. *J Neurosci.* 24(2):565-575.
- Alcamo EA, Chirivella L, Dautzenberg M, Dobрева G, Fariñas I, Grosschedl R, McConnell SK. 2008. Satb2 regulates callosal projection neuron identity in the developing cerebral cortex. *Neuron.* 57(3):364-377.
- Alzheimer A. 1907. Über eine eigenartige erkrankung der hirnrinde. *Zentralblatt für die gesamte Neurologie und Psychiatrie.* 18:177 - 179.
- Andersen OM, Reiche J, Schmidt V, Gotthardt M, Spoelgen R, Behlke J, von Arnim CA, Breiderhoff T, Jansen P, Wu X et al. 2005. Neuronal sorting protein-related receptor sorla/Ir11 regulates processing of the amyloid precursor protein. *Proc Natl Acad Sci U S A.* 102(38):13461-13466.
- Andersen OM, Schmidt V, Spoelgen R, Gliemann J, Behlke J, Galatis D, McKinsty WJ, Parker MW, Masters CL, Hyman BT et al. 2006. Molecular dissection of the interaction between amyloid precursor protein and its neuronal trafficking receptor sorla/Ir11. *Biochemistry.* 45(8):2618-2628.
- Anderson JJ, Holtz G, Baskin PP, Wang R, Mazzarelli L, Wagner SL, Menzaghi F. 1999. Reduced cerebrospinal fluid levels of alpha-secretase-cleaved amyloid precursor protein in aged rats: Correlation with spatial memory deficits. *Neuroscience.* 93(4):1409-1420.
- Ando Y, Nakamura M, Kai H, Katsuragi S, Terazaki H, Nozawa T, Okuda T, Misumi S, Matsunaga N, Hata K et al. 2002. A novel localized amyloidosis associated with lactoferrin in the cornea. *Lab Invest.* 82(6):757-766.
- Araki Y, Tomita S, Yamaguchi H, Miyagi N, Sumioka A, Kirino Y, Suzuki T. 2003. Novel cadherin-related membrane proteins, alcadeins, enhance the x11-like protein-mediated stabilization of amyloid beta-protein precursor metabolism. *J Biol Chem.* 278(49):49448-49458.
- Aranda-Anzaldo A. 2012. The post-mitotic state in neurons correlates with a stable nuclear higher-order structure. *Commun Integr Biol.* 5(2):134-139.
- Arbel-Ornath M, Hudry E, Boivin JR, Hashimoto T, Takeda S, Kuchibhotla KV, Hou S, Lattarulo CR, Belcher AM, Shakerdge N et al. 2017. Soluble oligomeric amyloid- β induces calcium dyshomeostasis that precedes synapse loss in the living mouse brain. *Mol Neurodegener.* 12(1):27.
- Arendt T, Brückner MK, Morawski M, Jäger C, Gertz H-J. 2015. Early neurone loss in alzheimer's disease: Cortical or subcortical? *Acta Neuropathologica Communications.* 3(1).
- Armada-Moreira A, Gomes JJ, Pina CC, Savchak OK, Gonçalves-Ribeiro J, Rei N, Pinto S, Morais TP, Martins RS, Ribeiro FF et al. 2020. Going the extra (synaptic) mile: Excitotoxicity as the road toward neurodegenerative diseases. *Front Cell Neurosci.* 14:90.
- Arvanitakis Z, Shah RC, Bennett DA. 2019. Diagnosis and management of dementia: A review. *JAMA.* 322(16):1589-1599.
- Ashraf AA, Dani M, So PW. 2020. Low cerebrospinal fluid levels of hemopexin are associated with increased alzheimer's pathology, hippocampal hypometabolism, and cognitive decline. *Front Mol Biosci.* 7:590979.
- Baek MJ, Kim K, Park YH, Kim S. 2016. The validity and reliability of the mini-mental state examination-2 for detecting mild cognitive impairment and alzheimer's disease in a korean population. *PLOS ONE.* 11(9):e0163792.
- Bai Y, Markham K, Chen F, Weerasekera R, Watts J, Horne P, Wakutani Y, Bagshaw R, Mathews PM, Fraser PE et al. 2008. The in vivo brain interactome of the amyloid precursor protein. *Mol Cell Proteomics.* 7(1):15-34.
- Barbiellini Amidei C, Fayosse A, Dumurgier J, Machado-Fragua MD, Tabak AG, van Sloten T, Kivimäki M, Dugravot A, Sabia S, Singh-Manoux A. 2021. Association between age at diabetes onset and subsequent risk of dementia. *JAMA.* 325(16):1640-1649.
- Bature F, Guinn B-A, Pang D, Pappas Y. 2017. Signs and symptoms preceding the diagnosis of alzheimer's disease: A systematic scoping review of literature from 1937 to 2016. *BMJ Open.* 7(8):e015746.
- Behl C, Davis JB, Lesley R, Schubert D. 1994. Hydrogen peroxide mediates amyloid beta protein toxicity. *Cell.* 77(6):817-827.
- Bekris LM, Yu CE, Bird TD, Tsuang DW. 2010. Genetics of alzheimer disease. *J Geriatr Psychiatry Neurol.* 23(4):213-227.

- Belloy ME, Napolioni V, Greicius MD. 2019. A quarter century of apoe and alzheimer's disease: Progress to date and the path forward. *Neuron*. 101(5):820-838.
- Blinkouskaya Y, Weickenmeier J. 2021. Brain shape changes associated with cerebral atrophy in healthy aging and alzheimer's disease. *Front Mech Eng*. 7.
- Bowes MP, Masliah E, Otero DA, Zivin JA, Saitoh T. 1994. Reduction of neurological damage by a peptide segment of the amyloid beta/a4 protein precursor in a rabbit spinal cord ischemia model. *Exp Neurol*. 129(1):112-119.
- Braithwaite SP, Stock JB, Lombroso PJ, Nairn AC. 2012. Protein phosphatases and alzheimer's disease. *Prog Mol Biol Transl Sci*. 106:343-379.
- Busche MA, Hyman BT. 2020. Synergy between amyloid- β and tau in alzheimer's disease. *Nature Neuroscience*. 23(10):1183-1193.
- Butterfield DA, Lauderback CM. 2002. Lipid peroxidation and protein oxidation in alzheimer's disease brain: Potential causes and consequences involving amyloid beta-peptide-associated free radical oxidative stress. *Free Radic Biol Med*. 32(11):1050-1060.
- Buxbaum JD, Thinakaran G, Koliatsos V, O'Callahan J, Slunt HH, Price DL, Sisodia SS. 1998. Alzheimer amyloid protein precursor in the rat hippocampus: Transport and processing through the perforant path. *J Neurosci*. 18(23):9629-9637.
- Caillé I, Allinquant B, Dupont E, Bouillot C, Langer A, Müller U, Prochiantz A. 2004. Soluble form of amyloid precursor protein regulates proliferation of progenitors in the adult subventricular zone. *Development*. 131(9):2173-2181.
- Cappai R. 2014. Making sense of the amyloid precursor protein: Its tail tells an interesting tale. *Journal of Neurochemistry*. 130(3):325-327.
- Carey RM, Balcz BA, Lopez-Coviella I, Slack BE. 2005. Inhibition of dynamin-dependent endocytosis increases shedding of the amyloid precursor protein ectodomain and reduces generation of amyloid beta protein. *BMC Cell Biol*. 6:30.
- Chasseigneaux S, Allinquant B. 2012. Functions of $\alpha\beta$, $\text{sapp}\alpha$ and $\text{sapp}\beta$: Similarities and differences. *Journal of Neurochemistry*. 120(s1):99-108.
- Chasseigneaux S, Dinc L, Rose C, Chabret C, Couplier F, Topilko P, Mauger G, Allinquant B. 2011. Secreted amyloid precursor protein β and secreted amyloid precursor protein α induce axon outgrowth in vitro through *egr1* signaling pathway. *PLoS ONE*. 6(1):e16301.
- Cheignon C, Tomas M, Bonnefont-Rousselot D, Faller P, Hureau C, Collin F. 2018. Oxidative stress and the amyloid beta peptide in alzheimer's disease. *Redox Biol*. 14:450-464.
- Cheng B, Mattson MP. 1992. Glucose deprivation elicits neurofibrillary tangle-like antigenic changes in hippocampal neurons: Prevention by *ngf* and *bfgf*. *Exp Neurol*. 117(2):114-123.
- Cho YY, Kwon OH, Park MK, Kim TW, Chung S. 2019. Elevated cellular cholesterol in familial alzheimer's presenilin 1 mutation is associated with lipid raft localization of β -amyloid precursor protein. *PLoS One*. 14(1):e0210535.
- Choi DW. 1987. Ionic dependence of glutamate neurotoxicity. *J Neurosci*. 7(2):369-379.
- Chow VW, Mattson MP, Wong PC, Gleichmann M. 2010. An overview of app processing enzymes and products. *Neuromolecular Med*. 12(1):1-12.
- Cimdins K, Waugh HS, Chrysostomou V, Lopez Sanchez MIG, Johannsen VA, Cook MJ, Crowston JG, Hill AF, Duce JA, Bush AI et al. 2019. Amyloid precursor protein mediates neuronal protection from rotenone toxicity. *Mol Neurobiol*. 56(8):5471-5482.
- Claasen AM, Guévremont D, Mason-Parker SE, Bourne K, Tate WP, Abraham WC, Williams JM. 2009. Secreted amyloid precursor protein- α upregulates synaptic protein synthesis by a protein kinase g-dependent mechanism. *Neurosci Lett*. 460(1):92-96.
- Coburger I, Dahms SO, Roeser D, Gührs KH, Hortschansky P, Than ME. 2013. Analysis of the overall structure of the multi-domain amyloid precursor protein (app). *PLoS One*. 8(12):e81926.
- Copanaki E, Chang S, Vlachos A, Tschäpe JA, Müller UC, Kögel D, Deller T. 2010. Sappalpha antagonizes dendritic degeneration and neuron death triggered by proteasomal stress. *Mol Cell Neurosci*. 44(4):386-393.
- Corbett NJ, Hooper NM, Chattopadhyay K, Basu SC. 2018. Soluble amyloid precursor protein α : Friend or foe? *Advances in Experimental Medicine and Biology*. 1112:177-183.
- Corder EH, Saunders AM, Risch NJ, Strittmatter WJ, Schmechel DE, Gaskell PC, Rimmler JB, Locke PA, Conneally PM, Schmechel KE. 1994. Protective effect of apolipoprotein e type 2 allele for late onset alzheimer disease. *Nat Genet*. 7(2):180-184.

- Corder EH, Saunders AM, Strittmatter WJ, Schmechel DE, Gaskell PC, Small GW, Roses AD, Haines JL, Pericak-Vance MA. 1993. Gene dose of apolipoprotein e type 4 allele and the risk of alzheimer's disease in late onset families. *Science*. 261(5123):921-923.
- Craft S, Asthana S, Schellenberg G, Baker L, Cherrier M, Boyt AA, Martins RN, Raskind M, Peskind E, Plymate S. 2000. Insulin effects on glucose metabolism, memory, and plasma amyloid precursor protein in alzheimer's disease differ according to apolipoprotein-e genotype. *Ann N Y Acad Sci*. 903:222-228.
- Criddle DN, Gillies S, Baumgartner-Wilson HK, Jaffar M, Chinje EC, Passmore S, Chvanov M, Barrow S, Gerasimenko OV, Tepikin AV et al. 2006. Menadione-induced reactive oxygen species generation via redox cycling promotes apoptosis of murine pancreatic acinar cells. *J Biol Chem*. 281(52):40485-40492.
- Csajbók É, Tamás G. 2016. Cerebral cortex: A target and source of insulin? *Diabetologia*. 59(8):1609-1615.
- Cummings JL, Morstorf T, Zhong K. 2014. Alzheimer's disease drug-development pipeline: Few candidates, frequent failures. *Alzheimers Res Ther*. 6(4):37.
- Cvetkovska V, Ge Y, Xu Q, Li S, Zhang P, Craig AM. 2022. Neurexin- β mediates the synaptogenic activity of amyloid precursor protein. *J Neurosci*.
- Daigle I, Li C. 1993. Apl-1, a caenorhabditis elegans gene encoding a protein related to the human beta-amyloid protein precursor. *Proc Natl Acad Sci U S A*. 90(24):12045-12049.
- Dar NJ, Glazner GW. 2020. Deciphering the neuroprotective and neurogenic potential of soluble amyloid precursor protein alpha (sapp α). *Cellular and Molecular Life Sciences*. 77(12):2315-2330.
- Dawkins E, Small DH. 2014. Insights into the physiological function of the β -amyloid precursor protein: Beyond alzheimer's disease. *Journal of Neurochemistry*. 129(5):756-769.
- Dawson GR, Seabrook GR, Zheng H, Smith DW, Graham S, O'Dowd G, Bowery BJ, Boyce S, Trumbauer ME, Chen HY et al. 1999. Age-related cognitive deficits, impaired long-term potentiation and reduction in synaptic marker density in mice lacking the beta-amyloid precursor protein. *Neuroscience*. 90(1):1-13.
- De Felice FG, Velasco PT, Lambert MP, Viola K, Fernandez SJ, Ferreira ST, Klein WL. 2007. Abeta oligomers induce neuronal oxidative stress through an n-methyl-d-aspartate receptor-dependent mechanism that is blocked by the alzheimer drug memantine. *J Biol Chem*. 282(15):11590-11601.
- de Wilde MC, Overk CR, Sijben JW, Masliah E. 2016. Meta-analysis of synaptic pathology in alzheimer's disease reveals selective molecular vesicular machinery vulnerability. *Alzheimers Dement*. 12(6):633-644.
- Demars MP, Bartholomew A, Strakova Z, Lazarov O. 2011. Soluble amyloid precursor protein: A novel proliferation factor of adult progenitor cells of ectodermal and mesodermal origin. *Stem Cell Res Ther*. 2(4):36.
- Demars MP, Hollands C, Zhao KaT, Lazarov O. 2013. Soluble amyloid precursor protein- α rescues age-linked decline in neural progenitor cell proliferation. *Neurobiol Aging*. 34(10):2431-2440.
- Deng J, Habib A, Obregon DF, Barger SW, Giunta B, Wang Y-J, Hou H, Sawmiller D, Tan J. 2015. Soluble amyloid precursor protein alpha inhibits tau phosphorylation through modulation of gsk3 β signaling pathway. *Journal of Neurochemistry*. 135(3):630-637.
- Dixon MC. 2008. Quartz crystal microbalance with dissipation monitoring: Enabling real-time characterization of biological materials and their interactions. *J Biomol Tech*. 19(3):151-158.
- Doody RS, Raman R, Farlow M, Iwatsubo T, Vellas B, Joffe S, Kieburtz K, He F, Sun X, Thomas RG et al. 2013. A phase 3 trial of semagacestat for treatment of alzheimer's disease. *N Engl J Med*. 369(4):341-350.
- Dorard E, Chasseigneaux S, Gorisse-Hussonnois L, Broussard C, Pillot T, Allinquant B. 2018. Soluble amyloid precursor protein alpha interacts with alpha3-na, k-atpase to induce axonal outgrowth but not neuroprotection: Evidence for distinct mechanisms underlying these properties. *Molecular neurobiology*. 55(7):5594-5610.
- Drummond E, Wisniewski T. 2017. Alzheimer's disease: Experimental models and reality. *Acta Neuropathol*. 133(2):155-175.
- Du J, Yi M, Zhou F, He W, Yang A, Qiu M, Huang H. 2021. S100b is selectively expressed by gray matter protoplasmic astrocytes and myelinating oligodendrocytes in the developing cns. *Mol Brain*. 14(1):154.
- Dupree EJ, Jayathirtha M, Yorkey H, Mihasan M, Petre BA, Darie CC. 2020. A critical review of bottom-up proteomics: The good, the bad, and the future of this field. *Proteomes*. 8(3).
- Dyrks T, Dyrks E, Masters CL, Beyreuther K. 1993. Amyloidogenicity of rodent and human beta a4 sequences. *FEBS Lett*. 324(2):231-236.
- Dziedziatowska M, Hill R, Hansen KC. 2014. Gelc-ms/ms analysis of complex protein mixtures. *Methods Mol Biol*. 1156:53-66.

- Edbauer D, Winkler E, Regula JT, Pesold B, Steiner H, Haass C. 2003. Reconstitution of gamma-secretase activity. *Nat Cell Biol.* 5(5):486-488.
- Egan MF, Kost J, Tariot PN, Aisen PS, Cummings JL, Vellas B, Sur C, Mukai Y, Voss T, Furtek C et al. 2018. Randomized trial of verubecestat for mild-to-moderate alzheimer's disease. *N Engl J Med.* 378(18):1691-1703.
- Ehehalt R, Keller P, Haass C, Thiele C, Simons K. 2003. Amyloidogenic processing of the alzheimer beta-amyloid precursor protein depends on lipid rafts. *J Cell Biol.* 160(1):113-123.
- Eimer WA, Vijaya Kumar DK, Navalpur Shanmugam NK, Rodriguez AS, Mitchell T, Washicosky KJ, György B, Breakefield XO, Tanzi RE, Moir RD. 2018. Alzheimer's disease-associated β -amyloid is rapidly seeded by herpesviridae to protect against brain infection. *Neuron.* 100(6):1527-1532.
- Engle SJ, Blaha L, Kleiman RJ. 2018. Best practices for translational disease modeling using human ipsc-derived neurons. *Neuron.* 100(4):783-797.
- Farrer LA, Cupples LA, Haines JL, Hyman B, Kukull WA, Mayeux R, Myers RH, Pericak-Vance MA, Risch N, van Duijn CM. 1997. Effects of age, sex, and ethnicity on the association between apolipoprotein e genotype and alzheimer disease. A meta-analysis. Apoe and alzheimer disease meta analysis consortium. *JAMA.* 278(16):1349-1356.
- Fernández-Calle R, Konings SC, Frontiñán-Rubio J, García-Revilla J, Camprubí-Ferrer L, Svensson M, Martinson I, Boza-Serrano A, Venero JL, Nielsen HM et al. 2022. Apoe in the bullseye of neurodegenerative diseases: Impact of the apoe genotype in alzheimer's disease pathology and brain diseases. *Mol Neurodegener.* 17(1):62.
- Ferrari A, Hoerndli F, Baechi T, Nitsch RM, Götz J. 2003. Beta-amyloid induces paired helical filament-like tau filaments in tissue culture. *J Biol Chem.* 278(41):40162-40168.
- Fischer O. 1907. Miliare nekrosen mit drüsigen wucherungen der neurofibrillen, eine regelmässige veränderung der hirnrinde bei seniler demenz. *Monatsschr Psychiatr Neurol.* 22:361-372.
- Fol R, Braudeau J, Ludewig S, Abel T, Weyer SW, Roederer JP, Brod F, Audrain M, Bemelmans AP, Buchholz CJ et al. 2016. Viral gene transfer of app α rescues synaptic failure in an alzheimer's disease mouse model. *Acta Neuropathol.* 131(2):247-266.
- Folstein MF, Folstein SE, McHugh PR. 1975. "Mini-mental state". A practical method for grading the cognitive state of patients for the clinician. *J Psychiatr Res.* 12(3):189-198.
- Foster EM, Dangla-Valls A, Lovestone S, Ribe EM, Buckley NJ. 2019. Clusterin in alzheimer's disease: Mechanisms, genetics, and lessons from other pathologies. *Front Neurosci.* 13:164.
- Furukawa K, Sopher BL, Rydel RE, Begley JG, Pham DG, Martin GM, Fox M, Mattson MP. 1996. Increased activity-regulating and neuroprotective efficacy of alpha-secretase-derived secreted amyloid precursor protein conferred by a c-terminal heparin-binding domain. *J Neurochem.* 67(5):1882-1896.
- Gandjour A. 2020. Willingness to pay for new medicines: A step towards narrowing the gap between nice and iqwig. *BMC Health Serv Res.* 20(1):343.
- Gauthier S, Rosa-Neto P, Morais J, Webster C. 2021. World alzheimer report 2021: Journey through the diagnosis of dementia. Alzheimer's Disease International.
- Glenner GG, Wong CW. 1984. Alzheimer's disease: Initial report of the purification and characterization of a novel cerebrovascular amyloid protein. *Biochem Biophys Res Commun.* 120(3):885-890.
- Goate A, Chartier-Harlin MC, Mullan M, Brown J, Crawford F, Fidani L, Giuffra L, Haynes A, Irving N, James L. 1991. Segregation of a missense mutation in the amyloid precursor protein gene with familial alzheimer's disease. *Nature.* 349(6311):704-706.
- Goldgaber D, Lerman MI, McBride OW, Saffiotti U, Gajdusek DC. 1987. Characterization and chromosomal localization of a cDNA encoding brain amyloid of alzheimer's disease. *Science.* 235(4791):877-880.
- Gong CX, Iqbal K. 2008. Hyperphosphorylation of microtubule-associated protein tau: A promising therapeutic target for alzheimer disease. *Curr Med Chem.* 15(23):2321-2328.
- Goodman Y, Mattson MP. 1994. Secreted forms of beta-amyloid precursor protein protect hippocampal neurons against amyloid beta-peptide-induced oxidative injury. *Exp Neurol.* 128(1):1-12.
- Gotoh N, Saito Y, Hata S, Saito H, Ojima D, Murayama C, Shigeta M, Abe T, Konno D, Matsuzaki F et al. 2020. Amyloidogenic processing of amyloid β protein precursor (app) is enhanced in the brains of alcadein α -deficient mice. *J Biol Chem.* 295(28):9650-9662.
- Goure WF, Krafft GA, Jeretic J, Hefti F. 2014. Targeting the proper amyloid-beta neuronal toxins: A path forward for alzheimer's disease immunotherapeutics. *Alzheimers Res Ther.* 6(4):42.
- Gralle M, Botelho MM, de Oliveira CL, Torriani I, Ferreira ST. 2002. Solution studies and structural model of the extracellular domain of the human amyloid precursor protein. *Biophys J.* 83(6):3513-3524.

- Grundke-Iqbal I, Iqbal K, Tung YC, Quinlan M, Wisniewski HM, Binder LI. 1986. Abnormal phosphorylation of the microtubule-associated protein tau (tau) in alzheimer cytoskeletal pathology. *Proc Natl Acad Sci U S A*. 83(13):4913-4917.
- Guo Q, Robinson N, Mattson MP. 1998. Secreted β -amyloid precursor protein counteracts the proapoptotic action of mutant presenilin-1 by activation of nf-kb and stabilization of calcium homeostasis. *Journal of Biological Chemistry*. 273(20):12341-12351.
- Gustafsen C, Glerup S, Pallesen LT, Olsen D, Andersen OM, Nykjær A, Madsen P, Petersen CM. 2013. Sortilin and sorla display distinct roles in processing and trafficking of amyloid precursor protein. *J Neurosci*. 33(1):64-71.
- Götz J, Chen F, van Dorpe J, Nitsch RM. 2001. Formation of neurofibrillary tangles in p301l tau transgenic mice induced by abeta 42 fibrils. *Science*. 293(5534):1491-1495.
- Habib A, Sawmiller D, Tan J. 2017. Restoring soluble amyloid precursor protein α functions as a potential treatment for alzheimer's disease. *J Neurosci Res*. 95(4):973-991.
- Halim A, Brinkmalm G, Rüetschi U, Westman-Brinkmalm A, Portelius E, Zetterberg H, Blennow K, Larson G, Nilsson J. 2011. Site-specific characterization of threonine, serine, and tyrosine glycosylations of amyloid precursor protein/amyloid β -peptides in human cerebrospinal fluid. *Proceedings of the National Academy of Sciences*. 108(29):11848-11853.
- Handel AE, Chintawar S, Lalic T, Whiteley E, Vowles J, Giustacchini A, Argoud K, Sopp P, Nakanishi M, Bowden R et al. 2016. Assessing similarity to primary tissue and cortical layer identity in induced pluripotent stem cell-derived cortical neurons through single-cell transcriptomics. *Hum Mol Genet*. 25(5):989-1000.
- Hardy JA, Higgins GA. 1992. Alzheimer's disease: The amyloid cascade hypothesis. *Science*. 256(5054):184-185.
- Hasebe N, Fujita Y, Ueno M, Yoshimura K, Fujino Y, Yamashita T. 2013. Soluble β -amyloid precursor protein alpha binds to p75 neurotrophin receptor to promote neurite outgrowth. *PLoS ONE*. 8(12):e82321.
- Hata S, Fujishige S, Araki Y, Kato N, Araseki M, Nishimura M, Hartmann D, Saftig P, Fahrenholz F, Taniguchi M et al. 2009. Alcadein cleavages by amyloid β -precursor protein (app) α - and γ -secretases generate small peptides, p3-alcs, indicating alzheimer disease-related γ -secretase dysfunction. *Journal of Biological Chemistry*. 284(52):36024-36033.
- Hegde RS, Bernstein HD. 2006. The surprising complexity of signal sequences. *Trends Biochem Sci*. 31(10):563-571.
- Hemdan ES, Zhao YJ, Sulkowski E, Porath J. 1989. Surface topography of histidine residues: A facile probe by immobilized metal ion affinity chromatography. *Proceedings of the National Academy of Sciences*. 86(6):1811-1815.
- Hintsch G, Zurlinden A, Meskenaite V, Steuble M, Fink-Widmer K, Kinter J, Sonderegger P. 2002. The calyntenins--a family of postsynaptic membrane proteins with distinct neuronal expression patterns. *Mol Cell Neurosci*. 21(3):393-409.
- Holmes C, Boche D, Wilkinson D, Yadegarfar G, Hopkins V, Bayer A, Jones RW, Bullock R, Love S, Neal JW et al. 2008. Long-term effects of abeta42 immunisation in alzheimer's disease: Follow-up of a randomised, placebo-controlled phase i trial. *Lancet*. 372(9634):216-223.
- Hornsten A, Lieberthal J, Fadia S, Malins R, Ha L, Xu X, Daigle I, Markowitz M, O'Connor G, Plasterk R et al. 2007. Apl-1, a caenorhabditis elegans protein related to the human beta-amyloid precursor protein, is essential for viability. *Proc Natl Acad Sci U S A*. 104(6):1971-1976.
- Huang WJ, Zhang X, Chen WW. 2016. Role of oxidative stress in alzheimer's disease. *Biomed Rep*. 4(5):519-522.
- Hutton M, Lendon CL, Rizzu P, Baker M, Froelich S, Houlden H, Pickering-Brown S, Chakraverty S, Isaacs A, Grover A et al. 1998. Association of missense and 5'-splice-site mutations in tau with the inherited dementia ftdp-17. *Nature*. 393(6686):702-705.
- Hyman BT, Phelps CH, Beach TG, Bigio EH, Cairns NJ, Carrillo MC, Dickson DW, Duyckaerts C, Frosch MP, Masliah E et al. 2012. National institute on aging-alzheimer's association guidelines for the neuropathologic assessment of alzheimer's disease. *Alzheimers Dement*. 8(1):1-13.
- Ikeda DD, Duan Y, Matsuki M, Kunitomo H, Hutter H, Hedgecock EM, Iino Y. 2008. Casy-1, an ortholog of calyntenins/alcadeins, is essential for learning in caenorhabditis elegans. *Proc Natl Acad Sci U S A*. 105(13):5260-5265.
- Ikegami S, Harada A, Hirokawa N. 2000. Muscle weakness, hyperactivity, and impairment in fear conditioning in tau-deficient mice. *Neurosci Lett*. 279(3):129-132.
- Iqbal K, Liu F, Gong C-X, Grundke-Iqbal I. 2010. Tau in alzheimer disease and related tauopathies. *Current Alzheimer Research*. 7(8):656-664.

- Iwagami M, Qizilbash N, Gregson J, Douglas I, Johnson M, Pearce N, Evans S, Pocock S. 2021. Blood cholesterol and risk of dementia in more than 1.8 million people over two decades: A retrospective cohort study. *Lancet Healthy Longev.* 2(8):e498-e506.
- Iwatsubo T, Odaka A, Suzuki N, Mizusawa H, Nukina N, Ihara Y. 1994. Visualization of a beta 42(43) and a beta 40 in senile plaques with end-specific a beta monoclonals: Evidence that an initially deposited species is a beta 42(43). *Neuron.* 13(1):45-53.
- Jarosz-Griffiths HH, Corbett NJ, Rowland HA, Fisher K, Jones AC, Baron J, Howell GJ, Cowley SA, Chintawar S, Cader MZ et al. 2019. Proteolytic shedding of the prion protein via activation of metallopeptidase adam10 reduces cellular binding and toxicity of amyloid- β oligomers. *Journal of Biological Chemistry.* 294(17):7085-7097.
- Jarrett JT, Berger EP, Lansbury PT. 1993. The carboxy terminus of the beta amyloid protein is critical for the seeding of amyloid formation: Implications for the pathogenesis of alzheimer's disease. *Biochemistry.* 32(18):4693-4697.
- Jin LW, Ninomiya H, Roch JM, Schubert D, Masliah E, Otero DA, Saitoh T. 1994. Peptides containing the terms sequence of amyloid beta/a4 protein precursor bind cell surface and promote neurite extension. *J Neurosci.* 14(9):5461-5470.
- Jones MC, Humphries JD, Byron A, Millon-Frémillon A, Robertson J, Paul NR, Ng DHJ, Askari JA, Humphries MJ. 2015. Isolation of integrin-based adhesion complexes. *Curr Protoc Cell Biol.* 66:9.8.1-9.8.15.
- Jonsson T, Atwal JK, Steinberg S, Snaedal J, Jonsson PV, Bjornsson S, Stefansson H, Sulem P, Gudbjartsson D, Maloney J et al. 2012. A mutation in app protects against alzheimer's disease and age-related cognitive decline. *Nature.* 488(7409):96-99.
- Jurga AM, Paleczna M, Kadluczka J, Kuter KZ. 2021. Beyond the gfap-astrocyte protein markers in the brain. *Biomolecules.* 11(9).
- Jutkowitz E, Kane RL, Gaugler JE, MacLehose RF, Dowd B, Kuntz KM. 2017. Societal and family lifetime cost of dementia: Implications for policy. *J Am Geriatr Soc.* 65(10):2169-2175.
- Kang J, Lemaire H-G, Unterbeck A, Salbaum JM, Masters CL, Grzeschik K-H, Multhaup G, Beyreuther K, Müller-Hill B. 1987. The precursor of alzheimer's disease amyloid a4 protein resembles a cell-surface receptor. *Nature.* 325(6106):733-736.
- Kang J, Müller-Hill B. 1990. Differential splicing of alzheimer's disease amyloid a4 precursor rna in rat tissues: Prea4(695) mrna is predominantly produced in rat and human brain. *Biochem Biophys Res Commun.* 166(3):1192-1200.
- Karantzoulis S, Galvin JE. 2011. Distinguishing alzheimer's disease from other major forms of dementia. *Expert Rev Neurother.* 11(11):1579-1591.
- Kashani A, Lepicard E, Poirel O, Videau C, David JP, Fallet-Bianco C, Simon A, Delacourte A, Giros B, Epelbaum J et al. 2008. Loss of vglut1 and vglut2 in the prefrontal cortex is correlated with cognitive decline in alzheimer disease. *Neurobiol Aging.* 29(11):1619-1630.
- Katoh M. 2020. Precision medicine for human cancers with notch signaling dysregulation (review). *Int J Mol Med.* 45(2):279-297.
- Katzman R, Terry R, DeTeresa R, Brown T, Davies P, Fuld P, Renbing X, Peck A. 1988. Clinical, pathological, and neurochemical changes in dementia: A subgroup with preserved mental status and numerous neocortical plaques. *Ann Neurol.* 23(2):138-144.
- Keller JN, Lauderback CM, Butterfield DA, Kindy MS, Yu J, Markesbery WR. 2000. Amyloid beta-peptide effects on synaptosomes from apolipoprotein e-deficient mice. *J Neurochem.* 74(4):1579-1586.
- Kim H, Kim D, Kim J, Lee HY, Park D, Kang H, Matsuda K, Sterky FH, Yuzaki M, Kim JY et al. 2020. Calsyntenin-3 interacts with both α - and β -neurexins in the regulation of excitatory synaptic innervation in specific schaffer collateral pathways. *J Biol Chem.* 295(27):9244-9262.
- Kimberly WT, LaVoie MJ, Ostaszewski BL, Ye W, Wolfe MS, Selkoe DJ. 2003. Gamma-secretase is a membrane protein complex comprised of presenilin, nicastrin, aph-1, and pen-2. *Proc Natl Acad Sci U S A.* 100(11):6382-6387.
- Kimura A, Hata S, Suzuki T. 2016. Alternative selection of β -site app-cleaving enzyme 1 (bace1) cleavage sites in amyloid β -protein precursor (app) harboring protective and pathogenic mutations within the a β sequence. *Journal of Biological Chemistry.* 291(46):24041-24053.
- Kinoshita A, Fukumoto H, Shah T, Whelan CM, Irizarry MC, Hyman BT. 2003. Demonstration by fret of bace interaction with the amyloid precursor protein at the cell surface and in early endosomes. *J Cell Sci.* 116(Pt 16):3339-3346.
- Knopman DS, Jones DT, Greicius MD. 2021. Failure to demonstrate efficacy of aducanumab: An analysis of the emerge and engage trials as reported by biogen, december 2019. *Alzheimers Dement.* 17(4):696-701.

- Koivisto L, Heino J, Häkkinen L, Larjava H. 1994. The size of the intracellular beta 1-integrin precursor pool regulates maturation of beta 1-integrin subunit and associated alpha-subunits. *Biochem J.* 300 (Pt 3):771-779.
- Koo EH, Squazzo SL, Selkoe DJ, Koo CH. 1996. Trafficking of cell-surface amyloid beta-protein precursor. I. Secretion, endocytosis and recycling as detected by labeled monoclonal antibody. *Journal of Cell Science.* 109(5):991-998.
- Kovalevich J, Langford D. 2013. Considerations for the use of sh-sy5y neuroblastoma cells in neurobiology. *Methods Mol Biol.* 1078:9-21.
- Kuhn PH, Wang H, Dislich B, Colombo A, Zeitschel U, Ellwart JW, Kremmer E, Rossner S, Lichtenthaler SF. 2010. Adam10 is the physiologically relevant, constitutive alpha-secretase of the amyloid precursor protein in primary neurons. *EMBO J.* 29(17):3020-3032.
- Kumar DK, Choi SH, Washicosky KJ, Eimer WA, Tucker S, Ghofrani J, Lefkowitz A, McColl G, Goldstein LE, Tanzi RE et al. 2016. Amyloid- β peptide protects against microbial infection in mouse and worm models of alzheimer's disease. *Sci Transl Med.* 8(340):340ra372.
- Larkin HD. 2023. Lecanemab gains fda approval for early alzheimer disease. *JAMA.*
- Lauderback CM, Kanski J, Hackett JM, Maeda N, Kindy MS, Butterfield DA. 2002. Apolipoprotein e modulates alzheimer's abeta(1-42)-induced oxidative damage to synaptosomes in an allele-specific manner. *Brain Res.* 924(1):90-97.
- Lee J, Retamal C, Cuitiño L, Caruano-Yzermans A, Shin JE, van Kerkhof P, Marzolo MP, Bu G. 2008. Adaptor protein sorting nexin 17 regulates amyloid precursor protein trafficking and processing in the early endosomes. *J Biol Chem.* 283(17):11501-11508.
- Leibson CL, Rocca WA, Hanson VA, Cha R, Kokmen E, O'Brien PC, Palumbo PJ. 1997. Risk of dementia among persons with diabetes mellitus: A population-based cohort study. *Am J Epidemiol.* 145(4):301-308.
- Li H, Wang B, Wang Z, Guo Q, Tabuchi K, Hammer RE, Südhof TC, Zheng H. 2010. Soluble amyloid precursor protein (app) regulates *transferrin* and *klotho* gene expression without rescuing the essential function of app. *Proceedings of the National Academy of Sciences.* 107(40):17362-17367.
- Lim GP, Chu T, Yang F, Beech W, Frautschy SA, Cole GM. 2001. The curry spice curcumin reduces oxidative damage and amyloid pathology in an alzheimer transgenic mouse. *J Neurosci.* 21(21):8370-8377.
- Lim J, Iftner T, Simon C. 2021. Native isolation of 3xha-tagged protein complexes to characterize protein-protein interactions. *Curr Protoc.* 1(2):e29.
- Lindwall G, Cole RD. 1984. Phosphorylation affects the ability of tau protein to promote microtubule assembly. *J Biol Chem.* 259(8):5301-5305.
- Liu M, Kuhel DG, Shen L, Hui DY, Woods SC. 2012. Apolipoprotein e does not cross the blood-cerebrospinal fluid barrier, as revealed by an improved technique for sampling csf from mice. *Am J Physiol Regul Integr Comp Physiol.* 303(9):R903-908.
- Lleó A, Núñez-Llaves R, Alcolea D, Chiva C, Balateu-Paños D, Colom-Cadena M, Gomez-Giro G, Muñoz L, Querol-Vilaseca M, Pegueroles J et al. 2019. Changes in synaptic proteins precede neurodegeneration markers in preclinical alzheimer's disease cerebrospinal fluid. *Mol Cell Proteomics.* 18(3):546-560.
- Lopes FM, Bristot IJ, Da Motta LL, Parsons RB, Klamt F. 2017. Mimicking parkinson's disease in a dish: Merits and pitfalls of the most commonly used dopaminergic in vitro models. *NeuroMolecular Medicine.* 19(2-3):241-255.
- Luo LQ, Martin-Morris LE, White K. 1990. Identification, secretion, and neural expression of appl, a drosophila protein similar to human amyloid protein precursor. *J Neurosci.* 10(12):3849-3861.
- Ma QL, Yang F, Rosario ER, Ubeda OJ, Beech W, Gant DJ, Chen PP, Hudspeth B, Chen C, Zhao Y et al. 2009. Beta-amyloid oligomers induce phosphorylation of tau and inactivation of insulin receptor substrate via c-jun n-terminal kinase signaling: Suppression by omega-3 fatty acids and curcumin. *J Neurosci.* 29(28):9078-9089.
- MacDermott AB, Mayer ML, Westbrook GL, Smith SJ, Barker JL. 1986. Nmda-receptor activation increases cytoplasmic calcium concentration in cultured spinal cord neurones. *Nature.* 321(6069):519-522.
- MacLeod R, Hillert EK, Cameron RT, Baillie GS. 2015. The role and therapeutic targeting of α -, β - and γ -secretase in alzheimer's disease. *Future Sci OA.* 1(3):FSO11.
- Madsen TD, Hansen LH, Hintze J, Ye Z, Jebari S, Andersen DB, Joshi HJ, Ju T, Goetze JP, Martin C et al. 2020. An atlas of o-linked glycosylation on peptide hormones reveals diverse biological roles. *Nature Communications.* 11(1).
- Mahase E. 2021a. Aducanumab: European agency rejects alzheimer's drug over efficacy and safety concerns. *BMJ : British Medical Journal (Online).* 375.

- Mahase E. 2021b. Three fda advisory panel members resign over approval of alzheimer's drug. *BMJ*. 373:n1503.
- Mahase E. 2023. Alzheimer's disease: Fda approves lecanemab amid cost and safety concerns. *BMJ*. 380:73.
- Mandal PK, Tripathi M, Sugunan S. 2012. Brain oxidative stress: Detection and mapping of anti-oxidant marker 'glutathione' in different brain regions of healthy male/female, mci and alzheimer patients using non-invasive magnetic resonance spectroscopy. *Biochem Biophys Res Commun*. 417(1):43-48.
- Mattson MP, Cheng B, Culwell AR, Esch FS, Lieberburg I, Rydel RE. 1993. Evidence for excitoprotective and intraneuronal calcium-regulating roles for secreted forms of the beta-amyloid precursor protein. *Neuron*. 10(2):243-254.
- Mattson MP, Cheng B, Davis D, Bryant K, Lieberburg I, Rydel RE. 1992. Beta-amyloid peptides destabilize calcium homeostasis and render human cortical neurons vulnerable to excitotoxicity. *J Neurosci*. 12(2):376-389.
- McCarron M, McCallion P, Reilly E, Mulryan N. 2014. A prospective 14-year longitudinal follow-up of dementia in persons with down syndrome. *J Intellect Disabil Res*. 58(1):61-70.
- Meziane H, Dodart JC, Mathis C, Little S, Clemens J, Paul SM, Ungerer A. 1998. Memory-enhancing effects of secreted forms of the beta-amyloid precursor protein in normal and amnesic mice. *Proc Natl Acad Sci U S A*. 95(21):12683-12688.
- Mittler R. 2017. Ros are good. *Trends Plant Sci*. 22(1):11-19.
- Monyer H, Goldberg MP, Choi DW. 1989. Glucose deprivation neuronal injury in cortical culture. *Brain Res*. 483(2):347-354.
- Mullan M, Crawford F, Axelman K, Houlden H, Lilius L, Winblad B, Lannfelt L. 1992. A pathogenic mutation for probable alzheimer's disease in the app gene at the n-terminus of beta-amyloid. *Nat Genet*. 1(5):345-347.
- Murphy MP, LeVine H. 2010. Alzheimer's disease and the amyloid-beta peptide. *J Alzheimers Dis*. 19(1):311-323.
- Müller U, Cristina N, Li ZW, Wolfer DP, Lipp HP, Rüllicke T, Brandner S, Aguzzi A, Weissmann C. 1994. Behavioral and anatomical deficits in mice homozygous for a modified beta-amyloid precursor protein gene. *Cell*. 79(5):755-765.
- Nakai M, Kawamata T, Taniguchi T, Maeda K, Tanaka C. 1996. Expression of apolipoprotein e mrna in rat microglia. *Neurosci Lett*. 211(1):41-44.
- Ndayisaba A, Kaindlstorfer C, Wenning GK. 2019. Iron in neurodegeneration - cause or consequence? *Front Neurosci*. 13:180.
- Nicoll JAR, Buckland GR, Harrison CH, Page A, Harris S, Love S, Neal JW, Holmes C, Boche D. 2019. Persistent neuropathological effects 14 years following amyloid- β immunization in alzheimer's disease. *Brain*. 142(7):2113-2126.
- Nikolaev A, McLaughlin T, O'Leary DD, Tessier-Lavigne M. 2009. App binds dr6 to trigger axon pruning and neuron death via distinct caspases. *Nature*. 457(7232):981-989.
- Nitsche A, Arnold C, Ueberham U, Reiche K, Fallmann J, Hackermüller J, Horn F, Stadler PF, Arendt T. 2021. Alzheimer-related genes show accelerated evolution. *Mol Psychiatry*. 26(10):5790-5796.
- Ohsawa I, Takamura C, Morimoto T, Ishiguro M, Kohsaka S. 1999. Amino-terminal region of secreted form of amyloid precursor protein stimulates proliferation of neural stem cells. *European Journal of Neuroscience*. 11(6):1907-1913.
- Monthly mortality analysis, england and wales: September 2022. 2022. <https://www.ons.gov.uk/peoplepopulationandcommunity/birthsdeathsandmarriages/deaths/bulletin/s/monthlymortalityanalysisenglandandwales/september2022>: Office for National Statistics (ONS); [accessed 2022 23/11].
- Orgogozo JM, Gilman S, Dartigues JF, Laurent B, Puel M, Kirby LC, Jouanny P, Dubois B, Eisner L, Flitman S et al. 2003. Subacute meningoencephalitis in a subset of patients with ad after abeta42 immunization. *Neurology*. 61(1):46-54.
- Paneni F, Beckman JA, Creager MA, Cosentino F. 2013. Diabetes and vascular disease: Pathophysiology, clinical consequences, and medical therapy: Part i. *Eur Heart J*. 34(31):2436-2443.
- Parsons CG, Danysz W, Dekundy A, Pulte I. 2013. Memantine and cholinesterase inhibitors: Complementary mechanisms in the treatment of alzheimer's disease. *Neurotoxicity Research*. 24(3):358-369.
- Parvathy S, Hussain I, Karran EH, Turner AJ, Hooper NM. 1999. Cleavage of alzheimer's amyloid precursor protein by alpha-secretase occurs at the surface of neuronal cells. *Biochemistry*. 38(30):9728-9734.
- Pavelescu LA. 2015. On reactive oxygen species measurement in living systems. *J Med Life*. 8 Spec Issue:38-42.

- Peh WY, Reimhult E, Teh HF, Thomsen JS, Su X. 2007. Understanding ligand binding effects on the conformation of estrogen receptor alpha-dna complexes: A combinational quartz crystal microbalance with dissipation and surface plasmon resonance study. *Biophys J*. 92(12):4415-4423.
- Perdivara I, Petrovich R, Allinquant B, Deterding LJ, Tomer KB, Przybylski M. 2009. Elucidation of o-glycosylation structures of the β -amyloid precursor protein by liquid chromatography-mass spectrometry using electron transfer dissociation and collision induced dissociation. *Journal of Proteome Research*. 8(2):631-642.
- Person F, Wilczak W, Hube-Magg C, Burdelski C, Möller-Koop C, Simon R, Noriega M, Sauter G, Steurer S, Burdak-Rothkamm S et al. 2017. Prevalence of β iii-tubulin (tubb3) expression in human normal tissues and cancers. *Tumour Biol*. 39(10):1010428317712166.
- Pettem KL, Yokomaku D, Luo L, Linhoff MW, Prasad T, Connor SA, Siddiqui TJ, Kawabe H, Chen F, Zhang L et al. 2013. The specific α -neurexin interactor calyntenin-3 promotes excitatory and inhibitory synapse development. *Neuron*. 80(1):113-128.
- Piersma SR, Warmoes MO, de Wit M, de Reus I, Knol JC, Jiménez CR. 2013. Whole gel processing procedure for gelc-ms/ms based proteomics. *Proteome Sci*. 11(1):17.
- Plant LD, Boyle JP, Smith IF, Peers C, Pearson HA. 2003. The production of amyloid beta peptide is a critical requirement for the viability of central neurons. *J Neurosci*. 23(13):5531-5535.
- Prillaman M. 2022. Heralded alzheimer's drug works - but safety concerns loom. *Nature*. 612(7939):197-198.
- Prince M, Knapp M, Guerchet M, McCrone P, Prina M, Comas-Herrera M, wittenberg A, Adelaja R, Hu B, King B et al. 2014. Dementia uk: Update. Alzheimer's Society.
- Qiu WQ, Walsh DM, Ye Z, Vekrellis K, Zhang J, Podlisny MB, Rosner MR, Safavi A, Hersh LB, Selkoe DJ. 1998. Insulin-degrading enzyme regulates extracellular levels of amyloid beta-protein by degradation. *J Biol Chem*. 273(49):32730-32738.
- Quiroz-Baez R, Rojas E, Arias C. 2009. Oxidative stress promotes jnk-dependent amyloidogenic processing of normally expressed human app by differential modification of alpha-, beta- and gamma-secretase expression. *Neurochem Int*. 55(7):662-670.
- Rajendran L, Honsho M, Zahn TR, Keller P, Geiger KD, Verkade P, Simons K. 2006. Alzheimer's disease beta-amyloid peptides are released in association with exosomes. *Proc Natl Acad Sci U S A*. 103(30):11172-11177.
- Ramassamy C, Krzykowski P, Averill D, Lussier-Cacan S, Theroux L, Christen Y, Davignon J, Poirier J. 2001. Impact of apoe deficiency on oxidative insults and antioxidant levels in the brain. *Brain Res Mol Brain Res*. 86(1-2):76-83.
- Ramazi S, Zahir J. 2021. Posttranslational modifications in proteins: Resources, tools and prediction methods. Database (Oxford). 2021.
- Ray B, Long JM, Sokol DK, Lahiri DK. 2011. Increased secreted amyloid precursor protein- α (sapp α) in severe autism: Proposal of a specific, anabolic pathway and putative biomarker. *PLoS One*. 6(6):e20405.
- Reardon S. 2023. Fda approves alzheimer's drug lecanemab amid safety concerns. *Nature*. 613(7943):227-228.
- Reed MJ, Damodarasamy M, Banks WA. 2019. The extracellular matrix of the blood-brain barrier: Structural and functional roles in health, aging, and alzheimer's disease. *Tissue Barriers*. 7(4):1651157.
- Reinhard C, Borgers M, David G, De Strooper B. 2013. Soluble amyloid- β precursor protein binds its cell surface receptor in a cooperative fashion with glypican and syndecan proteoglycans. *J Cell Sci*. 126(Pt 21):4856-4861.
- Rice HC, De Malmazet D, Schreurs A, Frere S, Van Molle I, Volkov AN, Creemers E, Vertkin I, Nys J, Ranaivoson FM et al. 2019. Secreted amyloid- β precursor protein functions as a gababr1a ligand to modulate synaptic transmission. *Science*. 363(6423):4827.
- Richter MC, Ludewig S, Winschel A, Abel T, Bold C, Salzburger LR, Klein S, Han K, Weyer SW, Fritz AK et al. 2018. Distinct *in vivo* roles of secreted app ectodomain variants app α and app β in regulation of spine density, synaptic plasticity, and cognition. *The EMBO Journal*. 37(11):e98335.
- Ring S, Weyer SW, Kilian SB, Waldron E, Pietrzik CU, Filippov MA, Herms J, Buchholz C, Eckman CB, Korte M et al. 2007. The secreted beta-amyloid precursor protein ectodomain app α is sufficient to rescue the anatomical, behavioral, and electrophysiological abnormalities of app-deficient mice. *J Neurosci*. 27(29):7817-7826.
- Robakis NK, Ramakrishna N, Wolfe G, Wisniewski HM. 1987. Molecular cloning and characterization of a cDNA encoding the cerebrovascular and the neuritic plaque amyloid peptides. *Proc Natl Acad Sci U S A*. 84(12):4190-4194.
- Roberts R, Knopman DS. 2013. Classification and epidemiology of mci. *Clin Geriatr Med*. 29(4):753-772.

- Roberts RO, Knopman DS, Mielke MM, Cha RH, Pankratz VS, Christianson TJ, Geda YE, Boeve BF, Ivnik RJ, Tangalos EG et al. 2014. Higher risk of progression to dementia in mild cognitive impairment cases who revert to normal. *Neurology*. 82(4):317-325.
- Roch JM, Masliah E, Roch-Levecq AC, Sundsmo MP, Otero DA, Veinbergs I, Saitoh T. 1994. Increase of synaptic density and memory retention by a peptide representing the trophic domain of the amyloid beta/a4 protein precursor. *Proceedings of the National Academy of Sciences*. 91(16):7450-7454.
- Rohan de Silva HA, Jen A, Wickenden C, Jen LS, Wilkinson SL, Patel AJ. 1997. Cell-specific expression of beta-amyloid precursor protein isoform mRNAs and proteins in neurons and astrocytes. *Brain Res Mol Brain Res*. 47(1-2):147-156.
- Rosen DR, Martin-Morris L, Luo LQ, White K. 1989. A drosophila gene encoding a protein resembling the human beta-amyloid protein precursor. *Proc Natl Acad Sci U S A*. 86(7):2478-2482.
- Rossjohn J, Cappai R, Feil SC, Henry A, McKinstry WJ, Galatis D, Hesse L, Multhaup G, Beyreuther K, Masters CL et al. 1999. Crystal structure of the n-terminal, growth factor-like domain of alzheimer amyloid precursor protein. *Nat Struct Biol*. 6(4):327-331.
- Ryan MM, Morris GP, Mockett BG, Bourne K, Abraham WC, Tate WP, Williams JM. 2013. Time-dependent changes in gene expression induced by secreted amyloid precursor protein-alpha in the rat hippocampus. *BMC Genomics*. 14:376.
- Sahlin C, Lord A, Magnusson K, Englund H, Almeida CG, Greengard P, Nyberg F, Gouras GK, Lannfelt L, Nilsson LN. 2007. The arctic alzheimer mutation favors intracellular amyloid-beta production by making amyloid precursor protein less available to alpha-secretase. *J Neurochem*. 101(3):854-862.
- Santillo S, Schiano Moriello A, Di Maio V. 2014. Electrophysiological variability in the sh-sy5y cellular line. *Gen Physiol Biophys*. 33(1):121-129.
- Schenk D, Barbour R, Dunn W, Gordon G, Grajeda H, Guido T, Hu K, Huang J, Johnson-Wood K, Khan K et al. 1999. Immunization with amyloid-beta attenuates alzheimer-disease-like pathology in the pdapp mouse. *Nature*. 400(6740):173-177.
- Schwartzentruber J, Foskolou S, Kilpinen H, Rodrigues J, Alasoo K, Knights AJ, Patel M, Goncalves A, Ferreira R, Benn CL et al. 2018. Molecular and functional variation in ipsc-derived sensory neurons. *Nat Genet*. 50(1):54-61.
- Seabrook GR, Smith DW, Bowery BJ, Easter A, Reynolds T, Fitzjohn SM, Morton RA, Zheng H, Dawson GR, Sirinathsinghji DJ et al. 1999. Mechanisms contributing to the deficits in hippocampal synaptic plasticity in mice lacking amyloid precursor protein. *Neuropharmacology*. 38(3):349-359.
- Selkoe DJ, Hardy J. 2016. The amyloid hypothesis of alzheimer's disease at 25 years. *EMBO Mol Med*. 8(6):595-608.
- Selkoe DJ, Podlisny MB, Joachim CL, Vickers EA, Lee G, Fritz LC, Oltersdorf T. 1988. Beta-amyloid precursor protein of alzheimer disease occurs as 110- to 135-kilodalton membrane-associated proteins in neural and nonneural tissues. *Proc Natl Acad Sci U S A*. 85(19):7341-7345.
- Selvackadunco S, Langford K, Shah Z, Hurley S, Bodi I, King A, Aarsland D, Troakes C, Al-Sarraj S. 2019. Comparison of clinical and neuropathological diagnoses of neurodegenerative diseases in two centres from the brains for dementia research (bdr) cohort. *Journal of Neural Transmission*. 126(3):327-337.
- Sengupta U, Nilson AN, Kayed R. 2016. The role of amyloid-beta oligomers in toxicity, propagation, and immunotherapy. *EBioMedicine*. 6:42-49.
- Shao CY, Mirra SS, Sait HB, Sacktor TC, Sigurdsson EM. 2011. Postsynaptic degeneration as revealed by psd-95 reduction occurs after advanced aβ and tau pathology in transgenic mouse models of alzheimer's disease. *Acta Neuropathol*. 122(3):285-292.
- Shi Y, Kirwan P, Livesey FJ. 2012. Directed differentiation of human pluripotent stem cells to cerebral cortex neurons and neural networks. *Nat Protoc*. 7(10):1836-1846.
- Silbert LC. 2007. Does statin use decrease the amount of alzheimer disease pathology in the brain? *Neurology*. 69(9):E8-11.
- Sinha P, Barocas JA. 2022. Cost-effectiveness of aducanumab to prevent alzheimer's disease progression at current list price. *Alzheimers Dement (N Y)*. 8(1):e12256.
- Skovronsky DM, Moore DB, Milla ME, Doms RW, Lee VM. 2000. Protein kinase c-dependent alpha-secretase competes with beta-secretase for cleavage of amyloid-beta precursor protein in the trans-golgi network. *J Biol Chem*. 275(4):2568-2575.
- Slanzi A, Iannoto G, Rossi B, Zenaro E, Constantin G. 2020. Models of neurodegenerative diseases. *Front Cell Dev Biol*. 8:328.

- Sokol DK, Chen D, Farlow MR, Dunn DW, Maloney B, Zimmer JA, Lahiri DK. 2006. High levels of alzheimer beta-amyloid precursor protein (app) in children with severely autistic behavior and aggression. *J Child Neurol.* 21(6):444-449.
- Soltani MH, Pichardo R, Song Z, Sangha N, Camacho F, Satyamoorthy K, Sanguenza OP, Setaluri V. 2005. Microtubule-associated protein 2, a marker of neuronal differentiation, induces mitotic defects, inhibits growth of melanoma cells, and predicts metastatic potential of cutaneous melanoma. *Am J Pathol.* 166(6):1841-1850.
- Soscia SJ, Kirby JE, Washicosky KJ, Tucker SM, Ingelsson M, Hyman B, Burton MA, Goldstein LE, Duong S, Tanzi RE et al. 2010. The alzheimer's disease-associated amyloid beta-protein is an antimicrobial peptide. *PLoS One.* 5(3):e9505.
- Steen E, Terry BM, Rivera EJ, Cannon JL, Neely TR, Tavares R, Xu XJ, Wands JR, de la Monte SM. 2005. Impaired insulin and insulin-like growth factor expression and signaling mechanisms in alzheimer's disease--is this type 3 diabetes? *J Alzheimers Dis.* 7(1):63-80.
- Stelzmann RA, Norman Schnitzlein H, Reed Murtagh F. 1995. An english translation of alzheimer's 1907 paper, über eine eigenartige erkrankung der hirnrinde. *Clinical Anatomy.* 8(6):429-431.
- Storey E, Katz M, Brickman Y, Beyreuther K, Masters CL. 1999. Amyloid precursor protein of alzheimer's disease: Evidence for a stable, full-length, trans-membrane pool in primary neuronal cultures. *European Journal of Neuroscience.* 11(5):1779-1788.
- Sun Q, Xie N, Tang B, Li R, Shen Y. 2017. Alzheimer's disease: From genetic variants to the distinct pathological mechanisms. *Front Mol Neurosci.* 10:319.
- Sze CI, Troncoso JC, Kawas C, Mouton P, Price DL, Martin LJ. 1997. Loss of the presynaptic vesicle protein synaptophysin in hippocampus correlates with cognitive decline in alzheimer disease. *J Neuropathol Exp Neurol.* 56(8):933-944.
- Sørensen BH, Rasmussen LJ, Broberg BS, Klausen TK, Sauter DP, Lambert IH, Aspberg A, Hoffmann EK. 2015. Integrin β 1, osmosensing, and chemoresistance in mouse ehrlich carcinoma cells. *Cell Physiol Biochem.* 36(1):111-132.
- Tan E, Chin CSH, Lim ZFS, Ng SK. 2021. Hek293 cell line as a platform to produce recombinant proteins and viral vectors. *Front Bioeng Biotechnol.* 9:796991.
- Tan JZA, Gleeson PA. 2019a. The role of membrane trafficking in the processing of amyloid precursor protein and production of amyloid peptides in alzheimer's disease. *Biochim Biophys Acta Biomembr.* 1861(4):697-712.
- Tan JZA, Gleeson PA. 2019b. The trans-golgi network is a major site for α -secretase processing of amyloid precursor protein in primary neurons. *Journal of Biological Chemistry.* 294(5):1618-1631.
- Tan VTY, Mockett BG, Ohline SM, Parfitt KD, Wicky HE, Peppercorn K, Schoderboeck L, Yahaya MFB, Tate WP, Hughes SM et al. 2018. Lentivirus-mediated expression of human secreted amyloid precursor protein-alpha prevents development of memory and plasticity deficits in a mouse model of alzheimer's disease. *Mol Brain.* 11(1):7.
- Tanokashira D, Mamada N, Yamamoto F, Taniguchi K, Tamaoka A, Lakshmana MK, Araki W. 2017. The neurotoxicity of amyloid β -protein oligomers is reversible in a primary neuron model. *Mol Brain.* 10(1):4.
- Tanzi RE, Gusella JF, Watkins PC, Bruns GA, St George-Hyslop P, Van Keuren ML, Patterson D, Pagan S, Kurnit DM, Neve RL. 1987. Amyloid beta protein gene: Cdna, mrna distribution, and genetic linkage near the alzheimer locus. *Science.* 235(4791):880-884.
- Teunissen CE, Verberk IMW, Thijssen EH, Vermunt L, Hansson O, Zetterberg H, van der Flier WM, Mielke MM, Del Campo M. 2022. Blood-based biomarkers for alzheimer's disease: Towards clinical implementation. *Lancet Neurol.* 21(1):66-77.
- Tharp WG, Sarkar IN. 2013. Origins of amyloid- β . *BMC Genomics.* 14:290.
- Togo K, Fukusumi H, Shofuda T, Ohnishi H, Yamazaki H, Hayashi MK, Kawasaki N, Takei N, Nakazawa T, Saito Y et al. 2021. Postsynaptic structure formation of human ips cell-derived neurons takes longer than presynaptic formation during neural differentiation in vitro. *Mol Brain.* 14(1):149.
- Trinkle-Mulcahy L. 2019. Recent advances in proximity-based labeling methods for interactome mapping. *F1000Res.* 8.
- Tseng BP, Green KN, Chan JL, Blurton-Jones M, LaFerla FM. 2008. Abeta inhibits the proteasome and enhances amyloid and tau accumulation. *Neurobiol Aging.* 29(11):1607-1618.
- Tönnies E, Trushina E. 2017. Oxidative stress, synaptic dysfunction, and alzheimer's disease. *Journal of Alzheimer's disease.* 57(4):1105-1121.

- Uchida Y, Gomi F, Murayama S, Takahashi H. 2013. Calsyntenin-3 c-terminal fragment accumulates in dystrophic neurites surrounding $\text{A}\beta$ plaques in tg2576 mouse and alzheimer disease brains: Its neurotoxic role in mediating dystrophic neurite formation. *Am J Pathol.* 182(5):1718-1726.
- Uchida Y, Nakano S, Gomi F, Takahashi H. 2011. Up-regulation of calsyntenin-3 by β -amyloid increases vulnerability of cortical neurons. *FEBS Lett.* 585(4):651-656.
- Um JW, Pramanik G, Ko JS, Song MY, Lee D, Kim H, Park KS, Südhof TC, Tabuchi K, Ko J. 2014. Calsyntenins function as synaptogenic adhesion molecules in concert with neurexins. *Cell Rep.* 6(6):1096-1109.
- Vagnoni A, Perkinton MS, Gray EH, Francis PT, Noble W, Miller CC. 2012. Calsyntenin-1 mediates axonal transport of the amyloid precursor protein and regulates $\text{A}\beta$ production. *Hum Mol Genet.* 21(13):2845-2854.
- Van Der Flier WM. 2005. Epidemiology and risk factors of dementia. *Journal of Neurology, Neurosurgery & Psychiatry.* 76(suppl_5):v2-v7.
- van Dyck CH, Swanson CJ, Aisen P, Bateman RJ, Chen C, Gee M, Kanekiyo M, Li D, Reyderman L, Cohen S et al. 2023. Lecanemab in early alzheimer's disease. *N Engl J Med.* 388(1):9-21.
- Vassar R, Bennett BD, Babu-Khan S, Kahn S, Mendiaz EA, Denis P, Teplow DB, Ross S, Amarante P, Loeloff R et al. 1999. B-secretase cleavage of alzheimer's amyloid precursor protein by the transmembrane aspartic protease bace. *Science.* 286(5440):735-741.
- Volpato V, Webber C. 2020. Addressing variability in ipsc-derived models of human disease: Guidelines to promote reproducibility. *Dis Model Mech.* 13(1).
- Walsh S, Merrick R, Milne R, Brayne C. 2021. Aducanumab for alzheimer's disease? *BMJ.* 374:n1682.
- Wang H, Kulas JA, Wang C, Holtzman DM, Ferris HA, Hansen SB. 2021. Regulation of beta-amyloid production in neurons by astrocyte-derived cholesterol. *Proc Natl Acad Sci U S A.* 118(33).
- Wang Z, Xu Q, Cai F, Liu X, Wu Y, Song W. 2019. Bace2, a conditional β -secretase, contributes to alzheimer's disease pathogenesis. *JCI Insight.* 4(1).
- Weyer SW, Klevanski M, Delekate A, Voikar V, Aydin D, Hick M, Filippov M, Drost N, Schaller KL, Saar M et al. 2011. App and aplp2 are essential at pns and cns synapses for transmission, spatial learning and ltp. *The EMBO Journal.* 30(11):2266-2280.
- White AR, Reyes R, Mercer JF, Camakaris J, Zheng H, Bush AI, Multhaup G, Beyreuther K, Masters CL, Cappai R. 1999. Copper levels are increased in the cerebral cortex and liver of app and aplp2 knockout mice. *Brain Res.* 842(2):439-444.
- Whittemore ER, Loo DT, Watt JA, Cotman CW. 1995. A detailed analysis of hydrogen peroxide-induced cell death in primary neuronal culture. *Neuroscience.* 67(4):921-932.
- WHO. 2017. Global action plan on the public health response to dementia 2017–2025.
- Wittenberg R, Knapp M, Hu B, Comas-Herrera A, King D, Rehill A, Shi C, Banerjee S, Patel A, Jagger C et al. 2019. The costs of dementia in england. *Int J Geriatr Psychiatry.* 34(7):1095-1103.
- Xie J, Brayne C, Matthews FE, collaborators MRCCFaAS. 2008. Survival times in people with dementia: Analysis from population based cohort study with 14 year follow-up. *BMJ.* 336(7638):258-262.
- Xu G, Ran Y, Fromholt SE, Fu C, Yachnis AT, Golde TE, Borchelt DR. 2015. Murine $\text{A}\beta$ over-production produces diffuse and compact alzheimer-type amyloid deposits. *Acta Neuropathol Commun.* 3:72.
- Yankner BA, Duffy LK, Kirschner DA. 1990. Neurotrophic and neurotoxic effects of amyloid beta protein: Reversal by tachykinin neuropeptides. *Science.* 250(4978):279-282.
- Yazaki M, Tagawa K, Maruyama K, Sorimachi H, Tsuchiya T, Ishiura S, Suzuki K. 1996. Mutation of potential n-linked glycosylation sites in the alzheimer's disease amyloid precursor protein (app). *Neuroscience letters.* 221(1):57-60.
- Yoon IS, Chen E, Busse T, Repetto E, Lakshmana MK, Koo EH, Kang DE. 2007. Low-density lipoprotein receptor-related protein promotes amyloid precursor protein trafficking to lipid rafts in the endocytic pathway. *FASEB J.* 21(11):2742-2752.
- Yu W, Datta A, Leroy P, O'Brien LE, Mak G, Jou TS, Matlin KS, Mostov KE, Zegers MM. 2005. Beta1-integrin orients epithelial polarity via rac1 and laminin. *Mol Biol Cell.* 16(2):433-445.
- Zayas JFa. 1997. Solubility of proteins. *Functionality of Proteins in Food.* 6-75.
- Zeng X, Ye M, Resch JM, Jedrychowski MP, Hu B, Lowell BB, Ginty DD, Spiegelman BM. 2019. Innervation of thermogenic adipose tissue via a calsyntenin 3 β -s100b axis. *Nature.* 569(7755):229-235.
- Zhang X, Song W. 2013. The role of app and bace1 trafficking in app processing and amyloid- β generation. *Alzheimers Res Ther.* 5(5):46.
- Zhang YW, Thompson R, Zhang H, Xu H. 2011. App processing in alzheimer's disease. *Mol Brain.* 4:3.
- Zhao J, Liu X, Xia W, Zhang Y, Wang C. 2020. Targeting amyloidogenic processing of app in alzheimer's disease. *Front Mol Neurosci.* 13:137.

- Zhao Y, Zhao B. 2013. Oxidative stress and the pathogenesis of alzheimer's disease. *Oxid Med Cell Longev*. 2013:316523.
- Zheng H, Jiang M, Trumbauer ME, Sirinathsinghji DJ, Hopkins R, Smith DW, Heavens RP, Dawson GR, Boyce S, Conner MW et al. 1995. Beta-amyloid precursor protein-deficient mice show reactive gliosis and decreased locomotor activity. *Cell*. 81(4):525-531.
- Zilkens RR, Davis WA, Spilsbury K, Semmens JB, Bruce DG. 2013. Earlier age of dementia onset and shorter survival times in dementia patients with diabetes. *Am J Epidemiol*. 177(11):1246-1254.